Dissertation Advisor: Author:

Professor Leonard I. Zon, M.D. Pulin Li

Chemical Genetics of Hematopoietic Stem Cell Transplantation

Abstract

Hematopoietic stem and progenitor cells (HSPCs) repopulate the blood system upon transplantation. A large-scale genetic approach to understand the factors that participate in successful engraftment has not been undertaken. In this thesis, I present the development of a novel live imaging-based competitive marrow repopulation assay in adult zebrafish, which allows fast and quantitative measurement of HSPC engraftment capability. Using this assay, a transplantation-based chemical screen was performed, which led to the discovery of 10 compounds that can enhance the marrow engraftment capability in zebrafish. Among them, the arachidonic acid-derived epoxyeicosatrienoic acids (EET), had conserved effects on both short- and long-term bone marrow engraftment in mice. Genetic analysis in zebrafish embryos demonstrated that EET acts through a Gα12/13-mediated receptor, which activates PI3K and induces transcription factors of the AP-1 family. This PI3K/AP-1 pathway directly induced the transcription of HSC marker, *runx1,* in embryos. The activation of PI3K by EET promoted HSPC migration and interactions

with niche cells. Our studies define a role for EETs in the development of blood stem cells during embryogenesis, and in engraftment in adult vertebrates. The other compounds discovered in the screen implicate additional novel signaling pathways involved in the HSPC engraftment process, which require further investigation. In summary, this thesis elucidated an important role of bioactive lipids in regulating HSC engraftment in adults and during embryo development. Systematically mapping out the regulatory network will tremendously benefit both the basic understanding of stem cell biology and the clinical manipulation to generate better stem cells for transplantation.

Contents

Citations to Published/Submitted Work

Parts of Chapters 2 and 3 have been written as one manuscript and submitted for publication as:

Li, P., Pugach, E.K., Riley, E.B., Panigrahy, D., Tamplin, O.J., Bowman, T.V., Heffner, G.C., McKinney-Freeman, S., Schlaeger, T.M., Daley, G.Q., Zeldin, D.C., and Zon, L.I. (2012). Epoxyeicosatrienoic Acids Enhance Hematopoietic Stem and Progenitor Cell Engraftment.

Parts of Chapters 1 and 4 are adapted from two previously published reviews:

Li, P., White, R.M., and Zon, L.I. (2011). Transplantation in zebrafish. Methods Cell Biol *105*, 403-417.

Li, P., and Zon, L.I. (2011). Stem Cell Migration: a Zebrafish Model. Methods Mol Biol. *750*, 157-68.

Parts of Chapter 2 includes the collaborative work I did for the following published papers:

Mosimann, C., Kaufman, C.K., **Li, P.**, Pugach, E.K., Tamplin, O.J., and Zon, L.I. (2011). Ubiquitous transgene expression and Cre-based recombination driven by the ubiquitin promoter in zebrafish. Development *138*, 169-177.

Pugach, E.K., **Li, P.**, White, R., and Zon, L. (2009). Retro-orbital injection in adult zebrafish. J Vis Exp.

Appendix 1, 2 and 3 have been published in their entirety in the following three original articles and/or review:

Zhang, L., Alt, C., **Li, P.**, White, R.M., Zon, L.I., Wei, X., and Lin, C.P. (2012) An optical platform for cell tracking in adult zebrafish. Cytometry A *81*, 176-182.

North, T.E., Goessling, W., Peeters, M., **Li, P.**, Ceol, C., Lord, A.M., Weber, G.J., Harris, J., Cutting, C.C., Huang, P., Dzierzak, E., and Zon, L.I. (2009) Hematopoietic stem cell development is dependent on blood flow. Cell *137*, 736-748.

Li, P., Zon, L.I. (2010) Resolving the controversy about N-cadherin and hematopoietic stem cells. Cell Stem Cell *6*, 199-202.

The work above has been reproduced by permission of the publishers and co-authors.

Acknowledgements

The generous support from many people, whom I either know personally or not, has made this thesis possible. The person to whom I owe the most for my graduate school experience is my extraordinary advisor, Leonard Zon. To me, he is not only an advisor on science, but also a mentor for life. Len's brilliant scientific insights, enthusiasm, positive attitude, and caring personality have deeply influenced me as a scientist, as well as a person. His constant encouragement makes me believe in myself and pursue the career I love. I am extremely grateful for his guidance!

As a graduate student at Harvard, one of the greatest things is being surrounded by the most brilliant scientists. I am thankful for the professors on my qualifying exam, dissertation advisory and defense committees: Drs. Jon Clardy, Randall Peterson, David Williams, Randall King, Stuart Orkin, Caroline Burns, and especially my chair, Amy Wagers, for her constant advice and being there for me all the time. I would also like to thank Dr. Lee Rubin for the fun teaching experience, and Drs. Stuart Schreiber and David Liu, who took me as a rotation student. All of this was made possible by the Chemical Biology program and the extremely helpful stuff: Melitta King, Samantha Reed, KeyAnna Schmiedl, and Jason Millberg.

The thesis could not be completed without the great collaborators: Dr. George Daley for offering advice and resources for the project and my career. Thanks to Thorsten Schlaeger and members of his lab, Sumon Datta and Philip Manos, for everything I learnt about chemical screen and imaging analysis. To Garrett Heffner,

Ronald Mathieu, Shannon McKinney-Freeman for everything about mice and FACS. To Yi Zhou and Tony Adibiase for the bioinformatics support. To Dr. Darryl Zeldin, Dipak Panigrahy, and Matthew Edin for the recent collaboration. To all the other people who generously shared their resources.

Science is not always easy, but I am lucky to be in a lab with many talented and wonderful people. I cannot say enough thank you to my previous and current labmates who have been an essential part of my graduate school training and helped me along the way: Trista North as my first mentor in the lab; Teresa Bowman and Xiaoying Bai, Eirini Trompouki, whom I always go to for scientific advice; Christian Mosimann, for just being Christian; Michelle Lin and Lili Jing for being like big sisters to me; Owen Tamplin, Rich White and Ellen van Rooijen for the memorable chats on the M2 shuttle; Yariv Houvras as a cool baymate. Thanks to the two extraordinary research assistants I have worked with: Emily Pugach and Elizabeth Riley, for bearing with me and helping me be organized. You make the "transplant" team productive and bench-work so much fun! To Bilguujin Dorjsuren and Vera Binder, who worked with me and gave me their trust. To the people who make the lab run smoothly: Bruce Barut, Dorothy Giarla, and many other people.

Thanks to the graduate students in the lab for simply being there and sharing the graduate school experience: Alison Taylor, Xiuning Le, Colleen Albacker, Narie Storer, Ellen Durand, Justin Tan, Jared Ganis. And especially my lovely baymates: Elizabeth Paik, Emily Huang, Cong Xu. You make going to lab every day such a pleasant experience! All the lunch break chats, weekend companions, out-of-lab fun… I will miss you all! To my other friends who came half way around

the world together, forming a new "family" here, and supporting each other throughout the past six years: Xiaolei Su, Chong Si, Chenjia Xu, Yikai Wang, Tengfei Zheng, Li Ye, Bingxin Lin, Jianing Liu, and Li Jiang. I cannot imagine being abroad without your friendship. To my fellow ChemBioers: Grace Chen, Rachael Wang, Craig Braun, and Louise Slater, for sharing this adventurous experience as the second class of the Chem Bio program.

I am grateful to Jinying Guo, Di Li, and many of my other teachers and mentors in the past 20+ years. Special thanks to the Yuan Pei undergraduate program at Peking University, especially my academic mentor Dr. Tingfang Zhang, for cultivating my interest in biology, and to Dr. Zengyi Chang for letting me have my first research experience in his lab for 2.5 years.

Finally, to my family. Mom and Dad, I cannot ask for better parents. You brought me to this world and became my first teachers. As I get older, I start to understand and appreciate the many decisions and sacrifices you made for me, and how critically they have influenced my life. When I decided to go far away for graduate school, you fully supported it. Thank you for the love and trust you gave me, which made me who I am and always motivates me to reach higher. My dear Victor, meeting you is the best gift ever. Thank you for being patient with my temper and silliness, and understanding and supporting all my decisions. Seeing you childishly enjoying your career as a scientist truly inspires me. Having you standing by me reminds me every day how lucky I am.

To my family,

for the never ending love,

support, and confidence

they have given me

Chapter 1

Introduction

Introduction

Somatic stem cells are specified during embryo development and assume their responsibility of regenerating damaged tissue in adults. Understanding this phenomenon is essential for improving stem cell-based therapy for treating patients with degenerative diseases or acutely damaged tissue. The hematopoietic system is truly the pioneer of stem cell-based therapy. Over the past decades hematopoietic stem cells (HSC) have been widely used for transplantation to treat life-threatening diseases, such as leukemia and bone marrow failure. Despite the successes of transplantation, unpredictable engraftment failure still jeopardizes patients' life. The fascinating nature of HSCs and the clinical needs for more reliable transplantation outcomes motivated me to study what factors regulate the engraftment processes of transplanted HSCs.

Hematopoietic Stem Cells

The hallmark of hematopoietic stem cells (HSCs) is their capability of being transplanted to engraft recipients and giving rise to all blood lineages, including erythroid, myeloid and lymphoid cells. Such bona fide HSCs are specified at an early stage during embryo development, in an evolutionarily conserved tissue, the aorta-gonad-mesonephro (AGM) region (Dzierzak and Speck, 2008). In the human fetus this takes place between day 27 and day 40 (Tavian et al., 2010). In mice, a similar developmental process happens around embryonic day (E) 10.5, when the cells from the embryonic tissue can be transplanted to repopulate adult recipients (Biosset and Robin, 2012). These cells first emerge from endothelial cells and form

hematopoietic clusters along the luminal side of the aortic wall. Later, they bud off the endothelial wall and travel to the fetal liver through circulation. Slightly later, transplantable HSCs are also found in other highly vascularized sites, including the placenta and yolk sac. In these transient hematopoietic tissues, HSCs undergo rapid proliferation. The number of HSCs is dramatically expanded by about 14-fold. After the expansion, HSCs migrate to the bone marrow, and finish this heroic odyssey (Dzierzak & Speck, 2008).

The bone marrow is composed of diverse types of cells, such as endothelial cells, stromal cells, adipocytes, osteoblasts and mature blood cells, which form a regulatory environment called the **niche** (Mercier et al., 2011). Upon receiving extrinsic signals from the niche, and under the control of an intrinsic regulatory network, HSCs make important decisions to either remain as a stem cell through the **self-renewal** mechanism, or **differentiate** into progenitor cells, which further become mature blood cells (Zon, 2010).

In adult humans, the daily demand for HSCs to differentiate into different types of mature blood cells is amazing. For example, an adult has 20-30 trillion red blood cells circulating, which count for about one quarter of the total human body cell number. These cells need to be completely replaced every 100-120 days. An adult also produces about 10^{11} neutrophils per day, most of which circulate in the blood for a mere 6 hours (Abass et al., 2012). Although the astronomical number of mature blood cells primarily arises from the rapid proliferation of lineage-specific **progenitors** or **precursors**, HSCs are the ultimate source of maintaining the appropriate ratio among different types of cells on the hematopoietic hierarchy.

Though under such high demand, this pool of stem cells generated during embryo development still lasts throughout the entire adult life without additional replenishment. How HSCs maintain their long lifetime, compared to differentiated blood cells, is still a mystery.

Hematopoietic Stem Cell Transplantation and Engraftment

Stem cell therapy is considered to be the Holy Grail for curing many types of otherwise incurable diseases. The most successful example is hematopoietic stem cells (HSC). HSCs have been widely used to treat life-threatening diseases, such as leukemia and bone marrow failure. The transplantation procedure is fairly simple. Recipients are previously conditioned with total body irradiation and/or chemotherapy to clear the niche. Purified HSCs or whole bone marrow cells are intravenously transfused. Once injected, the cells can find their way back to the bone marrow (BM), and lodge in the BM medullary cavity in less than 48 hours; this process is referred to as **homing** (Lapidot et al., 2005). HSC homing has not been observed in real time *in vivo* yet, but it is thought that this process shares similarities with neutrophil trans-endothelial migration during inflammatory responses and lymphocytes homing to lymphoid tissues. Existing genetic data support the hypothesis that the homing process involves chemokine attraction, reciprocal HSC-endothelial cell communication, active cell morphology changes and migration (Yang et al., 2001; Lapidot et al., 2005). Once entering the medullary cavity, whether HSCs and multipotent progenitors (MPPs) can be retained in the appropriate marrow space depends on various factors, which are not very well

understood. It is hypothesized that HSCs can also reenter the circulation, which has been observed even under homeostatic states to potentially serve the function of immune surveillance (Mazo et al., 2011). HSCs that successfully lodge into the niche can choose to undergo short-term and/or long-term self-renewal and differentiation; this is called **repopulation** or **engraftment**, and lasts months or years (Figure 1.1). However, some HSCs might also stay quiescent for various periods of time.

Hematopoietic stem cells can be obtained from different sources. The most common sources are either directly from bone marrow or mobilized HSCs from the peripheral blood. These HSCs usually require perfectly matched immune systems between the donor and recipient as characterized by the types of HLA (human leukecyte antigen), which makes the search for the appropriate donor a daunting task (Abass et al., 2012). Recently, HSCs were successfully purified from umbilical cord blood, and proven capable of engrafting recipients. Because of the relative immature features, the cord blood HSCs can be more compatible with recipients' immune system than bone marrow HSCs; therefore, only a partial matched HLA type is needed. Cord blood HSCs have been successfully used for treating children with leukemia. However, the insufficient number of HSCs per cord and delayed engraftment impair the application of cord blood to treating adult patients (Gluckman, 2011). The fascinating phenomena that HSCs can find their way home in the maze of the human body and the clinical demand for improving the engraftment capability of HSCs have attracted major research attention.

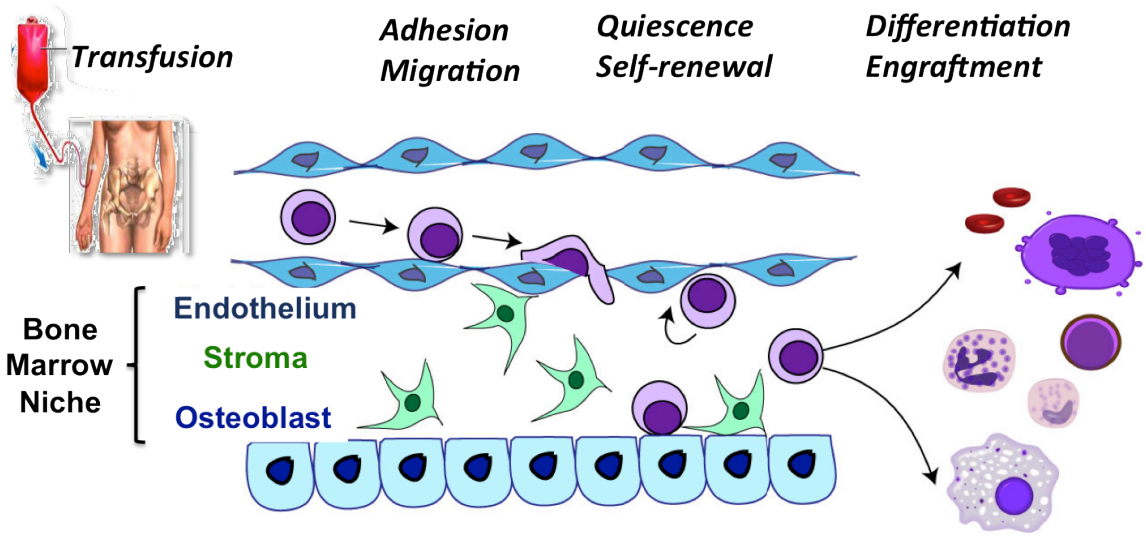

Figure 1.1 Illustration of human HSC transplantation and engraftment

HSCs or bone marrow cells are transfused intravenously. HSCs can then home to and lodge in the marrow niche, which is composed of multiple cell types, such as endothelium, stroma, osteoblasts, and many other cell types. This process involves active adhesion and migration. Once in the niche, HSCs make fate decisions among staying quiescence or entering self-renewal. Eventually, the final engraftment requires the differentiation of HSCs into multiple lineages of mature blood cells.

Regulators of HSC Engraftment

Thus far, the live process of a single HSC homing to and engrafting the bone marrow has not been observed. Many of the major breakthroughs that facilitated the understanding of the engraftment process were made using analogous processes in other cell types, such as lymphocytes and myelomonocytes. First, HSCs need to detect the correct environment to enter. The signaling by stromal-derived factor 1 (SDF-1) guides HSCs, which express the receptor CXCR4 to home to the marrow. The SDF-1/CXCR4 axis was originally discovered to be essential for the

attraction and retention of lymphocytes in the lymphoid organ. Genetic knockout mice also further demonstrated the requirement of this signaling for the trafficking of HSCs from fetal liver to bone marrow during embryo development in mice (Zou et al., 1998). Later on, it was also shown to play an important role in adult HSC homing to the bone marrow (Laird et al., 2008). This discovery led to the application of the opposite process, HSC mobilization. By blocking the SDF-1/CXCR4 signaling, HSCs can be mobilized into peripheral blood, and collected for transplantation (Lapidot et al., 2005). This chemokine guidance is also important for tumor cells to metastasize to a secondary site (Zlotnik et al., 2011). In addition to the SDF-1/CXCR4 signaling, stem cell factor (SCF) and its receptor, c-Kit also plays an important role in HSC homing, as well proliferation and cell-renewal (Kent et al., 2008).

Besides external signaling, homing also requires cell-cell interaction mediated by adhesion molecules. Integrins and very late antigen-4 (VLA-4)/the vascular cell adhesion molecule-1 (VCAM-1) mediate the HSC-endothelial interaction required for entering the marrow (Mazo et al., 1998; Papayannopoulou et al., 1995). These interactions were originally found to be essential for leukocytes slowing down and rolling on the endothelial wall before they undergo extravasation. Intra-cellularly, small GTPases, such as Rac, Cdc42 and Rho, are required to orchestrate the cell movement for efficient homing, retention and localization in the marrow (Cancelas et al., 2005; Gu et al., 2003; Williams et al., 2008; Yang et al., 2001). These small GTPases are the intermediate players in translating extracellular signals from cell membrane to the cytoskeleton, as well as regulating gene transcription in the nuclei. Another signaling component required for marrow engraftment is Gαs (Adams et al,

2009). Gαs mediates the signaling from hundreds of G protein-coupled receptors (GPCR), which are one of the most abundant cell surface receptors. Although many GPCRs utilize the same G trimeric protein complex composed of Gαs, β and γ subunits, how different ligand-receptor interactions lead to different cellular responses is unclear.

Once HSCs enter the bone marrow niche, extrinsic signaling from various niche cells, such as vascular and mesenchymal cells, influence HSC cell fate decisions to maintain quiescence, proliferate or differentiate. Signaling from the niche includes Angiopoietin/Tie2, Notch, etc (Arai et al., 2004; Bigas and Espinosa, 2012). Intrinsically, transcription factors and chromatin modifiers, such as Hox genes and polycomb group proteins mediate transcription repression thereby maintaining the self-renewal capabilities of HSCs. Reciprocally, HSCs might also participate in niche formation, although no published data have formally tested this hypothesis yet (Mercier et al., 2011).

Based on the studies in the past two decades, the complex steps leading to successful engraftment require finely tuned cellular responses. Each step involves a response to diverse external signals in the niche, dramatic cellular changes, and cell-cell interactions (Laird et al., 2008). Although some signaling pathways have been selected for study in the setting of hematopoietic stem cell transplantation, a large-scale forward genetic approach to systematically understand the factors that participate in successful engraftment has not been undertaken. Because of the complexity of the biological processes involved in HSC engraftment, it has to be appropriately studied with an *in vivo* animal model. Mouse models of marrow or

HSC transplantation can usually faithfully recapitulate the human process. However, the mouse is not the best model for large-scale forward genetic screening. Therefore, an animal model suitable for this purpose is greatly needed.

Zebrafish Hematopoiesis Models

Signaling pathways controlling HSCs are largely conserved across vertebrate species. Zebrafish embryonic hematopoiesis greatly resembles mammalian embryonic hematopoiesis. Details about zebrafish hematopoiesis during embryo development have been thoroughly described in several reviews (Davidson and Zon, 2004; Galloway and Zon, 2003). In summary, zebrafish embryonic hematopoiesis happens in two overlapping stages. The primitive wave only gives rise to lineage-committed erythroid and myeloid progenitors, while the definitive wave generates functional HSCs and all lineages found in the adult. The definitive HSCs can be identified by genetic markers, such as *runx1, cmyb,* and *CD41* (Kalev-Zylinska et al., 2002; Ma et al., 2011; Thompson et al., 1998). After being born in the AGM (aorta-gonad-mesonephro) region, HSCs will migrate to the temporary hematopoietic site, the CHT (caudal hematopoietic tissue) in zebrafish (Murayama et al., 2006). Eventually, the HSCs will colonize the kidney marrow, the equivalent of mammalian bone marrow, and become the juvenile and adult hematopoietic tissue.

Hematopoiesis in adult zebrafish is conserved with mammals (Davidson and Zon, 2004; Traver et al., 2003b). Zebrafish kidney marrow can rescue lethally irradiated or mutant zebrafish with hematopoietic defects (Stachura et al., 2011; Traver et al., 2003b; Traver et al., 2004). Flow cytometry analysis shows that

zebrafish WKM have similar forward scatter and side scatter profile to mouse or human bone marrow. Blood smear also confirms similar cellular features within the same type of blood cells between fish and mammals, with the exception of red blood cells, which still retain their nuclei after reaching maturation (Davidson and Zon, 2004; Traver et al., 2003). Transplanting adult zebrafish whole kidney marrow (WKM), which contains all the hematopoietic stem and progenitor cells, into lethally γ-irradiated fish can rescue the recipients with all the blood lineages fully repopulated (Traver et al., 2004). This proves the existence of HSCs in the kidney marrow.

Recently, White et al developed a transparent adult zebrafish, called *casper*, which is doubly mutant for *nacre* and *roy*, two genes essential for pigment cells. Organs such as the heart and blood vessels can be seen using standard stereomicroscopy. Using fluorescent transgenic zebrafish as marrow donors and *casper* as recipients allows for *in vivo* visual assessment of engraftment within the kidney marrow region without sacrificing the recipients (White et al., 2008). However, there can still be large individual variations of engraftment efficiency, which is likely caused by variability in the transplantation procedure due to the small fish body size. Having an internal HSC control population in a competitive transplantation setting can help solve this problem and generate more reproducible results. Despite the caveats, the zebrafish WKM transplantation model is still the most promising *in vivo* model for large-scale genetic or chemical genetic screens looking for regulators of HSC engraftment.

Arachidonic Acid-Derived Eicosanoids

Arachidonic acid (AA) is an important component of the cell lipid bi-layer membrane. It functions both as a structural component and signaling precursor. Upon extracellular stimulation, such as ligand binding to the IFN (Interferon) or 5-HT (5-hydroxytryptamine) receptors, phospholipase A_2 (PLA_2) is activated by phosphorylation and calcium influx. PLA_2 can release AA and/or lysophospholipids by catlytically hydrolyzing the sn-2 acyl bond of phospholipids from the cell membrane (Figure 1.2) (Carroll and McGiff, 2000). Free AA can be metabolized into versatile types of eicosanoids by different families of enzymes. Three major enzymatic pathways are involved in AA metabolism: cyclooxygenase (COX), lipoxygenase (LOX), and cytochrome P450 (CYP) pathways (Figure 1.2) (Carroll and McGiff, 2000). COX is the first enzyme in the metabolic pathway responsible for converting AA into various prostanoids, including prostaglandins, prostacyclin and thromboxane. Two *COX* genes have been identified in the human genome: *COX1* and *COX2*, the expression patterns of which are tissue-specific. LOX enzymes metabolize AA first into hydroperoxyeicosatetraenoic acids, which then can be metabolized into various leukotrienes. The human LOX family that uses AA as the main substrate includes *ALOX5, ALOX12*, and *ALOX15* (Haeggstrom and Funk, 2011).

Compared to the long-standing history of prostaglandins and leukotrienes, the finding that AA can be metabolized by CYP is relatively new. CYP is an enzyme superfamily, comprising hundreds of members, with varying enzymatic catalytic capabilities and substrate specificities. The majority of CYP enzymes are monooxygenase, which adds only one oxygen atom to the existing organic

substrates (Carroll and McGiff, 2000). In contrast, the enzymes involved in prostaglandin and leukotriene synthesis are mostly dioxygenases. Most of the well-studied CYP enzymes are involved in drug degradation or activation. Early studies using kidney tissues showed that AA can be omega-hydroxylated into mono-hydroxyeicosatetraenoic acids (HETE) or epoxydated into epoxyeicosatrienoic acids (EET) (Oliw & Oates, 1981; Oliw et al., 1982; Capdevila et al., 1981b, 1982; Morrison & Pascoe, 1981). These reactions are catalyzed by NADPH-dependent CYP enzymes (Capdevila et al., 1981b). The enzyme converting AA into 20- or 19-HETE turned out to be ω or ω-1 hydrolase (Oliw et al., 1982). The CYP enzymes responsible for synthesizing EETs were found to localize to the microsomal fraction of cells in multiple tissues and cell types. In human, the 2C and 2J subfamily of CYP are the major enzymes generating EETs (Lee et al., 2010). EETs have very short half-lives *in vivo*, and are quickly hydrolyzed into dihydroxyeicosatrienoic acids (DiHET), which are considered much less potent than EETs (Panigrahy et al., 2011b).

Interestingly, in normal rabbit kidney, the renal medulla can efficiently metabolize AA into prostaglandins. In contrast, with very minimal activity of COX, renal cortex predominantly converts AA into HETEs (Morrison et al, 1981). This is a perfect example of how different tissues or cells utilize different eicosanoids to achieve unique biological functions. Besides the tissue-specificity, the utilization of different CYP enzymes also shows species-specificity (Nelson et al., 1996).

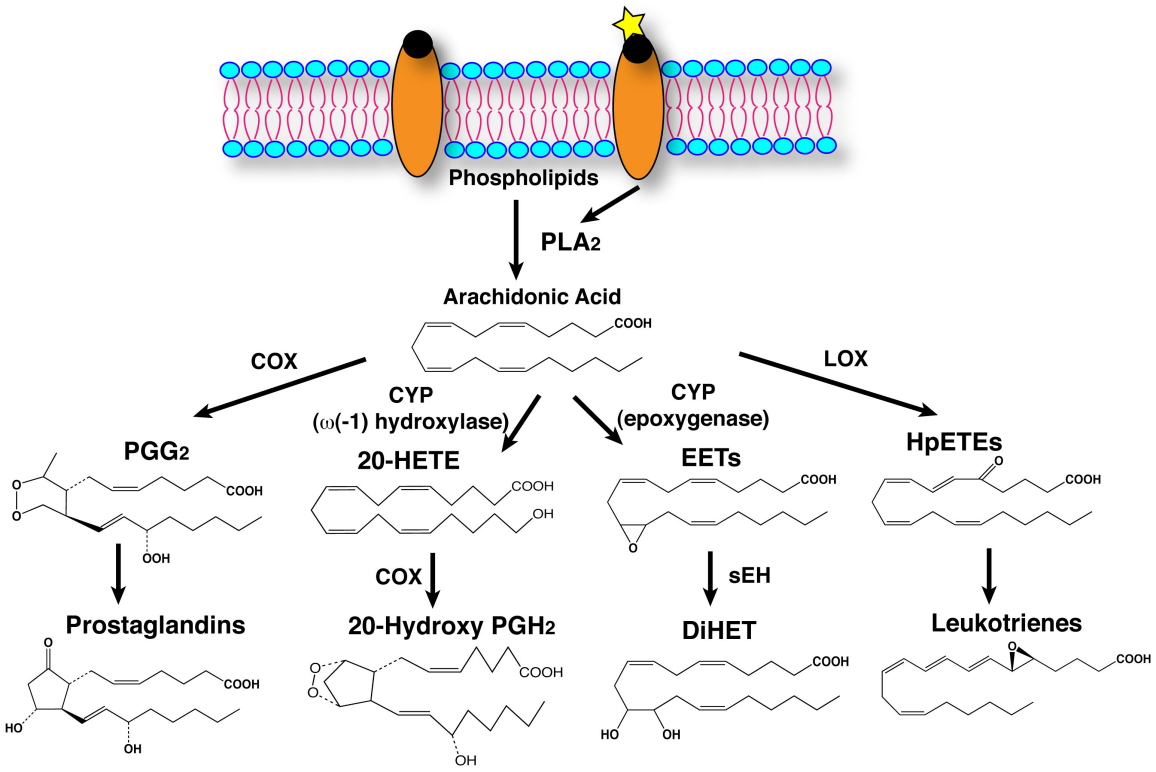

Figure 1.2 Arachidonic acid (AA)-derived eicosanoids

Upon stimulation, AA is released from the cell membrane by phospholipase A_2 (PLA_2), and further metabolized by different enzymes into different eicosanoids. COX: cyclooxygenase; CYP: cytochrome P450 enzyme families; sEH: soluble epoxide hydrolase; LOX: lipoxygenase; PGG_2: prostaglandin G_2; PGH_2: prostaglandin H_2; HETE: hydroxyeicosatetraenoic acid; EET: epoxyeicosatrienoic acid; DiHET: di-hydroxyeicosatrienoic acid; HpETE: hydroperoxyeicosatetraenoic acid.

Eicosanoids and Hematopoiesis

AA-derived eicosanoids play an important role in various physiological situations, especially in inflammatory and immune response. Therefore, most of the studies have centered on understanding how eicosanoids modulate the specialized cell functions of differentiated mature blood cells, such as macrophage migration

and platelet aggregation. In addition, a second major focus has been on how eicosanoids regulate the differentiation of hematopoietic progenitors (Vore et al., 1989). Studies of hematopoietic differentiation have utilized both primary hematopoietic progenitor cells and human leukemic cell culture. Usually during myeloid differentiation, with enhanced oxidative metabolic activity, AA metabolic enzymes are upregulated, which leads to the increased level of multiple eicosanoids. In cultured cells, exogenously added eicosanoids can either promote or block differentiation of myeloid or erythroid progenitor cells at various differentiation stages (Figure 1.3) (Ziboh et al., 1986). Similarly, chemically blocking certain metabolic enzymes can also block the terminal differentiation of progenitor cells (Visnjic et al., 1997). Although cytochrome P450-dependent eicosanoids are relatively young members of the family, their physiological effects are closely associated with hematopoiesis. It was originally reported that human peripheral blood neutrophils and bone marrow cells can convert AA into 19- and 20-HETE, in a cytochrome P450 and NADPH-dependent manner. These metabolites have potent CFU-E (colony forming unit erythroid) promoting activity on bone marrow cells within a nanomolar concentration range (Lutton et al., 1989).

Eicosanoids regulate hematopoiesis at several different levels of cell biology. Beside differentiation, prostaglandins and leukotrienes also regulate stem and progenitor cell proliferation and survival vs. apoptosis (Rizzo, 2002). In addition, it has been reported that bone marrow niche cells are also influenced by eicosanoids. Several growth factors, such as GM-CSF, TNF-α and IL-1, can stimulate bone marrow stromal cells to release AA, which can be further metabolized into various

eicosanoids (Geijsen et al., 2000; Rizzo et al., 1994). This might serve as one of the many mechanisms for niche cells to regulate hematopoiesis, or *vice versa*. However, thus far, studies on the role of eicosanoids on hematopoietic niche cells are very limited. This is a promising field to explore in the future.

Eicosanoids and Stem Cells

Besides affecting more differentiated progenitors, several studies have begun to elucidate the important role of eicosanoids on the stem cell population. Recently, our lab discovered Prostaglandin E_2 (PGE_2) could increase the HSC production in a chemical screen using the zebrafish embryo hematopoiesis model (North et al., 2007). Interesting, PGE_2 can also enhance adult bone marrow transplantation in mice. Currently, a degradation-resistant derivative of PGE_2, 16,16-dimethyl prostaglandin E_2 ($dmPGE_2$) is under clinical trials to test its efficacy in human umbilical cord HSC transplantation (unpublished data). It is thought that $dmPGE_2$ achieves such biological function through elevating the intracellular cAMP level, which in turn enhances β-catenin nuclear translocation by inhibiting GSK-3 kinase (North et al, 2010). This mechanism might explain the increase of HSC production during embryogenesis, since Wnt/β-catenin pathway is known to be essential for HSC specification in the AGM (Clements et al., 2011; Lengerke et al., 2008). However, the importance of Wnt in adult HSCs is quite controversial. Therefore, how $dmPGE_2$ enhances marrow engraftment and which cell population it directly acts on are less clear. Another group has shown pulse treatment with $dmPGE_2$ enhances HSC homing efficiency by two-fold via increasing the CXCR4 protein level on the cell

surface (Hoggatt et al., 2009). Other factors might also contribute to the total four-fold increase of competitive repopulating units by dmPGE_2 (Goessling et al., 2009; Hoggatt et al., 2009; North et al., 2007).

LOX enzymes are also required for normal HSC functions. It has been reported that *12/15-LOX*-deficient HSCs are severely compromised in their reconstitution capability as measured by competitive and serial transplantation assays (Kindler et al., 2010). The study also showed that the defects were mainly due to the loss of quiescence of long-term HSCs. Similarly, both prostaglandins and leukotrienes are also required for leukemia stem cells (LSC) to promote leukemia development. Loss of the *5-Lox* gene in mice impairs BCR-ABL-induced chronic myeloid leukemia (CML) (Chen et al., 2009). In another study using an *MLL-AF9*-induced mouse myelogenous leukemia (AML) model, expression of *Cox-1* and prostaglandin E receptor 1 (*Ptger1*) were upregulated in the leukemia stem cell population. Treating the mice with COX inhibitor, Indomethacin, dramatically reduced the LSC frequency (Wang et al., 2010).

The exploration of the role of eicosanoids on stem cells has just started. Although *LOX*-deficiency studies indicated the importance of leukotrienes in HSCs, the specific leukotriene(s) matching this role still need to be identified. Similarly, besides PGE_2, it is unclear if other prostaglandins also affect HSCs. Finally, the CYP-derived eicosanoids have not been studied in the context of HSCs. This aspect will be covered in this thesis.

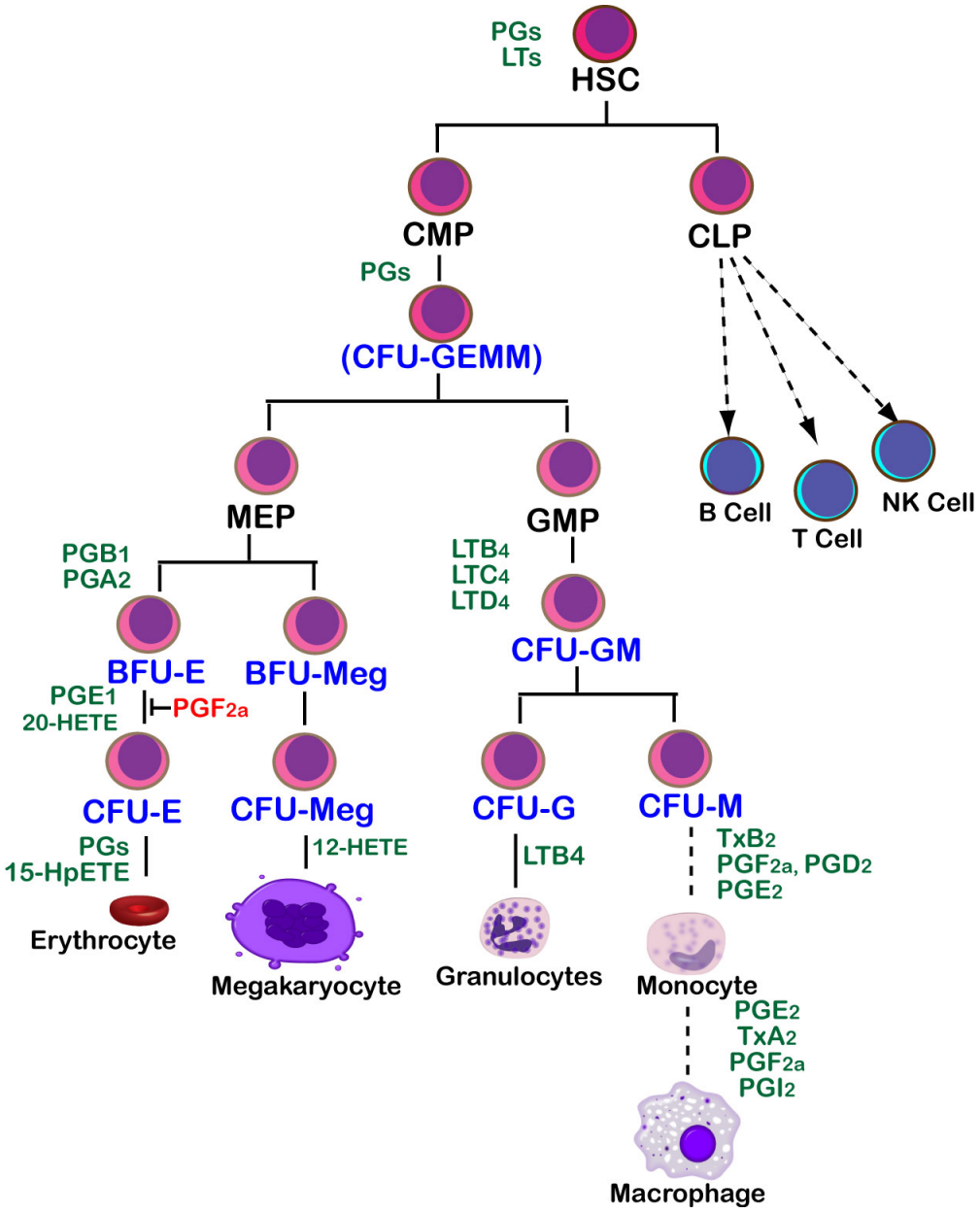

Figure 1.3 Arachidonic acid-derived eicosanoids regulate hematopoiesis

AA-derived eicosanoids have pleiotropic effects on normal hematopoiesis, from terminal differentiation to progenitor proliferation. Green labels represent positive effects, while red represents negative effects. PGs: prostaglandins in general; LTs: leukotrienes in general; Tx: thromboxane; CFU: colony forming unit; E, erythrocyte; Meg: megakaryocyte; G, granulocyte; M: monocyte; CMP: common myeloid progenitor; CLP: common lymphoid progenitor; MEP: megakaryocyte-erythroid progenitor; GMP: granulocyte-monocyte progenitor.

Summary of the Thesis

Understanding how HSCs achieve engraftment is important both as a basic biological question and for clinical application of stem cell therapy. In the following chapters of this thesis, I will describe the development of a competitive marrow transplantation assay in adult zebrafish, which allows quick visualization and quantification of the marrow engraftment capabilities *in vivo*. Using this assay, the first transplantation-based chemical screen was performed with a known-bioactive chemical library. The screen led to the discovery of ten chemicals involved in several novel pathways, which can enhance marrow engraftment. One example is a group of arachidonic acid-derived eicosanoids, epoxyeicosatrienoic acids (EETs). Evolutionarily conserved EETs can also promote both short-term and long-term marrow engraftment in mice. Using genetic knockdown and chemical suppressor screening in zebrafish embryos, we found that EET acts through a Gα12/13-mediated receptor, which activates PI3K and induces transcription factors of the AP-1 family. This PI3K/AP-1 pathway directly regulates the transcription of an HSC marker, *runx1,* in zebrafish embryos. Further study on the EET/PI3K pathway shows that PI3K activation is required for promoting HSPC migration and interactions with niche cells, and therefore engraftment.

In addition to the blood phenotype, EET also caused cell morphological and gene expression changes in the developing tail bud of zebrafish embryos. This tissue also utilizes the PI3K/AP-1 signaling/transcription cascade to induce ectopic *runx1* expression in the mesenchymal-like cells. Suppressor screening also identified an additional signaling and transcription regulatory network, which

shares some similarities with epithelial mesenchymal transition (EMT). This non-hematopoietic study might help to explain the previously reported observation that EETs can promote tumor metastasis and angiogenesis (Panigrahy et al., 2011b).

In summary, our studies define a role for EETs in the engraftment of HSCs in adult vertebrates, and HSC development during embryogenesis. The chemical screen also identified additional pathways important for regulating HSC engraftment. These discoveries may have clinical application in marrow or cord blood transplantation, as well as elucidate some basic regulatory mechanisms of stem cell engraftment. The success of the transplantation-based chemical screen might encourage the use of chemical genetic screening approaches to study complicated biological processes *in vivo*.

Chapter 2

Zebrafish Competitive HSPC Engraftment Model and Transplantation-Based Chemical Screen

Pulin Li[1,2], Emily K. Pugach[1], Richard M. White[1], Thorsten M. Schlaeger[1], and Leonard I. Zon[1,2,]*

[1] Stem Cell Program and Division of Hematology/Oncology, Children's Hospital Boston and Dana-Farber Cancer Institute, Howard Hughes Medical Institute, Harvard Stem Cell Institute, Harvard Medical School and, Boston, MA 02115, [2] Chemical Biology Program, Harvard University, Cambridge, MA 02138.

* To whom correspondence should be addressed
Address: 300 Longwood Avenue, Boston, MA 02115
Email: zon@enders.tch.harvard.edu

Attributions

The idea of developing a zebrafish competitive marrow transplantation was conceived by L. I. Zon and me. I undertook the experiments to create and optimize the competitive transplantation assay, and performed the pilot chemical tests with the assay. R. M. White invented the retro-orbital injection and I further refined the method. I designed, optimized, and performed the 480-bioactive chemical screen, with technical assistance from E. K. Pugach on the execution of the screen. T. M. Schleager and the CHB hESC core provided the chemical library, with the technical assistance from S. Datta and P. Manos. C. Mosimann developed the *ubi* transgenic zebrafish. I performed all of the chemical treatment in zebrafish embryos, did all the data analysis and literature research on the screen hits.

Introduction

The signature characteristic of adult stem cells is the capability to regenerate damaged tissue while maintaining their identity. The best understood example is hematopoietic stem cells (HSC), which are a rare cell population that gives rise to all the blood cells in the body. HSCs have been widely used to treat life-threatening diseases, such as leukemia and bone marrow failure. During transplantation, HSCs are intravenously transfused into patients previously conditioned with total body irradiation and/or chemotherapy to clear the niche. They travel in the circulation, home to the bone marrow, lodge into their niche, undergo proliferation and differentiation, and repopulate the blood system of the recipient. This process is termed engraftment (Laird et al., 2008). Clinical protocols have been well worked out for transplantation in humans, but unpredictable engraftment failure still jeopardizes the lives of patients.

In order to minimize engraftment failure, a better understanding of how HSCs achieve engraftment is essential. To tackle this question, animal models that can recapitulate the biology of human HSC transplantation are needed. The mouse system has been extensively used for competitive transplantation. Briefly, two alleles differing at the CD45 locus are used to distinguish among the two donors and the recipient. This proves to be the most quantitative method to determine whether a genetic mutation affects stem cell engraftment capability. However, because of the high cost and long latency, the mouse model has been mostly used to test a single hypothesis, such as the relative contribution of mutant to normal HSCs. In order to categorize pathways in relation to transplant engraftment in a more systematic way

and discover novel pathways, chemical or genetic screens are required. In order to achieve this goal, a higher-throughput and cost-effective assay needs to be developed.

The vertebrate model organism, *Danio rerio* (zebrafish), suits this purpose very well. Hematopoiesis in adult zebrafish is conserved with mammals (Davidson and Zon, 2004; Traver et al., 2003b). Zebrafish kidney marrow, the equivalent of mammalian bone marrow, can rescue lethally irradiated or mutant zebrafish with hematopoietic defects (Stachura et al., 2011; Traver et al., 2003b; Traver et al., 2004). In the latest rendition of transplant experiments, we utilized a *Tg(β-actin: GFP)* fish as donor. The wild-type recipient fish are irradiated at a sublethal dose of 25 Gy and are injected intra-cardiacally with the GFP expressing marrow. From 4 weeks to 3 months, GFP expression can be analyzed in the recipient animal by flow cytometry. At 4 weeks, significant reconstitution of the myeloid compartment is evident. Because myeloid cells have a short half-life, this gate gives the best estimate of engraftment in each animal. More recently, our lab has pioneered the use of *casper*, an adult zebrafish that is completely transparent. GFP+ kidney marrow engrafted in *casper* can be directly visualized over a 4 week period of time (White et al., 2008). However, due to the variability of the transplantation technique, it has been difficult to directly compare the engraftment capability of donor marrow cells in a precise way.

Driven by the needs of evaluating genetic and chemical effects on HSPCs in zebrafish, we took advantage of *casper* and developed a live imaging-based competitive transplantation system that enables a quick and quantitative evaluation

of the marrow engraftment capability. Pilot tests with chemicals targeting various important signaling pathways were performed to optimize the assay and chemical treatment conditions. The feasibility of testing hundreds of zebrafish per day with this assay allowed us to perform a chemical screen to identify compounds regulating engraftment. A chemical library of 480 chemicals of known bioactivities was screened using this competitive transplantation assay. After the primary screen and secondary round of confirmation, we found 10 compounds capable of significantly increasing marrow engraftment through blind scoring.

In conclusion, *in vivo* chemical screening using zebrafish competitive marrow transplantation provides a successful example of phenotypic screening in whole adult vertebrates. The discovery of novel repopulation modulators should provide a better understanding of signaling events that regulate homing and self-renewal, and may have clinical application in marrow or cord blood transplantation.

Results

In order to develop a competitive transplantation assay suitable for unbiased screening experiments, we evaluated the most recent advancement of transplantation techniques in zebrafish and further optimized several conditions, leading to the development of the imaging-based competitive marrow transplantation assay in zebrafish.

Optimizing the Myeloablative Conditions

Hematopoietic stem cells (HSC) reside in the marrow space surrounded by different cells that constitute a microenvironment called the niche. It has been postulated and indirectly proven that there are only a limited number of niches where HSCs can enter (Micklem et al., 1968). When the endogenous HSCs occupy the niche, transplanted HSCs have to compete with the endogenous cells for the limited space. In addition, the endogenous immune system forms a natural defensive barrier for exogenous cells to engraft. Therefore, to clear the endogenous niches and minimize the resistance from the endogenous immune system, myeloablative methods have been adapted both clinically in human patients and in animal models. Irradiation and/or chemotherapy are the most commonly used methods to pre-condition marrow transplantation recipients. Neutralizing antibodies against c-Kit have also been used to loosen up the interaction between the niche and the endogenous HSCs in immune-deficient mice (Czechowicz et al., 2007). Because of the lack of a zebrafish c-kit antibody and the potential high variability of injecting chemotherapy chemicals, a single dose of 25Gy radioactive

irradiation has been the pre-dominant method for pre-conditioning the wild-type zebrafish recipients. However, the 25Gy single irradiation is not an optimal condition, because it does not completely ablate the endogenous HSPCs and also causes high toxicity to the digestive system. We have also observed that irradiated recipients were often malnourished due to damage in the gut. Therefore, the effects of different irradiation regimens on the survival of *casper* zebrafish was tested. Splitting the 30Gy irradiation dose into equally divided double doses separated by 24 hrs (hours), or 40Gy equally into triple doses, dramatically increased the survival of irradiated zebrafish (Figure 2.1A). With the improved survival rate, one can increase the total dose of irradiation, and presumably ablate the endogenous hematopoietic system more efficiently. To test if this is true, 100,000 *Tg(β-actin:GFP)* WKM cells were transplanted into differently irradiated recipients. The engrafted recipients were imaged with a fluorescent microscope, and the GFP fluorescence intensity was measured within the kidney region. Animals receiving a 30Gy double-split dose or 40Gy triple-split dose both had increased survival and engraftment by 4 wpt (week post transplant) (Figure 2.1B). In order to maximize both the survival and the effectiveness of myelo-ablation, a double-split dose of 30Gy was chosen for future experiments.

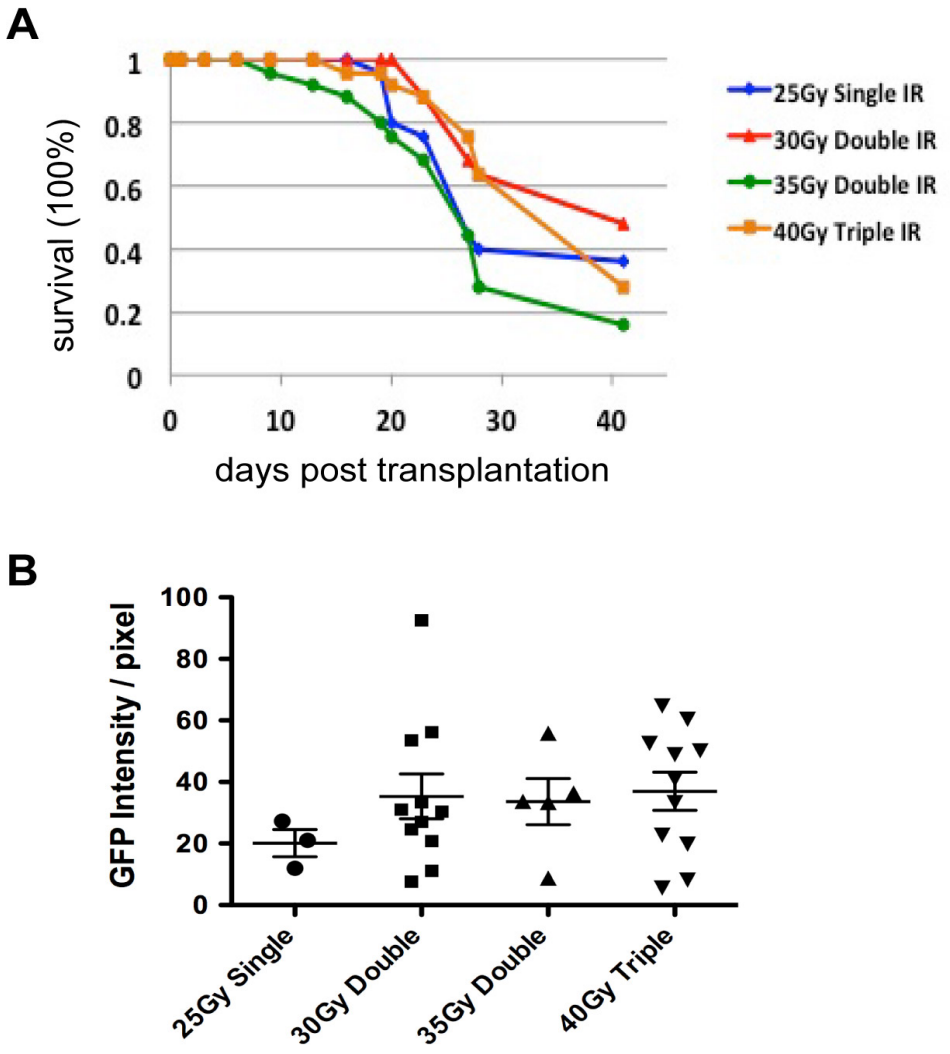

Figure 2.1 Optimizing the Myeloablative Conditions

(A) The survival curve of *casper* after various doses and conditions of irradiation. IR, irradiation. Single: single dose; Double: double-split dose; Triple: triple-split dose.
(B) The engraftment of 100,000 *Tg(β-actin:GFP)* WKM cells in *casper* receiving various doses of irradiation. The engraftment was quantified by the GFP fluorescence intensity in the kidney region.

Optimize the Injection Technique

Traditionally, chemicals or cells are infused into the blood circulation of adult zebrafish via intra-cardiac injection. Although, zebrafish have much stronger repair and regeneration capability after cardiac injury compared to human or mouse, this method still causes very high procedure-associated mortality. R. M. White introduced the new retro-orbital injection, inspired by the practice in mouse transplantation. Cells or chemicals can be injected into the sinus venous behind the eye (Figure 2.2A, B). To test how fast the injected substances get into circulation, we injected Dextran-conjugated TexasRed dyes with a molecular weight of 70,000 or 3,000. Within 15min after injection, the dye distributed in the circulation system of the whole fish, including the tail fin, the most distal tissue (Figure 2.2C, D). The 70,000 dye stays in the vascular system with minimal diffusion for the first 15mins, while the 3,000 dye can permeabilize the endothelial wall and diffuse into the surrounding tissue (data not shown). The kinetics of injected cells getting into circulation may differ from those of the chemical dye. Therefore, we injected red blood cells harvested from *Tg(lcr:GFP)* zebrafish into *casper*. GFP+ cells were seen in the circulation within 2 hrs after injection (Figure 2.2E). In order to observe the GFP+ cells in circulation immediately, a relatively large number of red blood cells (greater than 500,000) need to be injected due to the quick dilution by the endogenous GFP- cells.

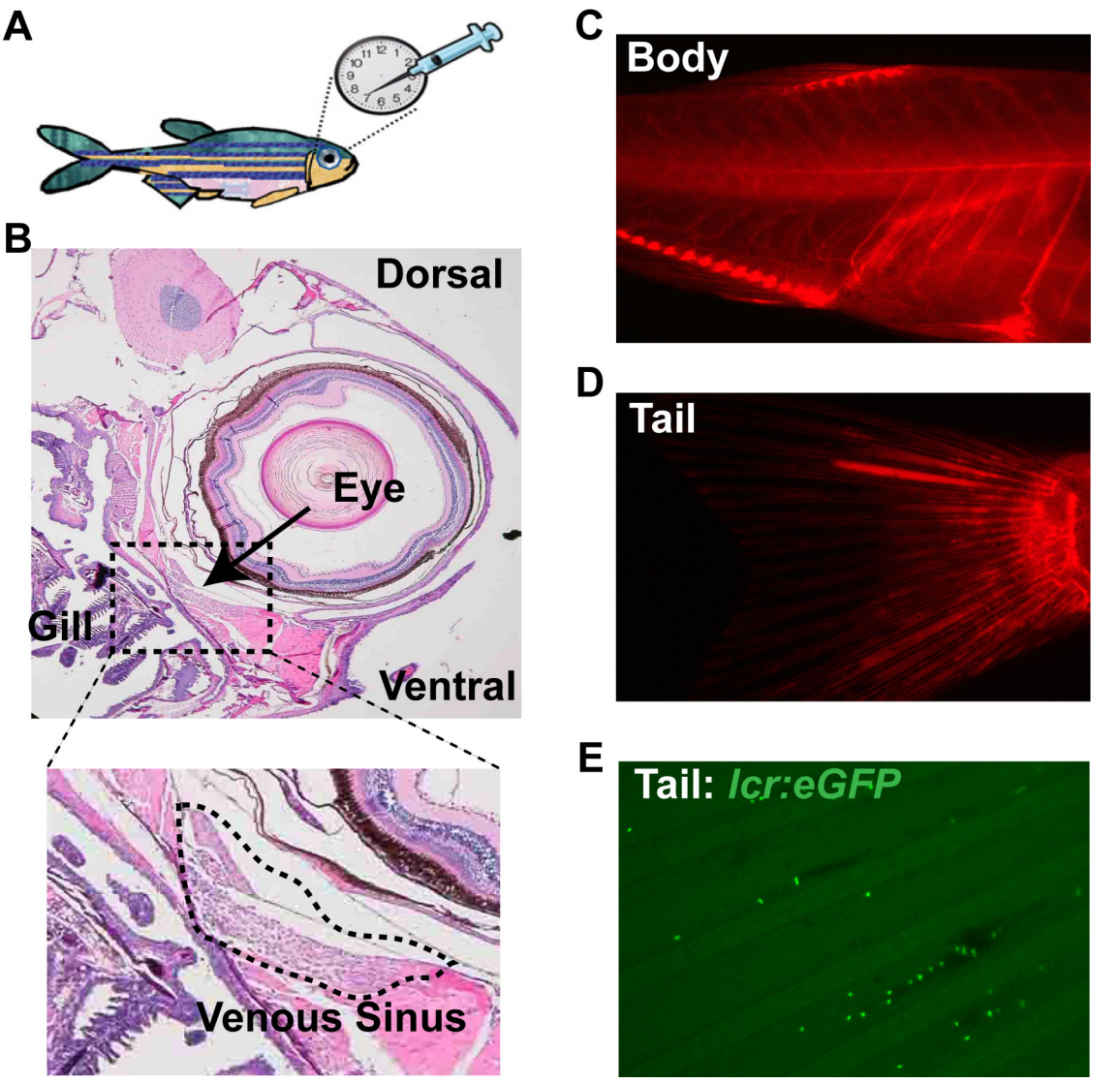

Figure 2.2 Retro-orbital injection in adult zebrafish

(A) Illustration of the location of retro-orbital injection. The needle aims at the spot on the eye equivalent to seven O'clock on a clock.
(B) Anatomy of the zebrafish eye region. The dashed box (top) represents the region where the needle (the black arrow) enters. Upon correct injection, the cells enter the venous sinus (bottom).
(C-D) 15min after retro-orbital injection with 70,000 Dextran-TexasRed dye. The dye enters the circulation and is distributed throughout the whole body (C) and the tail fin (D).
(E) 2hrs after retro-orbital injection with 500,000 *Tg(lcr:GFP)* red blood cells. GFP+ cells circulate in the recipient's peripheral blood.

Comparison of the Engraftment Capabilities of Different Transgenic Strains

Using *casper* as the WKM transplantation recipient allows for *in vivo* visual assessment of homing and engraftment. However, due to the variation among recipients and the subtle differences of injection techniques, it is difficult to quantify the engraftment with a single marrow transplantation. The solution is to have an internal control. We designed a double-color labeled competitive transplantation assay, in which donor marrows labeled with two different colors are transplanted into the same recipient. While one of the two donor populations stays consistent, the other donor population can be chemically or genetically manipulated. This way, the effect of the chemical or genetic changes on marrow engraftment can be standardized based on the engraftment of unmanipulated marrow population.

In order to develop such a competitive transplantation assay, two transgenic zebrafish strains labeled with different fluorescence proteins are needed as donors, such as GFP and DsRed. Ideally, to make the quantification of engraftment from the two donors comparable, the promoters driving GFP and DsRed expression should be the same. For example, *Tg(lyz:GFP)* and *Tg(lyz:DsRed)* both label macrophages (Figure 2.3) (Hall et al., 2007), while *Tg(gata1:GFP)* and *Tg(gata1:DsRed)* both label erythroid progenitors and some mature red blood cells in adult zebrafish (Long et al., 1997). These transgenic lines only label a very specific subset of blood cells. Therefore, they are not appropriate for evaluating the engraftment capability of the WKM population, although they are well suited for studying specific progenitor/precursor populations.

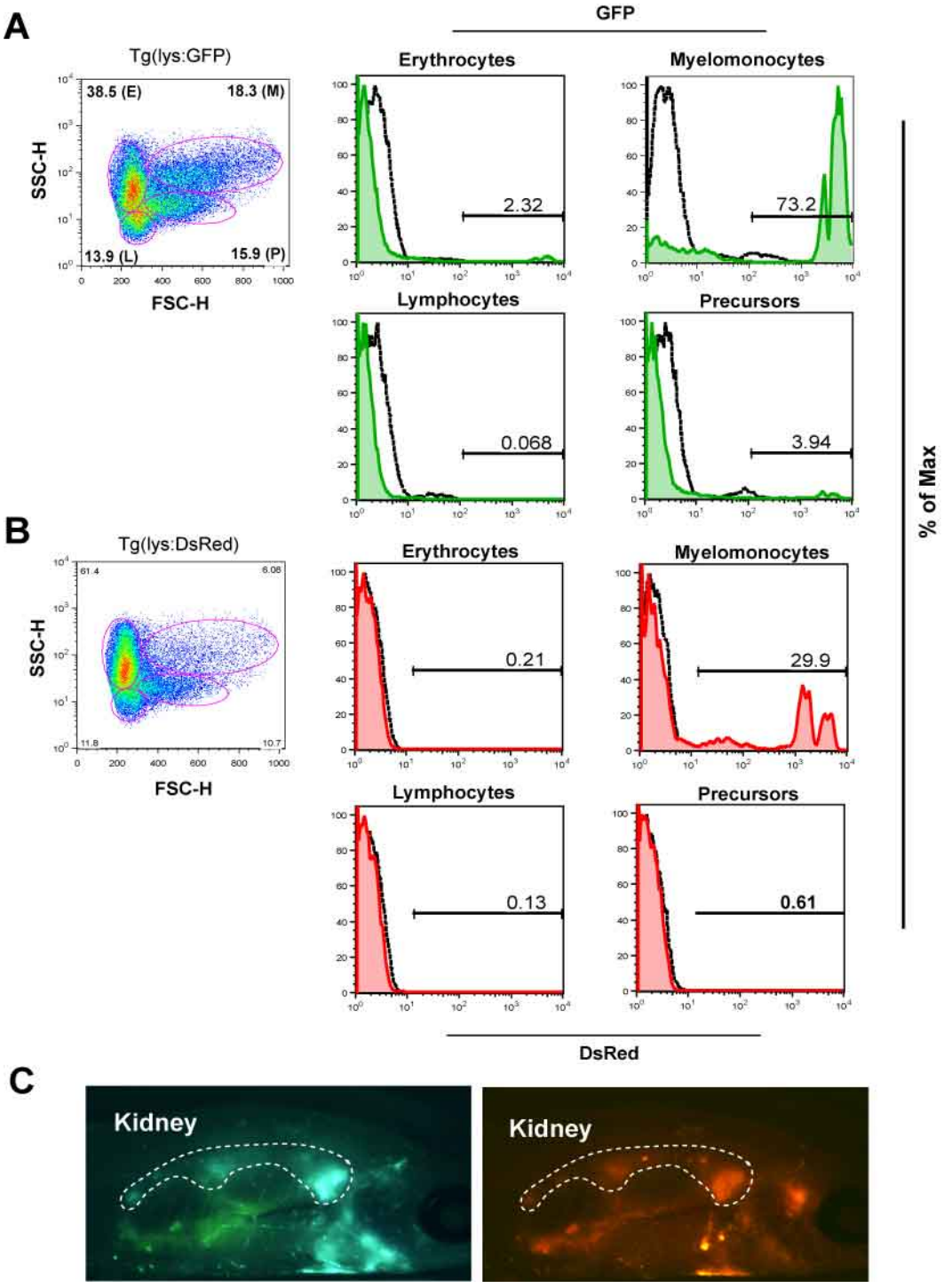

Figure 2.3 Transgenic zebrafish labeling myeloid cells

(A) and (B) WKM FACS analysis of *Tg(lyz:GFP)* and *Tg(lyz:DsRed)*
(C) Fluorescence microscopy of kidney of *casper* following competitive WKM transplantation of 100,000 *Tg(lyz:GFP)* and 100,000 *Tg(lyz:DsRed)*, 2wpt.

The most widely used ubiquitous transgenic zebrafish is *Tg(β-actin:GFP)* (Traver et al., 2003b). GFP is driven by the zebrafish ubiquitous promoter *β-actin*, and labels the majority of the white blood cell and progenitor populations in the kidney marrow (Figure 2.4A). Due to the lack of a *Tg(β-actin:DsRed)* line, a commercially available transgenic zebrafish, Red Glofish® was used as the red donor. Red Glofish® is a double transgenic fish with *β-actin:DsRed2* and *mlc:DsRed* (Blake, 2010). There are a series of Glofish® expressing different fluorescence proteins under the control of the same promoters, including a green line zsGreen. The majority of the kidney marrow cells in both the Red and Green Glofish® are labeled with fluorescent proteins (Figure 2.4B). The Red Glofish® WKM was also able to engraft recipient fish (figure 2.4C); however, when the zsGreen WKM was transplanted at various cell doses or with different injection methods, the recipients were never showed any GFP+ cells (data not shown). We speculated that this could be due to silencing of the transgene, which is associated with multiple copies of short transgenes in tandem and might also reflect the position effect of the specific transgene insertion location (Garrick et al., 1998). However, we never officially tested the hypothesis. Eventually, the *Tg(β-actin:GFP)* and Red Glofish® were chosen as the donors for the competitive transplantation assay.

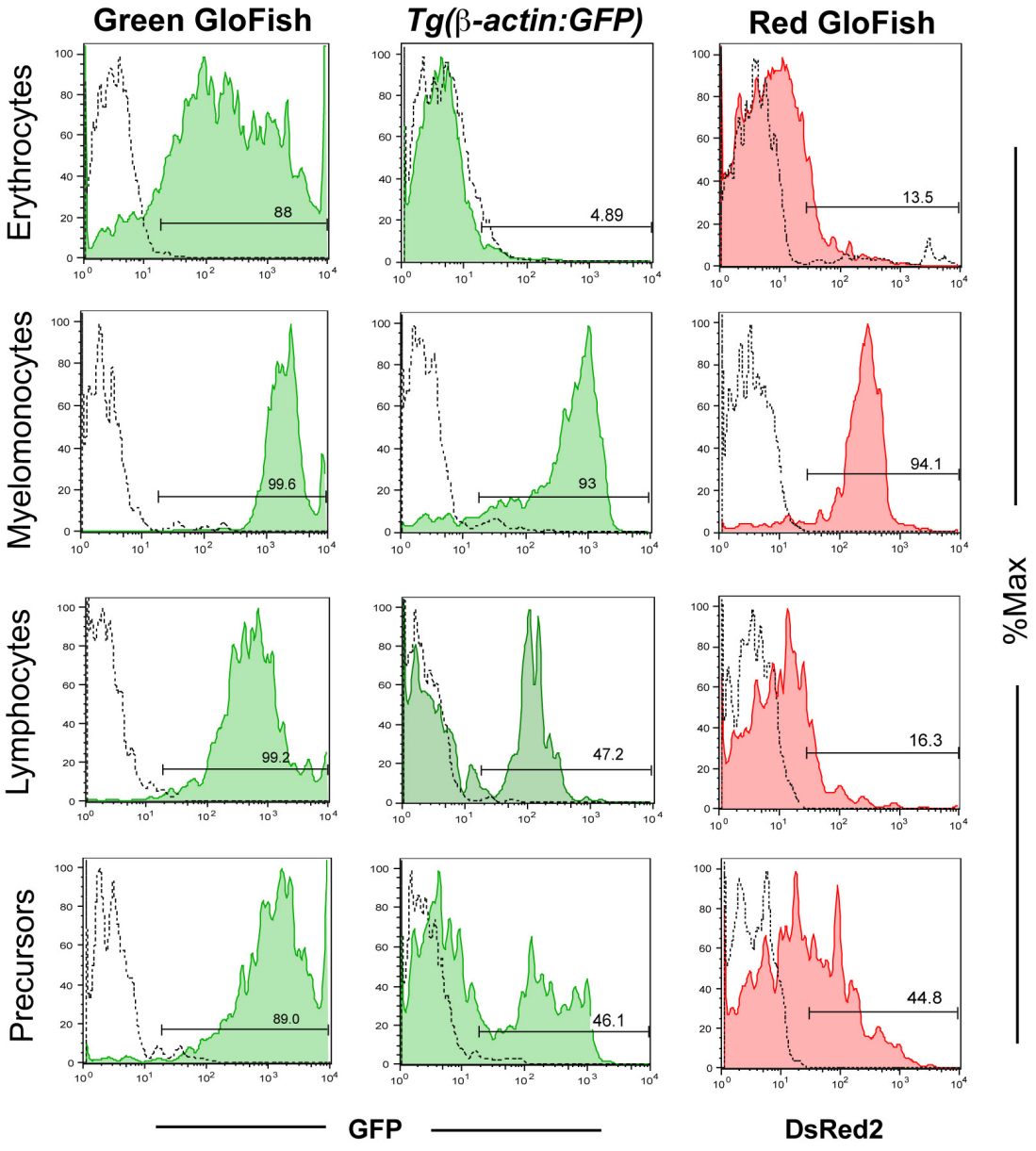

Figure 2.4 FACS analysis of ubiquitous transgenic zebrafish strains

Dashed black line represents the negative control. The blood lineages are gated based on the forward scatter and side scatter of the whole kidney marrow (Traver et al., 2003).

A Zebrafish Marrow Competitive Transplantation Assay Allows Direct Visualization and Quantification of Engraftment *in vivo*

With the optimized conditions, we standardized the zebrafish competitive marrow transplantation assay. Whole kidney marrow (WKM) cells were harvested from two transgenic donors, *Tg(β-actin:GFP)* and RedGlo® fish (Figure 2.5A). The two marrow populations were co-injected retro-orbitally into sublethally irradiated *casper* zebrafish. Donor-derived fluorescent cells can be directly visualized with a fluorescent stereoscope (Figure 2.5B). The average GFP or DsRed2 fluorescence intensities were measured within the same region using ImageJ. After subtracting the background fluorescence intensity, the relative engraftment was calculated by $G/R=(G_{kidney}-G_{background})/(R_{kidney}-R_{background})$. Taking this non-invasive live imaging approach, the same recipients can be repeatedly imaged over time to monitor the engraftment kinetics, even up to 3 months. Engraftment was evident in the recipient kidney as early as 2 weeks post transplant (wpt). By 4 wpt, with further proliferation and differentiation, donor-derived mature hematopoietic cells can be observed in recipients' circulation as well as in epidermis as tissue residential macrophages. At 8 wpt, donor-derived lymphoid cells also repopulate the recipient immune system. In these transplants, the long-term survival of recipients is compromised due to multiple reasons, including immune rejection, which can greatly benefit from MHC matching (de Jong et al., 2011). This perspective will be discussed in more details in Chapter 4. In all the later experiments, we have been assessing engraftment 4 wpt, mainly examining the progenitor repopulation capability.

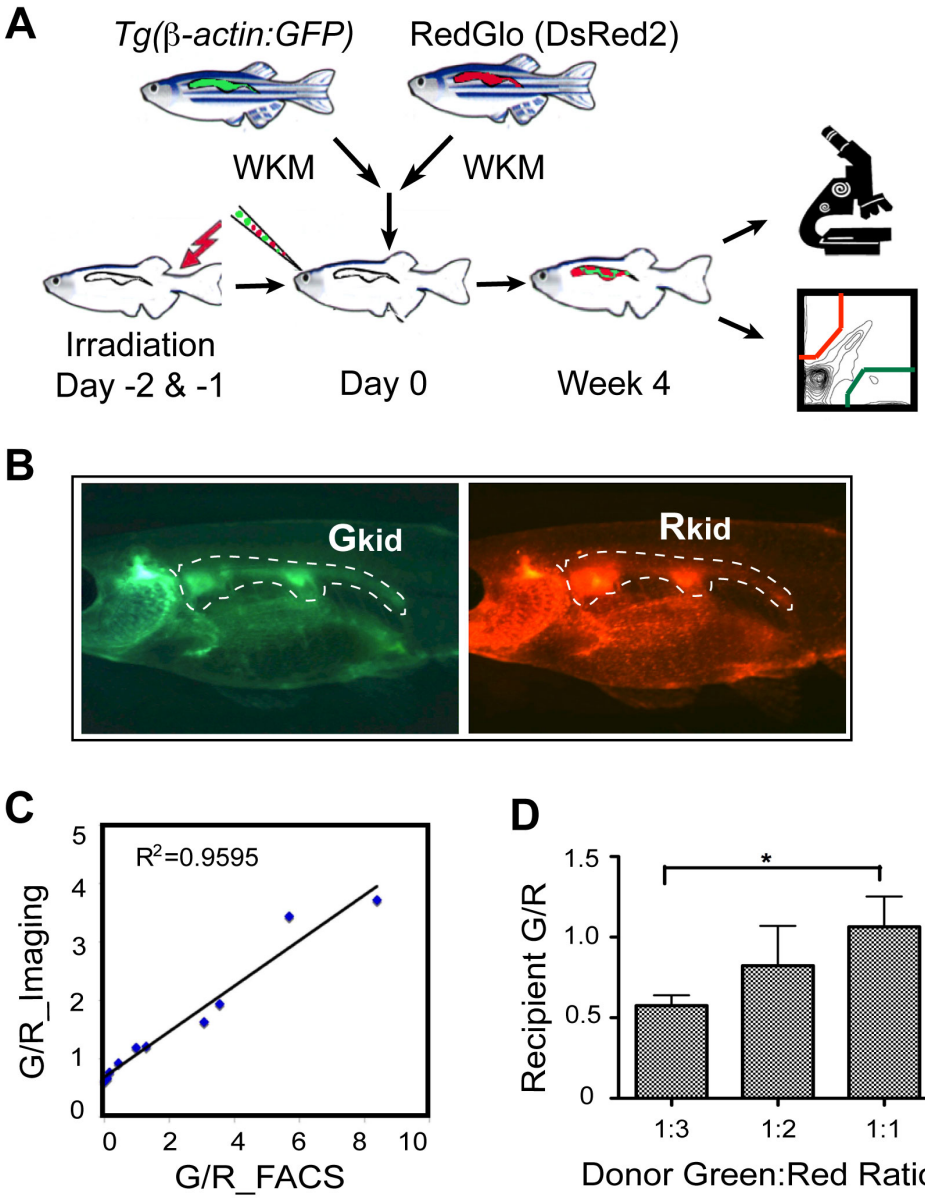

Figure 2.5 Zebrafish whole kidney marrow (WKM) competitive transplantation assay

(A) Schematic of zebrafish WKM competitive transplantation in adult zebrafish. wpt, week post transplant.
(B) Representative images of recipients co-engrafted with GFP and DsRed2 donor marrows. G_{kid}, kidney GFP intensity; R_{kid}, kidney DsRed2 intensity.
(C) The linear correlation of the relative engraftment results from FACS analysis and imaging analysis.
(D) Limiting dilution competitive transplant in zebrafish. A total number of 100,000 donor cells were transplanted. * Student's t test p values < 0.05.

To evaluate the accuracy of the imaging-based analysis of marrow engraftment, recipients were dissected after imaging, and their WKM were subjected to FACS (fluorescence-activated cell sorting). The ratio between the percentages of GFP+ and DsRed2+ cells was compared to the G/R ratio of the same recipient based on imaging. The two results were linearly correlated (R^2=0.9595), validating the quantitative success of this imaging-based approach (Figure 2.5C). In order to apply this novel competitive transplantation system to the study of HSPC engraftment process, the sensitivity of the assay was assessed. The donor marrow cells at green-to-red ratios of 1:3, 1:2, and 1:1 were transplanted with a total number of transplanted cells at 200,000. An increase of average G/R fluorescence intensity was observed accompanying the increasing donor green-to-red ratio (Figure 2.5D). Within the donor cell dose and ratio range assayed above, the zebrafish competitive marrow transplantation system can detect the change of relative engraftment capability in the donor cell populations.

Adult Zebrafish Competitive Marrow Transplantation Can Detect Chemical Effects on Marrow Engraftment

To test if the zebrafish competitive transplantation system is suitable for chemical screening, green marrow cells were treated *ex vivo* with chemicals known to enhance HSPC engraftment. dmPGE_2 (16, 16-dimethyl-prostaglandin E_2) is a stabilized derivative of PGE_2, which binds to the E prostanoid (EP) receptor (North et al., 2007). BIO activates the Wnt pathway by inhibiting GSK-3β (Goessling et al,, 2009). The chemicals were incubated with the green marrow cells for 4 hrs at room

temperature and washed off. The green marrow cells were mixed with untreated red marrow and transplanted together (20,000 GFP WKM vs. 80,000 DsRed2 WKM). Similar to the observation in mice, $dmPGE_2$ and BIO both enhanced zebrafish WKM engraftment capability at 4 wpt (Figure 2.6). Next, the colors of competitor and test donors were switched, and the increase of engraftment efficiency by $dmPGE_2$ treatment of the test donor was still evident (data not shown).

Additional chemicals targeting other well-conserved signaling pathways were also tested using this assay in order to assess the throughput of the assay. These chemicals also showed various effects on engraftment, although the definitive roles of the chemicals need to be further confirmed (data not shown). In conclusion, direct visualization of competitive marrow repopulation greatly facilitates the developmental, physiological or pathological study of HSCs and progenitors by providing a novel platform for the assay of specific genes or chemicals that could alter homing, engraftment or self-renewal.

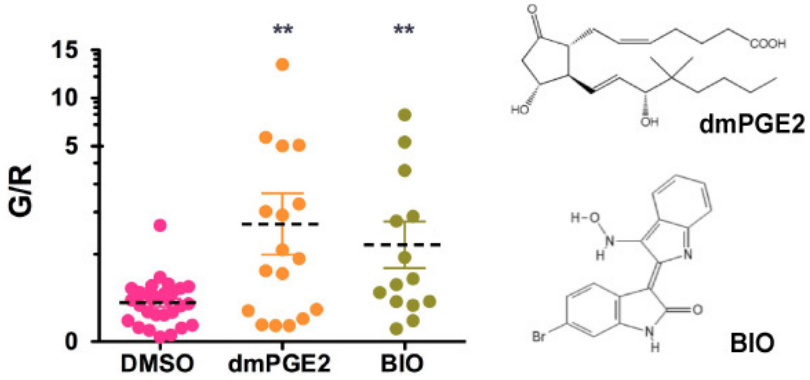

Figure 2.6 Use of the zebrafish competitive transplantation assay to evaluate chemical effects on marrow engraftment.

GFP+ marrow cells were treated *in vitro* at room temperature for 4 hrs with DMSO, 10μM $dmPGE_2$, or 0.5μM BIO. ** Student's t test p values<0.005.

A Chemical Screen Identified Novel Regulators of HSPC Engraftment

Although competitive transplantation in the mouse has been the gold standard for studying HSCs, it has been mostly used to test a single hypothesis such as the relative contribution of mutant to normal HSCs. Because of the high cost and labor intensity, an unbiased chemical screen has not been done to categorize pathways in relation to transplant engraftment. Using this novel competitive WKM transplantation assay in zebrafish, we can handle hundreds of animals per day with dramatically reduced cost. Therefore, we performed the first marrow-transplantation-based chemical screen with the Biomol ICCB Known Bioactive Library, which covers 480 diverse compounds with known bioactivities (Figure 2.7).

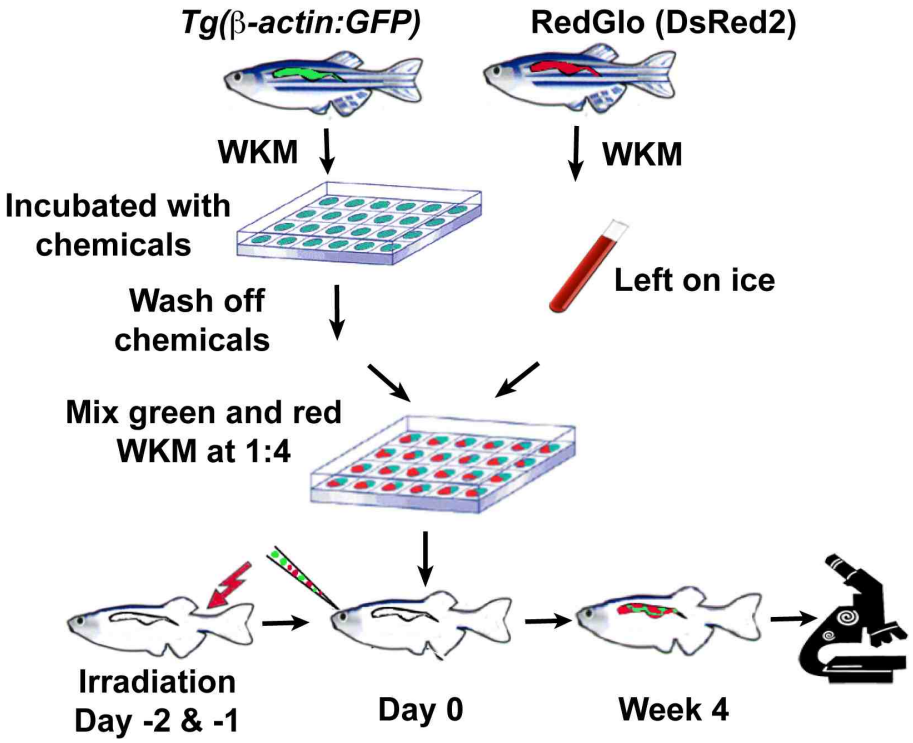

Figure 2.7 Schematic of the chemical screen based on adult zebrafish competitive transplantation

The GFP marrow was pre-treated with various chemicals *ex vivo* for 4hrs at room temperature. The chemicals were washed off before transplantation. Fresh DsRed2 WKM was mixed with the GFP marrow and injected at a dose of 20,000 Green cells and 80,000 Red WKM cells per recipient. 10 recipients were transplanted per chemical treatment group. The recipients were allowed to recover for 4 weeks before the engraftment was read out by imaging. We were able to screen 20-25 chemicals per day. Each independent screen day, a DMSO negative control and a dmPGE_2 positive control were included in the plate. After the G/R was calculated for each chemical treatment group, the DMSO group is normalized to an average G/R=1, and the rest of the treatment groups were normalized accordingly.

After the primary screen and secondary round of confirmation, we found 10 compounds capable of significantly increasing the G/R ratio through blind scoring, including PGE_2, and Ro 20-1724. PGE_2 functions through the Gαs-coupled receptor and activates cAMP signaling pathway (Goessling et al., 2009). Ro 20-1724 inhibits PDE4 (phosphodiesterase 4), the enzyme degrading cAMP, and therefore elevates cAMP level. Therefore, both chemicals activate the cAMP-dependent pathways. The screen results further confirm the importance of cAMP in marrow engraftment. The other screen hits target novel pathways that have not been linked to HSPC engraftment (Figure 2.8, Table 2.1).

Table 2.1 Hits from Adult Zebrafish WKM Competitive Transplantation-Based Chemical Screen

Compound ID	Compound Name	Screen Concentra-tion (μM)	Mechanism
CHC000005	1,2-Didecanoyl-glycerol (10:0) (DAG)	5	Bioactive lipids/ PKC activator
CHC000006	1,2-Dioctanoyl-sn-glycerol (DOG)	5	Bioactive lipids/ PKC activator
CHC000008	(±)11,12-Epoxyeicosatrienoic acid (11,12-EET)	0.5	Bioactive lipid/ arachidonic acid metabolite
CHC000018	(±)14,15-Epoxyeicosatrienoic acid (14,15-EET)	0.5	Bioactive lipid/ arachidonic acid metabolite
CHC000064	AM-580	5	Nuclear receptor ligands/ Retinoid RAR agonist
CHC000146	TTNPB	5	Nuclear receptor ligands/ Retinoid RAR agonist
CHC000081	C-PAF	5	PAF receptor agonist
CHC000142	S-Farnesyl-L-cysteine methyl ester (FCME)	5	Bioactive lipids/ MDR ATPase activator
CHC000097	Farnesylthioacetic acid (FTA)	5	Bioactive lipids/ Carboxymethylation inhibitor
CHC000135	Prostaglandin E_2 (PGE_2)	5	Bioactive lipids/ Prostaglandin EP receptor agonist
CHC000259	Ro 20-1724	5	phosphodiesterase (PDE4) inhibitor

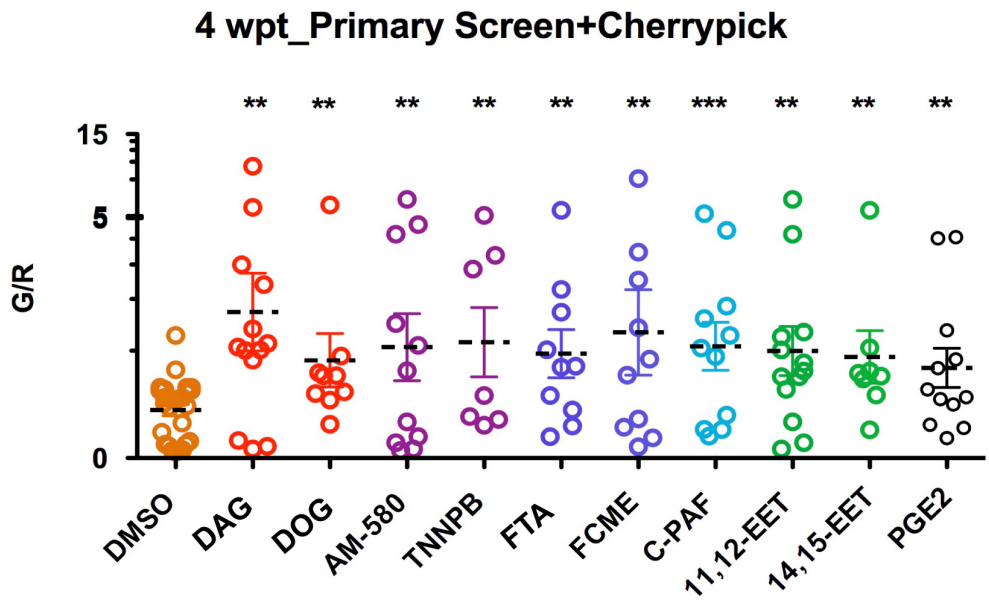

Figure 2.8 Chemical screen hits enhance short-term kidney marrow engraftment in adult zebrafish. (referring to Table 2.1 for the acronyms)

Some Hits Have Effects on Embryonic Hematopoiesis

In order to explore their other potential roles on HSPCs, the hit chemicals were also tested for effects on embryonic hematopoiesis. In the zebrafish embryo, hematopoiesis happens in two waves, primitive and definitive, similar to mammalian hematopoiesis (Davidson and Zon, 2004). The primitive wave only transiently generates embryonic erythrocytes and myeloid cells, while definitive HSPCs emerge from the hemogenic endothelium of the AGM (aorta-gonad-mesonephros region) and last the whole life (Bertrand et al., 2010; Boisset et al., 2010; Davidson and Zon, 2004; Kissa and Herbomel, 2010; Orkin and Zon, 2008). The definitive HSPCs enter circulation, then travel to and engraft in the caudal hematopoietic tissue (CHT), a secondary hematopoietic site equivalent to the mouse fetal liver (Murayama et al., 2006; Orkin and Zon, 2008). Because we were more

interested in the HSPCs that last the lifetime of the fish, we focused on the time window after primitive hematopoiesis and during the specification and trafficking of the definitive HSPCs. Various drug doses were tested. We found some of the screen hits, such as the two farnesyl analogs, FTA and FCME, could increase the definitive HSPC markers, *runx1/c-myb* in the AGM, while the RAR agonist, AM-580, decreased the expression of these markers (Figure 2.9). Interestingly, we found one chemical, 11.12-EET, can increase both the HSPC marker expression in the AGM and the trafficking of definitive HSPCs from AGM to CHT (Figure 2.9).

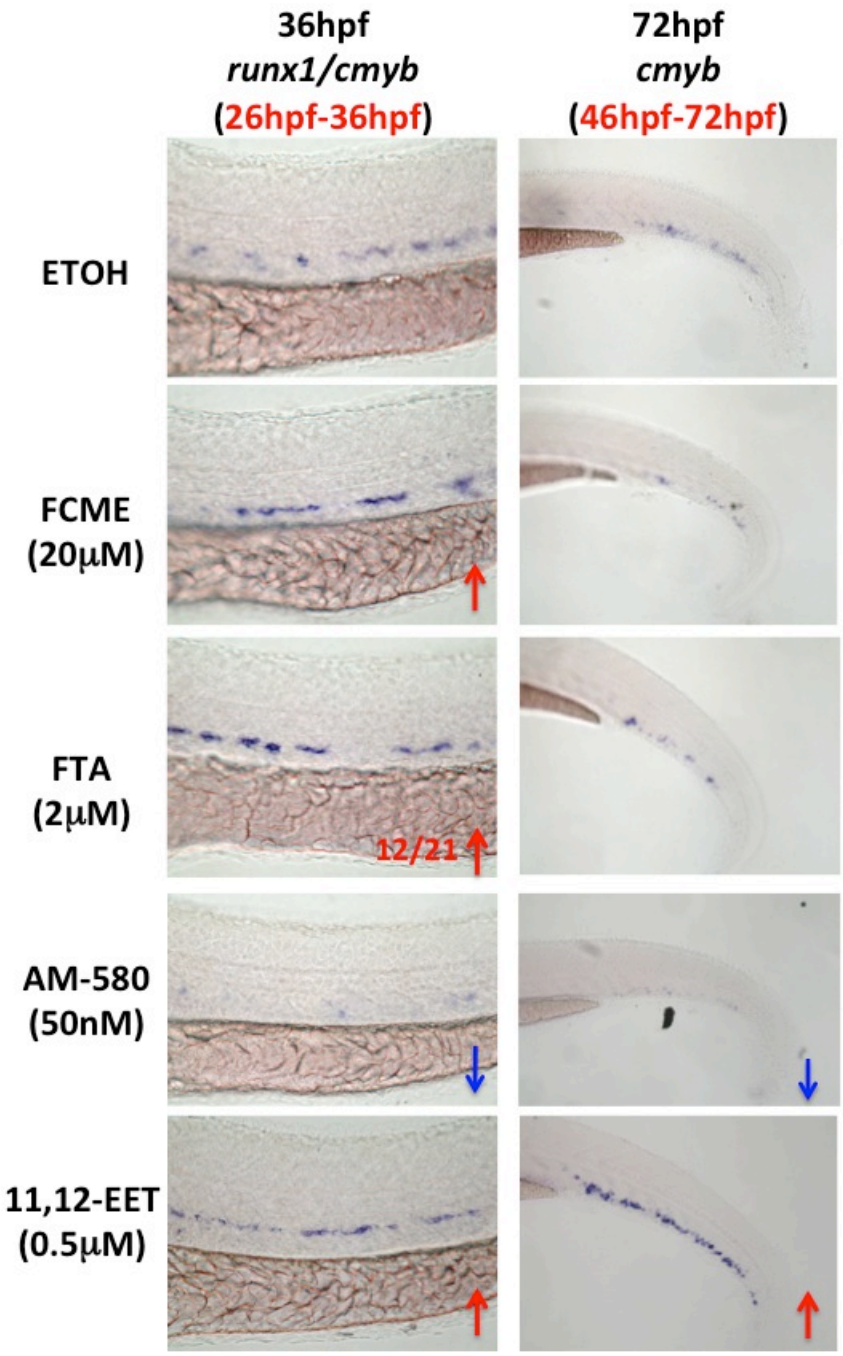

Figure 2.9 Effects of screen hits on embryonic definitive hematopoietic stem and progenitor cells

Embryos were treated with chemicals during the time window indicated above the figures. HSC markers were examined in the AGM (aorta-gonad-mesonephros) at 36hpf (left column) and CHT (caudal hematopoietic tissue) at 72 hpf (right column). Blue arrows indicate decrease, and red arrows indicate increase.

Developing Transgenic Zebrafish Lines with More Ubiquitous Labeling of Blood Cells

Several zebrafish transgenic lines have been previously described to have ubiquitous expression patterns, including the zebrafish *h2afx*, *tbp*, *β-actin* control elements (Kwan et al., 2007; Burket et al., 2008; Gillette-Ferguson et al., 2003), and the *Xenopus laevis*-derived *elongation factor 1a* promoter (*XlEef1a1*) (Johnson and Krieg, 1994). However, the expression of fluorescence proteins driven by these transgenes is not truly ubiquitous in the adult zebrafish blood compartment. For example, the *Tg(β-actin:GFP)* have the majority of their white blood cells labeled with GFP, but not their red blood cells (Figure 2.4). Recently, Christian Mosimann et al in our lab BLAST-searched using the human Ubiquitin peptide ORF as a query and identified the predicted zebrafish gene locus *zgc:172187* on linkage group 5, referred to here as zebrafish *ubiquitin B* (*ubi*). The zebrafish *ubi* gene features a 71 bp non-coding first exon, a 2 kb spanning intron, followed by a second exon encoding a multimeric (8 repeats) Ubiquitin peptide precursor, a gene structure homologous to *ubi* loci in other species. Using PCR, we cloned a 3.5kb sequence from BAC *CH211-202A12* immediately upstream of the *ATG* start codon at the 5' end of exon 2 that is analogous to the previously reported *Drosophila* and human *ubi* control region fragments (Lee et al., 1988; Schaefer et al., 2001; Schorpp et al., 1996) and includes the putative intron/exon splice junctions. Stable transgenic lines were constructed using this piece of regulatory element driving the expression of GFP or mCherry, annotated as *Tg(ubi:GFP)* and *Tg(ubi:mCherry)* (Mosimann et al., 2011).

ubi Expresses in All Blood Cell Types

We sought to analyze *ubi* expression in the hematopoietic system and profiled the blood expression of adult *ubi:EGFP* and *ubi:mCherry* heterozygous transgenic zebrafish using flow cytometric analysis of dissected WKM (Traver et al., 2003), the major hematopoietic tissue in adult zebrafish. The analyzed *ubi:EGFP* and *ubi:mCherry* transgenic lines showed robust fluorophore expression in all resolvable blood cell gates (Figure 2.10) and in the vast majority of cells in these respective populations, including erythroid, myeloid, and lymphoid lineages, plus precursor cell population. This is in stark contrast to *β-actin* promoter-driven EGFP transgenics, which overall show weaker expression in hematopoietic lineages, particularly in erythrocytes, which barely express *β-actin:EGFP* (Figure 2.4).

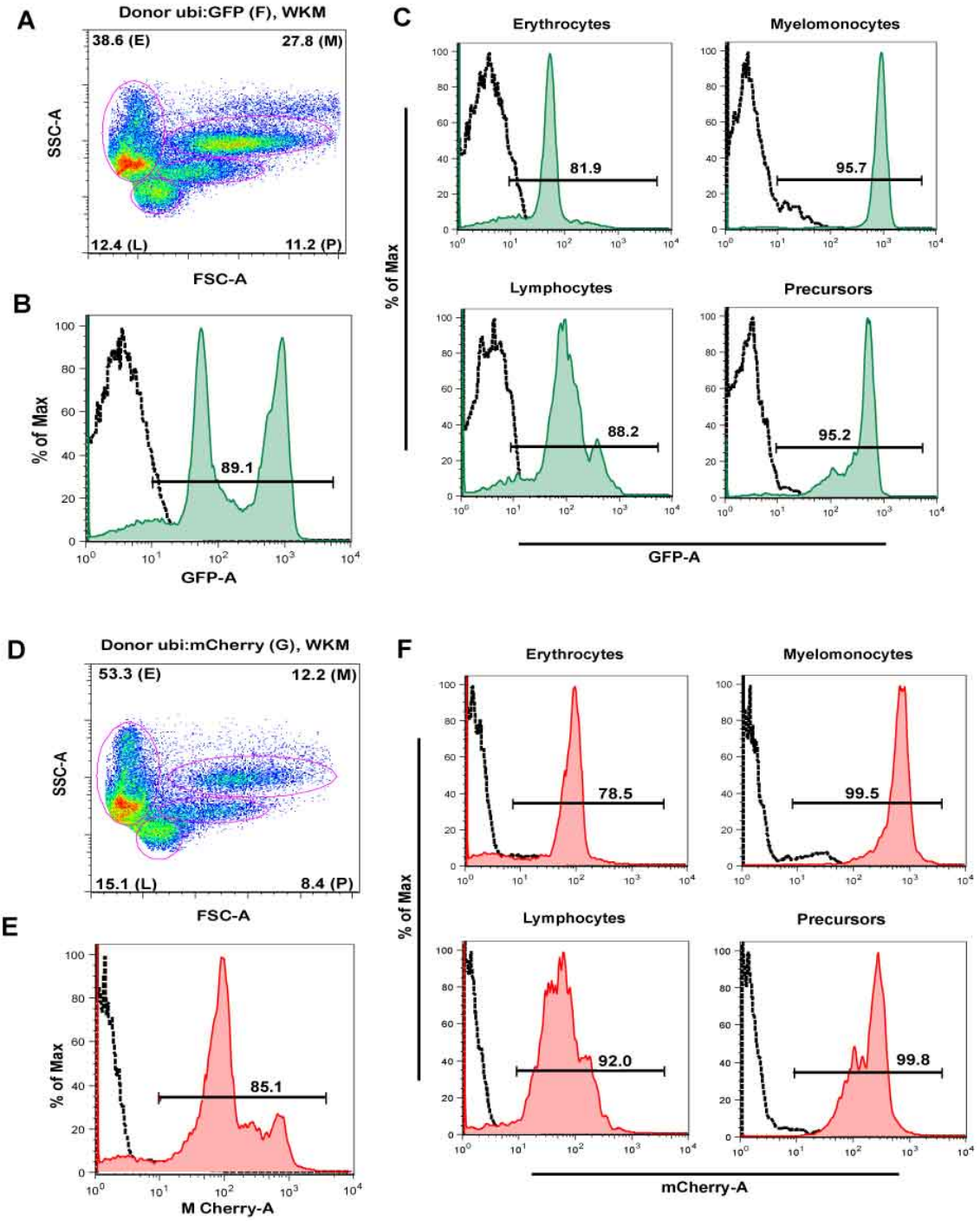

Figure 2.10 *ubi*-driven transgenes express in all blood cell lineages.

Representative flow cytometry analysis of *Tg*(*–3.5ubi-EGFP*) (A-C) and *Tg*(*–3.5ubi-mCherry*) (D-F) adult whole kidney marrow (WKM).
(A) (D) Separation of blood cell populations by forward and side scatter.
(B) (E) The majority of all WKM express EGFP or mCherry.
(C) (F) The individual subpopulations express EGFP or mCherry.

This broad hematopoietic expression should therefore allow assessment of multilineage engraftment in transplantation experiments using *ubi:EGFP* or *ubi:mCherry*. To test this application, we isolated WKM from either *ubi:mCherry* or *ubi:EGFP* heterozygous adults, and performed retro-orbital WKM transplantation into irradiated *roy*$^{-/-}$; *nacre*$^{-/-}$ (*casper*) (White et al., 2008) transparent recipients to allow for easy visualization. Three weeks post-transplantation, the transparent *casper* recipients showed strong localized fluorescence marking the kidney territory (Figure 2.11E, 2.11E). Flow cytometry analysis of WKM from these *casper* recipients revealed chimeric contribution of fluorophore-expressing donor cells to all light-scatter resolvable blood cell populations, as described above (Figure 2.11, 2.12). We have successfully monitored *ubi:EGFP* and *ubi:mCherry* WKM-transplanted *casper* recipients with long-term transplants over 3 months post transplant, as well as performed transplantation with mixed *ubi:EGPF* and *ubi:mCherry* populations in competitive transplants, without detecting any diminishing fluorophore intensity (Figure 2.13). *ubi*-driven transgenic reporters are therefore suitable reagents for hematopoietic transplantation experiments, and their true multilineage expression offers a clear advantage over previously used transgene reporters.

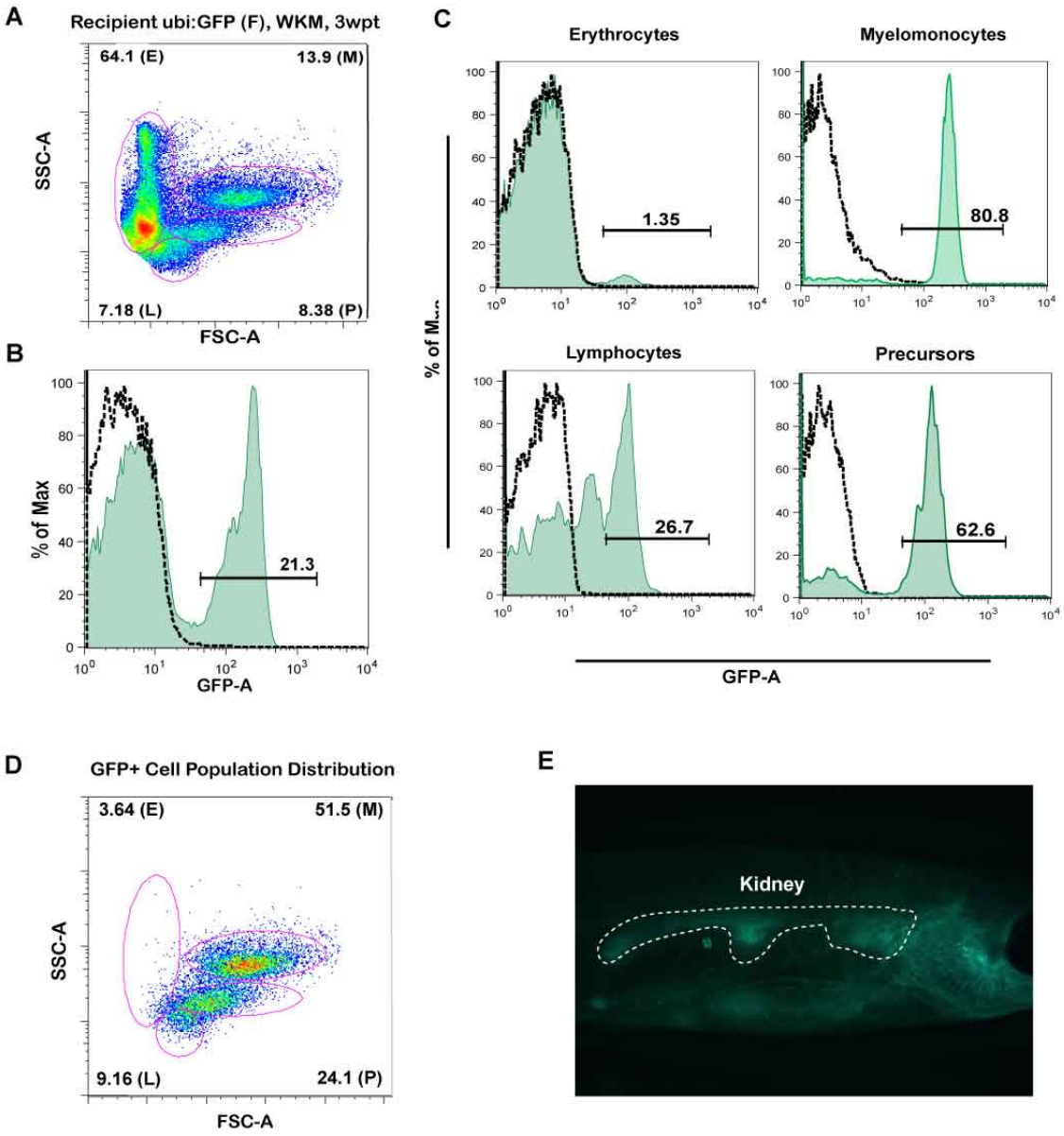

Figure 2.11 Whole kidney marrow transplantation using *ubi:EGFP*.

Cells isolated from *Tg*(*–3.5ubi-EGFP*) adult WKM were transplanted via retro-orbital injection into irradiated *casper* recipient adults and read-out 3 wpt for EGFP blood chimerism by flow cytometry (A-D) and fluorescence microscopy (E).
(A) Separation of the recipient's blood cell populations by forward and side scatter.
(B) Overall and (C) different lineage engrafted with EGFP+ donor-derived cells.
(D) The distribution of donor-derived GFP+ cells in different blood lineages.
(E) Live imaging of the recipient engrafted with GFP+ donor-derived marrow.

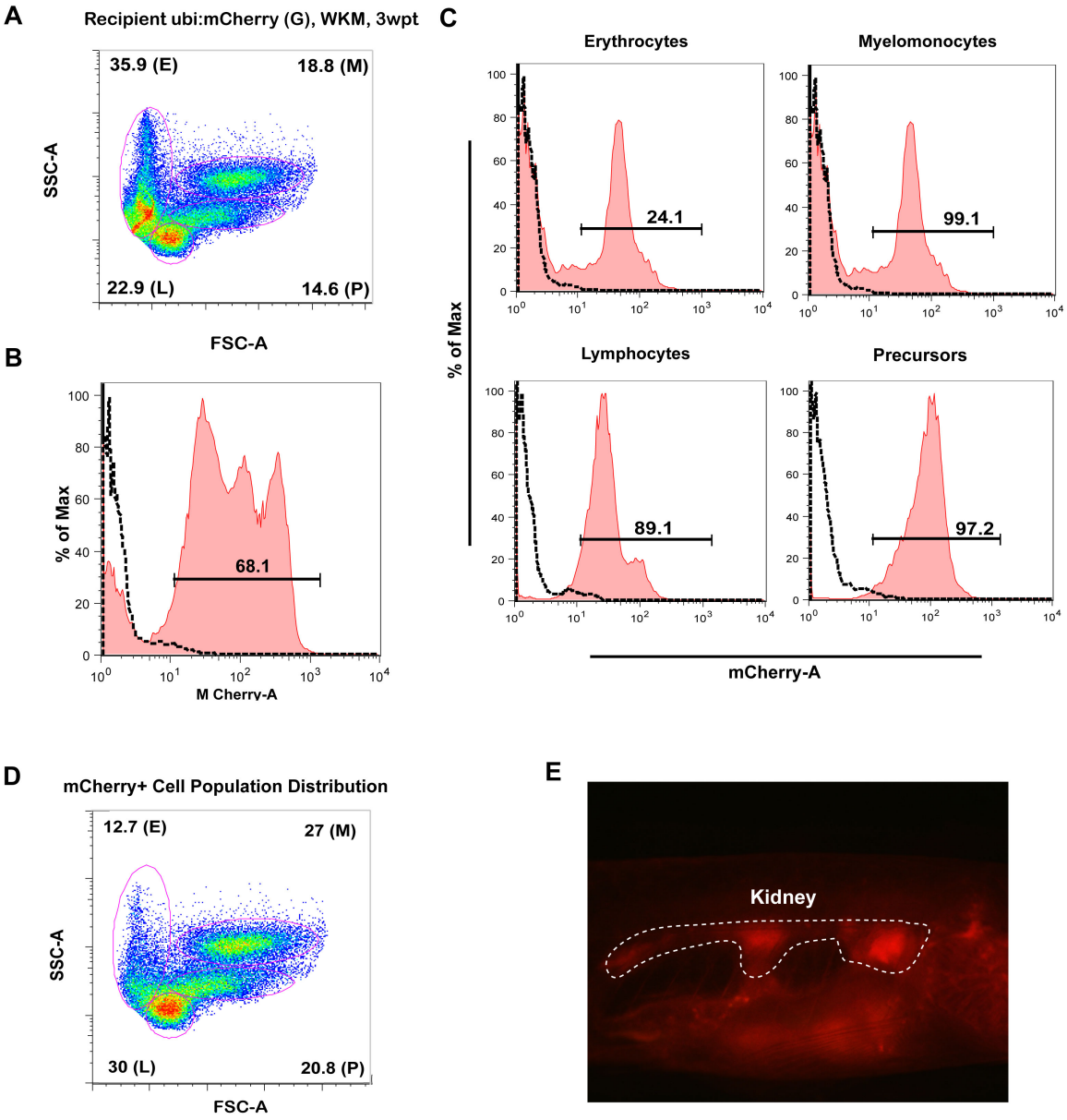

Figure 2.12 Whole kidney marrow transplantation using *ubi:mCherry.*

Cells isolated from *Tg*(*–3.5ubi-mCherry*) adult WKM were transplanted via retro-orbital injection into irradiated *casper* recipient adults and read-out 3 weeks post transplant (wpt) for mCherry blood chimerism by flow cytometry (A-D) and fluorescence microscopy (E).
(A) Separation of the recipient's blood cell populations by forward and side scatter.
(B) Overall and (C) different lineage engrafted with mCherry+ donor-derived cells.
(D) The distribution of donor-derived mCherry+ cells in different blood lineages.
(E) Live imaging of the recipient engrafted with mCherry+ donor-derived marrow.

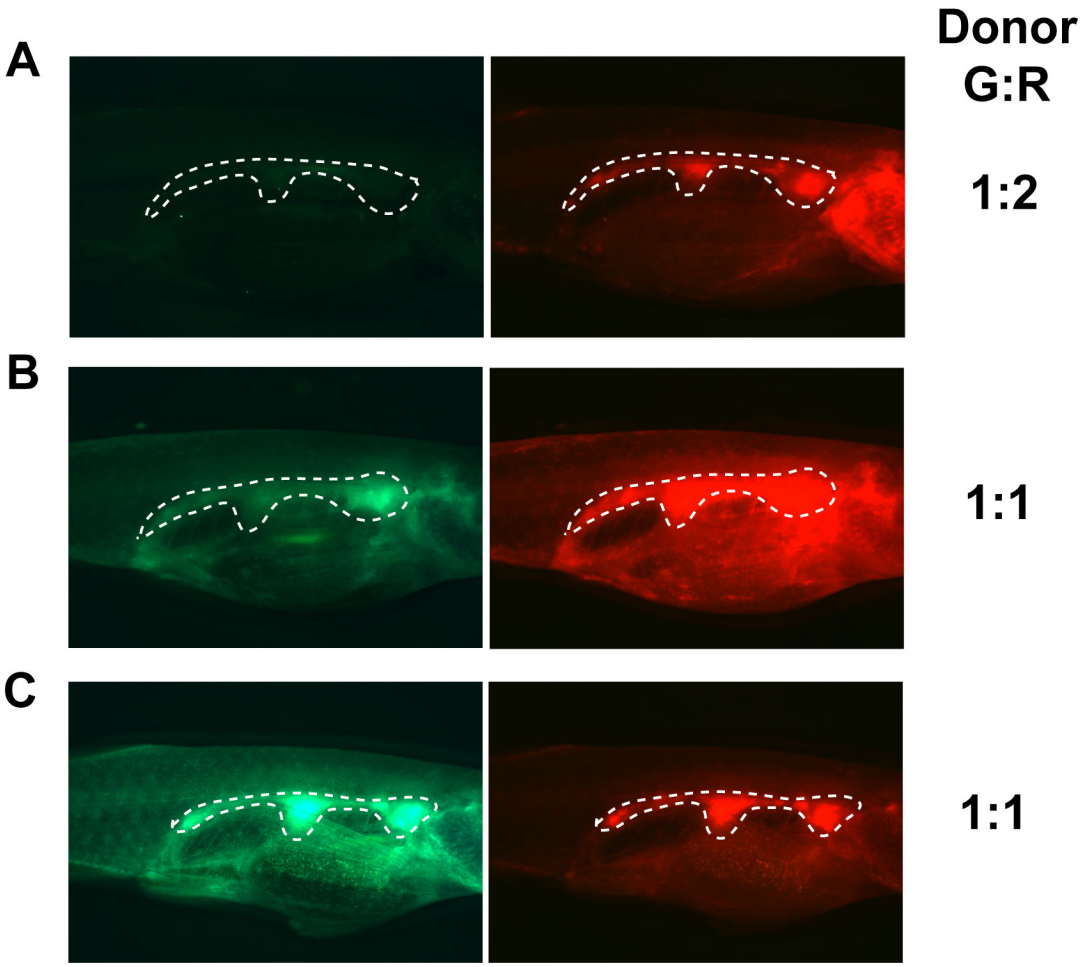

Figure 2.13 Competitive transplantation with *ubi* transgenic zebrafish

Tg(ubi:EGFP) and *Tg(ubi:mCherry)* donor marrows were transplanted at either a G:R ratio of 1:2 (33,000:66,000) (A) or 1:1 (50,000:50,000), and recipients were imaged at 4 wpt. At the ratio of 1:2, all the recipients were only engrafted with mCherry donor-derived cells. At the ratio of 1:1, half of the recipients were engrafted with both EGFP+ and mCherry+ cells.

Discussion

In summary, we evaluated multiple factors to produce an optimal transplantation model. These factors included donor zebrafish strains, myeloablation conditions, donor cell ratios, injection techniques, readout time-points and quantification method. Eventually, we were able to develop a live imaging-based adult zebrafish marrow competitive transplantation assay. This assay allows fast quantification of marrow engraftment capability. The system can be used to evaluate the effect of genetic mutations or transgene effects on adult HSPCs. We demonstrated that dmPGE_2 and/or GSK-3β inhibitor treatment of GFP+ marrows for 4 hrs could dramatically increase the marrow repopulation capability in zebrafish. Using this assay, the first chemical screen in adult vertebrates was performed *in vivo*. This approach defined critical pathways regulating HSPC engraftment in vertebrates, represented by 10 chemicals. These hits include PGE_2, which is the positive control of the screen. The other hits target novel pathways that have not been linked to HSPC engraftment. Some compounds also increased HSC formation in zebrafish embryos, indicating that some pathways might be common to different developmental stages.

The Variability of Marrow Transplantation and Engraftment

Due to the complexity of whole-organism level physiology and the biological processes involved in engraftment, transplantation has always been a relatively variable experimental approach, even within the genetically homogeneous mouse population. Zebrafish have a more diverse genetic background than mice. After

multiple-generations of inbreeding to create more homogenous zebrafish populations, fertility rates decline, presenting one of the greatest challenges of zebrafish husbandry (Monson and Sadler, 2010). Although homozygous diploid clonal zebrafish strains can be created by embryo manipulation at early stages, whether they will have the same inbreeding and fertility issues still needs to be tested over time (Mizgirev and Revskoy, 2010). Therefore, all adult zebrafish transplantation performed to date has been on a genetically non-homogenous population. This genetic heterogeneity may be a major cause of the large standard deviation of the engraftment level within each experimental group. On the other hand, this might more accurately reflect the reality of transplantation engraftment in the human population, more so in fact than the clonal mouse model, since patients undergoing marrow or HSC transplantation have very diverse genetic backgrounds. In addition, the low cost of zebrafish husbandry allows the sampling of a large number of animals for more rigorous statistical analysis.

Another major cause of the engraftment variability comes from the injection technique itself. Due to the small size of zebrafish, only 3-5ul of liquid can be injected through retro-orbital or intra-cardiac injection. The total blood volume of a single adult zebrafish is between 20-50ul by estimation, depending on the size of the fish. Therefore, this introduces a huge technical challenge to efficiently and consistently deliver the full volume into the animal. We hope with the experimental design of competitive transplantation, one donor can serve as an internal/technical control for the injection. From our experience, this enables us to quantify the relative engraftment capability changes with a relatively small number of recipients,

otherwise almost impossible to achieve with single marrow transplantation. However, the consistency of this competitive transplantation assay can certainly benefit from the development of better injection technique in the future.

A third factor that can introduce major variability is the heterogeneity of the donor population. Similar to the recipients, the donors are not clonal either. The heterogeneity of fluorescence strength among siblings from the same stable transgenic parent pair has been known for years (Akitake et al., 2011). This phenomenon has also been observed in other model organisms too, which is different from the position effect (Dobie et al., 1996). In order to have enough cells for 200 recipients, we pooled kidney marrows from multiple sibling donors together, which might also help to normalize the fluorescence intensity level. But the variability from experiment to experiment is still not marginal. Therefore we always normalize G/R relative to the DMSO control of each experiment (making the average G/R of DMSO equal to 1) before combining the data from any independent experiments.

Retinoic Acid Receptor Agonists

Retinoic acids have long been known to play a role in hematopoiesis. They bind to a family of nuclear hormone receptors, called retinoic acid receptor (RAR), which then form functional heterodimer with retinoic X receptor (RXR) (Means and Gudas, 1995). Among the seven RAR agonists in the chemical screen library only two structurally highly related compounds, AM-580 and TTNPB were scored positive in the screen. These two compounds have distinctive chemical moieties from the other

agonists, which include all-trans retinoic acid (ATRA) used for treating acute promyelocytic leukemia (Figure 2.14) (Degos and Wang, 2001). This structure difference might lead to the different agonistic effects on RAR or specific binding to other unknown targets. However, false negative results are quite common in a screening project, partially due to the subjective choice of a single concentration tested in the screen. Further tests with appropriate dose titration across multiple structurally different RAR agonists are necessary before making any definitive conclusion.

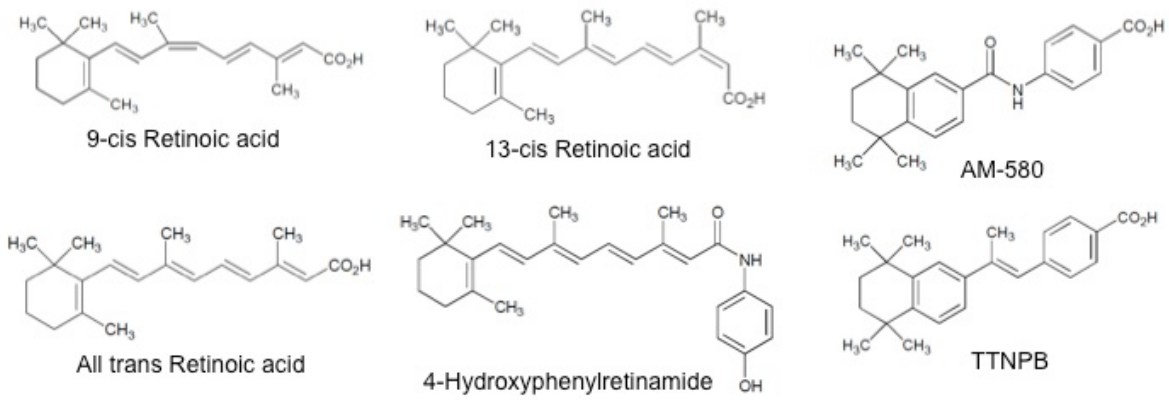

Figure 2.14 Chemical structures of different retinoic acid receptor agonists.

The hits from the screen, AM-580 and TTNPB, share similar structure characteristics, while the rest closely resemble ATRA (all-trans retinoic acid), which were not scored as positive in the screen.

Farnesylation-Related Chemicals

S-farnesyl-L-cysteine methyl ester (FCME) was annotated in the chemical library as an MDR ATPase activator, and farnesylthioacetic acid (FTA) is a protein carboxymethylation inhibitor. However, the chemical structures of both compounds

greatly resemble farnesyl cysteine, the intermediate product for protein farnesylation modification (Figure 2.15A). Farnesylation is a type of post-translational modification in which a farnesyl group is attached to the CAXX tail at the C-terminus of a given protein. Three enzymes are required for this sequential modification reaction: farnesyl transferase (FTase) which attaches the farnesyl diphosphate to the cysteine at the C-terminus, CAAX protease (RCE1) which cleaves the –AAX off the C-terminus, and the CAAX methyltransferase (ICMT) which attaches a methyl group (-CH_3) to the bare C-terminus (Figure 2.15) (Zhang and Casey, 1996). A parallel modification with geranylgeranyl group employs similar principles, and shares the same enzymes of RCE1 and ICMT. Together, these types of modification are called prenylation. FTA blocks the third step of C-terminal carboxylation by inhibiting ICMT. Based on the structural similarity between FCME and FTA, we hypothesize that FCME might also inhibit ICMT. In addition, we only observed the positive effect of farnesyl analogs, but not geranylgeranyl analogs (data not shown).

Prenylation changes the membrane affinity of the protein, and therefore modifies its intracellular localization. Many proteins are regulated by this process, such as the RAS and Rho small GTPase family, some phosphatases and kinases, nuclear lamins, and centromeric proteins CENP-E&-F. Most of the proteins have a preference for either farnesylation or geranylgeranylation, although not exclusive (Winter-Vann and Casey, 2005). The importance of this process has been exemplified by knockout mice. *Rce1*-null mice die between E15.5 and first week of life (Kim et al., 1999). *Icmt*-null mice have severe anemia and liver defects, and die

at E11.5 (Bergo et al., 2001). Conditional knockout of *Rce1* in the blood compartment of the *Kras2*-driven MPD (myeloproliferative disorder) mouse model (*Rce1*$^{fl/fl}$*Kras2*$^{LSL/+}$*Mx1-Cre*) causes accelerated MPD, while knocking out *Icmt* in the same mice (*Icmt*$^{fl/fl}$*Kras2*$^{LSL/+}$*Mx1-Cre*) ameliorates MPD (Wahlstrom et al., 2008). The effects of knocking out *Rce1* or *Icmt* on MPD development might reflect different means of modulation of Ras protein activity, but it clearly shows the importance of prenylation in regulating hematopoiesis. Marrow engraftment requires small GTPases, such as Rho and Rac, whose localization and activities are also regulated by prenylation. Therefore, further examination of the role of this pathway in the context of HSPC engraftment might generate interesting insights into how engraftment is regulated through lipid modification.

Discussion Summary

In summary, despite some of the caveats associated with the zebrafish competitive marrow transplantation, it is still a very powerful assay for determining short-term engraftment. More importantly, it is amenable for performing chemical or genetic screening for HSPC engraftment, therefore making it a useful platform to tackle the question *in vivo*. The screen hits need further optimization with dose titration and validation by bone marrow transplantation experiments in mice. The interesting categories of hits indicate some intriguing biological mechanisms behind HSPC engraftment.

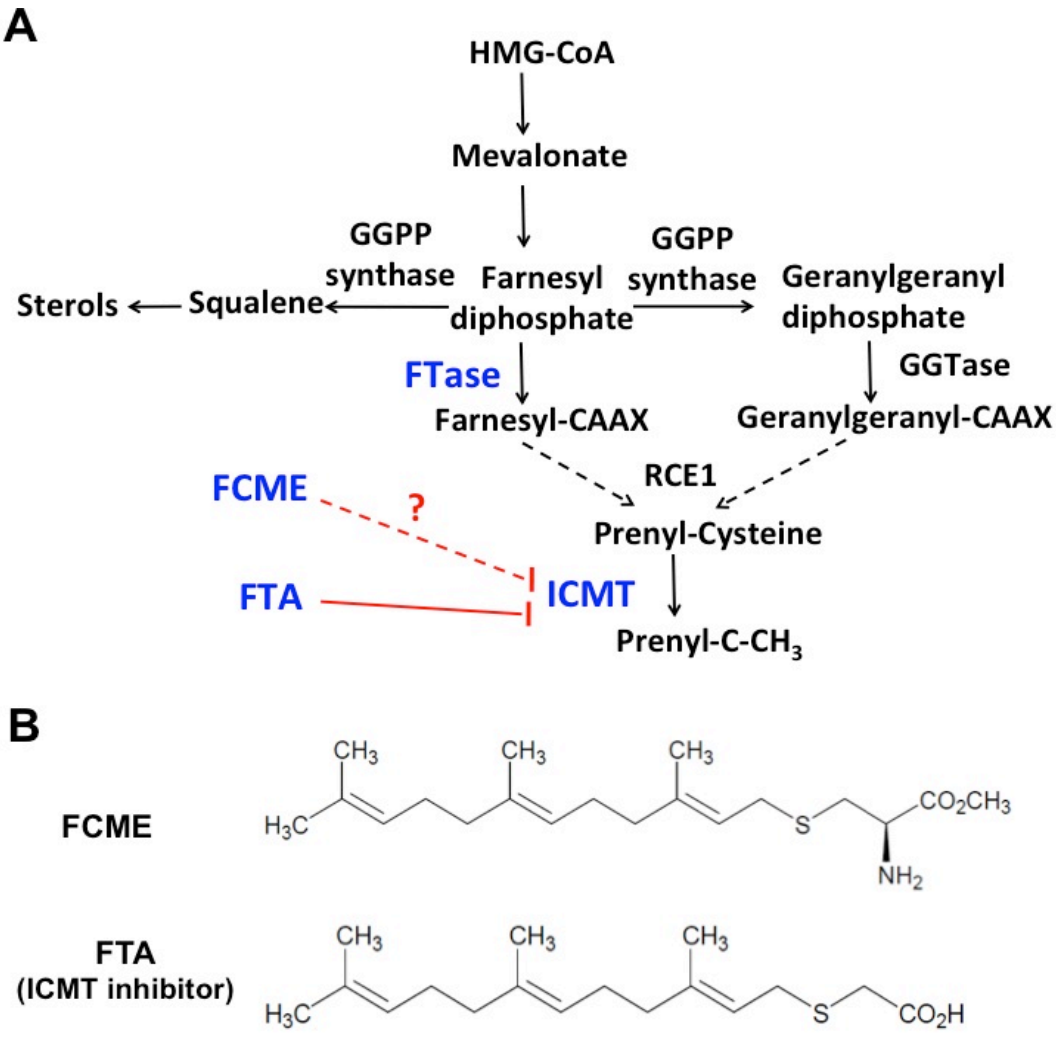

Figure 2.15 Protein prenylation pathway and chemical inhibitors

(A) Prenylation pathway: the substrates farnesyl diphosphate or geranylgeranyl diphosphate are synthesized from HMG-CoA, which is part of the sterol synthesis pathway. The two substrates are attached to proteins with C-terminal CAAX tail by farnesyl transferase (FTase) or geranygeranyl transferase (GGTase). The prenyl-CAAX intermediate products are processed by the enzyme, RCE1 (CAAX prenyl protease) to lose the AAX amino acids. The final step is catalyzed by ICMT (protein-S-isoprenylcysteine O-methyltransferase) which attaches a methyl group to the bare C-terminus. FTA is a known ICMT inhibitor. The target of FCME is unclear.
(B) Chemical structures of FCME and FTA. The methyl ester group in FCME is not stable in water, which can be quickly degraded to lose the methyl group.

Material and Methods

Zebrafish strains

Zebrafish were maintained in accordance with Animal Research Guidelines at Children's Hospital Boston. The following transgenic or mutant zebrafish lines were used in the experiments: GreenGlo® and RedGlo® zebrafish were purchased from 5D Tropical and authorized for research use (Blake, 2010). zsGreen or *DsRed2* are overexpressed under the *mlc* (myosin light chain) and *β-actin* dual promoters. Tg(*β-actin:GFP), Tg(lyz:GFP), Tg(lyz:DsRed), Tg(ubi:EGFP) and Tg(ubi:mCherry), and casper* lines were previously described (Kikuchi et al., 2011; White et al., 2008).

Adult Kidney Marrow Competitive Transplantation

Briefly, GFP+ marrow cells are competed against DsRed2+ marrow cells. The donor animals have ubiquitous GFP based on *β-actin*-driven expression and a ubiquitous DsRed2 based on a commercially available GloFish®. The two marrows are mixed at a certain ratio and co-injected into *casper* recipients. We used the ratio of average GFP intensity over average DsRed2 intensity within the same kidney region as the measurement of relative engraftment efficiency (G/R). The higher the ratio, the more competitive the green cells are.

Adult zebrafish donors are anaesthetized with 0.2% tricaine before blood and kidney collection. Peripheral blood is obtained from adult *casper* by cardiac puncture with micropipette tips coated with heparin and collected into 0.9XPBS containing 5% FCS. About 3-5 million red blood cells can be harvested from one

donor. To dissect whole kidney marrow (WKM), a ventral midline incision is made on the donor fish. Whole kidney is dissected out and placed into ice-cold 0.9XPBS containing 5% FCS. Single-cell suspensions are generated by aspiration followed by filtration through a 40-μm nylon mesh filter into a 50ml conical tube. The flow-though part is diluted with a final volume of 25ml and centrifuged at 1,500rpm for 8 minutes. The supernatant is discarded and the pellet cells are resuspended in 1ml 0.9XPBS containing 5% FCS. The number of cells alive is counted with a hemacytometer. On average, 500,000-700,000 cells can be harvested per donor. Finally, the peripheral blood and kidney marrow cells are centrifuged at 1,500rpm for 8 minutes, resuspended in 0.9XPBS containing 5% FCS and mixed at a certain ratio and concentration. Ten- to fourteen-week old *casper* recipients are sublethally irradiated with 30Gy γ-irradiation, split by two doses, 15Gy each at both 2d and 1d before transplantation. Recipients are anesthetized in tricaine. 4ul of the cell suspension mixture above is injected into the circulation retro-orbitally through a Hamilton syringe (26s gauge, 10ml volume). Usually 50,000-200,000 marrow cells plus 100,000-200,000 peripheral blood cells are able to rescue the recipient. Recipients are kept in still fish water supplemented with anti-fungal reagents to reduce infection for one week with minimal feeding, and then placed into the communal system with circulating water and a reduced amount of food.

Imaging-Based Quantification of Engraftment in Adult Zebrafish

Transplanted recipients can be anesthetized in tricaine and visualized over time on a Zeiss Discovery V8 stereomicroscope with a 1.2X PlanApo lens and GFP/DsRed

filters. Images are captured using AxioVision software and for each recipient, two images are taken with GFP or DsRed filter respectively. The images are all saved in .tif format and analyzed using ImageJ software. The kidney region is manually selected for every fish and the average fluorescence intensities per pixel of both GFP and DsRed are measured within the same region (G_{kid} and R_{kid}). Background for each image is measured in a region outside the fish (G_{bkg} and R_{bkg}), and subtracted from the correlated kidney fluorescence intensity. The relative engraftment level was calculated as $G/R= (G_{kid} - G_{bkg}) / (R_{kid} - R_{bkg})$. For the chemical screen, the average G/R in the DMSO group was normalized to 1, and all the other groups were normalized according to DMSO.

Chemical Screen

Adult zebrafish transplantation-based chemical screen was done at the hESC core at Children's Hospital Boston. The ICCB Known Bioactive Library was purchased from BIOMOL (Enzo Life Sciences). WKM (Whole kidney marrow) was incubated in 0.9xDPBS plus 5% heat-inactivated FBS for 4 hrs at room temperature, at a density of 1000 cells/μl. Chemicals were diluted at a 1:200 ratio. Chemicals used for the secondary round of screening for confirmation were from a different aliquot of the library, independent of the primary screen plate. The original solvent of $dmPGE_2$ (Cayman, #14750) was evaporated with nitrogen gas and resuspended in DMSO, and used at 10μM for chemical treatment. The other chemicals used for this study are: BIO (EMD), 0.5μM.

Chapter 3

Epoxyeicosatrienoic Acids Enhance Hematopoietic Stem and Progenitor Cell Engraftment

Pulin Li[1,2], Emily K. Pugach[1], Elizabeth B. Riley[1], Dipak Panigrahy[3], Owen J. Tamplin[1], Teresa V. Bowman[1], Garrett C. Heffner[1], Shannon McKinney-Freeman[4], Thorsten M. Schlaeger[1], George Q. Daley[1], Darryl C. Zeldin[5], and Leonard I. Zon[1,2,]*

[1] Stem Cell Program and Division of Hematology/Oncology, Children's Hospital Boston and Dana-Farber Cancer Institute, Howard Hughes Medical Institute, Harvard Stem Cell Institute, Harvard Medical School and, Boston, MA 02115, [2] Chemical Biology Program, Harvard University, Cambridge, MA 02138, [3] Vascular Biology Program, Children's Hospital Boston, Boston, MA 02115, [4] Department of Hematology, St. Jude Children's Research Hospital, Memphis, TN 38105-3678, [5] Division of Intramural Research, National Institute of Environmental Health Sciences, National Institutes of Health, Research Triangle Park, NC 27709

* To whom correspondence should be addressed
Address: 300 Longwood Avenue, Boston, MA 02115
Email: zon@enders.tch.harvard.edu

Attributions

I designed and performed the chemical screen leading to the discovery of EETs as novel regulators of HSPC engraftment. I performed all the mouse bone marrow and HSPC transplantation experiments, peripheral blood analysis and bone marrow stem and progenitor cell analysis, with technical advice from T. V. Bowman, G. C. Heffner and S. McKinney-Freeman. I designed and performed the chemical suppressor screening, the morpholino experiments in zebrafish embryos, the western blotting and qRT-PCR experiments in human cell lines, with some technical assistance from E. K. Pugach and E. B. Riley. I designed and performed the time-lapse confocal imaging analysis with the imaging technical assistance from O. J. Tamplin. C. R. Lee, M. L. Edin from D. C. Zeldin's laboratory and D. Panigrahy provided the *Tg*(*Tie2:CYP2C8)* transgenic mice. I analyzed all the data above.

I designed and prepared mRNA for the microarray and RNA-seq experiments. The microarray was performed by the Molecular Genetics Core Facility at Children's Hospital Boston, supported by NIH-P50-NS40828 and NIH-P30-HD18655. The microarray raw data was processed and analyzed by A. Dibiase. The RNA-seq was sequenced by the Whitehead Institute, and analyzed by R. M. White.

Introduction

In Chapter 2, I described the zebrafish whole kidney marrow (WKM) competitive transplantation assay and the chemical screen based on this assay. The screen led to the discovery of multiple novel chemicals that can modulate the hematopoietic stem and progenitor cell (HSPC) engraftment capability in zebrafish. This includes a group of lipids, epoxyeicosatrienoic acids (EETs) that can enhance marrow transplantation efficiency. EETs are biosynthesized from arachidonic acid by cytochrome P450 enzymes, especially members of the 2C and 2J families in mammals (Figure 3.1A) (Panigrahy et al., 2011b; Pfister et al., 2010). EETs have very short half-life in vivo, and are quickly degraded by soluble epoxide hydrolase into dihydroxyeicosatrienoic acids (DHETs), which have much less potent bioactivities in general. EETs regulate various physiological and pathological processes, such as vascular tone, inflammation, angiogenesis, and tumor growth/metastasis (Michaelis et al., 2005; Panigrahy et al., 2011b; Pfister et al., 2010).

Each step leading to engraftment involves a response to diverse external signals in the niche, dramatic cellular changes, and cell-cell interactions (Laird et al., 2008). Signaling by stromal-derived factor 1 (SDF-1) and stem cell factor (SCF) guides HSCs that express the receptors, CXCR4 and c-KIT respectively, to home to the marrow (Lapidot et al., 2005). Prostaglandin E_2 (PGE_2) enhances the homing efficiency, as well as the number of HSCs (Goessling et al., 2009; Hoggatt et al., 2009; North et al., 2007). Gαs signaling, which can be activated by PGE_2, is required for marrow engraftment (Adams et al, 2009). Integrins and other adhesion molecules mediate the HSC-endothelial interaction essential for entering the marrow (Mazo et al.,

1998; Papayannopoulou et al., 1995). Small GTPases, such as Rac and Cdc42, are required to orchestrate cell movement for efficient homing, retention and localization (Cancelas et al., 2005; Gu et al., 2003; Williams et al., 2008; Yang et al., 2001). Once HSCs enter the bone marrow niche, extrinsic signaling from various niche cells, such as vascular and mesenchymal cells, influence HSC cell fate decisions to maintain quiescence, proliferate or differentiate; reciprocally, HSCs might also participate in niche formation (Mercier et al., 2011).

Here, we show pulse treatment with EETs can enhance whole marrow engraftment both in zebrafish and mice. Genetic analysis in zebrafish embryos demonstrated that EET acts through a Gα12/13-mediated receptor, which activates PI3K and induces transcription factors of the AP-1 family. This PI3K/AP-1 pathway directly induced the transcription of HSC marker, *runx1,* in embryos. The autonomous activation of PI3K in HSPCs by EET promoted HSPC migration and interactions with niche cells. Our studies define a role for EETs in the development of blood stem cells during embryogenesis, and in engraftment in adult vertebrates. This discovery may have clinical application in marrow or cord blood transplantation.

Results

EETs Promote Marrow Engraftment in Zebrafish

From the chemical screening described in Chapter 2, we identified 10 chemicals that were able to enhance marrow engraftment capabilities. Among them are epoxyeicosatrienoic acids (EET), eicosanoids derived from arachidonic acid through the cytochrome P450 epoxygenase pathway, especially 2C and 2J in humans (Figure 3.1A) (Panigrahy et al., 2011b; Pfister et al., 2010). Four isomers of EETs exist in vivo: 5,6-EET, 8,9-EET, 11,12-EET and 14,15-EET.

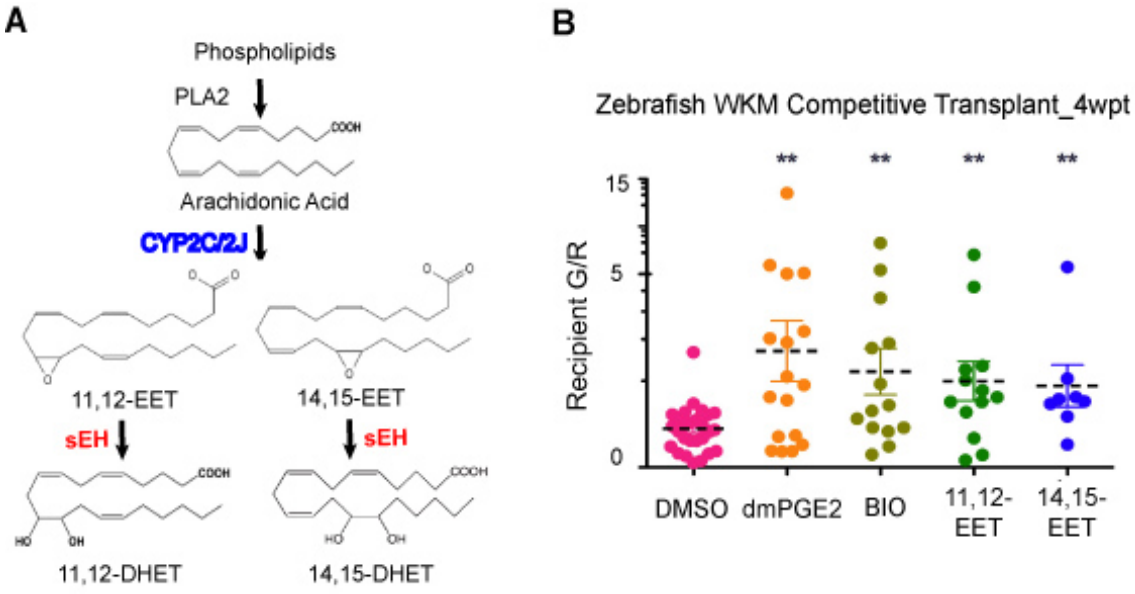

Figure 3.1. EETs enhance marrow engraftment capabilities in zebrafish.

(A) EET metabolic pathway
(B) Chemical treatment enhanced engraftment in zebrafish. GFP+ marrow cells were treated *in vitro* with DMSO, 10μM $dmPGE_2$, 0.5μM BIO, 0.5μM 11,12-EET or 0.5μM 14,15-EET for 4 hrs. ** Student's t test p values<0.005.

Both (±)11,12-EET and (±)14,15-EET increased the marrow engraftment in zebrafish at 0.5 μM concentration (Figure 3.1B). In this chapter, the follow-up studies on understanding the signaling and molecular mechanism of EETs are reported.

EETs Promote Adult HSPC Engraftment in Mammals

To test if the effects of EETs are conserved in mammals, we performed competitive whole bone marrow (WBM) transplantation in mice. 20,000 CD45.1 WBM cells were treated with 11,12-EET or DMSO for 4hrs, at room temperature. After washing off the chemicals, the treated marrow cells were competitively transplanted with 200,000 non-treated CD45.2 WBM. Consistent with results from zebrafish, 11,12-EET also enhanced short-term donor-derived WBC (white blood cell) chimerism by 4 wpt in mice. The effect was particularly prominent in myeloid cells, the earliest indicator of engraftment (Figure 3.2A). EET-treated WBM yielded enhanced repopulation, relative to control, for at least 24 weeks, as indicated by the increased number of recipients with long-term multi-lineage engraftment (Figure 3.2B). Enhanced short-term and long-term engraftment suggest that EET may impact both LT-HSC and progenitor cells, perhaps by establishing a competitive advantage at the very early stage of engraftment.

To genetically modify the concentration of EETs, we utilized *Tg*(*Tie2:CYP2C8*) mice, which overexpresses one of the human cytochrome P450 epoxygenases, *CYP2C8*, under the regulation of mouse *Tie2* promoter (Lee et al., 2010; Panigrahy et al., 2011a) (Figure 3.1A). Tie2 is expressed by endothelial cells and HSPCs (Arai et

al., 2004). These transgenic mice produce higher level of EETs than their wild type siblings (Lee et al., 2010; Panigrahy et al., 2011a). At steady-state conditions, *Tg*(*Tie2:CYP2C8*) mice have normal peripheral blood cell counts (Figure 3.3A) and numbers of HSPCs in the bone marrow (Figure 3.3B). We performed a limiting dilution competitive transplant to further challenge the HSPCs (Figure 3.3C), and found that *Tg(Tie2:CYP2C8)* donor marrow cells had a 4-fold increase of long-term competitive repopulating units (Figure 3.3D, Table 3.1). The difference between transplantation and homeostatic hematopoiesis indicates the biological aspect regulated by EET is specifically involved in HSPC engraftment.

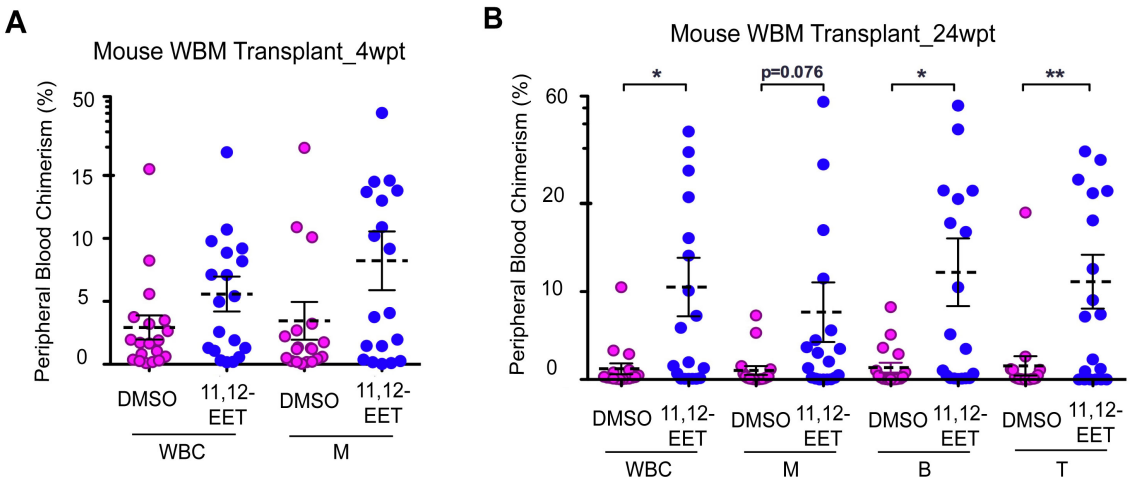

Figure 3.2. EET treatment enhances marrow engraftment capabilities in mammals.

Mouse whole bone marrow (WBM) competitive transplant: DMSO or 2μM 11,12-EET treated 20,000 CD45.1 bone marrow cells were transplanted together with 200,000 untreated CD45.2 bone marrow cells. WBC, white blood cell; M, myeloid cells. B, B cells; T, T cells. * Student's t test p values < 0.05, ** student's t test p values<0.005.
(A) EET enhanced short-term engraftment at 4wpt.
(B) EET enhanced long-term multilineage engraftment at 24wpt.

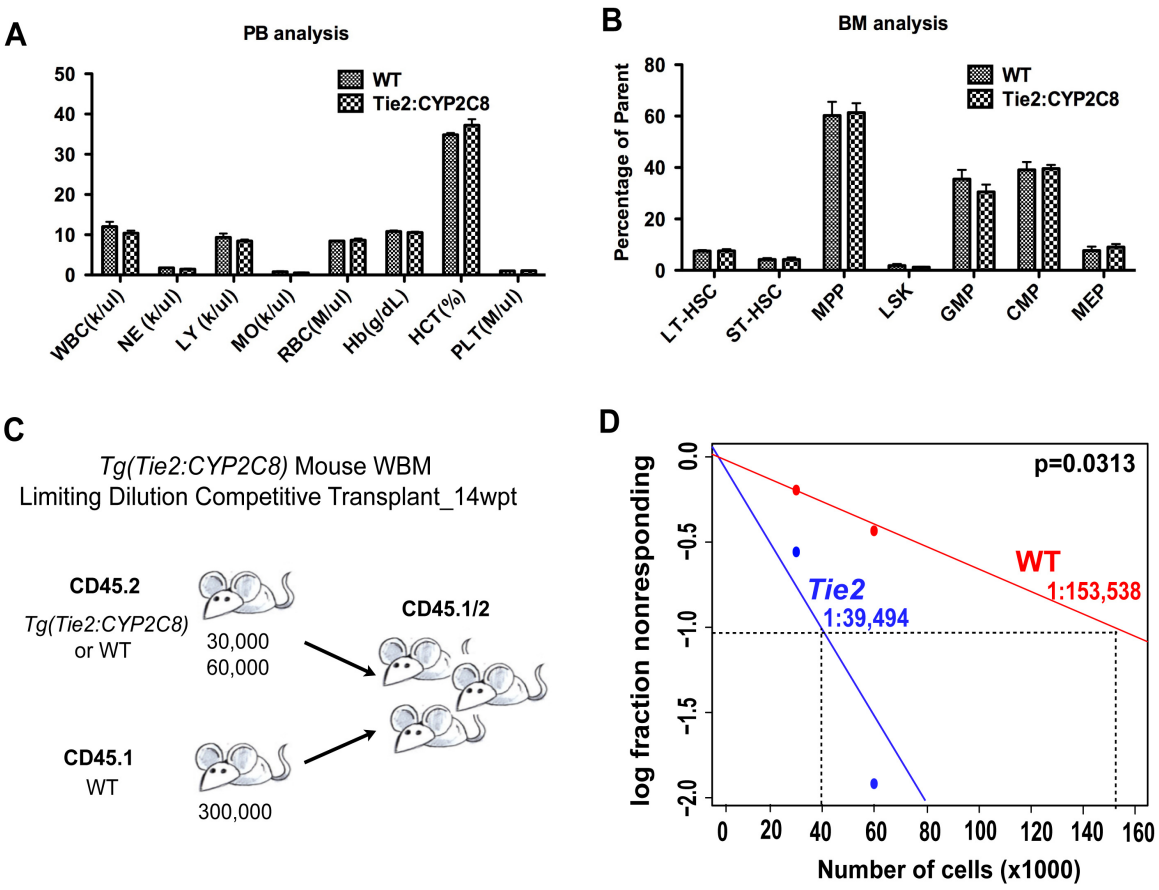

Figure 3.3. *Tg(Tie2:CYP2C8)* mice have normal hematopoiesis at homeostasis but competitive advantage in transplantation.

(A) Complete blood count (CBC) of the *Tg(Tie2:CYP2C8)* mice (n=4). WBC, white blood cell; NE, neutrophil granulocytes; LY, lymphocytes; MO, monocytes; RBC, red blood cells; Hb, hemoglobin; HCT, hematocrit; PLT, platelets.
(B) Bone marrow analysis of the *Tg(Tie2:CYP2C8)* mice (n=3). LT-HSC, long-term HSC (Lin- c-Kit+Sca-1+CD150+CD48-); ST-HSC, short-term HSC (Lin- c-Kit+Sca-1+CD150+CD48+); MPP, multipotent progenitor (Lin- c-Kit+Sca-1+CD150-CD48+); LSK: Lin-Sca-1+c-Kit+; GMP: granulocyte-macrophage progenitor (Lin- c-Kit+Sca-1-CD34+FcγR^{high}); CMP: common myeloid progenitor (Lin- c-Kit+Sca-1-CD34+FcgR^{mid}); MEP: megakaryocyte-erythroid progenitor (Lin- c-Kit+Sca-1-CD34-FcgR^{low}).
(C-D) Limiting dilution competitive transplant with *Tg(Tie2:CYP2C8).* 30,000 or 60,000 wild type or transgenic CD45.2 whole bone marrow cells were transplanted with 300,000 CD45.1 wild type marrow cells, into CD45.1/2 recipients. The frequency of long-term competitive repopulating unit (CRU) was calculated by ELDA (Hu and Smyth, 2009).

Table 3.1. *Tg(Tie2:CYP2C8)* Limiting Dilution Competitive Transplantation_14wpt

	Peripheral Blood CD45.2+CD45.1- Chimerism			
	Total	Myeloid	B Cells	T Cells
WT_30k_001	0.023	0	0	0.12
WT_30k_003	1.76	0.27	3.36	1.41
WT_30k_004	0.048	0.033	0.096	0
WT_30k_005	**6.46**	**18.7**	**1.91**	**2.87**
WT_30k_006	2.29	1.43	3.82	0.25
WT_30k_007	0.38	0.12	0.32	0
2C8_30k_001	0.012	0.048	0	0
2C8_30k_002	0.21	0.036	0.036	0
2C8_30k_003	**2.37**	**1.4**	**1.28**	**5.7**
2C8_30k_004	0.19	0.19	0.029	0.21
2C8_30k_005	**50.9**	**14.2**	**75.1**	**66.7**
2C8_30k_006	0.11	0.039	0.17	0.1
2C8_30k_007	**11.2**	**12**	**14.2**	**5.49**
WT_60k_001	0.77	0.4	1.05	0.98
WT_60k_002	0.069	0.072	0	0.035
WT_60k_003	0.52	1.1	0.57	0
WT_60k_005	**5.14**	**2.27**	**4.42**	**9.49**
WT_60k_006	0.11	0.082	0.069	0.048
WT_60k_007	**11.3**	**9.97**	**9.21**	**18.2**
2C8_60k_001	**2.87**	**2.13**	**1.39**	**7.49**
2C8_60k_002	**3.36**	**2.23**	**1.93**	**8.8**
2C8_60k_003	**23.7**	**19.8**	**30.8**	**18.2**
2C8_60k_004	**11.4**	**4.16**	**13**	**18.6**
2C8_60k_005	0.73	0.3	1.18	0.14
2C8_60k_006	**1.94**	**1.09**	**1.01**	**5.01**
2C8_60k_007	**11.6**	**4.23**	**12.7**	**17.1**

2C8: *Tie2:CYP2C8* transgenic mice; WT: Wild type mice
Mice with >1% chimerism in all three lineages (myeloid, B and T cells) were considered as engraftment (as shaded in grey).

EETs Induce *runx1* Transcription and HSPC Engraftment During Zebrafish Embryo Development

To understand the molecular mechanism of EET regulation of HSPC engraftment, EET effects on HSPCs during embryo development were studied. In the zebrafish embryo, HSCs emerge from the hemogenic endothelium of the AGM (aorta-gonad-mesonephros region), similar to mammals (Bertrand et al., 2010; Boisset et al., 2010; Davidson and Zon, 2004; Kissa and Herbomel, 2010; Orkin and Zon, 2008). The HSPCs enter circulation, then travel to and engraft in the caudal hematopoietic tissue (CHT), a secondary hematopoietic site equivalent to the mouse fetal liver (Figure 3.4A) (Murayama et al., 2006; Orkin and Zon, 2008). The trafficking of HSPCs in embryos shares some similar signaling pathways employed by adult HSCs during homing and engraftment, such as SCF/C-KIT and SDF-1/CXCR4 (Laird et at, 2008).

Various doses of 11,12-EET and different treatment time windows were studied during HSPC development in zebrafish embryos. Treatment of embryos with 11,12-EET during 24-36 hpf dramatically increased the embryonic HSPC marker, *runx1* (Figure 3.4B) (Kalev-Zylinska et al., 2002; Soza-Ried et al., 2010). To examine the later effect of *runx1* upregulation in AGM, the HSPC behavior during CHT colonization was studied. EET was washed off at 48 hpf and the embryos were allowed to develop for another 24 hrs, during which time HSPCs from AGM would migrate to and engraft in the CHT. The number of HSPCs in CHT was quantified by using a transgenic zebrafish expressing *mCherry* under the mouse *Runx1+23* enhancer that specifically labels definitive HSPCs (Bee et al., 2009; Nottingham et al.,

2007). Confocal microscopy showed a significant increase of the number of HSPCs colonizing the CHT region with EET (Figure 3.4C, D).

We confirmed the increase of number of HSPCs engrafting the CHT with another conserved embryonic HSPC marker, *cmyb* (Figure 3.4E). EET also induced robust *runx1* expression ectopically in the posterior tail region (Figure 3.4F). In E14.5 mouse embryos, *Runx1* was detected in the developing limb digits, a region anatomically similar to zebrafish fin fold (Levanon et al., 2001). These *runx1+* cells in zebrafish tail might represent a population of undifferentiated precursor cells for the future tail fin. EETs specifically induce *runx1* in stem and progenitor cells in the hemogenic endothelium and tail.

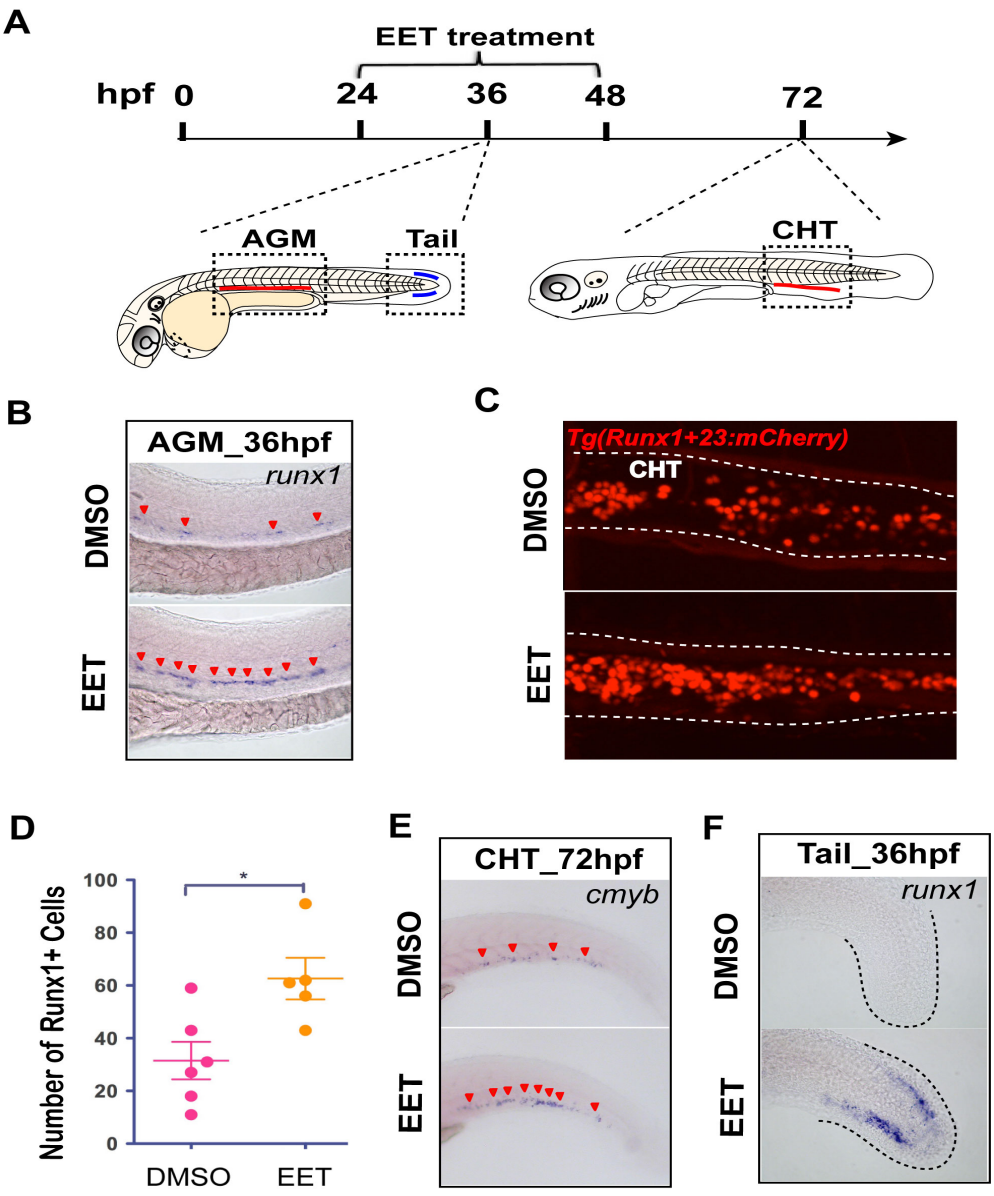

Figure 3.4. EETs induce *runx1* expression and enhance HSPC engraftment in zebrafish embryos

(A) Schematic of HSPC development and chemical treatment in zebrafish embryos. hpf, hour post fertilization; AGM, aorta-gonad-mesonephros; CHT, caudal hematopoietic tissue.
(B) EET increased *runx1* expression in the AGM.
(C-D) EET enhanced the number of HSPCs engrafted in the CHT. Using a transgenic zebrafish expressing *mCherry* under the mouse *Runx1+23* enhancer to specifically label definitive HSPCs. *mCherry+* cell number was quantified with ImageJ. * Student's t test p values < 0.05.
(E) EET increased HSPC marker *cmyb* in the CHT at 72hpf.
(F) EET induced ectopic *runx1* in the non-hematopoietic cells in the tail.

Immediate Induction of AP-1 Transcription Factors Is Required for EET-Induced *runx1* Expression

Although *runx1* has been well accepted as a HSC marker in embryos, the mechanism by which *runx1* transcription is induced during development is not completely understood. To study how EETs induced *runx1* expression, we performed microarray analysis on EET-treated 36 hpf embryos. Surprisingly, only 68 transcripts were up or down-regulated by EET treatment, including a subset of genes upregulated in zebrafish tail fin regeneration, such as *fn1* and *mvp*, and genes essential for cholesterol metabolism, such as *hmgcs1* and *cyp51a* (Table 3.2 and 3.3) (Yoshinari et al., 2009). Most of the up-regulated genes were confirmed by whole-mount *in situ* hybridization. A group of transcription factors belonging to the AP-1 (Activation Protein 1) family, such as *fosl2* and *junb*, were both induced by EET treatment and fin regeneration (Figure 3.5A).

AP-1 transcripts can be rapidly induced by many stimuli (Jochum et al., 2001). Fixing embryos at different time-points upon EET treatment showed a robust induction of AP-1 within 1 hr (25 hpf) and *runx1* after 4 hrs (28 hpf) (Figure 3.5B, C). To examine if AP-1 was an immediate early gene induced by EET, cycloheximide was used to block translation. *Runx1* transcription was completely blocked by cycloheximide at 28 hpf (Figure 3.5D), but not AP-1 expression at 25 hpf (Figure 3.5E). EET-induced signaling transduction directly activated AP-1 transcription, while *runx1* upregulation is dependent on the *de novo* protein synthesis of one or more upstream regulators.

Table 3.2 Microarray Analysis of 11,12-EET-treated 36 hpf Zebrafish Embryos List of Genes with Increased Expression

probe	mean.fc	q	gene
Dr.14719.1.A1_at	4.359432	0	ARF1
Dr.24471.1.A1_at	2.896713	0.079602	PALLADIN
Dr.19888.1.S1_at	2.52457	0	VED
DrAffx.2.81.A1_at	2.114362	0.015873	CYP51A1
Dr.12110.1.S1_at	2.097974	0	SC4MOL
Dr.4938.1.S1_at	1.998925	0.015873	FADS2
Dr.22219.1.S1_at	1.997586	0.079602	ACTN2
Dr.16634.1.A1_at	1.749673	0.015873	AK128797
Dr.20131.2.A1_at	1.516192	0	CLU
Dr.13651.1.A1_at	1.47763	0.028986	FBP1
Dr.16392.1.A1_at	1.413491	0	C6
Dr.11572.1.A1_at	1.30334	0.015873	WDR34
Dr.2051.1.S1_at	1.158936	0	HMGCS1
Dr.25093.1.A1_s_at	1.157838	0.037736	TAR3
Dr.24233.1.S1_at	1.148094	0	FN1
Dr.9617.1.A1_at	1.094222	0	SOCS3
Dr.23811.1.A1_at	1.072796	0.079602	MOGAT1
Dr.10130.2.A1_at	0.971631	0	FOSL2
Dr.967.1.S1_at	0.967481	0	MMP9
Dr.9642.1.A1_at	0.844911	0.015873	ASPN
Dr.19560.1.S1_at	0.781171	0.028986	INSIG1
Dr.22334.1.S1_at	0.747641	0	MS4A4A / ms4a17a.11
Dr.19560.1.S2_at	0.720476	0.015873	INSIG1
Dr.2487.1.S1_at	0.710377	0.037736	UPB1
Dr.10326.1.S1_at	0.704015	0.079602	JUNB
Dr.1089.1.S1_at	0.701168	0.015873	THBS3
Dr.25191.1.S1_at	0.635516	0.015873	IDH1
Dr.737.1.A1_at	0.543973	0.037736	JUNB
Dr.26534.1.A1_at	0.502621	0.079602	INSIG1
Dr.7010.1.S1_at	0.475427	0.074713	ELOVL7
Dr.24562.1.S1_a_at	0.387242	0.066667	MVP

Table 3.3 Microarray Analysis of 11,12-EET-treated 36 hpf Zebrafish Embryos List of Genes with Decreased Expression

probe	mean.fc	q	gene
Dr.20008.1.S1_at	-0.234813	0.074713	SLC25A5
AFFX-Dr-acta1-5_at	-0.290608	0.037736	ACTA1
Dr.6826.1.S1_at	-0.381291	0.083333	COL1A1b
Dr.20272.1.A1_at	-0.395476	0.034722	SNRP70
Dr.5531.3.S1_at	-0.405781	0.015873	KRT15
Dr.12425.1.S1_at	-0.415358	0.034722	KRT17
Dr.1377.1.A1_at	-0.440683	0.015873	COL1A2
Dr.24292.5.S1_at	-0.467295	0	KRT15
Dr.15266.1.A1_at	-0.51983	0.015873	CHRNG
Dr.24487.1.A1_at	-0.526189	0.079602	KRT8
Dr.3484.1.S1_at	-0.529253	0.074713	sap30bp
Dr.5439.2.S1_at	-0.566989	0.079602	NSFL1C
Dr.2539.1.A1_at	-0.577588	0.015873	wu:fy25c05
Dr.24399.1.A1_at	-0.579821	0	ARGLU1B
Dr.4681.1.A1_at	-0.61717	0	TTN
Dr.23502.1.A1_at	-0.781435	0	APOE
Dr.14514.1.S1_a_at	-0.999159	0	RPL13
Dr.18173.1.A1_at	-1.131191	0.015873	MPP2
Dr.17747.1.S1_at	-1.366207	0.015873	SCEL
Dr.9478.4.S1_at	-3.077714	0.079602	MPX
Dr.12749.1.A1_at	-3.319542	0.023256	RHCG

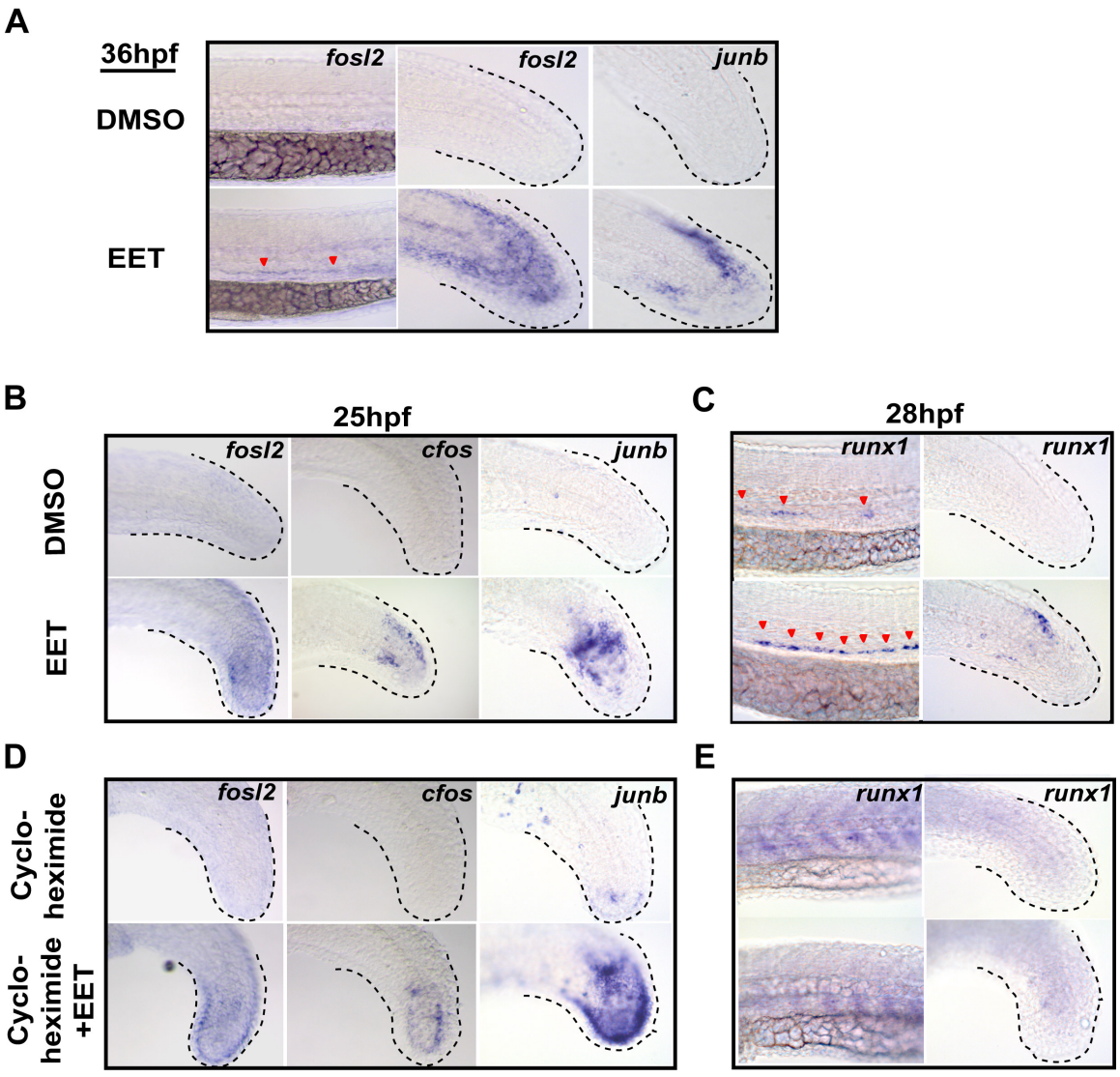

Figure 3.5. EET induces AP-1 transcription, but not *runx1* transcription, independent of translation.

All treatments started at 24 hpf with 5uM 11,12-EET.
(A) EET induced AP-1 family transcription factors, represented by *fosl2* and *junb*.
(B) EET quickly induced AP-1 within 1hr of treatment.
(C) *Runx1* was induced by EET after 4hr of treatment.
(D) AP-1 induction was not dependent on *de novo* protein synthesis. Wild type embryos were incubated with 300μM cycloheximide, a translation blocker, for 30 min before the addition of EET.
(E) *Runx1* transcription required *de novo* protein synthesis. Same treatment with cycloheximide as (C) blocked *runx1* transcription.

To evaluate the function of AP-1 during AGM HSC induction, AP-1 members were individually knocked down with anti-sense morpholinos in zebrafish embryos. *fosl2* at a high dose completely inhibited EET-induced upregulation of *runx1* in both AGM and tail, without affecting basal-level *runx1* expression (Figure 3.6). Double knockdown of *fosl2* and *cfos*, at a much lower dose, synergistically blocked both EET-induced and basal-level *runx1* transcription, showing the Fos family is required for both endogenous and induced *runx1* transcription (Figure 3.6). Fos members form heterodimers with Jun family for transcriptional regulation (Jochum et al., 2001). Different Jun members were studied by morpholino knockdown. The results showed the specific requirement for *junb*, but not *c-jun*, to induce *runx1* transcription both in the AGM and tail (Figure 3.6). At a slightly higher dose, *Junb* morphants had circulation defects. The lower doses of *junb* morpholino demonstrated specific decreased *runx1* expression independent of circulation.

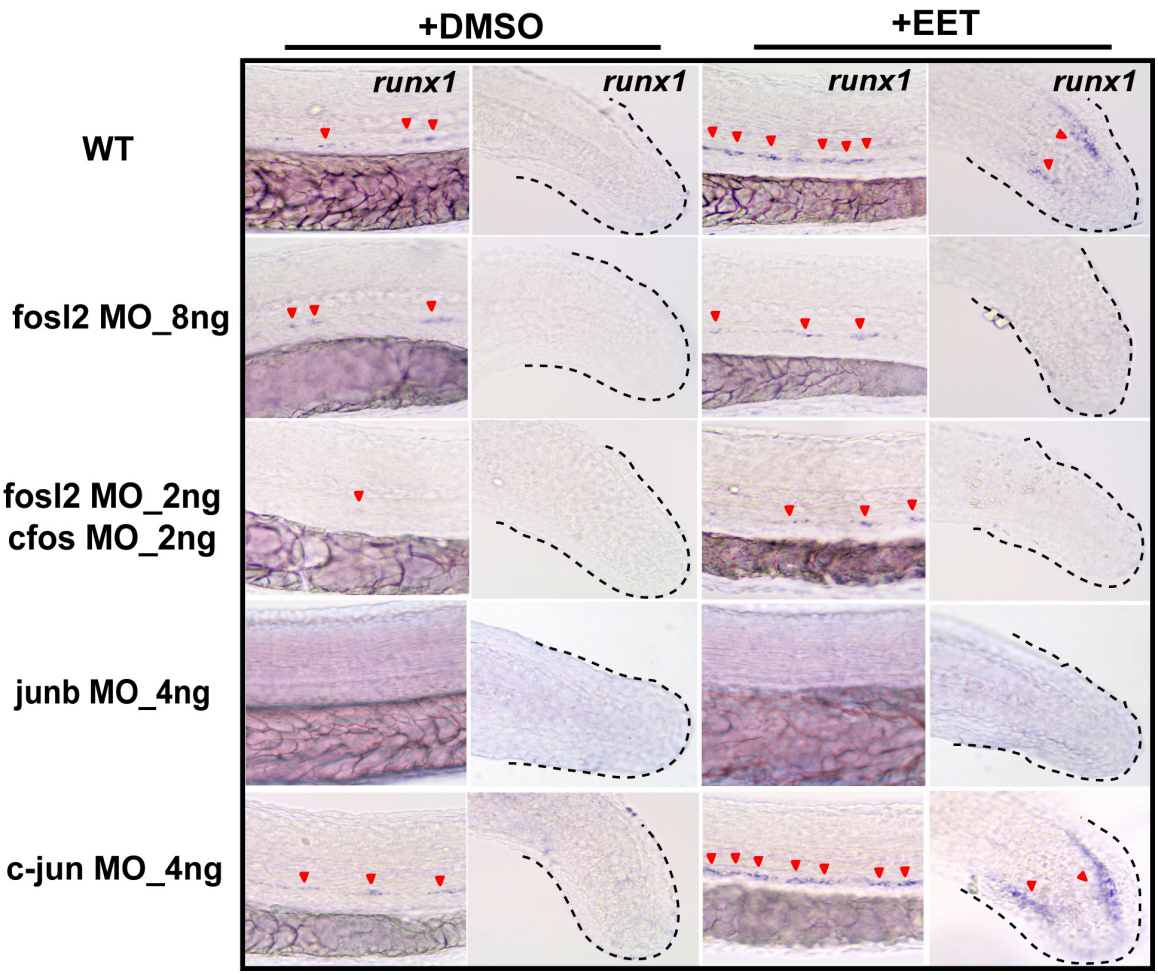

Figure 3.6. AP-1 transcription factors are required for *runx1* upregulation.

AP-1 was required for *runx1* transcription. 8ng morpholino (MO) targeting *fosl2* ATG site did not decrease basal level of *runx1* (DMSO), but blocked EET-induced *runx1* transcription (EET). Double morpholinos against both *fosl2* and *cfos* at low doses (2ng each) synergistically decreased both the basal-level and EET-induced *runx1*. Morpholino against *junb* (2ng) also completely inhibited *runx1* transcription. Wild-type zebrafish embryos were injected with *c-jun* morpholino at 4ng/embryo, the highest concentration tolerated by the embryos. Knocking down *c-jun* did not affect EET-induced *runx1* expression.

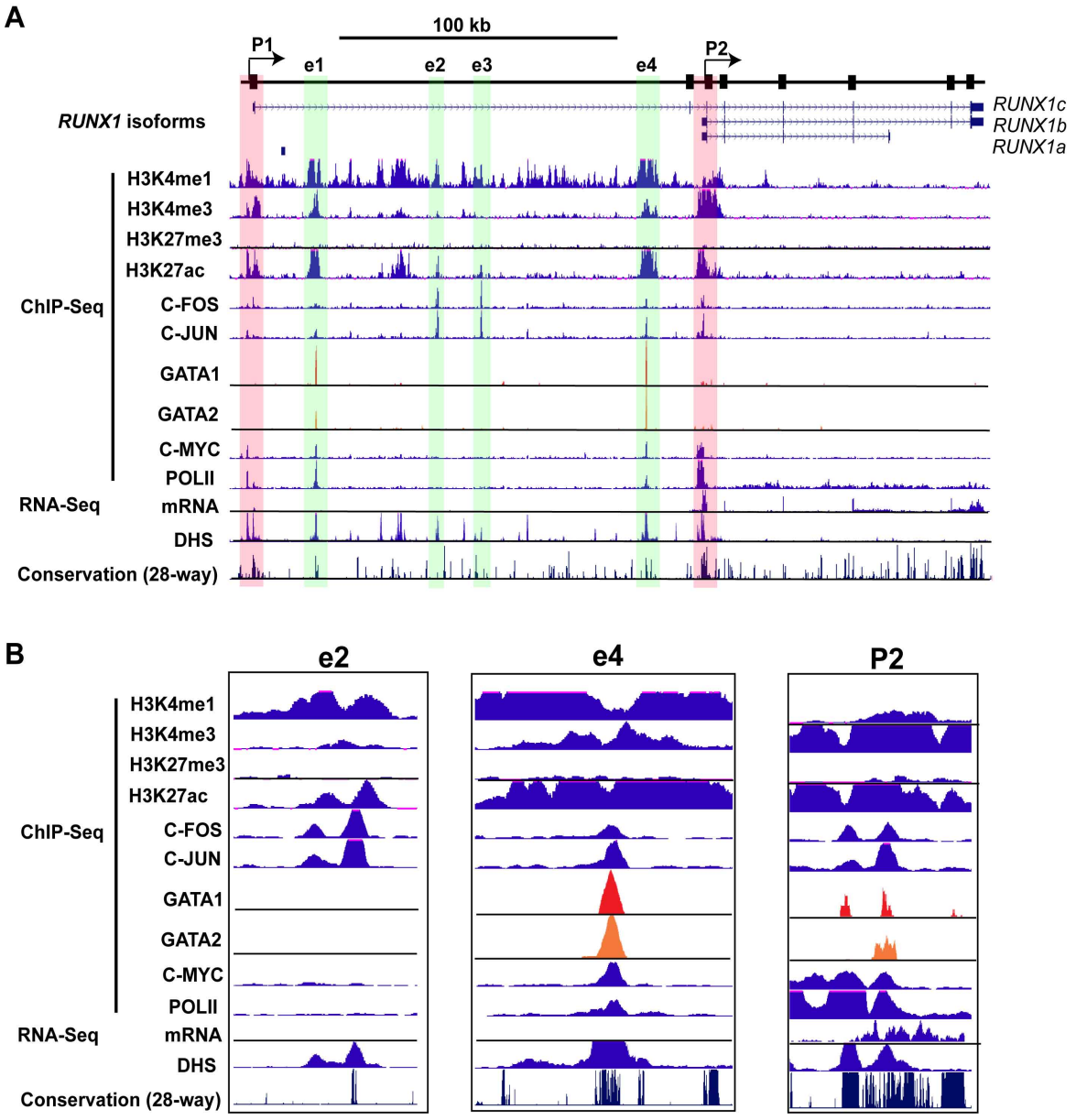

Figure 3.7. AP-1 binding sites on *RUNX1* DNA in human K562 cells

(A) ChIP-Seq, RNA-Seq, DHS (DNase I Hypersensitivity) mapping, and 28-way conservation analysis for human *RUNX1* locus were retrieved and analyzed on Encode. Two representatives of the AP-1 family member, C-FOS and C-JUN, showed multiple identical peaks, including the two alternative promoters (P1 and P2), and the enhancer region within the first intron (e1, e2, e3 and e4).
(B) Zoom-in images of the AP-1 binding sites on *RUNX1*. AP-1 binding on e2, e4, and P2 correlates with transcription activation mark H3K27ac (Creyghton et al., 2010), and open chromatin structure by DHS. The binding on e4 and P2 are highly evolutionarily conserved.

These observations on Jun family member knockdown are consistent with the mouse mutant phenotype. *Junb*-deficient embryos died in utero due to vascular defects (Jochum et al., 2001). Knockout of *c-Jun* did not cause any abnormality intrinsic to the hematopoietic or endothelial compartment (Eferl et al., 1999). In addition, myeloid-specific deficiency of *Junb* caused myeloproliferative disorder, supporting the important role of *Junb* in hematopoietic cells (Passegue et al., 2001).

The genetic studies above demonstrated that AP-1 is upstream of *runx1*. To evaluate if AP-1 directly binds to *runx1* transcriptional regulatory elements, we further examined ChIP-Seq data from the ENCODE Consortium database (Birney et al., 2007). The transcription of *RUNX1* utilizes two promoters, spaced by a >100kb enhancer region (Bee et al., 2009; Challen and Goodell, 2010). ChIP-Seq in K562 human leukemia cells showed strong binding sites of AP-1 family members at the evolutionarily conserved regions of *RUNX1* promoters, especially P2, as well as at the enhancer sites in the first intron (Figure 3.7). Different AP-1 members had the same binding sites on the *RUNX1* regulatory region. This suggests that AP-1 is a direct regulator of *RUNX1*.

EETs Signal Through a Gα12/13-Mediated Receptor

Despite the dramatic biological effects of EETs, efforts to identify and clone the EET receptor have been unsuccessful. Several recent studies indicated that EETs bind to a receptor on the extracellular membrane (Chen et al., 2007; Yang et al., 2008). Using UV-activated cross-linking between radioactively labeled EET analog and cells, an unknown 47 kDa cell membrane protein was shown to directly bind

EETs (Chen et al., 2011). The estimated size of the receptor is within the typical range of G protein-couple receptors (GPCR). Due to the similarity between EETs and other eicosanoids, the majority of which target GPCRs, we hypothesize that EETs might also bind one or multiple GPCR(s). All GPCRs are coupled to at least one type of the G-trimeric proteins composed of α-, β-, γ- subunits, required for activating diverse secondary signaling messengers. Even though more than 1000 GPCRs have been annotated in the human genome, there are a fairly small number of Gα subunits: Gαs, Gαi, Gαq, Gα12/13 (Lappano and Maggiolini, 2011). Different methods were used to block Gα proteins in zebrafish embryos: chemical inhibitors for Gαs (adenylate cyclase inhibitor SQ22536, PKA inhibitor H89), injecting pertussis toxin mRNA to block Gαi (Slusarski et al., 1997), and morpholino knockdown of individual Gαq (*gna11, gna14, gna15/16* and *gnaq*) and Gα12/13 (*gna12, gna13a, gna13b*). Blocking Gαs or Gαi did not affect EET-induced *runx1* expression (Figure 3.8A,B); however, knocking down the zebrafish orthologs of human *GNA13*, *gna13a* and *gna13b* together, or *gna12* alone partially blocked the EET effects (Figure 3.8C,D). Considering the potential redundancy of Gα12 and Gα13, we did triple knockdown of *gna12, gna13a* and *gna13b*. The triple morpholinos completely blocked EET-induced expression of *runx1*, *fosl2* and genes involved in cholesterol metabolism, such as *hmgcs1* (Figure 3.8E). This strongly supports that EETs act through a receptor mediated by Gα12/13.

Figure 3.8 EETs signal through a Gα12/13-mediated receptor.

(A) Inhibiting Gas downstream signaling with adenylate cyclase inhibitor SQ22536 (50uM) did not block EET-induced *runx1* expression.
(B) Representative images of knocking down *gna13a/b* or *gna12* alone. Only partial inhibition was observed.
(C) Quantification of the effects of inhibiting Gαs or Gαi on *runx1* expression. Embryos were categorized into two groups with either normal or increased *runx1* expression level. The bar graph represented the percentage of embryos in each group. PtxA, pertussis toxin A, 3pg, inhibiting GαI; H89, 5μM, PKA inhibitor; SQ22536, 50μM.
(D) Synergistic effects of knocking down *gna12/13* on *runx1* expression in zebrafish embryos. Morpholinos against *gna13a/b* (1ng each) or *gna12* (2ng) partially blocked *runx1* expression. Triple morpholinos against *gna12, gna13a* and *gna13b* (0.67ng each) completely blocked *runx1*. Embryos were categorized into three groups with either decreased, normal or increased *runx1* expression level. The bar graph represented the percentage of embryos in each group.
(E) *Gna12/13a/13b* is required for EET-induced multiple gene expression (see also Figure S5).

Figure 3.8 EETs signal through a Gα12/13-mediated receptor. (Continued)

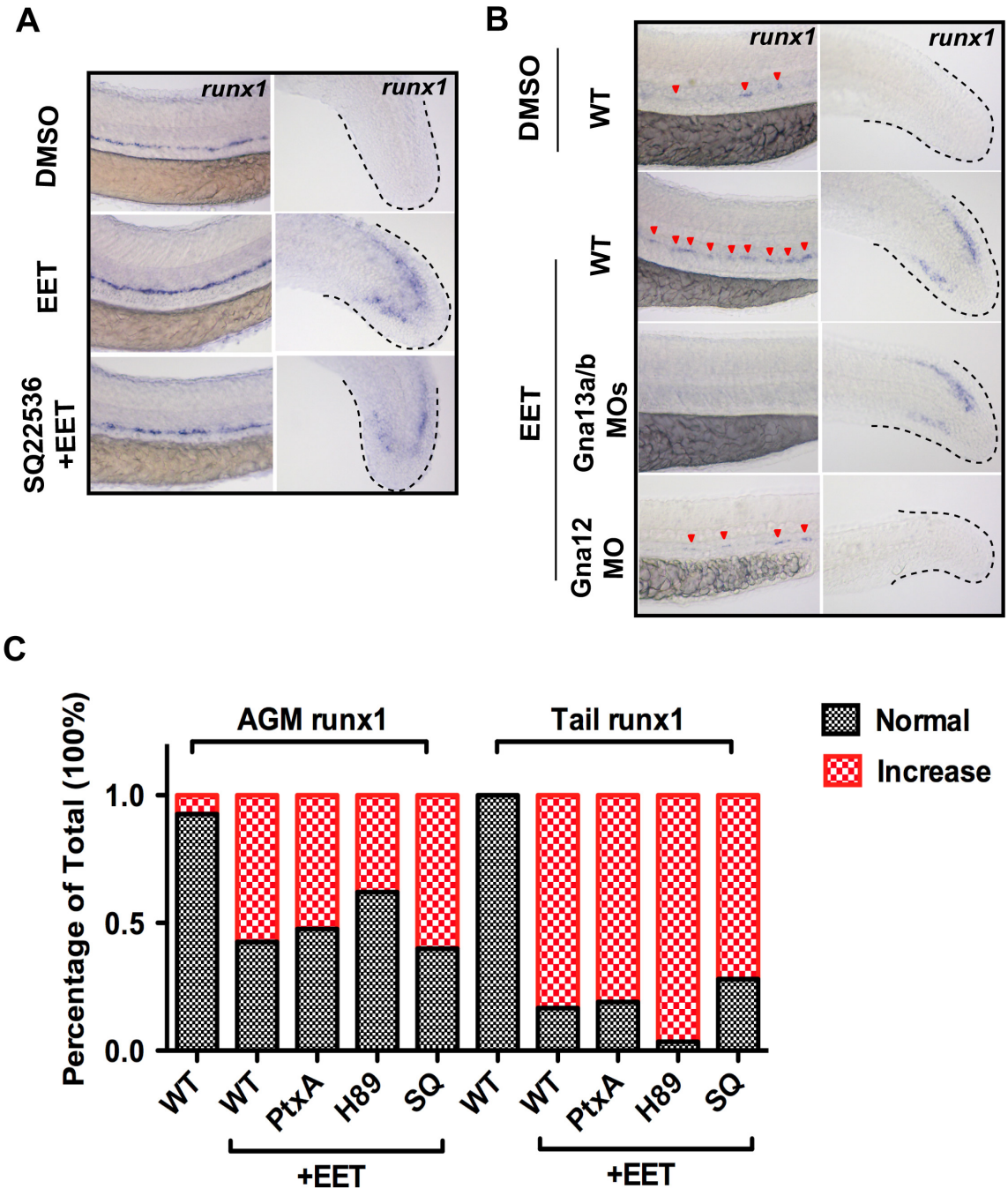

Figure 3.8 EETs signal through a Gα12/13-mediated receptor. (Continued)

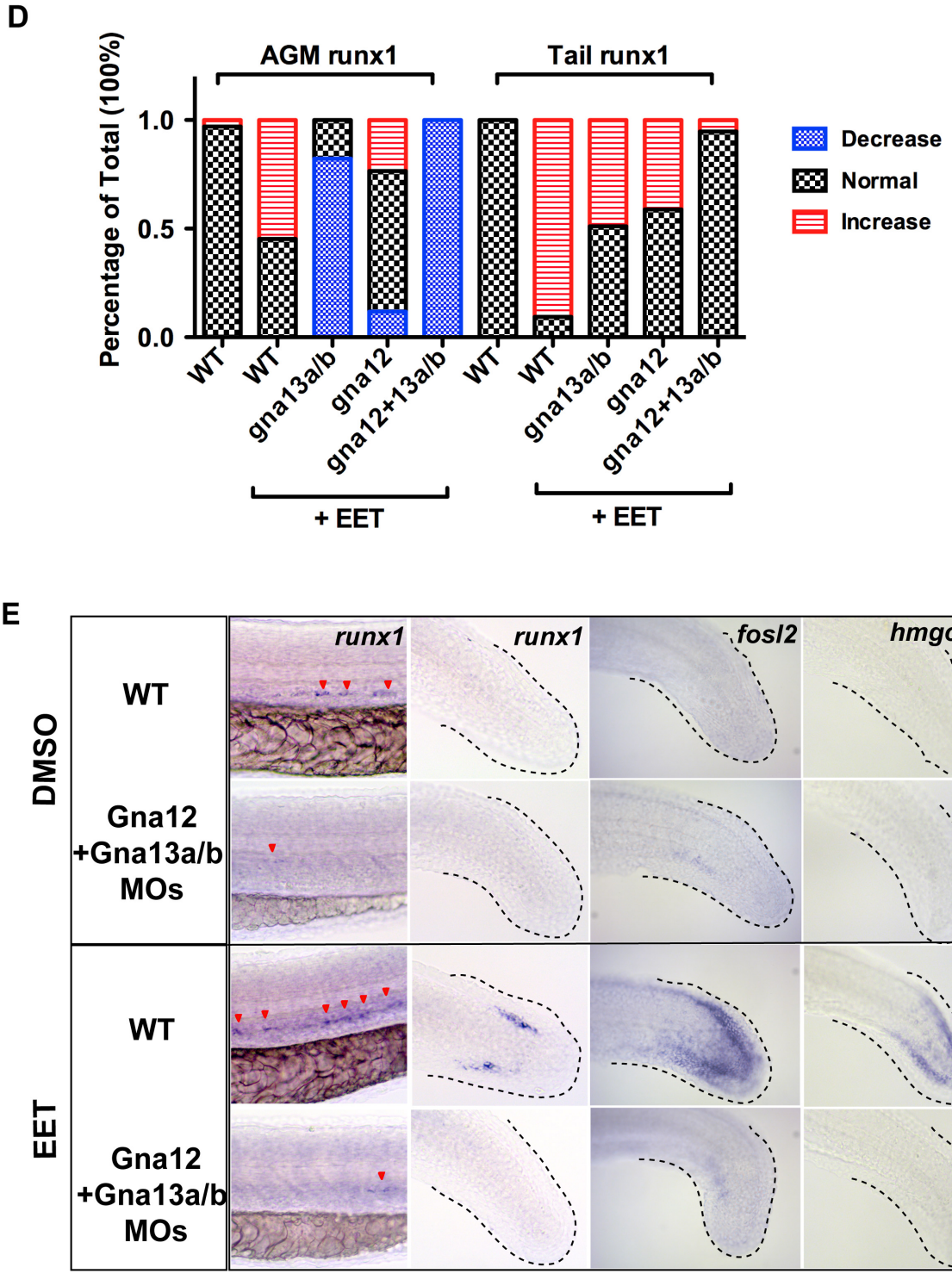

Activation of PI3K Is Required for EET-Induced AP-1 and *runx1* Expression

Many different signaling pathways have been proposed to be downstream of EETs, in a cell- and tissue-type dependent manner (Michaelis and Fleming, 2006; Panigrahy et al., 2011b; Yang et al., 2007). In search for the pathway(s) responsible for the EET effects on HSPC engraftment, we performed a chemical suppressor screen in zebrafish embryos. Upon EET treatment, upregulation of AP-1 and *runx1* are the earliest markers relevant to HSPCs. Using these markers, we examined if small molecules could inhibit the response to EETs.

We incubated 23.5 hpf embryos for 30 min with chemicals targeting the pathways previously reported to be downstream of EETs. 11,12-EET was added at 24 hpf (Figure 3.9A). Multiple PI3K inhibitors (LY294002, Wortmannin, and PI-103) completely suppressed EET-induced *runx1* expression, both in the AGM and the tail (Figure 3.9B). In contrast, MEK1/2 inhibitor (U0126) had no effect on *runx1* expression (Figure 3.9B). *fosl2* and *junb* expression were also blocked by LY294002, but not by U0126 (Figure 3.9C). LY294002 had a negligible effect on *hmgcs1*, while U0216 completely blocked *hmgcs1* (Figure 3.9D). The mutually exclusive effects of inhibiting PI3K and MAPK pathway provide an example where single ligand stimulation activates genetically separable signaling pathways.

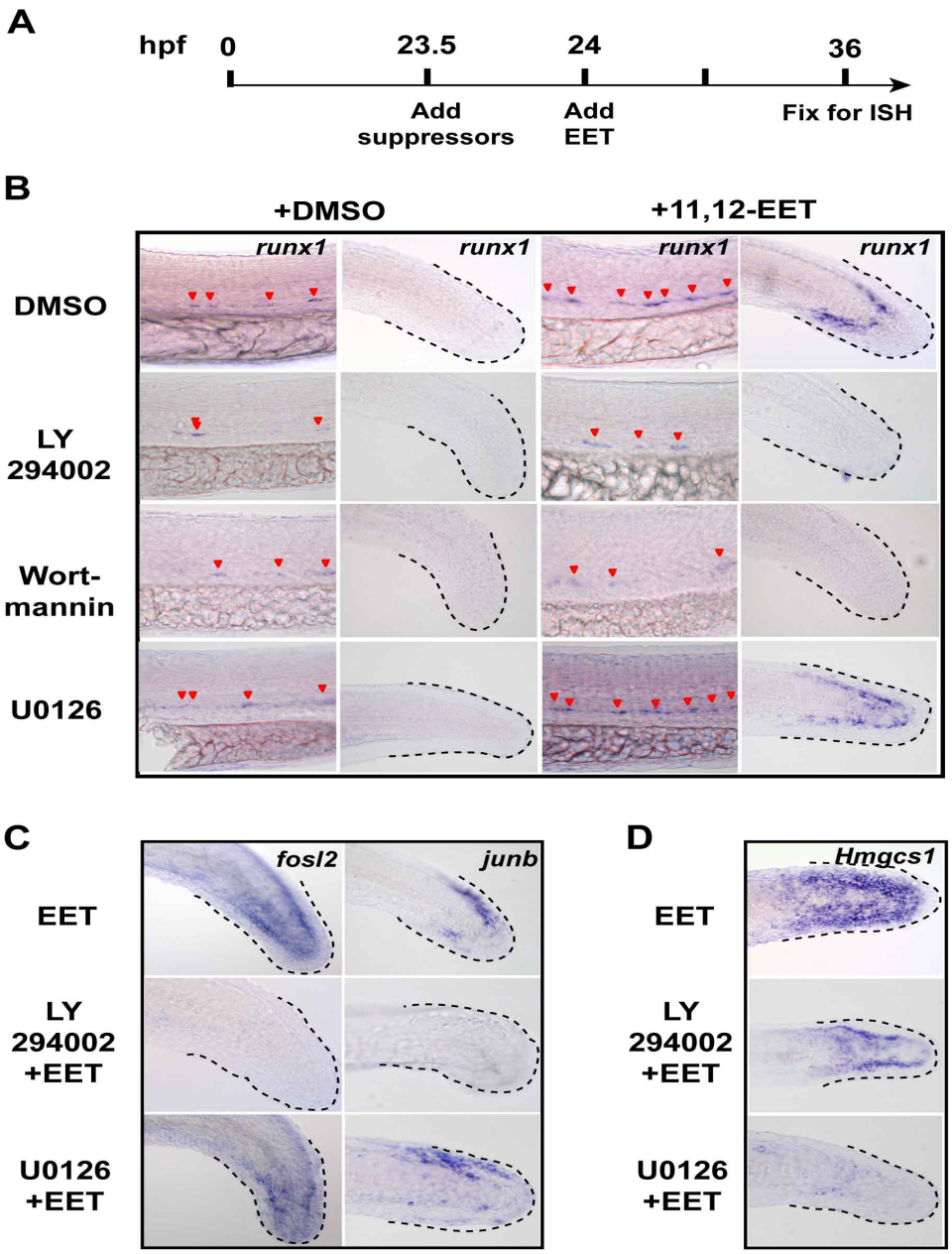

Figure 3.9. EET-induced PI3K activation leads to AP-1/*runx1* expression

(A) Schematic of chemical suppressor screen to identify EET downstream signaling pathways. ISH, *in situ* hybridization.
(B) PI3K inhibitors, LY294002 (10μM) and Wortmannin (2μM) completely blocked EET-induced induction of *runx1* in both AGM and tail, while MEK1/2 inhibitor U0126 (30μM) had no effect on *runx1* expression.
(C) Inhibiting PI3K , not MEK1/2, completely blocked EET-induced AP-1 expression.
(D) Inhibiting MEK1/2, not PI3K, completely blocked EET-induced cholesterol metabolism gene expression.

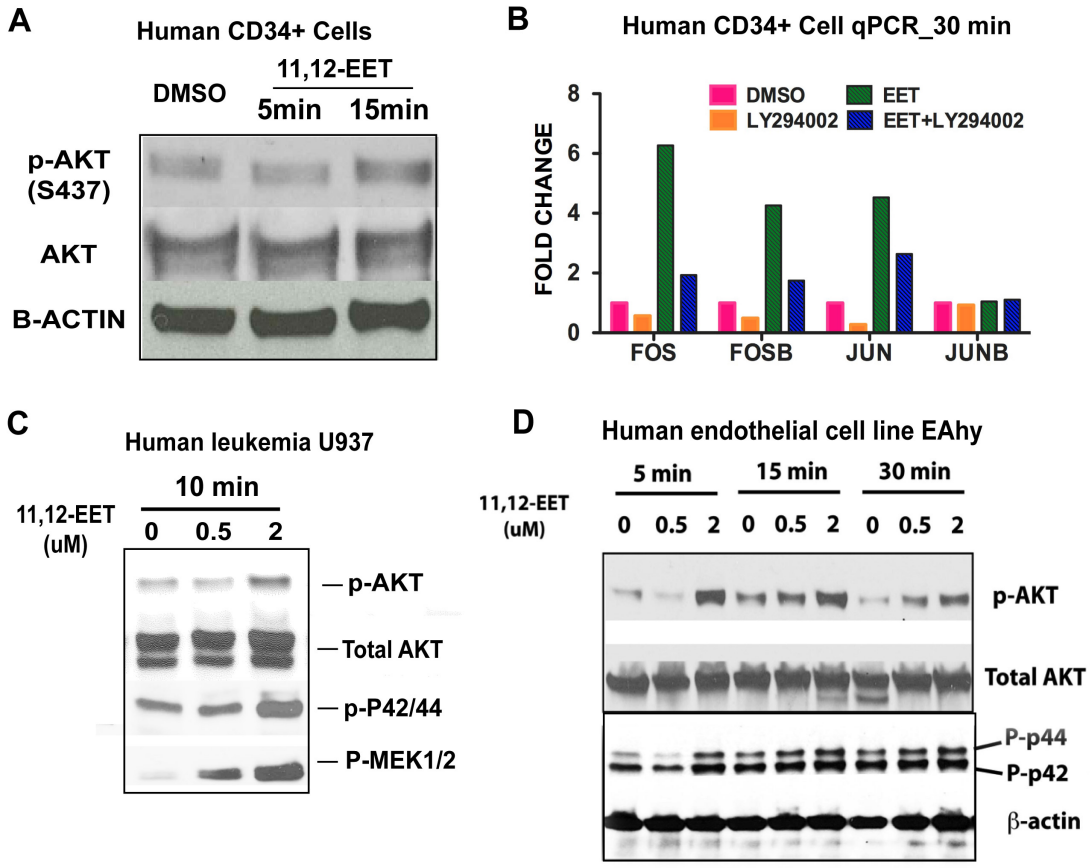

Figure 3.10 EETs induce PI3K activation and AP-1 transcription cell-autonomously.

(A) EET activated PI3K autonomously in human mobilized CD34+ HSPCs. Western blotting for phosphorylated AKT as an indicator of PI3K activation.
(B) EET induced the transcription of multiple AP-1 factors in human peripheral blood mobilized CD34+ HSPCs. Inhibition of PI3K with 10μM LY294002 reduced the magnitude of EET-induced AP-1 expression.
(C) EET activated PI3K and MAPK pathways in a cell-autonomous fashion in human leukemia cell line U937.
(D) EET activated PI3K and MAPK pathways in a cell-autonomous fashion in human immortalized endothelial cell line EAhy.

Activation of PI3K in HSPCs Is Required for the Enhancement of Engraftment

To test if the activation of these signaling pathways is autonomous to HSPCs, we performed western blot analysis on EET-treated human mobilized CD34+ HSPCs isolated from peripheral blood. EET quickly induced phosphorylation of AKT, as an indicator of PI3K activation (Figure 3.10A). qRT-PCR also confirmed that EET could induce multiple AP-1 members, especially the FOS family, in a PI3K-dependent manner (Figure 3.10B). Similarly, PI3K activation and ERK phosphorylation were also observed in human leukemia U937 and immortalized endothelial EAhy cell lines treated with EET (Figure 3.10C, D).

We tested if PI3K activation is responsible for enhanced transplantation engraftment. Mouse WBM was pre-incubated with LY294002 for 30 min before the addition of 11,12-EET. We found LY294002 blocked EET-induced enhancement of long-term multi-lineage engraftment in mice (Figure 3.11). The cell-autonomous activation of PI3K is completely required for enhancing HSPC engraftment.

To directly observe how EETs regulate HSPC behavior during engraftment, we studied HSPC engraftment during zebrafish embryo development. The process of HSPCs from AGM traveling to and engrafting CHT is comparable to the murine HSC trafficking from AGM to fetal liver (Murayama et al., 2006). We used the transgenic zebrafish described before (*Runx1+23:EGFP*, instead of *Runx1+23:mCherry*) to specifically label HSPCs (Tamplin et al, unpublished data). Endothelial cells were marked with *kdrl:DsRed*. The double transgenic embryos were treated with DMSO, 11,12-EET or LY294002 between 24-48 hpf. Chemicals were washed off and the embryos were imaged by time-lapse confocal between 54-64 hpf. At the beginning

of imaging, which is 54 hpf, HSPCs have already started migrating out of AGM and engrafting CHT. DMSO or EET-treated embryos had similar numbers of HSPCs that had already arrived at the CHT at this timepoint (Figure 3.12A), while LY-treated embryos had fewer engrafted cells (Figure 3.13A). Over the next 10 hrs, the number of HSPCs in DMSO or LY-treated embryos was relatively unchanged, while a significant accumulation of HSPCs was seen in EET-treated embryos (Figure 3.12A). Individual HSPCs were traced over time to observe their behavior. The migration routes of single cells were tracked using ImageJ (Figure 3.12B). We found EET dramatically enhanced HSPC migration. On average, HSPCs in EET-treated embryos migrated longer distance at a higher speed than in DMSO-treated embryos (Figure 3.12C, D).

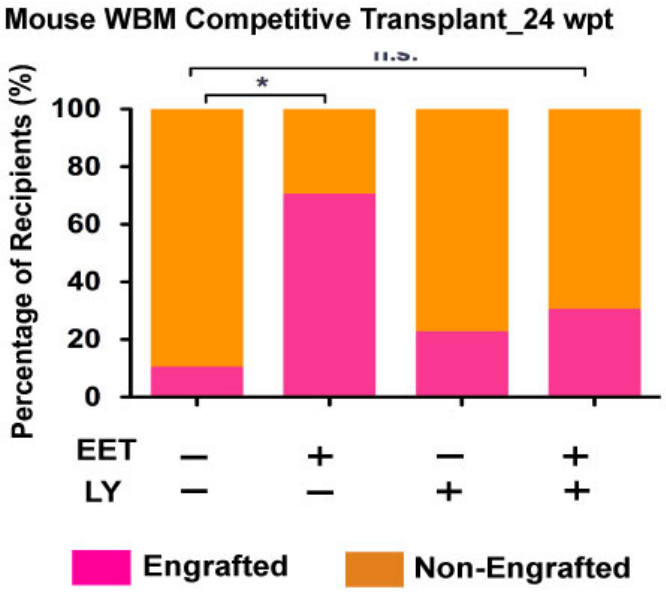

Figure 3.11 EETs enhance mouse engraftment in a PI3K-dependent manner.

20,000 CD45.1+ WBM cells were pre-incubated with DMSO or 10μM LY294002 for 30 min, before 2μM 11,12-EET was added and incubated for 4 hrs. * Student's t test p values < 0.05; n.s., not significant.

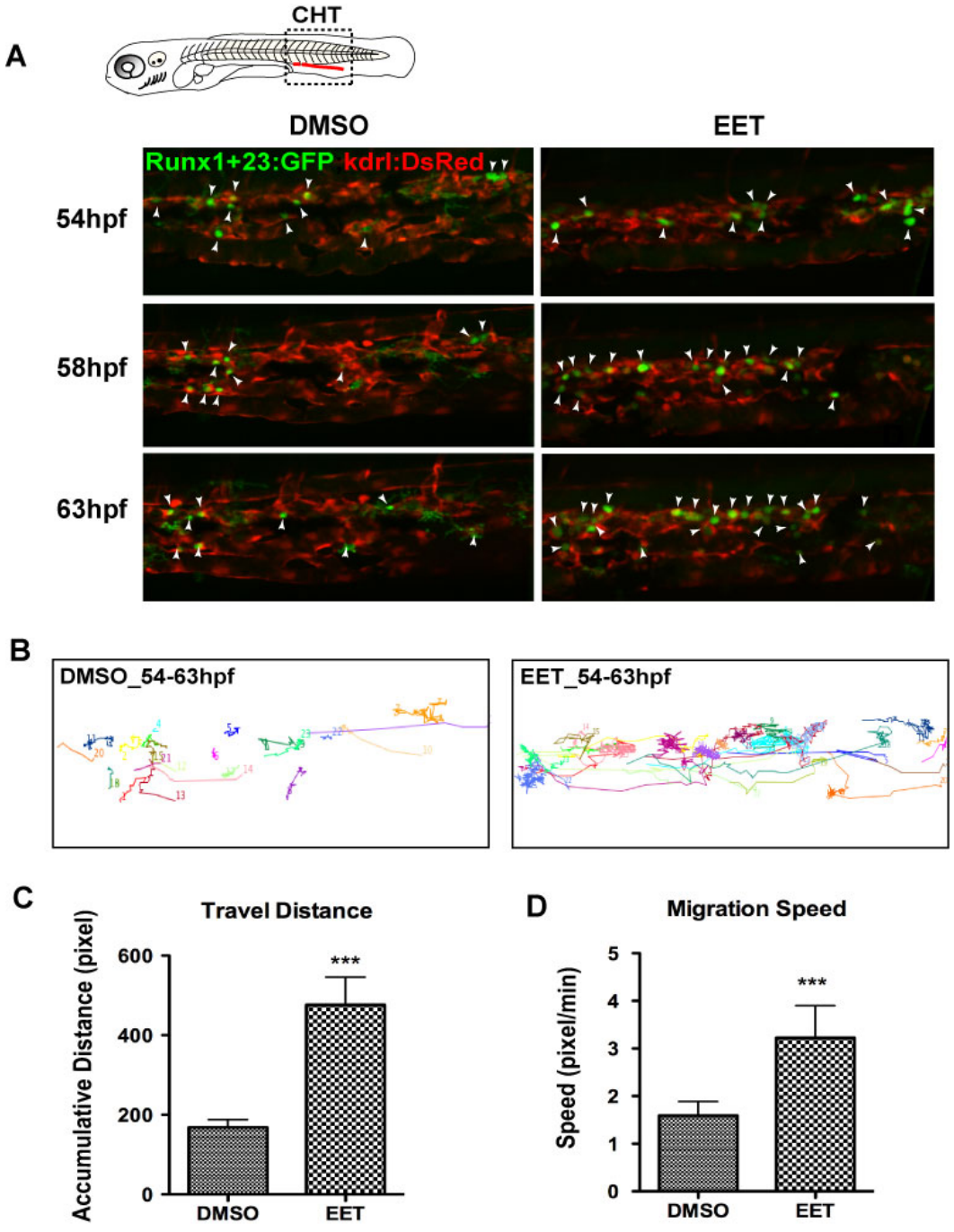

Figure 3.12 EETs enhance engraftment by modulating HSPC migration.

(A) Time-lapse confocal imaging of HSPCs engrafting zebrafish embryo caudal CHT between 54-64hpf. HSPCs: *Runx1+23:GFP*; endothelial cells: *kdrl:DsRed*. Embryos were treated between 24-48hpf. White arrowheads point to HSPCs.
(B) Tracking individual HSPC migration with ImageJ and MTrackJ.
(C-D) Quantification of average HSPC travel distance (C) and migration speed (D). *** Student's t test p values<0.0005.

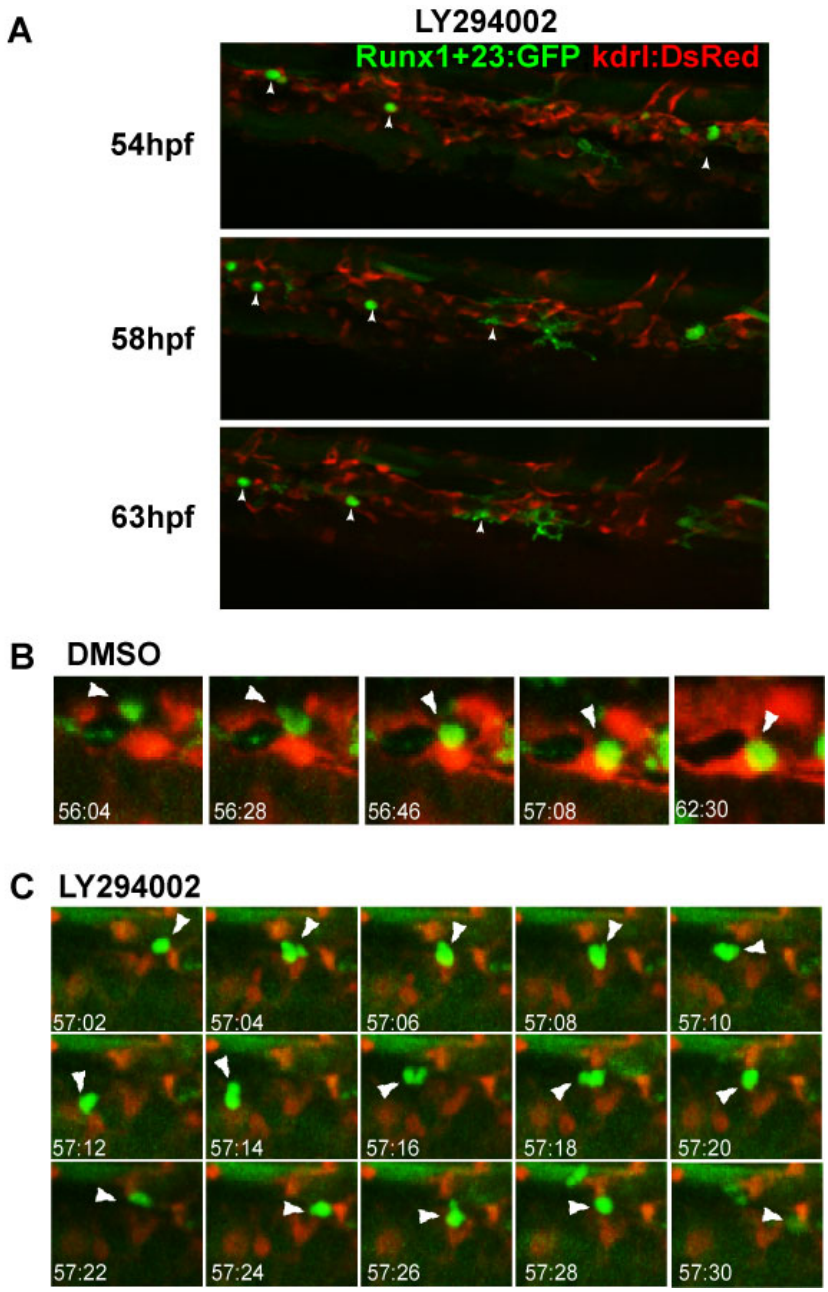

Figure 3.13. PI3K activation regulates HSPC migration and interaction with endothelial niche cells.

(A) Time-lapse confocal imaging of HSPCs engrafting zebrafish embryo caudal CHT between 54-64hpf. HSPCs: *Runx1+23:GFP*; endothelial cells: *kdrl:DsRed*. Embryos were treated between 24-48hpf. White arrowheads point to HSPCs. For DMSO-treated control, see Figure 3.12A.
(B)(C) Timelapse imaging the individual HSPC behavior during the engraftment of CHT in zebrafish embryos treated with DMSO (B) or LY294002 (C).

Despite the increased migration, HSPCs in the EET group maintained a close contact with endothelial cells and did not show any higher tendency to leave the CHT. In EET-treated embryos, there were more productive interactions between endothelial cells and HSPCs to form new niches, meaning more accumulated engraftment events. In contrast, in LY-treated embryos, the circulation was relatively normal and *GFP+* HSPCs still travelled through CHT. The HSPCs rarely made successful contact with endothelial cells, which led to failed engraftment (Figure 3.13C). EETs enhance engraftment by combined effects of enhanced HSPC migration and improved interactions with the niche in a PI3K-dependent manner.

Discussion

The zebrafish whole kidney marrow (WKM) transplantation-based chemical screening identified new chemicals/pathways regulating marrow engraftment, including a novel group of chemicals, epoxyeicosatrienoic acids (EETs). EETs enhanced marrow engraftment after transplantation in zebrafish and promoted both short- and long-term engraftment in mice in a PI3K-depdent manner. The source of EETs in the marrow could involve endothelial cell expression, as has been previously shown (Pfister et al, 2010). A gene expression study reported mouse *Cyp2j6*, a cytochrome P450 epoxygenase, is one of the 93 genes enriched in normal HSCs, in comparison to mobilized HSCs, leukemic HSCs and normal MPPs (multi-potent progenitors) (Forsberg et al., 2010). Our studies establish a role of EETs in regulating HSPC migration and interaction with niche cells.

EETs Alter the Cellular Behavior of HSPCs During Engraftment

By directly tracking the behavior of individual HSPC engrafting CHT, we found EETs dramatically enhanced HSPC migration and modulate adhesion properties (Figure 3.12). After crossing the endothelial barrier, instead of staying locally where they extravasated, a higher percentage of HSPCs in EET-treated embryos migrated away from the initial niche and then initiated new niche formation. The empty niche was then available for HSPC engraftment. This suggests that there is specific signal exchange between the migrating HSPC and endothelial cells in the niche, involving a fine balance between migration and adhesion. Pre-treatment of marrow cells or whole zebrafish embryos with EETs might modulate the migratory and adhesive

properties of HSPCs in a PI3K-dependent manner. PI3K and one of its downstream effectors, AKT, are required for migration and adhesion of many cell types. Two recent studies indicated a negative role of AKT in regulating HSC homing and engraftment (Buitenhuis et al., 2010; Kharas et al., 2010). In our studies, when hematopoietic or endothelial cells were pre-treated with EETs, PI3K activation only lead to a transient phosphorylation of AKT (Figure 3.10). This is distinct from over-expressing a constitutively active form of AKT (Buitenhuis et al., 2010; Kharas et al., 2010). In contrast to 24 hr inhibition of AKT in those studies, we did not see an increase of engraftment with short-term incubation with PI3K inhibitor, LY294002 (Figure 3.11). This could be due to the different inhibitors used and the duration of inhibition, thereby differentially affecting the fine balance between migration and adhesion.

One caveat with the experiments in embryos is that the whole embryo is immersed in EETs. Establishing cell-autonomous effects can be difficult. In the mouse transgenic experiments, the *Tg*(*Tie2:CYP2C8*) mouse donor marrows can secrete higher level of EETs. HSPCs and niche cells might each receive high EET signals. It has been reported that constitutive Akt activation in endothelial cells caused HSPC expansion (Kobayashi et al., 2010). Nevertheless, the transplantation experiments with transient EET exposure demonstrate a cell autonomous role of EETs on blood cells.

Regulation of *runx1* Transcription

In the process of pursuing the molecular mechanism of EET effects, we found EET-induced PI3K activation also led to increased transcription of the stem cell marker, *runx1*, in zebrafish embryos. As a HSC marker in embryo development, the transcription of *Runx1* requires hematopoietic master regulators, such as Scl and Gata2 (Nottingham et al., 2007). Meanwhile, *Runx1* is also expressed in multiple non-hematopoietic progenitor cells, such as hair follicle stem cells and cardiac muscle progenitors (Hoi et al., 2010; Kubin et al., 2011; Osorio et al., 2008; Osorio et al., 2011). The transcriptional regulation of *Runx1* in these non-hematopoietic cells has not been well understood. EETs induced *runx1* in both hematopoietic and non-hematopoietic progenitor cells in zebrafish embryos, arguing for a general transcriptional regulatory mechanism of *runx1*. Consistent with the hypothesis, the requirement of AP-1 for *runx1* induction was genetically established (Figure 3.6). In agreement with our finding, another group independently discovered *FOSL2/RUNX1* are part of the transcriptional module for mesenchymal transformation of glioblastoma through bioinformatics analysis (Carro et al., 2010). The ChIP-Seq data showed binding of AP-1 to both promoter and multiple enhancer regions of *RUNX1* in human K562 cells (Figure 3.7). The binding sites in the promoter regions, especially P2, are evolutionarily conserved and co-bound by RNA POLII (Figure 3.7). RNA-Seq data showed the short transcript initiated from the P2 promoter is the dominant isoform in K562 cells, which is different from what has been reported in human HSCs (Challen and Goodell, 2010). The AP-1-bound regions were also labeled with active marks, such as H3K4me and H3K27ac (Figure 3.7). This supports that AP-1 could activate *runx1* transcription directly. A suggestion of co-operation with

hematopoietic master regulators was found based on conserved sites in the first intron region, where AP-1 colocalizes with GATA1/2 (e1, e4 in Figure 3.7). This co-operation has also been indicated in human umbilical vein endothelial cells (Linnemann et al., 2011). Some AP-1-bound regions were also found devoid of GATA1/2 (e2, e3 in Figure 3.7). The versatile binding capabilities enable AP-1 to regulate *RUNX1* expression in different cell types, in collaboration with cell type-specific master transcription factors.

EETs also induce AP-1 in HSPCs *in vitro*. It is possible that AP-1 is also required for engraftment, although we did not formally test this hypothesis. In contrast to AP-1, the increase of *runx1* transcription was only observed in embryos. This suggests that AP-1 is not sufficient to induce *runx1* expression by itself, and *runx1* induction in the adult marrow is not required for engraftment. In support of this, *Mx-Cre*-mediated *Runx1* inactivation in adult murine HSCs does not affect stem cell maintenance (Ichikawa et al., 2004). The enhanced engraftment by EETs is likely through other pathways downstream of PI3K activation.

Direct target of EETs

Despite the potent biological effects, the receptor(s) for EETs are unknown. It has long been proposed that EETs bind to a GPCR (G-protein coupled receptor) (Chen et al., 2011; Node et al., 2001; Yang et al., 2008). For the first time we provided genetic evidence showing Gα12/13 is required for EET effects, supporting the GPCR hypothesis. The 12/13 family Gα subunits have been shown to play an important role in regulating cell migration during embryonic vasculogenesis and

cancer invasion (Kelly et al., 2006; Offermanns et al., 1997). In addition to our finding that EETs modulate HSPC migration behavior (Figure 3.12), it has also been reported that EETs promote angiogenesis and cancer cell motility (Jiang et al., 2007; Michaelis et al., 2005; Nithipatikom et al., 2010; Panigrahy et al., 2011a). The similar cellular aspects regulated by Gα12/13 and EETs further indicate that signaling through the EET receptor is mediated by Gα12/13, although other Ga subunits may be used also.

The effects of EET on HSPCs may be therapeutically useful. During marrow transplant, HSPC chimerism over time is critical, and the time to adequate neutrophil engraftment is an important milestone for treatment success. EET seems to also have a prominent effect on progenitor engraftment, as shown by increased chimerism early after transplantation. Previously it was found $dmPGE_2$, or $dmPGE_2$ in combination with Wnt activator (BIO), increased the engraftment rate in bone marrow competitive transplantation at a limited donor cell dose (Goessling et al., 2009; North et al., 2007). Both PGE_2 and EETs are arachidonic acid-derived eicosanoids. These small lipids are locally derived near wounds, and may facilitate progenitor recruitment, engraftment, and proliferation. Despite their common origin, the underlying molecular mechanism and cell biology are different. $dmPGE_2$ modulates both homing and HSPC numbers via cAMP pathway, while EETs have a more dramatic effect on cell migration and adhesion through PI3K activation. Because of the different and complimentary effects of $dmPGE_2$ and EETs, treatment of HSPCs with both PGE_2 and EETs might lead to faster and safer engraftment in patients.

Material and Methods

Zebrafish strains and husbandry

Zebrafish were maintained in accordance with Animal Research Guidelines at Children's Hospital Boston. The following transgenic zebrafish were used in the study: RedGlo® zebrafish, Tg(*β-actin:GFP), casper*, Tg(*kdrl:DsRed2*), Tg*(Runx1+23:mCherry)* and Tg(*Runx1+23:GFP*). RedGlo® zebrafish was purchased from 5D Tropical and authorized for research use (Blake, 2010). *DsRed2* is overexpressed under the *mlc* (myosin light chain) and *β-actin* promoters. *Tg(β-actin:GFP), casper* and Tg(*kdrl:DsRed2*) lines were previously described (Kikuchi et al., 2011; White et al., 2008). *Tg(Runx1+23:mCherry)* and *Tg(Runx1+23:GFP)* were constructed and provided by Owen J. Tamplin (unpublished data). The +23 enhancer region of mouse Runx1 was used to drive HSPC-specific expression (Bee et al., 2009).

Zebrafish embryo morpholino and mRNA injection

Morpholinos were obtained from Gene Tools, LLC. Morpholinos and mRNA were injected into one to two cell-stage embryos. See Table 3.4 for morpholino sequences. All of the morpholinos used in the study target the translation initiation site (ATG). All of the morpholinos were tested at 2, 4, and 6 ng to decide the effective dosage.

There are 5 types of Gα subunits and 16 functional *gna* loci in human. In zebrafish, they are *Gαs (gnas, gnal), Gαi (gnai1, gnai2, gnai2l, gnai3, gnaia, gnat1,*

gnat2, gnao1a, gnao1b, gnaz), Gαq/11 (gnaq, gna11, gna14, gna14a), Gα12/13 (gna12, gna12l, gna13a, gna13b), and *Gαv (gnav)*. To block different types of Gα subunits individually in zebrafish embryos, different approaches were used. To inhibit Gαi in general, *PtxA* (Pertussis toxin A) mRNA was in vitro transcribed with SP6 and injected into 1-cell stage zebrafish embryo at 3 pg/embryo with morphological defects but no general toxicity (Addgene, Plasmid 16678) (Slusarski et al., 1997). To inhibit Gαq and Gα12/13, morpholinos were designed to inhibit each one (Table 3.4).

Table 3.4 Zebrafish Morpholino Sequences

Gene	Ref Seq	MO sequence (5'→3')	Reference
junb	NM_213556	CGGTTGCTCCATTTTTG TTGACATG	(Meder et al., 2010)
fosl2	NM_001082998	ATGTCCCGGTGTAATCC TGGTACAT	Gene Tools
c-jun	NM_199987	TTCCATCTTGGTAGACA TAGAAGGC	Gene Tools
c-fos	NM_205569	CGGCGTTAAGGCTGGTA AACATCAT	Gene Tools
gna12	NM_001013277	CGCACCACGCCAGCCAT CCTGTCCA	(Lin et al., 2005)
gna13a	NM_001012243	AAATCCGCCATCTTTGT AGTAGCGA	(Lin et al., 2005)
gna13b	NM_001013263	AGGAAATACGCCATCTT TGTGCAAC	(Lin et al., 2005)
gna15/16	NM_001003626	TGTAGCACCATCTCCAG CAGCCCAT	Gene Tools
gnaq	NM_001144799	CATGATTCTCCCTGTCA CTTCACAA	Gene Tools
gna11	NM_001007773	AGGCCATCATCGACTCT AAAGTCAT	Gene Tools
gna14	NM_001003753	CGCCTGATAAACAGCAC TCCTCCAT	Gene Tools

Screen and chemical treatment

Adult zebrafish transplantation-based chemical screen was done at the hESC core at Children's Hospital Boston. The ICCB Known Bioactive Library was purchased from BIOMOL (Enzo Life Sciences). WKM (Whole kidney marrow) was incubated in 0.9xDPBS plus 5% heat-inactivated FBS for 4 hrs at room temperature, at a density of 1000 cells/μl. Chemicals were diluted at a 1:200 ratio. All the embryo treatment with 11,12-EET started at 24 hpf. The suppressors were added 30 min prior to EET. 0.5μM 11,12-EET and 14,15-EET were used for zebrafish whole kidney marrow treatment; 2 μM 11,12-EET for mouse bone marrow treatment; 5 μM 11,12-EET for zebrafish embryo treatment.

Chemicals used for the secondary round of screening for confirmation were from a different aliquot of the library, independent of the primary screen plate. 11,12-EET (Cayman Chemical, Cat. # 50511) was resuspended in DMSO with original organic solvent evaporated. The following chemicals were used for zebrafish marrow treatment: $dmPGE_2$ (Cayman, #14750), 10 μM; BIO (EMD), 0.5 μM. For the chemical suppressor screen, zebrafish embryos were incubated with inhibitors at three different concentrations. The highest effective concentration without causing general toxicity is listed below.

Table 3.5 Chemicals for Suppressor Screen in Zebrafish Embryos

Chemical Name	Source	Highest Concentration	Pathway
SB 203580	Tocris	100 μM	p38
PD98059	Calbiochem	50 μM	MEK1
U0126	Tocris	30 μM	MEK1/2
GW5074	Tocris	50 μM	C-RAF
LY294002	Sigma	10 μM	PI3K
wortmannin	Sigma	1 μM	PI3K AKT
PI-103	Cayman	10 μM	PI3K
rapamycin	Enzo Life Sciences	50 μM	mTOR
H89	Sigma	5 μM	PKA
SQ22536	Sigma	100 μM	Adenylate Cyclase
GW9662	Cayman Chemicals	5 μM	PPARg antagonist
BADGE	Tocris	10 μM	PPARg antagonist
PP2	Sigma	10 μM	SRC
Tyrphostin AG1478	Sigma	30 μM	EGFR
GM6001	Enzo Life Sciences	25 μM	MMP
SU 5402	Tocris	30 μM	FGF/VEGF
Indomethacin	Sigma	20 μM	COX
L-NAME	Sigma	10 μM	NOS
SU1498	EMD	50 μM	VEGF
NSC 23766	Tocris	50 μM	RAC
SP600125	Tocris	40 μM	JNK

Adult zebrafish WKM competitive transplantation

Adult zebrafish kidney marrow was dissected, processed into single-cell suspension and injected retro-orbitally. Recipients at 4 wpt (week post transplant) were anesthetized with 0.2% Tricaine in fish water and imaged using a Zeiss Discovery V8 fluorescence stereomicroscope with GFP/RFP filters. Images were analyzed with ImageJ. For detailed description, see Chapter 2.

Imaging acquisition and quantification in zebrafish embryos

For live imaging of embryos, zebrafish embryos were embedded in agarose as described before (Bertrand et al., 2010). Single-frame image or time-lapse Movie was taken on a spinning disk confocal microscope with an incubation chamber. Images were taken every 2 minutes. Images were processed and quantified using Fluorender and ImageJ. To track the cell migration routes, MTrackJ plugin was used together with ImageJ (Meijering et al., 2009). The number of pixels along the track measures the total travel distance. The average migration speed is calculated by the ratio between total travel distance and travel time.

Mouse bone marrow transplantation and chimerism analysis

All mice were maintained according to IACUC approved protocols in accordance with Children's Hospital Boston animal research guidelines. 9-week-old CD45.1 and CD45.2 (C57/BL6) mice were purchased from Jackson laboratories. 14-week-old Tg(*Tie2:CYP2C8*) mice in the CD45.2 (C57/BL6) background and wild type siblings were provided by C. R. Lee and D. C. Zeldin (Lee et al., 2010). All recipients received an 11Gy split dose of γ-irradiation prior to transplantation. For the chemical treatment, 20,000 CD45.1 WBM cells were treated at room temperature for 4 hrs with 2 μM 11,12-EET and/or 10μM LY294002. Chemicals were washed off before cells were retro-orbitally injected with 200,000 fresh CD45.1/2 mouse WBM cells into CD45.2 recipients. Each treatment condition included 8-10 recipients per experiment with 2 biological repeats. In the limiting dilution competitive transplant, 30,000 or 60,000 CD45.2 wild type or transgenic WBM were injected with 300,000

CD45.1 WBM into CD45.1/2 recipients (n=7). Peripheral blood was stained with lineage-specific antibodies and analyzed every four weeks on LSRII (BD Biosciences) to assess engraftment. The following antibodies were used: Gr1 (RB6-8C5), Mac1 (M1/70), B220 (RA3-B2), CD3 (145-2C11), and Ter119 from eBioscience; CD45.1 and CD45.2 from BD Biosciences. Animals with 1% chimerism in myeloid, T, and B cell lineages were considered to have multilineage engraftment.

Mouse bone marrow analysis

FACS analysis was performed on the mouse whole bone marrow with the following antibody staining: Sca-1(E13-161.7), CD48 (HM48-1), FcgR (2.4G2), CD4 (GK1.5), CD8 (53-6.7), and Ter119 from BD Biosciences; c-Kit (2B8), and CD34 (RAM34) from eBioscience; CD150 (TC15-12F12.2) from Biolegend; Mac1, Gr1 and B220 from Invitrogen; Goat-anti-Rat IgG PE-TexRed from SouthernBiotech.

Mouse peripheral blood CBC and chimerism analysis

Tg(Tie2:CYP2C8) or wild-type sibling mice were bled. Complete blood count (CBC) was performed on HEMAVET HV950 (Drew Scientific, Inc).

Cell culture

U937 (ATCC, CRL-1593.2) was cultured in RPMI media supplemented with 10% FBS, 100 U/mL penicillin and 100µg/mL streptomycin. EA.hy926 (ATCC, CRL-2922) supplemented with 10% FBS and 1xHAT supplement (Gibco). Cells were split 2-3 times per week. Before chemical treatment, cells were serum starved for 12-16 hrs.

Human $CD34^+$ cells, isolated from the peripheral blood of granulocyte colony-stimulating factor mobilized healthy volunteers, were obtained from the Yale Center of Excellence in Molecular Hematology. The frozen cells were thawed and expanded in StemSpan medium (Stem Cell Technologies Inc.) with 1× CC100 cytokine mix (Stem Cell Technologies Inc.), 200 U/mL penicillin and 200μg/mL streptomycin for 6 days. Cells were stained and analyzed for CD34, CD38 and CD133 surface marker expression before use. For the in vitro stimulation, expanded CD34+ cells were starved with StemSpan medium without cytokines for 1 hr, and the treated with 2 μM 11,12-EET. PI3K inhibitor, LY294002, was added 30 min before EET.

Western blotting

Cell lysates were prepared with 1x RIPA buffer (Thermo Scientific) and applied for western with the following antibodies from Cell Signaling Technology: phospho-Akt (S437) (D9E), pan Akt (C67E7), phospho-p44/42 MAPK (Erk1/2) (Thr202/Tyr204) (D13.14.4E), phospho-MEK1/2 (Ser217/221) (41G9); and β-Actin (Invitrogen).

qRT-PCR

Total RNA was extracted with Trizol/Chloroform. cDNA was made with reverse transcription (SuperScript III Reverse Transcriptase Kit, Invitrogen). qPCR was performed on BioRad C1000 Real-Time Machine (384-well). Primers were designed by qPrimerDepot (http://primerdepot.nci.nih.gov/) and verified.

Table 3.6 Primers for qPCR with Human Cells

GENE	REF SEQ	FORWARD (5'-->3')	REVERSE (5'-->3')
GAPDH	NM_002046	AAGGTGAAGGTCGGAGTCAA	AATGAAGGGGTCATTGATGG
JUNB	NM_002229	GAACAGCCCTTCTACCACGA	AGGCTCGGTTTCAGGAGTTT
FOSL2	NM_005253	TTATCCCGGGAACTTTGACA	TGAGCCAGGCATATCTACCC
FOS	NM_005252	CTACCACTCACCCGCAGACT	GTGGGAATGAAGTTGGCACT
FOSB	NM_006732	ACCCTCTGCCGAGTCTCAAT	GAAGGAACCGGGCATTTC
JUN	NM_002228	GAGGGGGTTACAAACTGCAA	TCTCACAAACCTCCCTCCTG

Genome-wide expression analysis

Total RNA was extracted from 36hpf zebrafish embryos treated with DMSO or 5uM 11,12-EET between 24-36hpf, with 3 biological replicates each. Microarray hybridization was performed with the Affymetrix GeneChip Zebrafish Genome Array. Hybridized microarray was background-corrected, normalized and multiple-tested using Goldenspike (http://www2.ccr.buffalo.edu/halfon/spike/) in R/Bioconductor (Choe et al, 2005). Genes with $q<0.1$ by SNR test were considered differentially expressed.

Statistics

The correlation between image- and FACS-based analysis was simulated by linear regression. Limiting dilution competitive transplantation data were analyzed ELDA (Hu and Smyth, 2009). The rest of the statistics were done with student t-test.

Acknowledgements

We would like to thank C. R. Lee and M. L. Edin for providing reagents; Y. Zhou, A. Dibiase, S. Datta, P. Manos, and R. Mathieu for technical assistance; E. Trompouki for the GATA1/2 ChIP-Seq data. We are grateful to R. M. White for bioinformatics analysis and insightful discussion; T. E. North and C. Mosimann for helpful discussion and critical comments. The publically available ChIP-Seq, RNA-Seq and DHS data were obtained from ENCODE Consortium database, especially provided by the following groups: Broad Institute and B. E. Bernstein at MGH; M. Snyder, M. Gerstein and S. Weissman at Yale University; P. Farnham at UC Davis; K. Struhl at Harvard University; B. Wold at Caltech; R. Myers at Stanford; Illumina gene expression group; and UW ENCODE group. L.I.Z. and G.Q.D. are Howard Hughes Medical Institute investigators. L.I.Z. and P.L. are supported by NIH 1R01HL097794-03. This research was funded, in part, by the Intramural Research Program of the NIH, National Institute of Environmental Health Sciences (Z01 ES025034 to D.C.Z). L.I.Z. is a founder and stockholder of Fate, Inc. and a scientific advisor for Stemgent. G.Q.D. is a member of the Scientific Advisory Boards of MPM Capital, Inc., Epizyme, Inc., and iPierian, Inc.

Chapter 4

Concluding Discussion and Future Directions

Concluding Discussion

In the work described in this thesis, we developed a competitive marrow transplantation assay in adult zebrafish, which allows quick visualization and quantification of marrow engraftment capabilities *in vivo*. Using this assay, the first transplantation-based chemical screen was performed with a known-bioactive chemical library. The screen led to the discovery of ten chemicals involved in several novel pathways that can enhance marrow engraftment. One example is a group of arachidonic acid-derived lipids, epoxyeicosatrienoic acids (EETs). EETs can also promote both short-term and long-term marrow engraftment in mice. Using genetic knockdown and chemical suppressor screening in zebrafish embryos, we found that EET acts through a Gα12/13-mediated receptor, which activates PI3K and induces transcription factors of the AP-1 family. This PI3K/AP-1 pathway directly induced the transcription of HSC marker, *runx1,* in embryos. The activation of PI3K by EET is required for promoting HSPC migration and interactions with niche cells, and therefore engraftment. In addition to the blood phenotype, EET also caused cell morphological and gene expression changes in the tail bud of zebrafish embryos. The signaling and transcription regulatory network indicate these changes share some similarities with epithelial mesenchymal transition (EMT). These findings may help explain the previously reported observation that EETs can promote tumor metastasis and angiogenesis.

Our studies define a role for EETs in the engraftment of HSCs in adult vertebrates, and HSC development during embryogenesis. The chemical screen also identified additional pathways important for regulating HSC engraftment. These

discoveries may have clinical application in marrow or cord blood transplantation, may help elucidate basic regulatory mechanisms of stem cell engraftment, and encourage the use of chemical screening approaches to study complicated biological processes.

Engraftment Rejection and Zebrafish Immunology

The immune system protects organisms from foreign, "non-self" insults such as bacteria, parasites, and viruses; therefore, it also creates a barrier for allogeneic transplantation. In human patients, a myeloablative regimen is taken before allogeneic transplantation, and immune suppressants are given to the patients to reduce the likelihood of acute rejection.

Adult zebrafish have both innate and adaptive immune systems, and as in human and mice, the adaptive immune system is the biggest barrier for allogeneic transplantation of stem cells and tumors (Lieschke and Trede, 2009). We have taken a similar approach of γ-irradiation, as in humans, to suppress the recipient's immune system before transplantation. With our current irradiation regimen, when high doses of irradiation are used to completely eradicate the recipient's immune system, the general toxicity in the digestive system causes rapid death of the recipients, which cannot be rescued by hematopoietic transplantation. The overall survival of the recipients is greatly compromised. Sublethal irradiation regimen was used to partially ablate the immune system. Consequently, recipients recover their endogenous immune competency by about 4 weeks post-irradiation causing the

long-term engraftment levels to become extremely variable, especially in the recipients with relatively low chimerism during the short-term engraftment period.

The incomplete ablation of the endogenous immune system creates a second barrier for optimal long-term engraftment, which is the mismatched immune systems between the donor and recipient. The molecular cues used by immune cells to distinguish 'self' from 'non-self' are based on the MHC (major histocompatibility complex) molecules. MHC is a family of proteins presented at the cell membrane of virtually all somatic cells as recognition tag for innate and adaptive immune system cells, especially T cells and natural killer (NK) cells. In human bone marrow transplantation, the donor and recipient's MHC types, which are called HLA (human leukocyte antigen) in human, are matched to reduce the potential host rejection and graft-versus-host disease (Abbas et al., 2012). MHCs have been well studied in humans, and laboratory mice have become isogenic at MHC loci due to decades of inbreeding. In contrast, the MHC types in zebrafish have turned out to be very complicated and less well understood. Therefore, all of the transplantation described in this thesis has been performed without MHC-matched donors and recipients.

The lack of optimal myeloablative regimen and the mismatch of MHC between donors and recipients create a barrier for assessing long-term engraftment in adult zebrafish. Additionally, the water-living conditions of zebrafish make it difficult to create a near-sterile environment for post-transplantation care. Potential infections also compromise the survival of transplanted recipients. Due to the survival curve of fish treated in the non-optimal conditions mentioned above, we decided to analyze

engraftment levels at 4 wpt, before the recipients recover their endogenous immune systems. The early engraftment level is also meaningful as it represents the progenitor engraftment level. Further, in humans the early neutrophil count in patients undergoing HSC transplantation is a very important clinical index in predicting survival and long-term engraftment.

The Implications from the Transplantation-Based Chemical Screen

Among the 480 chemicals tested in the screen library, we identified 10 chemicals that can enhance marrow engraftment to different extents. The efficacy of the other hits, besides EETs, needs to be tested in the mouse competitive transplantation assay with careful dose titration. Some of the hits target the same pathway, which is reassuring. In general, structure activity relationship should be studied by testing chemicals with similar structures as the hits, or structurally different chemicals sharing the same target. This will help clarify the exact pathways targeted by the hits.

The transplantation-based chemical screen is quite low throughput; therefore, the chemical space covered by the screen is very small. However, our screen had a relatively high hit rate compared to *in vitro* cell culture-based chemicals screens. Several reasons contribute to this: 1) One potential issue with large diversity-based chemical libraries is that the pharmacokinetics and bioavailability of the chemicals are unknown. Chemicals with poor bioavailability will definitively be scored as negative in the screen. The 480 chemicals in the library we chose are known to have bioactivities and most of them have identified targets. This increases the likelihood

of the chemicals perturbing certain molecular pathways. 2) Protein or cell-based screens usually use *in vitro* readouts with one or two dimensional measurements. Our screen design is extremely high-content. Chemical treatment can affect many different cellular aspects, such as proliferation, migration, adhesion, apoptosis vs. survival, which can all affect the final readout as the relative level of engraftment. Therefore, one single *in vivo* assay is more than the sum of several different *in vitro* assays. This also increases the likelihood of chemicals having an effect on the final readout. It will be interesting to test all the hits in specific assays assessing which cellular aspect they have an impact on, such as *in vitro* migration and proliferation, and *in vivo* homing assays. In conclusion, low-throughput but high-content screens like this can also yield interesting results.

The EET Receptor(s)

Even though it has been almost two decades since the discovery of EETs, the direct receptor(s) that EETs bind to is still unknown. The literature on this topic is also quite controversial, because the majority of published data had only indirect evidence on the identity of the receptor. Until recently, the research led by Dr. William Campbell had observed the direct physical binding between a modified EET and an unknown 47kDa cell membrane protein (Chen et al., 2011). The same paper also confirmed the expression of this putative receptor on the cell membrane in human leukemia U937 cell line, and primary bovine endothelia cells, but not in the HEK293T cells. The authors hypothesized that this putative receptor is a GPCR (G-protein coupled receptor), and overexpressed more than 70 orphan GPCRs in the

HEK293T cells. None of these GPCRs bind to EETs. Although this study did not lead to the identification of the EET receptor, it generated very important information and encouraged the further pursuit of this mysterious receptor.

We also hypothesized the hypothetical EET receptor is a GPCR based on the following facts: First, the majority of known arachidonic acid-derived lipids target GPCRs. EETs share very similar chemical structures with prostaglandins and leukotrienes. Since ligand-GPCR binding is very promiscuous, and usually a single lipid binds to multiple GPCRs with differential affinities, we hypothesize that even the GPCRs with known ligands cannot be excluded from the list of candidate EET receptors. In addition, using genetic knockdown approaches, we demonstrated the requirement of Gα12/13 for EET-induced gene expression in zebrafish embryos. This further supports the GPCR hypothesis, although it is also possible that Gα12/13 is in a parallel pathway to EET-induced signaling.

Based on the information above, we decided to compare the GPCR expression profiles in cells that express the EET receptor on the membrane, with the ones that do not bind to EETs. Beside U937 cell line which has been shown to be positive for the EET receptor, we also biochemically demonstrated that a human immortalized endothelial cell line, EAhy, can also respond to 11,12-EET and increase the pAKT level (Figure 3.10). In contrast, the putative receptor is not present on the surface of HEK193T cells. We extracted poly-A enriched mRNA from these three cell lines for RNA-seq. We performed comparative transcriptome analysis, looking for the GPCRs differentially expressed in the responsive and non-responsive cell lines.

The data have been independently analyzed by Richard M. White in our lab and Dr. Guy Sauvageau's lab at University of Montreal. To our surprise, each cell type only has about 70-80 annotated GPCRs with detectable levels of mRNA expression. The tow analysis generated similar results. Strictly based on fold-change without statistic tests, 37 GPCRs are enriched in either U937 and/or EAhy cells. Upon application of statistical constraints to the datasets based on $q<0.05$, 15 GPCRs remain. With this manageable list, we have started loss-of-function studies. We have annotated the zebrafish orthologs of most of these candidates. Since 11,12-EET causes dramatic gene expression phenotypes, knocking down the fish orthologs with morpholinos in embryos may generate even cleaner results than knockdowns of the receptors in cell lines. In addition, the mRNA expression patterns of the candidates and/or the size of the protein can be used for prioritization. However, some GPCRs belong to specific GPCR families comprising multiple paralogues with high DNA sequence similarities, such as the C-C chemokine receptor family. A one-to-one relationship does not exist when comparing the human and zebrafish genome. Therefore, in such situations, knocking down the candidate receptors in the human cell lines is a more reasonable approach. These different candidates can be knocked down in U937 or EAhy cell lines with shRNA, and the effects on AKT-phosphorylation upon EET treatment can be examined by western blotting or phospho-flow cytometry.

Though the aforementioned experiments are feasible, caution should be taken when doing this type of analysis, especially when interpreting the potential false-negative results. First, the original biochemical identification of the 47kDa receptor

is based on the presence of the protein on the cell membrane. Many scenarios can lead to the absence of the protein but presence of the mRNA in the "non-responding" cells. For example, the translation of the mRNA into proteins is only initiated upon certain stimulation; or the proteins are made but instead of being translocated to the membrane, they remain in the cytoplasm. In either case, the GPCR will not be considered a candidate because the mRNA is not differentially expressed. Second, the band of 47kDa might not reflect the actual size of the protein. Post-translational modification, such as glycosylation, can increase the perceived molecular weight of the modified protein, and proteolysis triggered by signals can make the actual protein smaller than the one predicted based on the genomic sequence. Third, as mentioned above, some GPCRs belong to multi-member families, and one ligand can bind to multiple receptors within the same family. For example, PGE_2 (prostaglandin E_2) binds to four known receptors. It is possible that EETs bind to two different receptors on two different non-responder cell lines, which requires special attention when performing the differential expression analysis. Last but not the least, GPCRs can form homodimers, heterodimers or even oligomers, depending on the specific ligand and the presence/absence of binding partners (Kaczor and Selent, 2011; Maurice et al., 2011). When performing gain-of-function analysis, overexpressing a single candidate receptor might not result in the optimal binding to EETs.

Despite the caveats with this genetic approach, it provides a new angle for looking at this receptor puzzle. We have already started the loss-of-function study in zebrafish embryos, and are in preparation for similar experiments in human cell

lines. In the meantime, this receptor is also being pursued by other labs using biochemical binding assays combined with updated mass spectrometry technologies. We are hoping to get the answer in the near future.

The Cell Autonomy vs. Non-Autonomy Effects

In the situation of whole kidney marrow or bone marrow transplantation, a mixed population of cells was exposed to EETs, including mature white blood cells, red blood cells, endothelial cells, mesenchymal cells, and other cell types. Knowing which cell population(s) is/are the direct responding cells is important for understanding how EETs enhance engraftment. Because the receptor of EETs is unknown, the direct target cells cannot be separated by FACS. Therefore, the best approach for identification of the relevant cell type is to sort out different cell populations and treat them separately with EETs. In mice, different phenotypic HSPC populations can be finely purified based on cell surface markers.

We sorted Lin-c-Kit+Sca-1+CD150+CD48-CD34- long-term HSCs from wild type mice, and treated them with EETs. However, we did not see a significant increase in long-term engraftment with sorted cells. This result can have multiple explanations. One seemingly obvious scenario is when the whole kidney/bone marrow is exposed to EETs, the direct responding cells are not the phenotypic LT-HSCs. EETs are known to have effects on endothelial cells and some types of mature blood cells (Fleming, 2007; Spector, 2009). It is possible that EET directly modulate some other cells types, which can have a secondary effect on HSCs, for example, by secreting cytokines and grow factors upon EET stimulation. In fact, it has been reported that

14,15-EET can induce the production of FGF_2 (fibroblast growth factor 2) in endothelial cells (Zhang et al., 2006). If this hypothesis is true, it suggests that the quality of HSCs may be improved by modulating their niche cells. Testing this hypothesis is not an easy task, due to the complexity of bone marrow components. One possible experiment is to sort out different niche cell types, such as endothelial or stromal cells, and incubate these cells with EET for a period of time. The conditioned media from this treatment can then be collected and applied to purified HSPCs, which can later be transplanted. This experimental design assumes whatever the intermediate signaling molecule is soluble, and the effect on HSPCs is not dependent on the physical cell-cell interaction.

Another less obvious explanation for why EET-treatment of LT-HSCs alone did not enhance the engraftment is EET might affect a specific HSC population separate from phenotypic LT-HSCs. Based on previously published microarray data, the phenotypic LT-HSCs express higher level of cytochrome P450 enzymes than ST-HSC and progenitors. It is possible that the phenotypic LT-HSCs can already synthesize high-level of EETs, and are therefore self-sufficient. In contrast, treating phenotypic ST-HSCs with EETs may compensate for their lack of the LT-HSC signature, and therefore, make them act more LT-HSC–like. To formally test this hypothesis, different HSPC populations need to be purified first, treated with EETs separately, and then transplanted.

Both the non-autonomous and the autonomous models can be interesting. Even more interesting is that EET might affect both stem cells and the niche. Both stem cells and endothelial cells are capable of synthesizing high levels of EETs, which may

be employed as a means of communication between different cell populations to coordinate the responses to various environmental fluctuations.

Transplanting Limited Numbers of HSCs

From the competitive transplantation experiment we noticed that the effect of EET on engraftment was only significant when a low dose of whole bone marrow cells were transplanted in an extreme competition situation. For example, 20,000 wild type donor whole bone marrow cells competing with 200,000 competitors can only result in long-term multi-lineage engraftment in about 20% of the recipients. In contrast, 200,000 donor cells competing with 200,000 competitors can engraft 90-100% of the recipients. With EET treatment, there was a dramatic increase of the percentage of recipients with long-term engraftment in the 20,000 cell group, while 200,000 cells still engrafted sufficiently, and no significant difference of the average chimerism among the recipients was observed. This special effect in the extreme competition situation has also been reported on other pathways. For example, in *vitro* treatment with $dmPGE_2$ for 2hrs had very similar effects as EET (North et al, 2007). Another example is the immediate early response gene *EGR1*. $Egr^{-/-}$ bone marrow cell performed normally in non-competitive transplantation, at a cell dose as low as 25,000. In the competitive transplantation situation, $Egr^{-/-}$ bone marrow had a significant increase of long-term myeloid engraftment at a 25,000 cell dose, but not 100,000 (Min et al, 2008).

These observations raise a mysterious but fascinating question: do stem cells behave differently within a large group of stem cells versus as a single stem cell?

Within 20,000-25,000 whole bone marrow cells, there are on average only 1-2 LT-HSCs. One hypothetical rationalization for this differential behavior of stem cells is that the number of "healthy" niche cells after irradiation is extremely limited. Therefore far fewer stem cells can engraft than what is expected, especially in a competitive transplantation situation. However, if this is the case, we would expect to see that EET or dmPGE_2 treated bone marrow cells have a higher chimerism in the 200,000 v.s. 200,000 group, because they will be more competitive at occupying the niche than the control population. Therefore, the niche hypothesis is not a likely explanation. A second hypothesis is that HSCs can communicate to each other and sense the quantity and quality of other stem cells. In the situation with a saturated number of HSCs, some stem cells might receive suppressive signals from other stem cells to enter quiescence. Therefore, when looking at the output from a large population of stem cells, the effects of EETs or PGE_2 will be masked by the population behavior. In the situation of limited number of HSCs, the same chemical effect can be amplified and become detectable. To test this pure theoretical hypothesis, more advanced single stem cell analysis is required, such as single cell transcriptome and proteomics analysis, single cell *in vivo* tracking, etc.

Future Directions

Generate MHC-Matched Donor/Recipients

Due to the immune rejection discussed above, some alternative zebrafish systems have been adapted to allow long-term engraftment, such as using younger larvae as recipients without any immune-suppressive regimen. The major maturation events for immune competence occur between 2-4 weeks post fertilization. It has been shown that transplanting adult kidney marrow cells into 2-day old *gata1*$^{-/-}$ embryos rescued the otherwise lethal mutant phenotype with continued contribution of donor marrow cells to the recipient's hematopoiesis up to 8 months (Traver et al., 2003a). This shows the plasticity of the immune system during development.

Another approach is to try to match the MHC types between donor and recipient zebrafish. Our lab has shown that the Type I MHC cluster on zebrafish chromosome 19 plays a major role on immune rejection (de Jong et al., 2011). We have genotyped *casper* zebrafish and found they are homozygous for this chromosome 19 locus (unpublished data). The next step is to breed the transgenic donors into *casper*, and select the progenies with homozygous MHC types on chromosome 19 matching *casper*. The genomic differences between zebrafish and human MHC genes is that in the zebrafish genome, they are distributed among multiple chromosomes; while in the human genome, they all cluster in a single genomic locus (Graser et al., 1998; Sambrook et al., 2005). This creates challenges for a perfect MHC match.

Alternatively, Streisinger and co-worker have created isogenic zebrafish lines by applying a heat-shock procedure at the one cell stage. The resulting completely homozygous zebrafish strain is called clonal zebrafish (Streisinger et al., 1981). Within the clonal strain, all individuals have the same MHC genotype, therefore immune barriers concerns are eliminated. Recently several labs were able to generate tumor models in these clonal zebrafish, and showed that transplantation within the same family of clonal zebrafish can improve tumor transplantability (Mizgireuv and Revskoy, 2006; Smith et al., 2010).

To improve the transplantation efficiency and fully benefit from the imaging power provided by the zebrafish, one promising future direction is to generate a clonal *casper* strain and model transplantation and diseases in this strain. This requires remaking the fluorescence transgenic donors in the same strain, which is not a trivial task. However in the long-term, this would be an ideal system for direct visualization of engraftment and elimination of immune rejection. However, cautions need to be taken when inbreeding these clonal strains, since it has been reported that highly inbred zebrafish strains have decreased fertility and epigenetic silencing of transgenes.

Identify *bona fide* HSCs in Adult Zebrafish

After more than two decades of studies in mice, subpopulations of bone marrow cells can be purified and characterized by fluorescence-activated cell sorting (FACS). For example long-term HSCs can be highly enriched using a combination of more than eight surface proteins/antibodies (Kiel et al., 2005). However, in zebrafish this

technique is critically lagging, due to a lack of antibodies targeting zebrafish cell surface proteins. Though the existence of long-term HSCs in zebrafish WKM is widely recognized through serial transplantation, the *bona fide* zebrafish HSCs cannot be prospectively identified. I have tested some mouse antibodies (B220, CD4, CD8, Mac-1, Gr1, c-Kit and Sca-1) with zebrafish kidney marrow cells in hopes of species cross-reactivity. But due to the low conservation of these surface markers, none of the antibodies generated signal with zebrafish cells. Generating new antibodies against zebrafish surface proteins is a critical step towards fully embracing the potential of this model organism in stem cell research.

Stem cells can also be marked using transgenic techniques to express fluorescent proteins under the control of stem cell-specific promoters. With the highly efficient transgenic techniques in zebrafish and fast expanding toolbox of fluorescent proteins, the generation of multi-color transgenic zebrafish employing the combination of multiple stem cell markers is a feasible approach to increase the purity of stem cells. In addition, multi-color transgenic zebrafish would facilitate the live tracking and imaging of cell populations *in vivo* through fluorescence microscopy (Ignatius and Langenau, 2009).

Construct a Lipid Regulatory Network in HSCs

The vast majority of literature studying the intrinsic and extrinsic regulators of hematopoietic stem cells focuses on macromolecules, such as cytokines, chemokines, growth factors and transcription factors (Zon, 2010). However, as in other cell types, HSCs are exposed to many different types of stimuli *in vivo*, such as

carbohydrates, nucleic acids, and lipids. They utilize these non-protein components to signal and make fate decisions. Cells constantly metabolize and secrete lipids, just like proteins. From our novel discovery of EETs, and others' previously published data (North et al, 2007; Kindler et al., 2010), it has become clear that arachidonic acid-derived eicosanoids, or bioactive lipids in general, play an important role in the regulation of hematopoietic stem cells. Besides extrinsic factors, lipids are also essential intracellular signaling molecules. As discussed in Chapter 3, one of the direct downstream signaling pathways responsible for EET-induced engraftment is the PI3K pathway. PI3K is a lipid kinase that phosphorylates phosphoinositides, which are also lipids.

With the advancement of small molecule analytical tools, more and more bioactive lipids are being identified. For example, eicosanoids refer to the oxygenated derivatives from three different 20-carbon essential fatty acids, which include arachidonic acid (AA), eicosapentaenoic acid (EPA) and dihomo-γ-linolenic acid (DGLA). EPA and DGLA can also be metabolized by pathways parallel to the AA metabolic pathways. The same COX and LOX enzymes that generate prostaglandins and leukotrienes from AA can also convert DGLA into different series of eicosanoids. In general, AA-derived eicosanoids have pro-inflammatory effects, while DGLA-derived eicosanoids are considered to be anti-inflammatory (Kapoor and Huang, 2006). The opposite physiological effects and the potential competition for the same enzymes between AA and DGLA indicate that the balance among different bioactive lipids might be important for the biological output.

The important roles of eicosanoids, or lipids in general, on regulating stem cells have just begun to be appreciated. AA-derived eicosanoids are much better studied than the EPA and DGLA derivatives. They can function intracellularly, as autocrine or paracrine factors, or long-range hormones. Their receptors can be either expressed on the cytoplasmic membrane or inside cells. One famous example is the essential role of retinoids, the active metabolites of vitamin A, during embryo development. Fetal Vitamin A Deficiency leads to multiple developmental problems, including hematopoietic defects.

To systematically study the lipid regulatory network in stem cells, gene expression analysis is helpful for profiling the lipid metabolic enzymes and signaling pathway components in stem cells. In fact, some published microarray analysis has indicated certain stem cell populations might have a unique lipid signature. For example, among the 76 genes highly and specifically enriched in long-term quiescent mouse HSCs, the cytochrome P450 family member *Cyp2j6* is on the list (Forsberg et al., 2010). With the improvement of the sensitivity of mass spectrometry technology, directly profiling the lipid components among different types of hematopoietic stem and progenitor cells will become feasible. Comparing the biochemical data with gene expression profiles might yield a systematic map of the network.

Functionally testing the roles of these bioactive lipids on stem cells is more straightforward than studying protein function, because as small molecules, lipids can be directly added to cells or administered to animals. Combining multiple lipids that might potentially interplay with each other in various assays can quickly

delineate the functional interaction among them. For example, using the competitive marrow transplantation assay in adult zebrafish, multiple different eicosanoids can be mixed at various ratios and used for pulse-treatment of the marrow cells. It will be interesting to examine whether combining members of the AA-derived eicosanoids can have additive effects, or mixing AA-derived eicosanoids with DGLA-derived eicosanoids might cancel the effects of each other.

Genetic and Chemical Screening with Transplantation Model in Zebrafish

Transplantation has been an indispensible experimental approach in stem cell research. It is the gold standard for identifying adult somatic stem cells, as well as the cell of origin for cancer. Zebrafish have emerged as an important animal model in cancer studies in the past decade. Teleost fish can acquire spontaneous cancers in almost all organs after exposure to water-borne carcinogens (Spitsbergen et al., 2000a, b). In addition, transgenic tumor models of tissue-specific promoter-driven oncogene expression have been developed, such as melanoma (Patton et al., 2005), T/B cell acute lymphoid leukemia (Langenau et al., 2003; Sabaawy et al., 2006), and embryonal rhabdomyosarcoma (Langenau et al., 2007). A variety of transplantation techniques have been developed to study the nature of these tumors and compare them with human tumors; for example, serial transplantation to identify the self-renewal potential of over-proliferative cells, limiting dilution transplantation to estimate the frequency of self-renewing cells in a tumor, and purified sub-population transplantation to identify specific cancer stem cells (Frazer et al., 2009; Langenau et al., 2007; Smith et al., 2010). In addition to zebrafish-derived tumors,

xenotransplantation of human tumor cells into larval or immune-suppressed adult zebrafish has greatly broadened the spectrum of cancer questions that can be studied in zebrafish (Topczewska et al., 2006). Using the transparent zebrafish as recipients, one can directly visualize tumor cell proliferation and dissemination (White et al., 2008).

Anticancer drug discovery and development is recognized as having been highly inefficient in the past; the issues root in the high rate of compound attrition, the relatively small number of patients available for Phase I/II testing, and the finite R&D budgets of the biopharmaceutical industry. To ameliorate these problems, the high rate of ineffective compounds entering clinical trials must be decreased, which requires a better way of preclinical screening. Mouse xenograft testing has been an invaluable step in almost all the successful cancer therapies developed in the modern era. However, mouse xenografts have very poor predictive value on the outcome of clinical trials partially because of a failure to represent the enormous genetic diversity of tumors in patients (Sharpless and Depinho, 2006). In this regard, a zebrafish xenotransplantation model can accommodate a more diverse range of tumors in a less labor-intensive way, which can be used for large-scale assessment of tumor response and modeling resistance. Such large-scale approaches can potentially increase the success of cancer drug development.

A high-throughput imaging system based on the LED fluorescence macroscope has been developed for screening fish transplanted with fluorescently labeled T-ALL (Smith et al., 2010). Combining the imaging power and throughput in zebrafish, tumor transplantation-based screening approaches hold promise for accelerating

the discovery of the molecular mechanisms of cancer and the development of novel drugs.

Summary of Future Directions

In summary, the zebrafish competitive transplantation assay is still in its primitive form. More technical trouble-shooting can be done to improve the efficiency and reproducibility of this assay. In addition, to fully address the autonomy question, developing methods to purify HSCs in zebrafish should be paramount. This thesis documents a novel transplantation-based chemical screen, which led to the discovery of novel components in the HSC regulatory network. With the accumulation of knowledge through unbiased screening, a systematic study on the relationships among different pathways can be undertaken to ultimately construct a comprehensive signaling network regulating HSPC engraftment. A particularly striking aspect is the capacity for different bioactive lipids to form a signaling network in HSCs. Systematically mapping out the regulatory nodules will tremendously benefit both the basic understanding of stem cell biology and the clinical manipulation to generate better stem cells for transplantation. By demonstrating the feasibility of transplantation-based chemical screen, we hope similar screening will be done in adult zebrafish, to study different types of adult stem cells and cancer initiating cells.

Bibliography

Abbas, A.K., Lichtman, A.H., and Pillai, S.: Cellular and Molecular Immunology. Philadelphia: W. B. Saunders, 2012. Print

Akitake, C.M., Macurak, M., Halpern, M.E., and Goll, M.G. (2011). Transgenerational analysis of transcriptional silencing in zebrafish. Dev Biol *352*, 191-201.

Arai, F., Hirao, A., Ohmura, M., Sato, H., Matsuoka, S., Takubo, K., Ito, K., Koh, G.Y., and Suda, T. (2004). Tie2/angiopoietin-1 signaling regulates hematopoietic stem cell quiescence in the bone marrow niche. Cell *118*, 149-161.

Bee, T., Ashley, E.L., Bickley, S.R., Jarratt, A., Li, P.S., Sloane-Stanley, J., Gottgens, B., and de Bruijn, M.F. (2009). The mouse Runx1 +23 hematopoietic stem cell enhancer confers hematopoietic specificity to both Runx1 promoters. Blood *113*, 5121-5124.

Bergo, M.O., Leung, G.K., Ambroziak, P., Otto, J.C., Casey, P.J., Gomes, A.Q., Seabra, M.C., and Young, S.G. (2001). Isoprenylcysteine carboxyl methyltransferase deficiency in mice. J Biol Chem *276*, 5841-5845.

Bertrand, J.Y., Chi, N.C., Santoso, B., Teng, S., Stainier, D.Y., and Traver, D. (2010). Haematopoietic stem cells derive directly from aortic endothelium during development. Nature *464*, 108-111.

Bigas, A., and Espinosa, L. (2012). Hematopoietic stem cells: to be or Notch to be. Blood.

Birney, E., Stamatoyannopoulos, J.A., Dutta, A., Guigo, R., Gingeras, T.R., Margulies, E.H., Weng, Z., Snyder, M., Dermitzakis, E.T., Thurman, R.E*., et al.* (2007). Identification and analysis of functional elements in 1% of the human genome by the ENCODE pilot project. Nature *447*, 799-816.

Blake, A., Crockett, R., Essner, J., Hackett, P., Nasevicius A. (2010). Recombinant constructs and transgenic fluorescent ornamental fish therefrom. (U.S., Yorktown Technologies, L.P., Austin, TX(US)), pp. 31.

Boisset, J.C., van Cappellen, W., Andrieu-Soler, C., Galjart, N., Dzierzak, E., and Robin, C. (2010). In vivo imaging of haematopoietic cells emerging from the mouse aortic endothelium. Nature *464*, 116-120.

Buitenhuis, M., van der Linden, E., Ulfman, L.H., Hofhuis, F.M., Bierings, M.B., and Coffer, P.J. (2010). Protein kinase B (PKB/c-akt) regulates homing of hematopoietic progenitors through modulation of their adhesive and migratory properties. Blood *116*, 2373-2384.

Burns, K.D., Capdevila, J., Wei, S., Breyer, M.D., Homma, T., and Harris, R.C. (1995). Role of cytochrome P-450 epoxygenase metabolites in EGF signaling in renal proximal tubule. Am J Physiol *269*, C831-840.

Cancelas, J.A., Lee, A.W., Prabhakar, R., Stringer, K.F., Zheng, Y., and Williams, D.A. (2005). Rac GTPases differentially integrate signals regulating hematopoietic stem cell localization. Nat Med *11*, 886-891.

Carroll, M.A., and McGiff, J.C. (2000). A new class of lipid mediators: cytochrome P450 arachidonate metabolites. Thorax *55 Suppl 2*, S13-16.

Challen, G.A., and Goodell, M.A. (2010). Runx1 isoforms show differential expression patterns during hematopoietic development but have similar functional effects in adult hematopoietic stem cells. Exp Hematol *38*, 403-416.

Chen, Y., Falck, J.R., Manthati, V.L., Jat, J.L., and Campbell, W.B. (2011). 20-Iodo-14,15-epoxyeicosa-8(Z)-enoyl-3-azidophenylsulfonamide: photoaffinity labeling of a 14,15-epoxyeicosatrienoic acid receptor. Biochemistry *50*, 3840-3848.

Chen, Y., Sprung, R., Tang, Y., Ball, H., Sangras, B., Kim, S.C., Falck, J.R., Peng, J., Gu, W., and Zhao, Y. (2007). Lysine propionylation and butyrylation are novel post-translational modifications in histones. Mol Cell Proteomics *6*, 812-819.

Clements, W.K., Kim, A.D., Ong, K.G., Moore, J.C., Lawson, N.D., and Traver, D. (2011). A somitic Wnt16/Notch pathway specifies haematopoietic stem cells. Nature *474*, 220-224.

Creyghton, M.P., Cheng, A.W., Welstead, G.G., Kooistra, T., Carey, B.W., Steine, E.J., Hanna, J., Lodato, M.A., Frampton, G.M., Sharp, P.A., *et al.* (2010). Histone H3K27ac separates active from poised enhancers and predicts developmental state. Proc Natl Acad Sci U S A *107*, 21931-21936.

Czechowicz, A., Kraft, D., Weissman, I.L., and Bhattacharya, D. (2007). Efficient transplantation via antibody-based clearance of hematopoietic stem cell niches. Science *318*, 1296-1299.

Davidson, A.J., and Zon, L.I. (2004). The 'definitive' (and 'primitive') guide to zebrafish hematopoiesis. Oncogene *23*, 7233-7246.

de Jong, J.L., Burns, C.E., Chen, A.T., Pugach, E., Mayhall, E.A., Smith, A.C., Feldman, H.A., Zhou, Y., and Zon, L.I. (2011). Characterization of immune-matched hematopoietic transplantation in zebrafish. Blood *117*, 4234-4242.

Degos, L., and Wang, Z.Y. (2001). All trans retinoic acid in acute promyelocytic leukemia. Oncogene *20*, 7140-7145.

Dobie, K.W., Lee, M., Fantes, J.A., Graham, E., Clark, A.J., Springbett, A., Lathe, R., and McClenaghan, M. (1996). Variegated transgene expression in mouse mammary gland is determined by the transgene integration locus. Proc Natl Acad Sci U S A *93*, 6659-6664.

Eferl, R., Sibilia, M., Hilberg, F., Fuchsbichler, A., Kufferath, I., Guertl, B., Zenz, R., Wagner, E.F., and Zatloukal, K. (1999). Functions of c-Jun in liver and heart development. J Cell Biol *145*, 1049-1061.

Fleming, I. (2007). Epoxyeicosatrienoic acids, cell signaling and angiogenesis. Prostaglandins Other Lipid Mediat *82*, 60-67.

Forsberg, E.C., Passegue, E., Prohaska, S.S., Wagers, A.J., Koeva, M., Stuart, J.M., and F, I.L. (2010). Molecular signatures of quiescent, mobilized and leukemia-initiating hematopoietic stem cells. PLoS One *5*, e8785.

Frazer, J.K., Meeker, N.D., Rudner, L., Bradley, D.F., Smith, A.C., Demarest, B., Joshi, D., Locke, E.E., Hutchinson, S.A., Tripp, S.*, et al.* (2009). Heritable T-cell malignancy models established in a zebrafish phenotypic screen. Leukemia *23*, 1825-1835.

Garrick, D., Fiering, S., Martin, D.I., and Whitelaw, E. (1998). Repeat-induced gene silencing in mammals. Nat Genet *18*, 56-59.

Gillette-Ferguson, I., Ferguson, D.G., Poss, K.D., and Moorman, S.J. (2003). Changes in gravitational force induce alterations in gene expression that can be monitored in the live, developing zebrafish heart. Adv Space Res *32*, 1641-1646.

Gluckman, E. (2011). Milestones in umbilical cord blood transplantation. Blood Rev *25*, 255-259.

Goessling, W., North, T.E., Loewer, S., Lord, A.M., Lee, S., Stoick-Cooper, C.L., Weidinger, G., Puder, M., Daley, G.Q., Moon, R.T.*, et al.* (2009). Genetic interaction of

PGE2 and Wnt signaling regulates developmental specification of stem cells and regeneration. Cell *136*, 1136-1147.

Graser, R., Vincek, V., Takami, K., and Klein, J. (1998). Analysis of zebrafish Mhc using BAC clones. Immunogenetics *47*, 318-325.

Gu, Y., Filippi, M.D., Cancelas, J.A., Siefring, J.E., Williams, E.P., Jasti, A.C., Harris, C.E., Lee, A.W., Prabhakar, R., Atkinson, S.J.*, et al.* (2003). Hematopoietic cell regulation by Rac1 and Rac2 guanosine triphosphatases. Science *302*, 445-449.

Haeggstrom, J.Z., and Funk, C.D. (2011). Lipoxygenase and leukotriene pathways: biochemistry, biology, and roles in disease. Chem Rev *111*, 5866-5898.

Hall, C., Flores, M.V., Storm, T., Crosier, K., and Crosier, P. (2007). The zebrafish lysozyme C promoter drives myeloid-specific expression in transgenic fish. BMC Dev Biol *7*, 42.

Hoggatt, J., Singh, P., Sampath, J., and Pelus, L.M. (2009). Prostaglandin E2 enhances hematopoietic stem cell homing, survival, and proliferation. Blood *113*, 5444-5455.

Hoi, C.S., Lee, S.E., Lu, S.Y., McDermitt, D.J., Osorio, K.M., Piskun, C.M., Peters, R.M., Paus, R., and Tumbar, T. (2010). Runx1 directly promotes proliferation of hair follicle stem cells and epithelial tumor formation in mouse skin. Mol Cell Biol *30*, 2518-2536.

Hu, Y., and Smyth, G.K. (2009). ELDA: extreme limiting dilution analysis for comparing depleted and enriched populations in stem cell and other assays. J Immunol Methods *347*, 70-78.

Ichikawa, M., Asai, T., Saito, T., Seo, S., Yamazaki, I., Yamagata, T., Mitani, K., Chiba, S., Ogawa, S., Kurokawa, M.*, et al.* (2004). AML-1 is required for megakaryocytic maturation and lymphocytic differentiation, but not for maintenance of hematopoietic stem cells in adult hematopoiesis. Nat Med *10*, 299-304.

Ignatius, M.S., and Langenau, D.M. (2009). Zebrafish as a model for cancer self-renewal. Zebrafish *6*, 377-387.

Jiang, J.G., Ning, Y.G., Chen, C., Ma, D., Liu, Z.J., Yang, S., Zhou, J., Xiao, X., Zhang, X.A., Edin, M.L.*, et al.* (2007). Cytochrome p450 epoxygenase promotes human cancer metastasis. Cancer Res *67*, 6665-6674.

Jochum, W., Passegue, E., and Wagner, E.F. (2001). AP-1 in mouse development and tumorigenesis. Oncogene *20*, 2401-2412.

Johnson, A.D., and Krieg, P.A. (1994). pXeX, a vector for efficient expression of cloned sequences in Xenopus embryos. Gene *147*, 223-226.

Kaczor, A.A., and Selent, J. (2011). Oligomerization of G protein-coupled receptors: biochemical and biophysical methods. Curr Med Chem *18*, 4606-4634.

Kalev-Zylinska, M.L., Horsfield, J.A., Flores, M.V., Postlethwait, J.H., Vitas, M.R., Baas, A.M., Crosier, P.S., and Crosier, K.E. (2002). Runx1 is required for zebrafish blood and vessel development and expression of a human RUNX1-CBF2T1 transgene advances a model for studies of leukemogenesis. Development *129*, 2015-2030.

Kapoor, R., and Huang, Y.S. (2006). Gamma linolenic acid: an antiinflammatory omega-6 fatty acid. Curr Pharm Biotechnol *7*, 531-534.

Kelly, P., Stemmle, L.N., Madden, J.F., Fields, T.A., Daaka, Y., and Casey, P.J. (2006). A role for the G12 family of heterotrimeric G proteins in prostate cancer invasion. J Biol Chem *281*, 26483-26490.

Kent, D., Copley, M., Benz, C., Dykstra, B., Bowie, M., and Eaves, C. (2008). Regulation of hematopoietic stem cells by the steel factor/KIT signaling pathway. Clin Cancer Res *14*, 1926-1930.

Kharas, M.G., Okabe, R., Ganis, J.J., Gozo, M., Khandan, T., Paktinat, M., Gilliland, D.G., and Gritsman, K. (2010). Constitutively active AKT depletes hematopoietic stem cells and induces leukemia in mice. Blood *115*, 1406-1415.

Kiel, M.J., Yilmaz, O.H., Iwashita, T., Terhorst, C., and Morrison, S.J. (2005). SLAM family receptors distinguish hematopoietic stem and progenitor cells and reveal endothelial niches for stem cells. Cell *121*, 1109-1121.

Kikuchi, K., Holdway, J.E., Major, R.J., Blum, N., Dahn, R.D., Begemann, G., and Poss, K.D. (2011). Retinoic acid production by endocardium and epicardium is an injury response essential for zebrafish heart regeneration. Dev Cell *20*, 397-404.

Kim, E., Ambroziak, P., Otto, J.C., Taylor, B., Ashby, M., Shannon, K., Casey, P.J., and Young, S.G. (1999). Disruption of the mouse Rce1 gene results in defective Ras processing and mislocalization of Ras within cells. J Biol Chem *274*, 8383-8390.

Kissa, K., and Herbomel, P. (2010). Blood stem cells emerge from aortic endothelium by a novel type of cell transition. Nature *464*, 112-115.

Kobayashi, H., Butler, J.M., O'Donnell, R., Kobayashi, M., Ding, B.S., Bonner, B., Chiu, V.K., Nolan, D.J., Shido, K., Benjamin, L.*, et al.* (2010). Angiocrine factors from Akt-activated endothelial cells balance self-renewal and differentiation of haematopoietic stem cells. Nat Cell Biol *12*, 1046-1056.

Kubin, T., Poling, J., Kostin, S., Gajawada, P., Hein, S., Rees, W., Wietelmann, A., Tanaka, M., Lorchner, H., Schimanski, S.*, et al.* (2011). Oncostatin m is a major

mediator of cardiomyocyte dedifferentiation and remodeling. Cell Stem Cell *9*, 420-432.

Laird, D.J., von Andrian, U.H., and Wagers, A.J. (2008). Stem cell trafficking in tissue development, growth, and disease. Cell *132*, 612-630.

Langenau, D.M., Keefe, M.D., Storer, N.Y., Guyon, J.R., Kutok, J.L., Le, X., Goessling, W., Neuberg, D.S., Kunkel, L.M., and Zon, L.I. (2007). Effects of RAS on the genesis of embryonal rhabdomyosarcoma. Genes Dev *21*, 1382-1395.

Langenau, D.M., Traver, D., Ferrando, A.A., Kutok, J.L., Aster, J.C., Kanki, J.P., Lin, S., Prochownik, E., Trede, N.S., Zon, L.I.*, et al.* (2003). Myc-induced T cell leukemia in transgenic zebrafish. Science *299*, 887-890.

Lapidot, T., Dar, A., and Kollet, O. (2005). How do stem cells find their way home? Blood *106*, 1901-1910.

Lappano, R., and Maggiolini, M. (2011). G protein-coupled receptors: novel targets for drug discovery in cancer. Nat Rev Drug Discov *10*, 47-60.

Lee, C.R., Imig, J.D., Edin, M.L., Foley, J., DeGraff, L.M., Bradbury, J.A., Graves, J.P., Lih, F.B., Clark, J., Myers, P.*, et al.* (2010). Endothelial expression of human cytochrome P450 epoxygenases lowers blood pressure and attenuates hypertension-induced renal injury in mice. Faseb J *24*, 3770-3781.

Lee, H.S., Simon, J.A., and Lis, J.T. (1988). Structure and expression of ubiquitin genes of Drosophila melanogaster. Mol Cell Biol *8*, 4727-4735.

Lengerke, C., Schmitt, S., Bowman, T.V., Jang, I.H., Maouche-Chretien, L., McKinney-Freeman, S., Davidson, A.J., Hammerschmidt, M., Rentzsch, F., Green, J.B.*, et al.* (2008). BMP and Wnt specify hematopoietic fate by activation of the Cdx-Hox pathway. Cell Stem Cell *2*, 72-82.

Levanon, D., Brenner, O., Negreanu, V., Bettoun, D., Woolf, E., Eilam, R., Lotem, J., Gat, U., Otto, F., Speck, N.*, et al.* (2001). Spatial and temporal expression pattern of Runx3 (Aml2) and Runx1 (Aml1) indicates non-redundant functions during mouse embryogenesis. Mech Dev *109*, 413-417.

Lieschke, G.J., and Trede, N.S. (2009). Fish immunology. Curr Biol *19*, R678-682.

Lin, F., Sepich, D.S., Chen, S., Topczewski, J., Yin, C., Solnica-Krezel, L., and Hamm, H. (2005). Essential roles of G{alpha}12/13 signaling in distinct cell behaviors driving zebrafish convergence and extension gastrulation movements. J Cell Biol *169*, 777-787.

Linnemann, A.K., O'Geen, H., Keles, S., Farnham, P.J., and Bresnick, E.H. (2011). Genetic framework for GATA factor function in vascular biology. Proc Natl Acad Sci U S A *108*, 13641-13646.

Long, Q., Meng, A., Wang, H., Jessen, J.R., Farrell, M.J., and Lin, S. (1997). GATA-1 expression pattern can be recapitulated in living transgenic zebrafish using GFP reporter gene. Development *124*, 4105-4111.

Lutton, J.D., Schwartzman, M.L., and Abraham, N.G. (1989). Cytochrome P450 dependent arachidonic acid metabolism in hemopoietic cells. Adv Exp Med Biol *271*, 115-121.

Ma, D., Zhang, J., Lin, H.F., Italiano, J., and Handin, R.I. (2011). The identification and characterization of zebrafish hematopoietic stem cells. Blood *118*, 289-297.

Maurice, P., Kamal, M., and Jockers, R. (2011). Asymmetry of GPCR oligomers supports their functional relevance. Trends Pharmacol Sci *32*, 514-520.

Mazo, I.B., Gutierrez-Ramos, J.C., Frenette, P.S., Hynes, R.O., Wagner, D.D., and von Andrian, U.H. (1998). Hematopoietic progenitor cell rolling in bone marrow microvessels: parallel contributions by endothelial selectins and vascular cell adhesion molecule 1. J Exp Med *188*, 465-474.

Mazo, I.B., Massberg, S., and von Andrian, U.H. (2011). Hematopoietic stem and progenitor cell trafficking. Trends Immunol *32*, 493-503.

Means, A.L., and Gudas, L.J. (1995). The roles of retinoids in vertebrate development. Annu Rev Biochem *64*, 201-233.

Meder, B., Just, S., Vogel, B., Rudloff, J., Gartner, L., Dahme, T., Huttner, I., Zankl, A., Katus, H.A., and Rottbauer, W. (2010). JunB-CBFbeta signaling is essential to maintain sarcomeric Z-disc structure and when defective leads to heart failure. J Cell Sci *123*, 2613-2620.

Meijering, E., Dzyubachyk, O., Smal, I., and van Cappellen, W.A. (2009). Tracking in cell and developmental biology. Semin Cell Dev Biol *20*, 894-902.

Mercier, F.E., Ragu, C., and Scadden, D.T. (2011). The bone marrow at the crossroads of blood and immunity. Nat Rev Immunol *12*, 49-60.

Michaelis, U.R., Fisslthaler, B., Barbosa-Sicard, E., Falck, J.R., Fleming, I., and Busse, R. (2005). Cytochrome P450 epoxygenases 2C8 and 2C9 are implicated in hypoxia-induced endothelial cell migration and angiogenesis. J Cell Sci *118*, 5489-5498.

Michaelis, U.R., and Fleming, I. (2006). From endothelium-derived hyperpolarizing factor (EDHF) to angiogenesis: Epoxyeicosatrienoic acids (EETs) and cell signaling. Pharmacol Ther *111*, 584-595.

Micklem, H.S., Clarke, C.M., Evans, E.P., and Ford, C.E. (1968). Fate of chromosome-marked mouse bone marrow cells tranfused into normal syngeneic recipients. Transplantation *6*, 299-302.

Mizgireuv, I.V., and Revskoy, S.Y. (2006). Transplantable tumor lines generated in clonal zebrafish. Cancer Res *66*, 3120-3125.

Mizgirev, I., and Revskoy, S. (2010). Generation of clonal zebrafish lines and transplantable hepatic tumors. Nat Protoc *5*, 383-394.

Monson, C.A., and Sadler, K.C. (2010). Inbreeding depression and outbreeding depression are evident in wild-type zebrafish lines. Zebrafish *7*, 189-197.

Murayama, E., Kissa, K., Zapata, A., Mordelet, E., Briolat, V., Lin, H.F., Handin, R.I., and Herbomel, P. (2006). Tracing hematopoietic precursor migration to successive hematopoietic organs during zebrafish development. Immunity *25*, 963-975.

Nithipatikom, K., Brody, D.M., Tang, A.T., Manthati, V.L., Falck, J.R., Williams, C.L., and Campbell, W.B. (2010). Inhibition of carcinoma cell motility by epoxyeicosatrienoic acid (EET) antagonists. Cancer Sci *101*, 2629-2636.

Node, K., Ruan, X.L., Dai, J., Yang, S.X., Graham, L., Zeldin, D.C., and Liao, J.K. (2001). Activation of Galpha s mediates induction of tissue-type plasminogen activator gene transcription by epoxyeicosatrienoic acids. J Biol Chem *276*, 15983-15989.

North, T.E., Goessling, W., Walkley, C.R., Lengerke, C., Kopani, K.R., Lord, A.M., Weber, G.J., Bowman, T.V., Jang, I.H., Grosser, T.*, et al.* (2007). Prostaglandin E2 regulates vertebrate haematopoietic stem cell homeostasis. Nature *447*, 1007-1011.

Nottingham, W.T., Jarratt, A., Burgess, M., Speck, C.L., Cheng, J.F., Prabhakar, S., Rubin, E.M., Li, P.S., Sloane-Stanley, J., Kong, A.S.J.*, et al.* (2007). Runx1-mediated hematopoietic stem-cell emergence is controlled by a Gata/Ets/SCL-regulated enhancer. Blood *110*, 4188-4197.

Offermanns, S., Mancino, V., Revel, J.P., and Simon, M.I. (1997). Vascular system defects and impaired cell chemokinesis as a result of Galpha13 deficiency. Science *275*, 533-536.

Orkin, S.H., and Zon, L.I. (2008). Hematopoiesis: an evolving paradigm for stem cell biology. Cell *132*, 631-644.

Osorio, K.M., Lee, S.E., McDermitt, D.J., Waghmare, S.K., Zhang, Y.V., Woo, H.N., and Tumbar, T. (2008). Runx1 modulates developmental, but not injury-driven, hair follicle stem cell activation. Development *135*, 1059-1068.

Osorio, K.M., Lilja, K.C., and Tumbar, T. (2011). Runx1 modulates adult hair follicle stem cell emergence and maintenance from distinct embryonic skin compartments. J Cell Biol *193*, 235-250.

Panigrahy, D., Edin, M.L., Lee, C.R., Huang, S., Bielenberg, D.R., Butterfield, C.E., Barnes, C.M., Mammoto, A., Mammoto, T., Luria, A.*, et al.* (2011a). Epoxyeicosanoids stimulate multiorgan metastasis and tumor dormancy escape in mice. J Clin Invest.

Panigrahy, D., Greene, E.R., Pozzi, A., Wang, D.W., and Zeldin, D.C. (2011b). EET signaling in cancer. Cancer Metastasis Rev.

Papayannopoulou, T., Craddock, C., Nakamoto, B., Priestley, G.V., and Wolf, N.S. (1995). The VLA4/VCAM-1 adhesion pathway defines contrasting mechanisms of lodgement of transplanted murine hemopoietic progenitors between bone marrow and spleen. Proc Natl Acad Sci U S A *92*, 9647-9651.

Passegue, E., Jochum, W., Schorpp-Kistner, M., Mohle-Steinlein, U., and Wagner, E.F. (2001). Chronic myeloid leukemia with increased granulocyte progenitors in mice lacking junB expression in the myeloid lineage. Cell *104*, 21-32.

Patton, E.E., Widlund, H.R., Kutok, J.L., Kopani, K.R., Amatruda, J.F., Murphey, R.D., Berghmans, S., Mayhall, E.A., Traver, D., Fletcher, C.D.*, et al.* (2005). BRAF mutations are sufficient to promote nevi formation and cooperate with p53 in the genesis of melanoma. Curr Biol *15*, 249-254.

Pfister, S.L., Gauthier, K.M., and Campbell, W.B. (2010). Vascular pharmacology of epoxyeicosatrienoic acids. Adv Pharmacol *60*, 27-59.

Sabaawy, H.E., Azuma, M., Embree, L.J., Tsai, H.J., Starost, M.F., and Hickstein, D.D. (2006). TEL-AML1 transgenic zebrafish model of precursor B cell acute lymphoblastic leukemia. Proc Natl Acad Sci U S A *103*, 15166-15171.

Sambrook, J.G., Figueroa, F., and Beck, S. (2005). A genome-wide survey of Major Histocompatibility Complex (MHC) genes and their paralogues in zebrafish. BMC Genomics *6*, 152.

Schaefer, B.C., Schaefer, M.L., Kappler, J.W., Marrack, P., and Kedl, R.M. (2001). Observation of antigen-dependent CD8+ T-cell/ dendritic cell interactions in vivo. Cell Immunol *214*, 110-122.

Schorpp, M., Jager, R., Schellander, K., Schenkel, J., Wagner, E.F., Weiher, H., and Angel, P. (1996). The human ubiquitin C promoter directs high ubiquitous expression of transgenes in mice. Nucleic Acids Res *24*, 1787-1788.

Sharpless, N.E., and Depinho, R.A. (2006). The mighty mouse: genetically engineered mouse models in cancer drug development. Nat Rev Drug Discov *5*, 741-754.

Slusarski, D.C., Corces, V.G., and Moon, R.T. (1997). Interaction of Wnt and a Frizzled homologue triggers G-protein-linked phosphatidylinositol signalling. Nature *390*, 410-413.

Smith, A.C., Raimondi, A.R., Salthouse, C.D., Ignatius, M.S., Blackburn, J.S., Mizgirev, I.V., Storer, N.Y., de Jong, J.L., Chen, A.T., Zhou, Y.*, et al.* (2010). High-throughput cell transplantation establishes that tumor-initiating cells are abundant in zebrafish T-cell acute lymphoblastic leukemia. Blood *115*, 3296-3303.

Soza-Ried, C., Hess, I., Netuschil, N., Schorpp, M., and Boehm, T. (2010). Essential role of c-myb in definitive hematopoiesis is evolutionarily conserved. Proc Natl Acad Sci U S A *107*, 17304-17308.

Spector, A.A. (2009). Arachidonic acid cytochrome P450 epoxygenase pathway. J Lipid Res *50 Suppl*, S52-56.

Spitsbergen, J.M., Tsai, H.W., Reddy, A., Miller, T., Arbogast, D., Hendricks, J.D., and Bailey, G.S. (2000a). Neoplasia in zebrafish (Danio rerio) treated with 7,12-dimethylbenz[a]anthracene by two exposure routes at different developmental stages. Toxicol Pathol *28*, 705-715.

Spitsbergen, J.M., Tsai, H.W., Reddy, A., Miller, T., Arbogast, D., Hendricks, J.D., and Bailey, G.S. (2000b). Neoplasia in zebrafish (Danio rerio) treated with N-methyl-N'-nitro-N-nitrosoguanidine by three exposure routes at different developmental stages. Toxicol Pathol *28*, 716-725.

Stachura, D.L., Svoboda, O., Lau, R.P., Balla, K.M., Zon, L.I., Bartunek, P., and Traver, D. (2011). Clonal analysis of hematopoietic progenitor cells in the zebrafish. Blood *118*, 1274-1282.

Streisinger, G., Walker, C., Dower, N., Knauber, D., and Singer, F. (1981). Production of clones of homozygous diploid zebra fish (Brachydanio rerio). Nature *291*, 293-296.

Thompson, M.A., Ransom, D.G., Pratt, S.J., MacLennan, H., Kieran, M.W., Detrich, H.W., 3rd, Vail, B., Huber, T.L., Paw, B., Brownlie, A.J.*, et al.* (1998). The cloche and spadetail genes differentially affect hematopoiesis and vasculogenesis. Dev Biol *197*, 248-269.

Topczewska, J.M., Postovit, L.M., Margaryan, N.V., Sam, A., Hess, A.R., Wheaton, W.W., Nickoloff, B.J., Topczewski, J., and Hendrix, M.J. (2006). Embryonic and tumorigenic pathways converge via Nodal signaling: role in melanoma aggressiveness. Nat Med *12*, 925-932.

Traver, D., Paw, B.H., Poss, K.D., Penberthy, W.T., Lin, S., and Zon, L.I. (2003). Transplantation and in vivo imaging of multilineage engraftment in zebrafish bloodless mutants. Nat Immunol *4*, 1238-1246.

Traver, D., Winzeler, A., Stern, H.M., Mayhall, E.A., Langenau, D.M., Kutok, J.L., Look, A.T., and Zon, L.I. (2004). Effects of lethal irradiation in zebrafish and rescue by hematopoietic cell transplantation. Blood *104*, 1298-1305.

Visnjic, D., Batinic, D., and Banfic, H. (1997). Arachidonic acid mediates interferon-gamma-induced sphingomyelin hydrolysis and monocytic marker expression in HL-60 cell line. Blood *89*, 81-91.

Vore, S.J., Eling, T.E., Danilowicz, M., Tucker, A.N., and Luster, M.I. (1989). Regulation of murine hematopoiesis by arachidonic acid metabolites. Int J Immunopharmacol *11*, 435-442.

Wang, Y., Krivtsov, A.V., Sinha, A.U., North, T.E., Goessling, W., Feng, Z., Zon, L.I., and Armstrong, S.A. (2010). The Wnt/beta-catenin pathway is required for the development of leukemia stem cells in AML. Science *327*, 1650-1653.

White, R.M., Sessa, A., Burke, C., Bowman, T., LeBlanc, J., Ceol, C., Bourque, C., Dovey, M., Goessling, W., Burns, C.E.*, et al.* (2008). Transparent adult zebrafish as a tool for in vivo transplantation analysis. Cell Stem Cell *2*, 183-189.

Williams, D.A., Zheng, Y., and Cancelas, J.A. (2008). Rho GTPases and regulation of hematopoietic stem cell localization. Methods Enzymol *439*, 365-393.

Winter-Vann, A.M., and Casey, P.J. (2005). Post-prenylation-processing enzymes as new targets in oncogenesis. Nat Rev Cancer *5*, 405-412.

Yang, F.C., Atkinson, S.J., Gu, Y., Borneo, J.B., Roberts, A.W., Zheng, Y., Pennington, J., and Williams, D.A. (2001). Rac and Cdc42 GTPases control hematopoietic stem cell shape, adhesion, migration, and mobilization. Proc Natl Acad Sci U S A *98*, 5614-5618.

Yang, S., Lin, L., Chen, J.X., Lee, C.R., Seubert, J.M., Wang, Y., Wang, H., Chao, Z.R., Tao, D.D., Gong, J.P.*, et al.* (2007). Cytochrome P-450 epoxygenases protect endothelial cells from apoptosis induced by tumor necrosis factor-alpha via MAPK and PI3K/Akt signaling pathways. Am J Physiol Heart Circ Physiol *293*, H142-151.

Yang, W., Tuniki, V.R., Anjaiah, S., Falck, J.R., Hillard, C.J., and Campbell, W.B. (2008). Characterization of epoxyeicosatrienoic acid binding site in U937 membranes using a novel radiolabeled agonist, 20-125i-14,15-epoxyeicosa-8(Z)-enoic acid. J Pharmacol Exp Ther *324*, 1019-1027.

Yoshinari, N., Ishida, T., Kudo, A., and Kawakami, A. (2009). Gene expression and functional analysis of zebrafish larval fin fold regeneration. Dev Biol *325*, 71-81.

Zhang, B., Cao, H., and Rao, G.N. (2006). Fibroblast growth factor-2 is a downstream mediator of phosphatidylinositol 3-kinase-Akt signaling in 14,15-epoxyeicosatrienoic acid-induced angiogenesis. J Biol Chem *281*, 905-914.

Zhang, F.L., and Casey, P.J. (1996). Protein prenylation: molecular mechanisms and functional consequences. Annu Rev Biochem *65*, 241-269.

Ziboh, V.A., Wong, T., Wu, M.C., and Yunis, A.A. (1986). Lipoxygenation of arachidonic acid by differentiated and undifferentiated human promyelocytic HL-60 cells. J Lab Clin Med *108*, 161-166.

Zou, Y.R., Kottmann, A.H., Kuroda, M., Taniuchi, I., and Littman, D.R. (1998). Function of the chemokine receptor CXCR4 in haematopoiesis and in cerebellar development. Nature *393*, 595-599.

Zon, L.I. (2010) Intrinsic and extrinsic control of haematopoietic stem-cell self-renewal. Nature *453*, 306-313.

Appendix 1

Epoxyeicosatrienoic Acids Induce Epithelial-Mesenchymal Transition-Like Program in the Developing Zebrafish Tail

Pulin Li[1,2] , and Leonard I. Zon[1,2,]*

[1] Stem Cell Program and Division of Hematology/Oncology, Children's Hospital Boston and Dana-Farber Cancer Institute, Howard Hughes Medical Institute, Harvard Stem Cell Institute, Harvard Medical School and, Boston, MA 02115, [2] Chemical Biology Program, Harvard University, Cambridge, MA 02138,

* To whom correspondence should be addressed
Address: 300 Longwood Avenue, Boston, MA 02115
Email: zon@enders.tch.harvard.edu

Introduction

Chapter 3 has been compiled as an independent manuscript for submission, mainly focusing on the effects of EETs (epoxyeicosatrienoic acids) on hematopoiesis. However, the effects of EETs are not restricted to the hematopoietic compartment. Additional analysis on EET-caused phenotypes of the developing zebrafish embryo tail is documented in Appendix 1. This part includes detailed description of the cellular phenotype, signaling transduction, and gene transcriptional network. The phenotype observed here is closely related to certain tumor metastasis. These additional results will contribute to the understanding of the basic signaling and molecular mechanism of EETs, especially in the context of promoting tumor metastasis.

Results

EET Effect Is Specific for Embryos Older than 24 hpf

In the chemical screen, both 11,12- and 14,15-EET could increase zebrafish kidney marrow engraftment. Therefore, we tested the effects of both EETs on embryonic hematopoiesis. Treating zebrafish embryos with 5 μM 11,12-EET between 24-36 hpf increased both AGM and tail *runx1* expression, while 14,15-EET increased AGM *runx1* at 2 μM without affecting circulation. Although 5 μM 14,15-EET also induced ectopic *runx1* expression in the tail, the embryos had circulation defects; therefore, the effect on AGM was compromised (Figure A1.1). Because 11,12-EET does not cause circulation defects at a dose that can induce robust *runx1* expression, we only used 11,12-EET in the following experiments. To see if EET has an effect on younger embryos, we treated embryos at different stages, and did in situ for both *runx1* and mesoderm markers, such as *eve1* and *papc*. We did not observe any effect of EET on embryos younger than 16 hpf (Figure A1.2A, B). However, in embryos older than 24 hpf, EET caused the expansion of the mesoderm marker, *eve1*, in the tail bud (Figure A1.2C). Therefore, EET modulates specific populations of undifferentiated progenitor cells at a specific developmental stage.

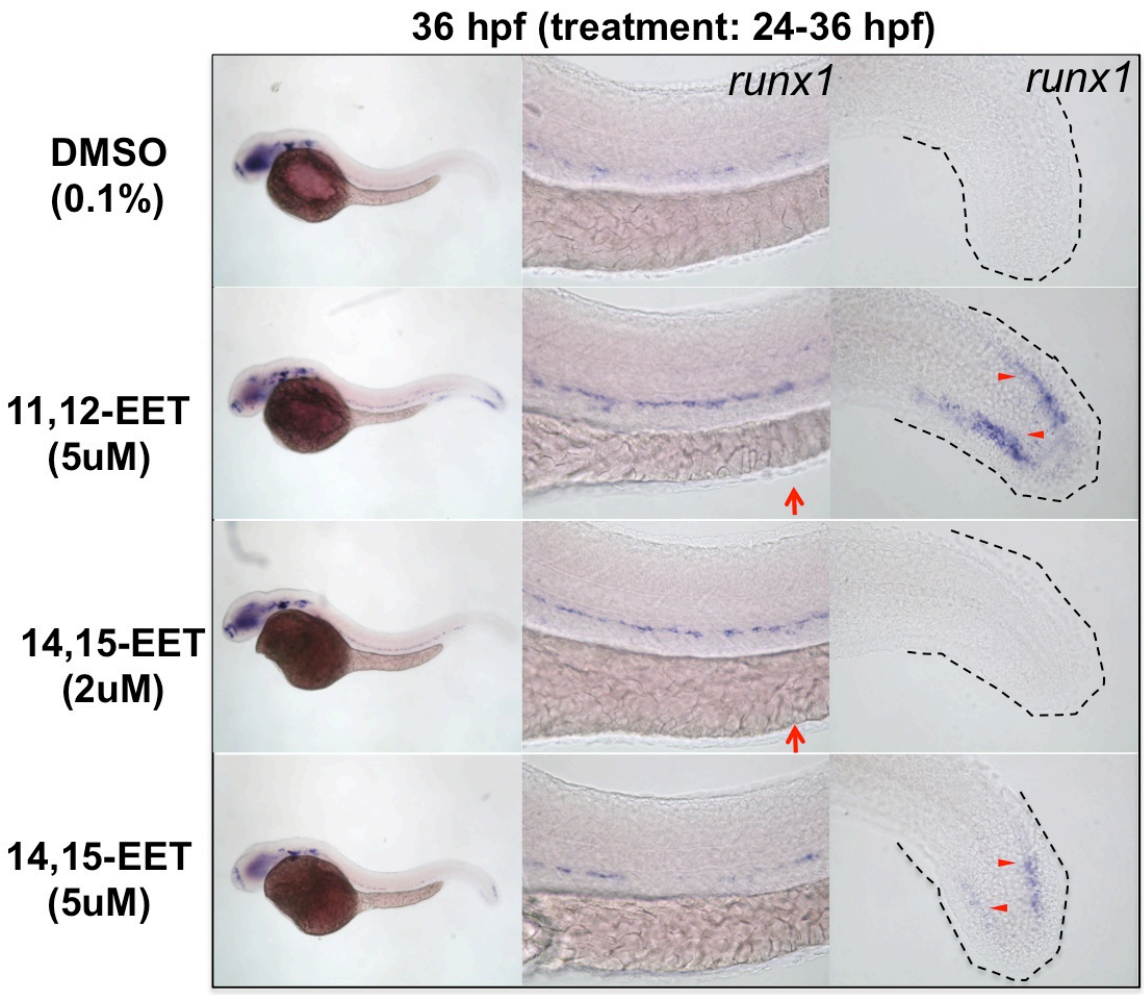

Figure A1.1 11,12- and 14,15-EET showed different dose response dynamics.

11,12-EET induced runx1 expression both in the AGM and tail at 5 μM, while 14,15-EET increased runx1 in the AGM at 2uM, and tail at 5uM. The effect of 14,15-EET on AGM runx1 expression at 5 μM is compromised by disrupted circulation.

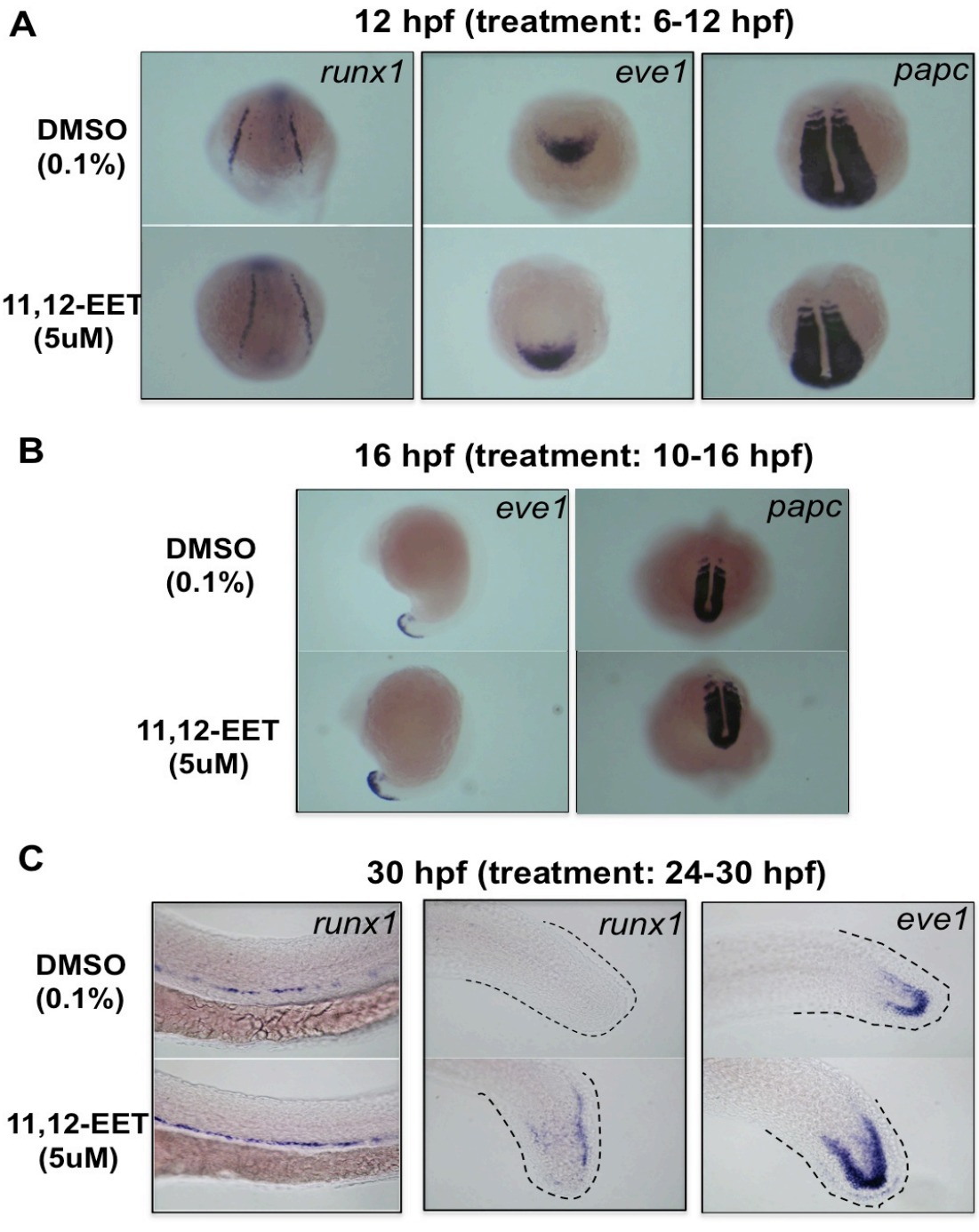

Figure A1.2 EET effect is specific on embryos older than 24 hpf.

(A) Embryos treated with 5 μM 11,12-EET between 6-12 hpf and fixed at 12 hpf.
(B) Embryos treated with 5 μM 11,12-EET between 10-16 hpf and fixed at 16 hpf.
(C) Embryos treated with 5 μM 11,12-EET between 24-30 hpf and fixed at 30 hpf.

One of the simplest explanations why the EET effect is so time-sensitive is the presence or absence of the EET receptor. However, because the EET receptor has not been identified, this hypothesis is difficult to test. Another possibility is the specific cell population in the tail bud only reaches a certain developmental stage at 24 hpf. To test this hypothesis, the ectopic *runx1+* cells must be identified. Many in situ markers were tested, such as neural crest markers *(snai2, c-kit)*, blood markers *(scl, lmo2, gata1, cmyb)*, endothelial marker *(flk, vegf)*, and other *runx* genes *(runx2a, runx2b, runx3)*. None of the above genes is expressed by these *runx1+* cells. However, we did find that the *runx1+* cell population overlaps with the cells positive for *cxcr4a,* a chemokine receptor essential for HSC homing and tumor metastasis (Figure A1.3) (Zlotnik et al., 2011). In addition, one of the *cxcr4* ligands, *sdf1b*, is expressed in the tail bud at 24hpf at a very high level (zfin.org). It can be interesting to see if EET is functionally interacting with SDF-1/CXCR4.

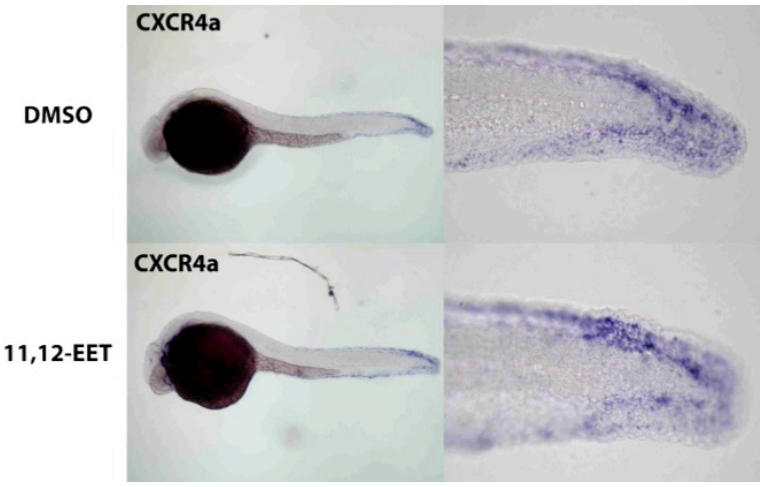

Figure A1.3 *runx1+* cells overlap with *cxcr4a+* cells in the tail bud

Embryos were treated with 5μM 11,12-EET or DMSO between 24-30 hpf. In situ hybridization with *cxcr4a* or *cxcr4b* probes was performed at 30 hpf. *cxcr4a* had high expression levels in the tail bud, but *cxcr4b* was not detected in the tail. EET treatment did not significantly change the mRNA level of *cxcr4a*.

EET Induced Morphological Changes That Resemble EMT in the Embryo Tail

Upon EET treatment of zebrafish embryos starting at 24hpf, we noticed a rapid cell morphological change in the tail bud region. The peridermal and epidermal epithelial cells started to become round and packed on the surface of the tail bud within 1hr of EET treatment. The morphological changes are EET-dose dependent, starting from 5μM, and becoming very severe at 7.5 μM (Figure A1.4). Over time, the rounded cells loosen up and bud off from the skin. The phenotype is gradually resolved, probably due to the rapid breakdown of EETs in water and/or metabolism by the embryos. By 4 hr post drug treatment, the "bubbly skin" is no longer seen with the 5 μM EET-treated embryos, but the tail fin fold looked under-developed. The rounded cells on the surface do not show increased apoptosis within 1hr of treatment by TUNEL staining when the cell morphology change has already become obvious (data not shown). Therefore, we think the budding cells are not due to cellular toxicity, but rather changes of cell adhesion properties.

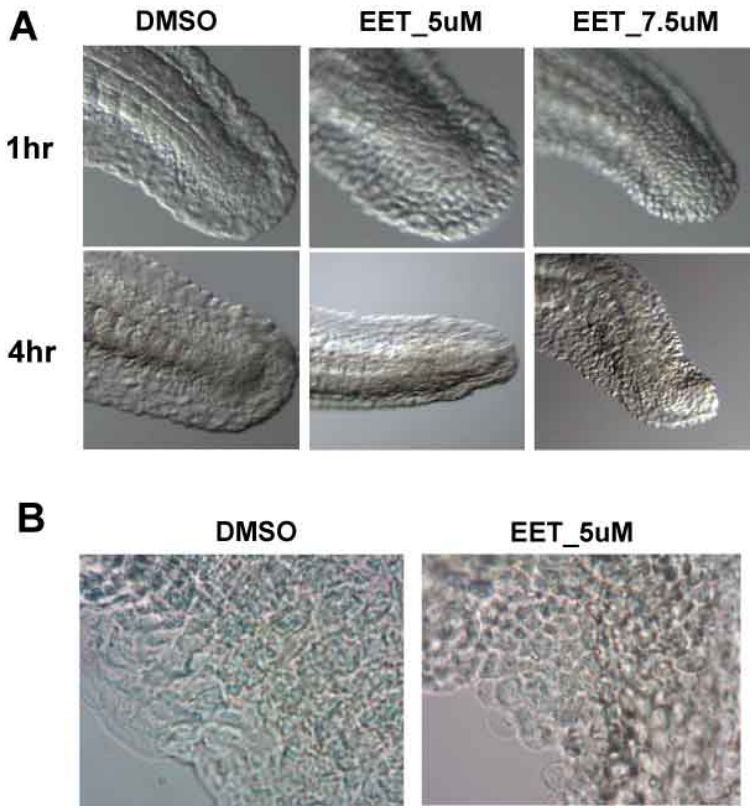

Figure A1.4 EET-induced cellular morphological change in the tail of zebrafish embryo

(A) Dose-dependent morphological changes in the tail. Treatment started at 24 hpf. (B) Higher resolution images of the cells rounding up in the tail within 1hr of EET treatment.

EET Activates the *Stat3/Fosl2/Runx1* Core Transcription Program Associated with Mesenchymal Cell Features

On the microarray list of EET-treated embryos, we noticed *socs3* is also upregulated. It is well known that both *SOCS3* and *AP-1* members are targets of *STAT* (Signal Transducer and Activator of Transcription) signaling (Ding et al., 2008). We decided to investigate the relationship between *stat3* and *AP-1/runx1* induction in

zebrafish embryos. *stat3* is highly expressed in the posterior epidermal superficial stratum between 24-36 hpf (zfin.org). Knocking down *stat3* completely abolished *runx1* induced *fosl2* and *runx1* expression in the tail and AGM, as well as basal level of AGM *runx1* expression (Figure A1.5A, B). In contrast, knocking down *stat5.1* and/or *stat5.2* did not block the effect (data not shown). Based on the genetic data, we propose a transcriptional regulation model (Figure A1.5C). A recent paper on mesenchymal transition of brain tumors also implicates this core transcription program as part of the network regulating brain tumor mesenchymal cell-like characteristics (Carro et al., 2010). Mesenchymal cells have unique adhesion properties and high migratory capabilities. Therefore, the mesenchymal-like phenotype induced by EET treatment might reflect a change in the cell adhesion and migration properties of the specific cell population in the embryo tail. This model can also explain the previous observation that EET has pro-tumorigenic, pro-metastatic, and pro-angiogenic effects (Panigrahy et al., 2011b).

It was previously reported that *Stat3* is required for mouse AGM HSC development (Takizawa et al., 2003). We performed in situ hybridization to analyze the expression pattern of *stat3* in the hematopoietic tissues in zebrafish embryos from 24 hpf to 36 hpf, but barely detected the expression of *stat3* in the AGM (data not shown). This can be either due to the insufficient sensitivity of the *stat3* in situ probe or the requirement for *stat3* at an earlier developmental stage preceding the AGM HSC specification.

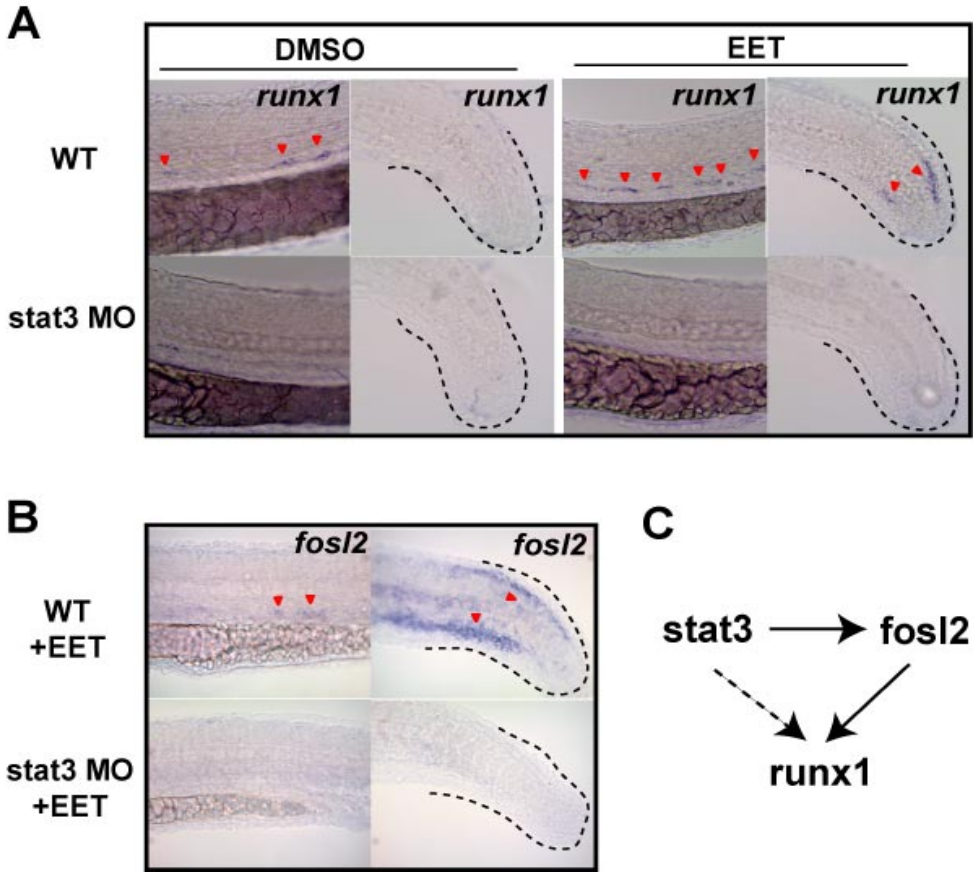

Figure A1.5 EET induced the activation of a mesenchymal cell transcription network.

(A) (B) knockdown of *stat3* in zebrafish embryos blocked EET-induced expression of *runx1* and *fosl2*. 2ng *stat3* morpholino was injected per embryo.
(C) The mesenchymal cell-like gene transcription network.

Additional Signaling Pathways Required for the Tail Phenotypes

In an attempt to identify signaling pathways downstream of EETs, we performed a chemical suppressor screen in zebrafish embryos. We found PI3K-AKT (LY294002 and Wortmannin) is required for the induction of *runx1* both in the AGM and tail (Figure 3.9). In addition, we also identified a few inhibitors that could specifically block the *runx1* induction in the tail without affecting AGM. For example,

the JNK inhibitor (SP600125) blocked both *runx1* and AP-1, but had no effects on the cholesterol metabolism genes (Figure A1.6A). EGFR (epidermal growth factor receptor) inhibitor (AG1498) could completely block both *AP-1/runx1* and the cholesterol metabolism genes (Figure A1.6A). This indicates EET-induced signaling requires the activation of a receptor tyrosine kinase (RTK) in the embryo tail bud, which in this case, is EGFR. One explanation is the EGFR pathway acts in parallel to the EET pathway, and is required for maintaining the correct identity of the cells in the tail. However, treating the embryos with the EGFR inhibitor by itself from 24 hpf did not cause any gross morphological changes in the embryo (data not shown). Another explanation is EGFR acts downstream of EET. It has been shown that in a kidney epithelial cell line, EET can transactivate EGF signaling pathway and result in the phosphorylation of EGFR within a few minutes (Burns et al., 1995). GPCRs transactivating RTKs have been reported in different systems and with different receptors, although the basic mechanism of transactivation is still unclear. So EET may transactivate EGFR in the embryo tail, although this hypothesis requires further biochemical testing.

Beside the effect on gene expression, we also examined what roles the suppressors might play in the EMT-like morphological changes in the tail. We pretreated the 24hpf embryos with the suppressors and incubated the embryos with EET for 1hr in the presence of the suppressors. We found JNK and EGFR inhibitors completely blocked the cell morphology change (Figure A1.6B). This further supports the hypothesis that JNK is downstream of EGFR. The translation inhibitor, cycloheximide, did not block the cell morphology change at all, which

indicates that EGFR-JNK activation resulted in the cell morphology change through direct signal transduction, without *de novo* protein synthesis.

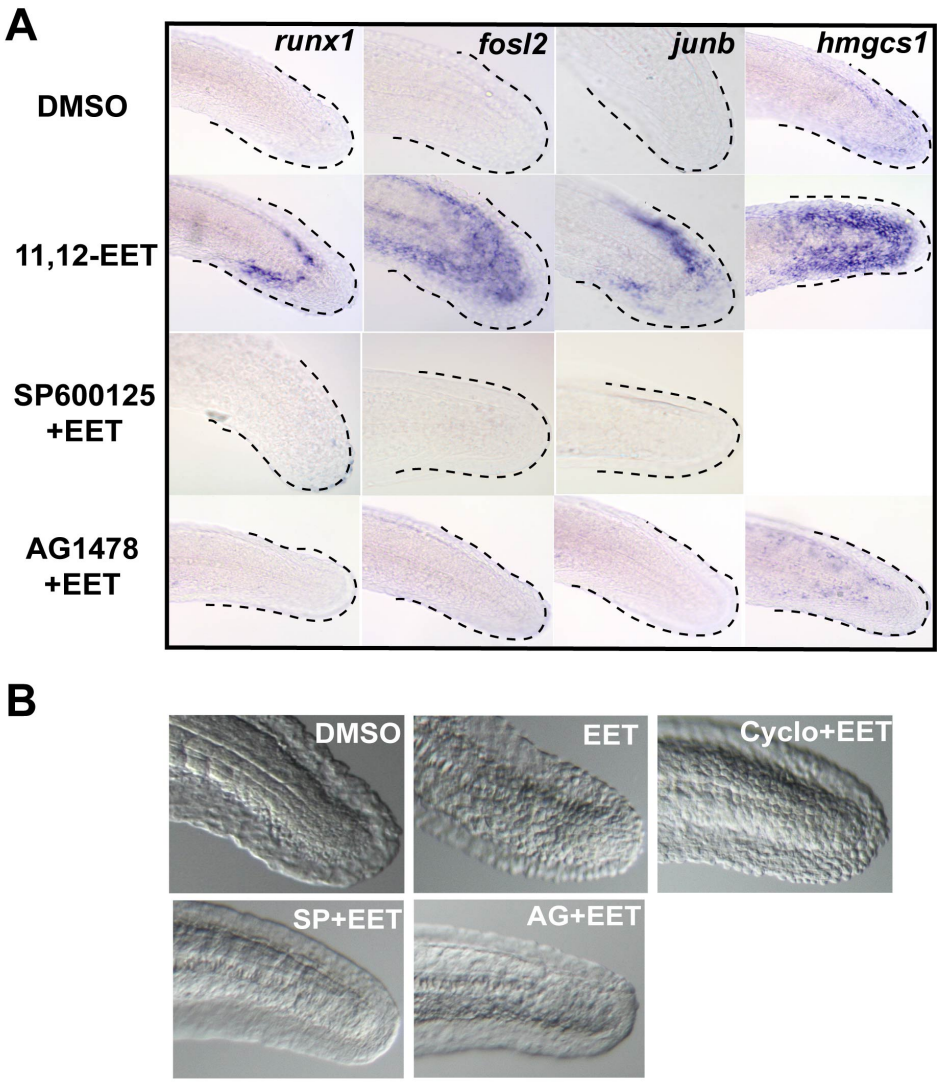

Figure A1.6 JNK and EGFR inhibitors blocked the tail phenotype.

Wild type zebrafish embryos were pre-incubated with inhibitors for 30 min at 24 hpf before 5μM 11,12-EET was added.
(A) JNK inhibitor (SP600125, 30μM) and EGFR inhibitor (AG1478, 20μM) blocked EET-induced *runx1* and AP-1 expression in the tail. AG1478 also suppressed the cholesterol metabolism gene expression.
(B) JNK and EGFR activation are required for the EET-induced cell morphology change in the tail (SP+EET and AG+EET), which is translation-independent (Cyclo+EET). SP, SP600125; AG, AG1478; Cyclo, cycloheximide.

JNK has been shown to promote cell migration through regulation of focal adhesion partially via phosphorylation of paxillin which changes cellular focal adhesion composition and assembly/disassembly dynamics, thereby leading to increased cell motility (Huang et al., 2004; Huang et al., 2003). This adhesion/migration change can also lead to transcriptional changes. One potential factor linking this cell morphology change and transcription regulation is Stat3. Phosphorylated STAT3 has been found to localize with focal adhesion complexes and directly interact with paxillin and focal adhesion kinase (Silver et al., 2004). JNK-mediated phosphorylation of paxillin can potentially exclude paxillin from the focal adhesion complexes, and lead to the nuclear translocation of p-STAT3. In fact, the nuclear translocation of p-STAT3 has been observed following 14,15-EET treatment of human breast cancer cell lines and dermal microvascular endothelial cells (Cheranov et al., 2008; Mitra et al., 2011). However, whether this adhesion-transcription relationship is causative or correlative requires further testing. Based on the observation above, EET-induced AP-1/*runx1* mRNA upregulation requires both PI3K-AKT pathway-dependent direct transcriptional regulation, and EGFR-JNK pathway-dependent cell adhesion changes (Figure A1.7).

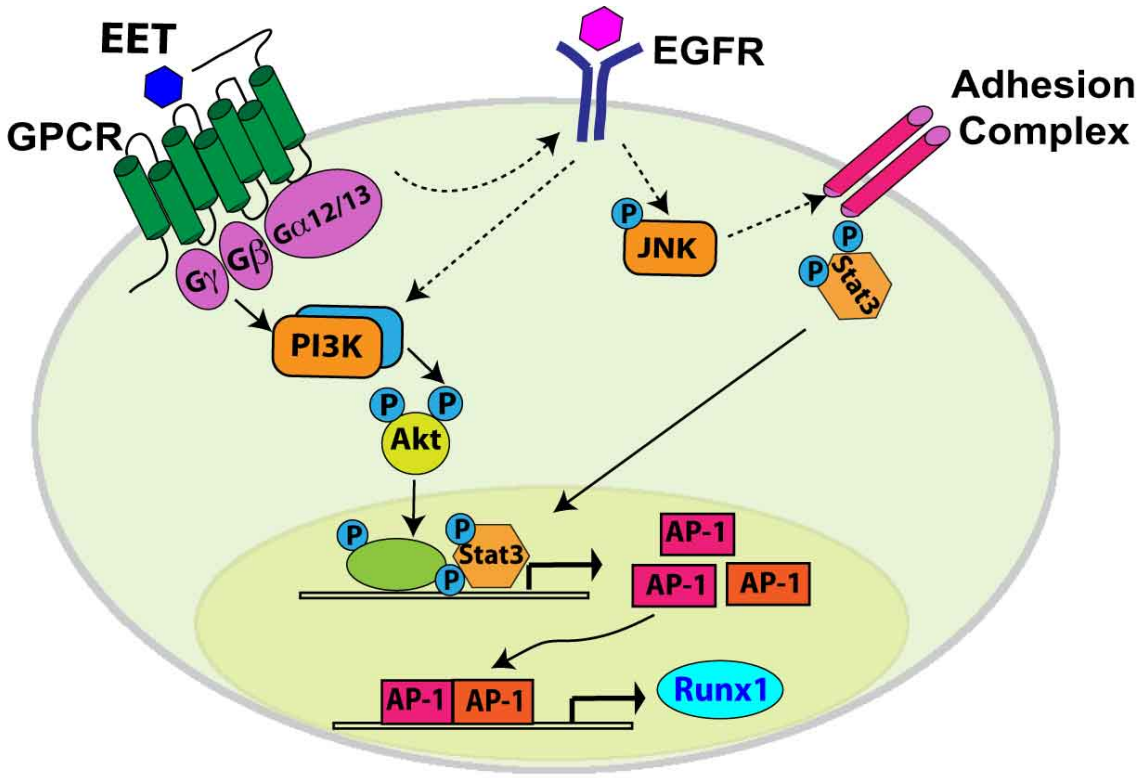

Figure A1.7 Proposed signaling model for EET-induced tail phenotype

In the zebrafish embryo tail bud, EET activates Gα12/13 through a hypothetical receptor, which crosstalks with EGFR. This leads to the activation of PI3K/AKT signaling pathway, which is require for inducing AP-1 transcription. EGFR signaling might also crosstalk with adhesion complexes, potentially through JNK signaling. This leads to the activation of Stat3, which is also required for induction of AP-1 transcription. Upregulated AP-1 levels induce *runx1* transcription.

Material and Methods

The chemical treatments and morpholino injection were performed under the same conditions as previously described in Material and Methods in Chapter 3, with some exception of the treatment time window as indicated in Figure A1.1 Additional chemicals used in the treatment are included in Table 3.5 with their corresponding concentrations. Additional morpholino sequences are listed in Table A1.1.

Table A1.1 Additional Zebrafish Morpholino Sequences

Gene	Ref Seq	MO sequence (5'→3')	Reference
stat3	NM_131479	GCCATGTTGACCCCTTA ATGTGTCG	Gene Tools
stat5.1	NM_194387	AATCCACACGGCCATGA TCACTCT	Gene Tools
stat5.2	NM_001003984	CGCCATGCCTGGCTAAG TTTTTAAC	Gene Tools

References

Burns, K.D., Capdevila, J., Wei, S., Breyer, M.D., Homma, T., and Harris, R.C. (1995). Role of cytochrome P-450 epoxygenase metabolites in EGF signaling in renal proximal tubule. Am J Physiol *269*, C831-840.

Carro, M.S., Lim, W.K., Alvarez, M.J., Bollo, R.J., Zhao, X., Snyder, E.Y., Sulman, E.P., Anne, S.L., Doetsch, F., Colman, H.*, et al.* (2010). The transcriptional network for mesenchymal transformation of brain tumours. Nature *463*, 318-325.

Cheranov, S.Y., Karpurapu, M., Wang, D., Zhang, B., Venema, R.C., and Rao, G.N. (2008). An essential role for SRC-activated STAT-3 in 14,15-EET-induced VEGF expression and angiogenesis. Blood *111*, 5581-5591.

Ding, B.B., Yu, J.J., Yu, R.Y., Mendez, L.M., Shaknovich, R., Zhang, Y., Cattoretti, G., and Ye, B.H. (2008). Constitutively activated STAT3 promotes cell proliferation and survival in the activated B-cell subtype of diffuse large B-cell lymphomas. Blood *111*, 1515-1523.

Huang, C., Jacobson, K., and Schaller, M.D. (2004). A role for JNK-paxillin signaling in cell migration. Cell Cycle *3*, 4-6.

Huang, C., Rajfur, Z., Borchers, C., Schaller, M.D., and Jacobson, K. (2003). JNK phosphorylates paxillin and regulates cell migration. Nature *424*, 219-223.

Mitra, R., Guo, Z., Milani, M., Mesaros, C., Rodriguez, M., Nguyen, J., Luo, X., Clarke, D., Lamba, J., Schuetz, E.*, et al.* (2011). CYP3A4 mediates growth of estrogen receptor-positive breast cancer cells in part by inducing nuclear translocation of phospho-Stat3 through biosynthesis of (+/-)-14,15-epoxyeicosatrienoic acid (EET). J Biol Chem *286*, 17543-17559.

Panigrahy, D., Greene, E.R., Pozzi, A., Wang, D.W., and Zeldin, D.C. (2011b). EET signaling in cancer. Cancer Metastasis Rev.

Silver, D.L., Naora, H., Liu, J., Cheng, W., and Montell, D.J. (2004). Activated signal transducer and activator of transcription (STAT) 3: localization in focal adhesions and function in ovarian cancer cell motility. Cancer Res *64*, 3550-3558.

Takizawa, M., Nobuhisa, I., Igarashi, K., Ueno, M., Nakashima, K., Kitamura, T., and Taga, T. (2003). Requirement of gp130 signaling for the AGM hematopoiesis. Exp Hematol *31*, 283-289.

Zlotnik, A., Burkhardt, A.M., and Homey, B. (2011). Homeostatic chemokine receptors and organ-specific metastasis. Nat Rev Immunol *11*, 597-606.

Appendix 2

An Optical Platform for Cell Tracking in Adult Zebrafish

Li Zhang,[1,2,3] Clemens Alt,[1] Pulin Li,[4] Richard M. White,[4] Leonard I. Zon,[4] Xunbin Wei,[3,5]*

Charles P. Lin[1]*

[1]Advanced microscopy program, Center for Systems Biology and Wellman Center for Photomedicine, Massachusetts General Hospital, Harvard Medical School, Boston, Massachusetts 02114
[2] School of Life Science, Fudan University, Shanghai 200433, China
[3]Institutes of Biomedical Sciences, Fudan University, Shanghai 200032, China
[4]Harvard Medical School, Howard Hughes Medical Institute, Harvard Stem Cell Institute, Children's Hospital, Boston, Massachusetts 02115
[5]Med-X Research Institute and School of Biomedical Engineering, Shanghai Jiaotong University, Shanghai 200240, China

*Correspondence to: Charles P. Lin, Ph.D.,
Email: lin@helix.mgh.harvard.edu or xunbinwei@gmail.com
or Xunbin Wei, Med-X Research Institute and School of Biomedical Engineering, Shanghai Jiao Tong University, 1954 Huashan Road, Shanghai, China 200240

Attributions

L. Zhang, C. Alt, and C. P. Lin developed and built the imaging platform. P. Li designed the biological experiment, provided the zebrafish for imaging, annotated the vascular system in the images, and partially involved in the imaging process with L. Zhang and C. Alt. R. M. White helped with the optimization of the anesthesia procedure. Everyone contributed to the writing of the manuscript.

Cytometry
PART A
Journal of the International Society for Advancement of Cytometry

An Optical Platform for Cell Tracking in Adult Zebrafish

Li Zhang,[1,2,3] Clemens Alt,[1] Pulin Li,[4] Richard M. White,[4] Leonard I. Zon,[4] Xunbin Wei,[3,5]* Charles P. Lin[1]*

[1]Advanced microscopy program, Center for Systems Biology and Wellman Center for Photomedicine, Massachusetts General Hospital, Harvard Medical School, Boston, Massachusetts 02114

[2] School of Life Science, Fudan University, Shanghai 200433, China

[3]Institutes of Biomedical Sciences, Fudan University, Shanghai 200032, China

[4]Harvard Medical School, Howard Hughes Medical Institute, Harvard Stem Cell Institute, Children's Hospital, Boston, Massachusetts 02115

[5]Med-X Research Institute and School of Biomedical Engineering, Shanghai Jiaotong University, Shanghai 200240, China

Received 18 March 2011; Revision Received 1 September 2011; Accepted 16 October 2011

Additional Supporting Information may be found in the online version of this article.

This article was originally intended for publication in the In Vivo Flow Cytometry special issue (volume 79A, issue 10, 2011).

Grant sponsor: China Scholarship Council (CSC); Grant number: 2008610061; Grant sponsor: NIH; Grant number: HL97794.

• Abstract

Adult zebrafish are being increasingly used as a model in cancer and stem cell research. Here we describe an integrated optical system that combines a laser scanning confocal microscope (LSCM) and an in vivo flow cytometer (IVFC) for simultaneous visualization and cell quantification. The system is set up specifically for non-invasive tracking of both stationary and circulating cells in adult zebrafish (casper) that have been engineered to be optically transparent. Confocal imaging in this instrument serves the dual purpose of visualizing fish tissue microstructure and an imaging-based guide to locate a suitable vessel for quantitative analysis of circulating cells by IVFC. We demonstrate initial testing of this novel instrument by imaging the transparent adult zebrafish casper vasculature and tracking circulating cells in CD41-GFP/Gata1-DsRed transgenic fish whose thrombocytes/erythrocytes express the green and red fluorescent proteins. In vivo measurements allow cells to be tracked under physiological conditions in the same fish over time, without drawing blood samples or sacrificing animals. We also discuss the potential applications of this instrument in biomedical research. © 2011 International Society for Advancement of Cytometry

• Key terms

In vivo flow cytometry (IVFC); in vivo confocal microscopy; circulating cells; adult zebrafish

Introduction

Zebrafish have become a powerful vertebrate model organism for both genetic and chemical screens because of its high degree of genetic conservation to human, its rapid development, small size, and cost-effectiveness (1). In particular, the zebrafish embryo is often used for studies of organ development because it is transparent and easy to image. The adult zebrafish, on the other hand, is commonly used in the studies of disease processes such as tumor growth, invasion, metastases, angiogenesis, and in stem cell and transplantation research as well. Up to date imaging studies have been limited to embryogenesis due to the opacity of the adult fish. Recently, a line of transparent adult zebrafish, named casper, have been created to facilitate in vivo visualization with fluorescence microscopy. This fish line is a double mutant that lacks both the pigmented melanocytes and reflective iridophores (2). This new model of adult zebrafish brought forth a possibility to longitudinally visualize complex biological processes in vivo at an anatomic resolution not readily achievable in murine or other systems. With the creation of the casper model comes a new opportunity (and need) to develop more advanced in vivo imaging and quantitative techniques to study cellular processes in the fish with single cell resolution and sensitivity.

Standard flow cytometry has been used in quantitative analysis of isolated cell populations from zebrafish, which often requires the fish to be sacrificed or a large number of fish to be sampled. However, a technique to track hematopoietic stem cell proliferation and differentiation after marrow transplantation, or cancer cell engraftment, growth, and metastasis, in the same fish over time, is currently not available. Our group has previously developed optical methods for in vivo tracking of stem

*Correspondence to: Charles P. Lin, Ph.D., Advanced Microscopy Program, Wellman Center for Photomedicine and Center for Systems Biology, Massachusetts General Hospital, BAR 804, Harvard Medical School, 50 Blossom Street, Boston, MA 02114 or Xunbin Wei, Med-X Research Institute and School of Biomedical Engineering, Shanghai Jiao Tong University, 1954 Huashan Road, Shanghai, China 200240.

Email: lin@helix.mgh.harvard.edu or xunbinwei@gmail.com

Published online in Wiley Online Library (wileyonlinelibrary.com)

DOI: 10.1002/cyto.a.21167

cells, cancer cells, and immune cells in live mice (3–5). A video rate laser scanning confocal microscope (LSCM) was optimized for live small animal imaging that is capable of imaging moving objects and searching for rare cells, as well as rapidly acquiring 3D data sets for assessing large tissue volumes (6). Complementing in vivo imaging, an in vivo flow cytometer (IVFC) was developed for real-time detection and enumeration of circulating fluorescent cells in mouse circulation (7,8), in which an excitation laser beam is focused to a slit across a blood vessel. Each time a fluorescently labeled cell crosses the laser slit, an emission is detected and counted. If applicable to zebrafish, these techniques allow comprehensive optical examination of live zebrafish over time without sacrifice or phlebotomy, therefore reducing the variations between individuals and reducing the overall number of zebrafish.

The typical fish circulation is a single circuit: heart-gills-body-heart. In contrast to mammals, the low-pressure circulatory system of the fish does not have strong pulsation associated with the heartbeat, and the difference in flow rates between arteries and veins is relatively small. However, unlike the flat part of the mouse ear commonly used for the IVFC measurements, the fish body has a dense 3D vascular network. Therefore, a confocal microscope is necessary to locate an appropriate vessel in the fish body with precise and consistent 3D positioning accuracy required for IVFC measurement. Here, we report the development of a dedicated system combining confocal microscopy and flow cytometry functionalities, so that both stationary and circulating cell populations can be tracked in transparent adult zebrafish in a single setting. Initial experiments to evaluate the two integrated techniques were undertaken in transgenic CD41-green fluorescent protein (GFP) casper fish whose circulating thrombocytes express the GFP, or in CD41-GFP/Gata1-DsRed transgenic casper fish whose red blood cells additionally express the DsRed. The vasculature was imaged after labeling with fluorescent dextrans.

Materials and Methods

This new system, for simultaneous confocal imaging and IVFC measurement in adult casper (Fig. 1), integrates two subsystems: a video rate LSCM (Fig. 1, path A), and an IVFC (Fig. 1, path B). The two paths share three continuous-wave lasers at 488 nm, (JDSU, Mipitas, CA: FCD488-020) 561 nm (Cobolt Jive Solna, Sweden; 561nm: 04-01), and 632.8 nm (Melles Griot, Rochester, NY: 05LHP991) for single-photon fluorescence excitation. A beamsplitter BS1 transmits 30% of

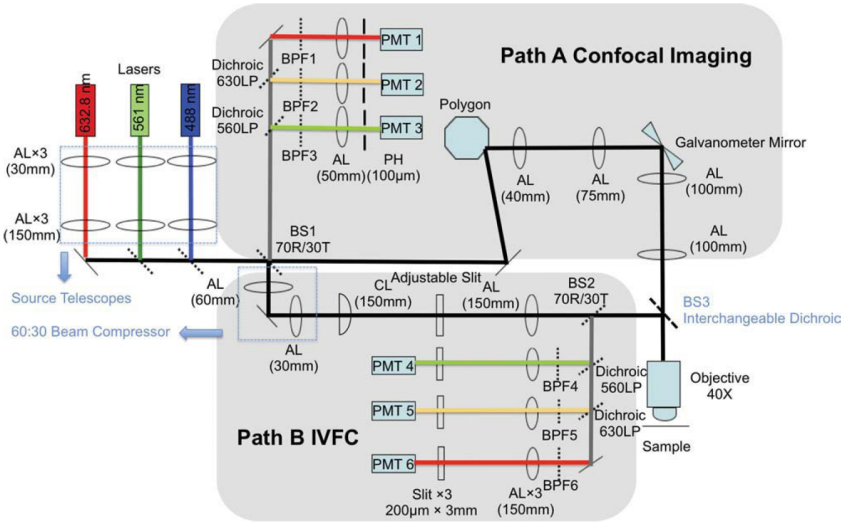

Figure 1. Schematic of the integrated system. BS1, BS2, 70R/30T beam splitters; BS3, interchangeable dichroic (see Materials and Methods for specific dichroic for different experimental settings); AL, achromatic lens; CL, cylindrical lens; BPF, band pass filters; PH, pinhole; PMT, photomultiplier tube; LP, long pass. [Color figure can be viewed in the online issue which is available at wileyonlinelibrary.com]

the laser power to the microscope and reflects 70% to the flow cytometer. The imaging beam is directed to a scanner comprising a spinning polygon (Lincoln Laser, Phoenix, AZ: DT-36-290-025) and a galvanometer mirror (Cambridge Technology: 6240H) that together form the raster scan. A 40 × objective lens (Olympus, Center Valley, PA: LUCPlanF1; 0.6NA; dry) focuses the excitation beam onto the sample and collects fluorescence photons emitted from the sample. On return, the fluorescence collected from the microscope is descanned, and reflected (70%) by BS1 onto the imaging confocal detectors, with 100 μm pinholes (corresponding to 5.11 times the airy disc) in front of the PMTs (photomultiplier tubes; Hamamatsu R3896, Japan) (PMT 1–3 in Fig. 1). The IVFC path is characterized by a cylindrical lens focusing the laser beam to a narrow slit ($\sim$5 μm wide at the sample). The length of the optical slit is controlled by an adjustable mechanical slit to match the diameter of the blood vessel to be measured. Photons emitted from fluorescent cells crossing the laser slit are collected by the same objective and reflected by BS3 and a 70R/30T beamsplitter BS2 to the IVFC confocal detectors with 200 μm × 2 mm slit apertures in front of the PMTs (PMT 4–6 in Fig. 1). The size of the slit aperture corresponds to 5 μm × 50 μm when imaged onto the sample plane. The key component of this hybrid system is the interchangeable dichroic beamsplitter BS3, which integrates the microscope and the IVFC beam paths by combining the different wavelengths. When the slot is empty, the system is set up for confocal imaging where up to three colors can be imaged simultaneously. By selecting dichroic beam splitters specific to the desired experiments, multicolor confocal imaging and multichannel IVFC are achievable. Thus, the system is highly adaptable to individual experimental needs. The laser power at the sample is 200 μW for the IVFC beams and less than 1 mW for the imaging beams.

The diameters of the laser beams were carefully adjusted at the back aperture of the microscope objective in order to fulfill the diverging requirements of the two optical modalities. For confocal imaging, over-filling the back aperture of the objective is desired to maximize numerical aperture (NA) and improve optical resolution and confocal sectioning. The beam diameter was adjusted to the desired size and divergence with a source telescope at each laser. For IVFC, NA is reduced by underfilling the back focal plane of the objective, accomplished with a 60:30 beam compressor that reduces the beam diameter of the beam incident on the objective back aperture. The result is a longer depth of focus that provides an excitation slit of uniform intensity over a depth of the maximum diameter of the blood vessel ($\approx$40 μm).

To focus the three excitation lasers at the same focal point, the 561 nm laser was chosen as the reference beam. A beam propagation analyzer (Mode Master, Coherent, St. Clara, CA) was used up to minimize the divergence and times-diffraction-limit factor (M^2) of the reference laser beam entering the confocal imaging system. Subsequently, the focal plane of the other two lasers (488 nm and 632.8 nm) was matched to the focal plane of the reference laser by slightly adjusting each respective source telescope, thus introducing beam divergence that minimizes chromatic aberrations. The alignment of the microscope was then verified and optimized in three dimensions using FocalCheck^{TM} fluorescence microscope test slide no. 1 (Invitrogen, Grand Island, NY: F36909). Focal alignment is achieved simultaneously in three colors by aligning the red, blue, and green rings of the FocalCheck^{TM} microspheres containing fluorescent red, blue, and green stains. Next, to ensure that the IVFC beams focus at the same focal plane as the imaging beams (even though the IVFC system had a longer depth of focus), the surface of a microscope slide was imaged using the 561 nm reflectance LSCM and brought into focus. Then, the 60:30 beam compressor in the IVFC beam path was adjusted until the image of the IVFC slit was sharpest and brightest on the slide surface. The alignment was verified by measuring the axial response function of both the LSCM and IVFC subsystems (plotting the two PMT output signals as the z position of the slide was translated $\pm$50 μm through the focus).

Animals

Adult zebrafish (2 months old) of the transparent casper line were used throughout the experiments. Preliminary low magnification imaging of the vasculature was performed using fli-GFP transgenic casper in which all vascular endothelial cells express the GFP. Subsequent LSCM and IVFC experiments were performed on the new system using CD41-GFP transgenic casper adults in which thrombocytes (nucleated equivalent of platelets in nonmammalian vertebrates (9)) were CD41+ (GFP+), and the vasculature was labeled by retro-orbital injection of 3 μl of a 70 kDa dextran conjugated to Texas Red (10). Additional experiments were performed using the CD41-GFP Gata1-DsRed double transgenic casper adults in which thrombocytes were GFP+ and a portion of the red blood cells were DsRed+. The vasculature of the double transgenic fish was labeled by injection of 2 μl of a 70 kDa dextran conjugated to Alexa Fluor 647. Zebrafish were maintained in E3 fish water under 28°C, pH 7.4 and salinity-controlled conditions. Zebrafish were anesthetized with tricaine in E3 fish water (4.2 ml (4 mg/ml) tricaine/100 ml fish water) before procedure. For imaging and IVFC experiments, they were anesthetized and placed in glass-bottom culture dishes. Fish were kept alive and returned into the tank within 15 min after the completion of the imaging and IVFC measurements.

In Vivo Multicolor Confocal Imaging

For confocal imaging experiments without in vivo flow cytometry, the interchangeable beam splitter (BS3) was removed. To image thrombocytes in CD41-GFP casper along with the vasculature, 488 nm and 561 nm lasers were used to excite GFP and Texas Red, respectively. GFP fluorescence was detected through a 525/50 nm band pass filter. Texas Red fluorescence was detected through a 610/60 nm band pass filter. Confocal images and movies were acquired with our custom iPhoton software at video rate (30 frames per second). The images were saved by averaging over 15 frames.

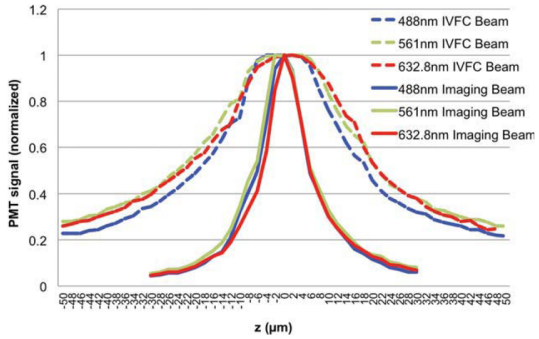

Figure 2. Axial response of LSCM and IVFC subsystems. The two subsystems were aligned to focus at the same plane. The system was designed so that the imaging subsystem had high axial resolution (solid lines, FWHM about 8 μm) while the IVFC subsystem had long depth of focus (dashed lines, FWHM about 40 μm). [Color figure can be viewed in the online issue which is available at wileyonlinelibrary.com]

In Vivo Flow Cytometry

For counting GFP+ thrombocytes in casper, a 552 nm edge dichroic beamsplitter (Semrock: FF552-Di02-25×36) was placed at BS3 to separate the wavelengths for vascular imaging (Texas Red; ex: 561 nm; em: 610/60 nm) from the wavelengths for IVFC cell counting (GFP; ex: 488 nm; em: 525/50 nm). The fish were placed on a rotating sample stage so that the selected blood vessel (seen from the imaging screen) could be oriented perpendicular to the laser slit, which excites individual fluorescently labeled cells as they flow though the laser focus. Thus, each cell generates a burst of fluorescent photons that can be detected as cell peaks. The IVFC trace was recorded in DT Measure Foundry and cell peaks were analyzed and counted by a custom Matlab program. Vessel images were overlaid with the image of excitation slit by ImageJ.

For simultaneous LSCM and two color IVFC measurement, BS3 was changed to a 605 nm edge dichroic beamsplitter (Semrock: FF605-Di02-25×36), which passes the 632.8 nm laser beam to excite the dextran-conjugated Alexa Fluor 647 (vasculature imaging), and reflects the 488 nm and 561 nm lasers beams to excite CD41-GFP and Gata1-DsRed circulating cells (IVFC measurement).

Results

To confirm that the two optical subsystems focus at the same focal plane, their respective axial response was measured. The light power was evenly split between the two subsystems by placing a 50R/50T beamsplitter at BS3. The confocal PMT signals from both the imaging and IVFC paths were recorded while a glass slide placed in the object plane was translated by ±50 μm through the focal plane. Figure 2 shows the axial response of the two subsystems using three lasers. Both the imaging beam and the IVFC beam have maximum axial response at $z = 0$, which has been defined as the location where the sharpest image was obtained. As designed, the imaging subsystem has a sharper axial response (full width at half maximum (FWHM) = 8 μm) for optical sectioning than the IVFC subsystem. The axial response of the IVFC beam has a FWHM of about 40 μm around the focal plane, therefore can probe the maximum diameter of a blood vessel that would be chosen for IVFC measurement.

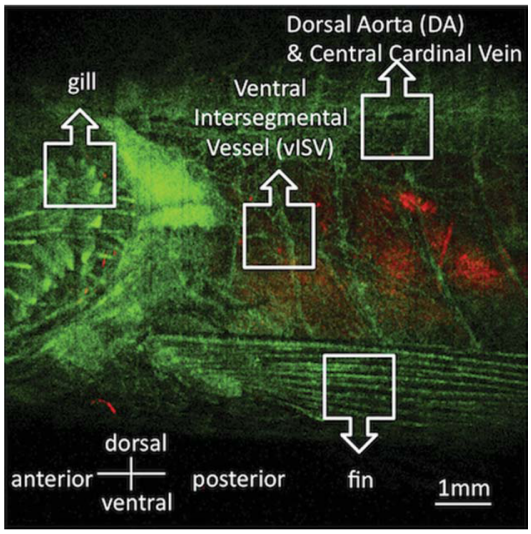

Figure 3. Image of vasculature of a fli-GFP casper where all blood vessel endothelial cells express the GFP. This image was taken with an existing confocal microscope in our laboratory at low magnification and long depth of field, to provide orientation. Because of the complex vascular network of the fish, it necessitates to perform IVFC under the guidance of 3D vasculature imaging using LSCM. Red is reflectance. [Color figure can be viewed in the online issue which is available at wileyonlinelibrary.com]

Preliminary survey of the fish vasculature was performed at low resolution using a fli-GFP transgenic casper zebrafish whose entire vasculature was labeled with the GFP (Fig. 3). To demonstrate the in vivo multicolor confocal imaging of vasculature with stationary and circulating cells in the adult zebrafish, we acquired both static images and real-time videos using the CD41-GFP casper fish whose thrombocytes express GFP; its vasculature was labeled with Texas Red (Fig. 4). We were able to visualize those thrombocytes that were sticking to the endothelium of blood vessel walls, as well as circulating thrombocytes in the blood stream. Individual GFP+ cells were observed flowing in the vessels in the skin and the muscle, and in inter-segmental vessels. Many GFP+ cells were also observed in the gills due to their rich vasculature, but a much smaller number of cells were seen circulating in the fin. Single inter-segmental arteries and veins were parallelly distributed at each transverse septum along the ventral side of the fish at depths of 120–200 μm underneath the surface of the fish skin (Fig. 4E), but the arteries and veins are not strictly arranged in alternating patterns. Intersegmental vessels were branches of a central artery or vein (Fig. 4F). Circulating thrombocytes were visible in the Supporting Information movies.

To demonstrate the *in vivo* cell quantification capability with our new system in the adult casper model, we used the

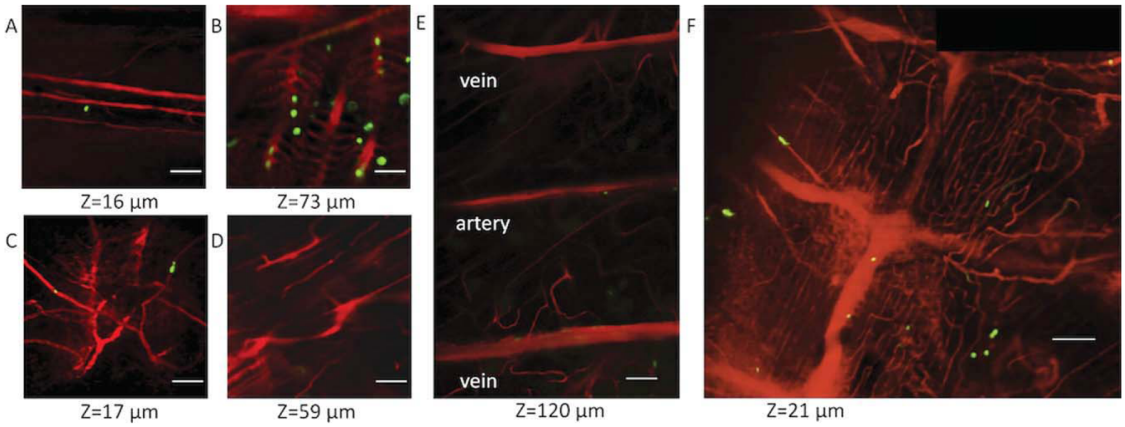

Figure 4. Images of vessels (Texas Red, red) and thrombocytes (GFP, green) at various regions and depths in a CD41-GFP casper. The imaging depth for each panel is indicated, relative to the surface of the fish (at $z = 0$). Images of vessels in (**A**) fin, (**B**) gills, (**C**) skin, (**D**) muscle, (**E**) inter-segmental vessels of parallel distribution, (**F**) caudal vein with inter-segmental veins. (C–E) were taken at different depth of the same location on the ventral side of the fish body. (E,F) are montages of several images. Scale bars are 50 μm. [Color figure can be viewed in the online issue which is available at wileyonlinelibrary.com]

same CD41-GFP fish with Texas Red labeled vasculature. With the guidence of 3D vascular imaging navigation, multiple vessels were located for IVFC test measurements (Figs. 5A and 5C). An overlaid image of the slit (blue) indicated the position of the IVFC excitation slit that was oriented perpendicularly to the vessels. Figures 5D–5F show 2 sec traces sampled from 60 sec traces recorded with the slit on the corresponding vessel in Figures 5A–5C. GFP+ cells were detected in skin vessels, (Fig. 5D) but the cell count was low. In the same fish, the cell count was much higher in the inter-segmental vessels (Figs. 5E and 5F). Comparing the inter-segmental arteries and veins, the former had narrower signal peaks and more uniform pulse width distributions, resulting in fewer overlapping peaks, making it easier to distinguish individual peaks in the arteries. The peak width histogram was computed and shown in Figure 5G.

To further demonstrate the multicolor capability of the combined LSCM and IVFC system, CD41-GFP/Gata1-DsRed double transgenic fish were used for counting two fluorescent cell populations (GFP+ thrombocytes and DsRed+ erythrocytes) while imaging the vasculature, labeled with a fluorescent dextran (Fig. 5H). Since DsRed+ red blood cells were much more abundant than GFP+ thrombocytes (about 40% of the whole blood was DsRed+), a small vessel near the skin surface was chosen for circulating cell counting to avoid frequently overlapping cell peaks. The two right panels in Figure 5H show example 2 sec traces taken from 60 sec recorded traces and show the difference in counting frequency and fluorescence intensity of the two circulating cell types.

The reproducibility of IVFC measurement in zebrafish is demonstrated in Figure 6 by measuring GFP+ thrombocytes in the same vascular locations of the same fish at three separate timepoints. The fish was anesthesized and recovered fully after each measurement (2 h apart), therefore the three time points shown in Figure 6 can be considered individual experiment. We were able to locate the same vessels each time by looking for the same vascular pattern and compared to previously stored images. IVFC data were recorded on two locations as shown in Figures 6A and 6B. The corresponding cell counts are shown in Figure 6C. The cell count for site A is the average of three 60 sec traces while at site B a single 60 sec trace was recorded for each measurement. Site B was a smaller vessel branch downstream of site A and gave a lower cell count. The cell count numbers at each site remained relatively constant.

Disscussion

We have developed an integrated optical platform that combines a LSCM with IVFC, enabling real-time 3D image capture and quantitative analysis of circulating cells in the adult zebrafish in vivo. The system can image to a depth of $\sim$180 μm with single cell resolution. To choose an optimal blood vessel for the IVFC measurement in the adult zebrafish model, the selected vessel should allow the cells of the population of interest to traverse the laser focus one at a time, with consistent flow rate, reasonable sample volume, and repeatable location. For these reasons, we do not use vessels in the fin or tail, even though these vessels are easy to visualize, because the flow rate is low and susceptible to external variables such as temperature and anesthesia. The vessels in skin and muscle have bright fluorescence signals and occasional high flow rates, but these vessels are small ($<$15 μm) and the cell counts are too low to obtain statistically meaningful results and to probe rare cells of interest (Fig. 5G). Moreover the passage of single cells through the small vessels can cause large variations in the flow rates. The inter-segmental vessels on the ventral side that are 120–200 μm underneath the skin, have diameters of 30–50 μm, and are regularly distributed, have constant flow during anesthesia, and it is easy to locate the same vessel repeatedly. Inter-segmental arteries provide the right combination of high

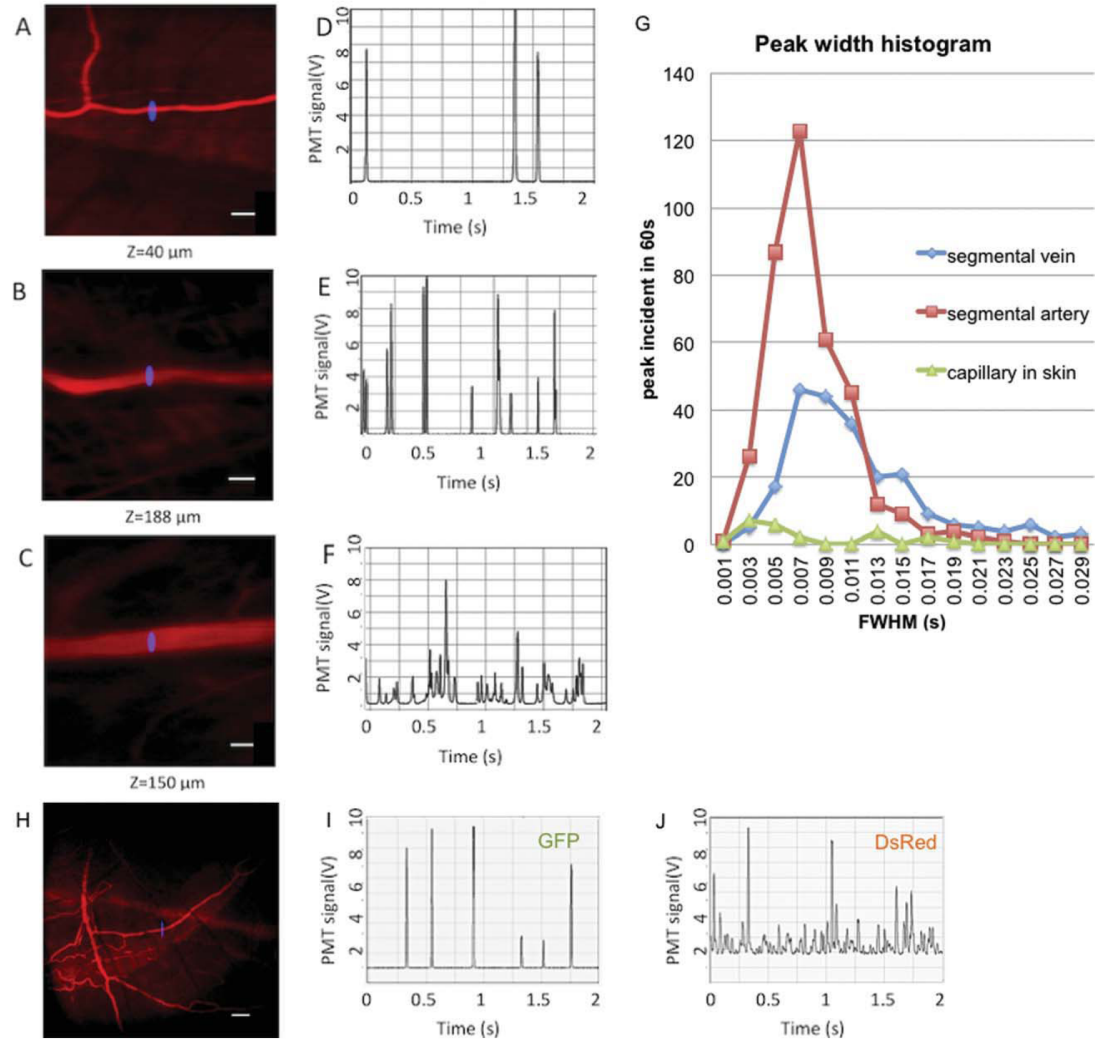

Figure 5. IVFC measurement with vessel imaging in transgenic casper. (**A**–**G**) IVFC and vessel imaging (Texas Red, red) in a CD41-GFP casper. An overlaid image of the slit indicated the position of IVFC excitation (blue). Images of (A) skin vessel, (**B**) inter-segmental artery, (**C**) inter-segmental vein, (**D**—**F**) corresponding IVFC traces. The *x*-axis denotes time in seconds, and *y*-axis is GFP fluorescence signal intensity in volts. For clarity only 2 sec of the 60 sec recorded traces are shown. G: IVFC peak width histogram of the 60 sec traces for the three vessels. **H**–**J**: Simultaneous vasculature imaging (dextran conjugated Alexa Fluor 647) and two color IVFC traces (**I**, DsRed cells; J, GFP cells) in a CD41-GFP Gata1-DsRed casper. Scale bars are 50 μm. [Color figure can be viewed in the online issue which is available at wileyonlinelibrary.com]

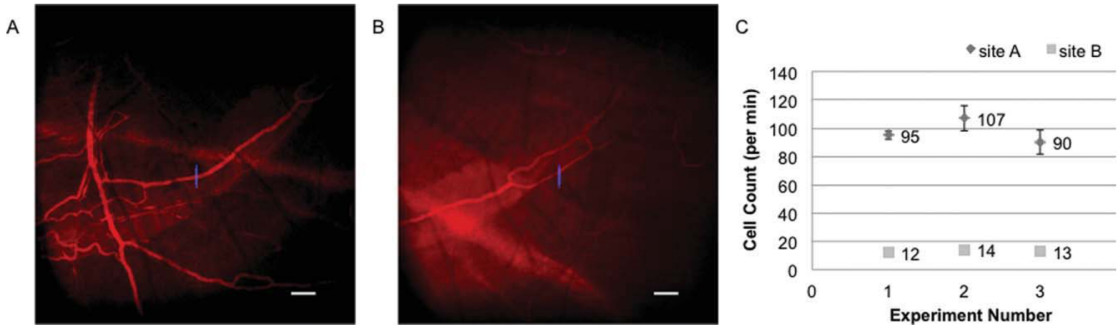

Figure 6. IVFC Reproducibility experiment. IVFC measuremnts of CD41-GFP thrombocytes performed at the same vascular locations of the same fish at three separate time points. The fish was allowed to recover in between the measurements. Site A was a small vessel and site B was a downstream branch. Vascular imaging was performed with the injection of 70 kDa dextran conjugated to Alex Fluor 647. Scale bars are 50 μm. [Color figure can be viewed in the online issue which is available at wileyonlinelibrary.com]

cell count with individual and distinguishable signal spikes. In inter-segmental veins, on the other hand, signal peaks frequently overlap, indicating that multiple cells passed through the slit. Therefore, inter-segmental arteries are the optimal choice for IVFC measurement at least in this CD41-GFP casper case. The optimum vessel size depends on how many cells of the population of interest are expected in the circulation. For counting rare cells, such as circulating tumor cells or transplanted stem cells and their progeny, a larger vessel such as the dorsal aorta or caudal artery may be needed.

The ventral inter-segmental arteries that we located in zebrafish for IVFC measurement have similar diameters as the ear arteries that were selected for IFVC measurements in mice (7). The peak width equals the time that a cell travels through the excitation slit, which is inversely porpotional to the blood flow speed. Comparison of the peak width histogram (Fig. 5G) with previous mouse data (7) shows that the flow velocity in the fish is ~3 times slower in the artery and ~1.5 time slower in the vein because of its low pressure circulatory system. For a flow velocity of ~1 mm/sec, the examed blood volume is about 0.06 μl/min in a 30 μm diameter vessel. Since an adult zebrafish has a total blood volume of ~20 μl (compared to ~2 ml for an adult mouse), the porportion of sampled volume in a 60 sec trace relative to the whole blood volume is about 30 fold higher in zebrafish than in mice, implying that it will be more likely to detect a very small number of cells circulating in a fish than in a mouse.

Our current imaging depth in the casper fish is approximately 180 μm for the LSCM. Deeper tissue imaging will be needed to access different organs such as the kidney (site of marrow engraftment) and liver (site of frequent metastasis) (11). We plan to add two-photon microscopy and adaptive optics to improve image depth in the future.

We observed that the dye injection and the laser powers used (200 μW for the IVFC beams and less than 1 mW for the imaging beams) appear well-tolerated by the fish. All fish were viable and recovered fully after the experment. We envision that as more fluorescent protein-based reporter fish become available, there will be less need for dye injection. Already the vasculature can be visualized without dye injection in the fli-GFP fish whose endothelial cells express the GFP, or in the Gata1-DsRed fish whose red blood cells (~40%) are DsRed+. Double- or triple-transgenic fish involving one of these strains are now being generated for simultaneous vascular imaging and monitoring of other cell populations of interest. Compared with current approaches to investigate adult zebrafish (phlebotomy or histological examination), the live imaging and IVFC methods enable longitudinal studies of cells within their natural environment with minimal invasiveness.

By applying imaging and quantitative techniques to transparent adult zebrafish casper model, our new system helps meet the needs for cancer and stem cell research using this emerging model. The combined LSCM and IVFC will enable both stationary and circulating cells to be tracked non-invasively over time. This system can be applied to monitoring tumor growth and metastases, and hematopoietic stem cell engraftment after transplantation, and follow up the same cohort of fish over time without affecting physiology of the fish. It can be used for identifying modifiers of tumor engraftment in genetic and chemical-based screens in adult zebrafish casper model as well (12).

Acknowledgments

Authors thank Joel Spencer for technical help and discussion, Alicia Calson for help with image acquisition, Ilya Shestopalov for fluorescent dye synthesis, and Mark Cronin-Golomb of Tufts University for the loan of the beam propagation analyzer.

Literature Cited

1. Tamplin OJ, Zon LI. Fishing at the cellular level. Nat Method 2010;7:600–601.
2. White RM, Sessa A, Burke C, Bowman T, LeBlanc J, Ceol C, Bourque C, Dovey M, Goessling W, Burns CE, et al. Transparent adult zebrafish as a tool for in vivo transplantation analysis. Cell Stem Cell 2008;2:183–189.
3. Sipkins DA, Wei X, Wu JW, Runnels JM, Cote D, Means TK, Luster AD, Scadden DT, Lin CP. In vivo imaging of specialized bone marrow endothelial microdomains for tumour engraftment. Nature 2005;435:969–973.
4. Lo Celso C, Fleming HE, Wu JW, Zhao CX, Miake-Lye S, Fujisaki J, Côté D, Rowe DW, Lin CP, Scadden DT. Live-animal tracking of individual haematopoietic stem/progenitor cells in their niche. Nature 2009;457:92–96.
5. Fan Z, Spencer JA, Lu Y, Pitsillides CP, Singh G, Kim P, Yun SH, Toxavidis V, Strom TB, Lin CP, et al. In vivo tracking of 'color-coded' effector, natural and induced regulatory T cells in the allograft response. Nat Med 2010;16:718–723.
6. Veilleux I, Spencer JA, Biss DP, Côté D, Lin CP. In vivo cell tracking with video rate multimodality laser scanning microscopy. IEEE J Sel Top Quant Electron 2008;14:10–18.
7. Novak J, Georgakoudi I, Wei X, Prossin A, Lin CP. In vivo flow cytometer for real-time detection and quantification of circulating cells. Opt Lett 2004;29:77–79.
8. Georgakoudi I, Solban N, Novak J, Rice WL, Wei X, Hasan T, Lin CP. In vivo flow cytometry: a new method for enumerating circulating cancer cells. Cancer Res 2004;64:5044–5047.
9. Lin HF, Traver D, Zhu H, Dooley K, Paw BH, Zon LI, Handin RI. Analysis of thrombocyte development in CD41-GFP transgenic zebrafish. Blood 2005;106:3803–3810.
10. Pugach EK, Li P, White RM, Zon LM. Retro-orbital Injection in Adult Zebrafish. JoVE 2009;34:1–3.
11. Kissa K, Murayama E, Zapata A, Cortes A, Perret E, Machu C, Herbomel P. Live imaging of emerging hematopoietic stem cells and early thymus colonization. Blood 2008;111:1147–1156.
12. Martin CP, Chang TY, Koo BK, Gilleland CL, Wasserman SC, Yanik MF. High-throughput in vivo vertebrate screening. Nat Methods 2010;7:634–636.

Appendix 3

Hematopoietic Stem Cell Development Is Dependent on Blood Flow

Trista E. North,[1,2,8] Wolfram Goessling,[1,3,4,5,8] Marian Peeters,[6] Pulin Li,[1] Craig Ceol,[1]

Allegra M. Lord,[1] Gerhard J. Weber,[1]James Harris,[2] Claire C. Cutting,[3] Paul Huang,[7]

*Elaine Dzierzak,[6] and Leonard I. Zon[1]**

[1]Stem Cell Program and Hematology/Oncology, Children's Hospital, Howard Hughes Medical Institute, Harvard Stem Cell Institute, Harvard Medical School, Boston, MA 02115, USA
[2]Department of Pathology, Beth Israel Deaconess Medical Center, Boston, MA 02115, USA
[3]Genetics Division
[4]Gastroenterology Division
Brigham and Women's Hospital, Boston, MA 02115, USA
[5]Medical Oncology, Dana-Farber Cancer Institute, Boston, MA 02115, USA
[6]Erasmus Stem Cell Institute, Erasmus Medical Center, 3000 DR Rotterdam, The Netherlands
[7]Cardiovascular Research Center, Massachusetts General Hospital, Boston, MA 02114, USA
[8]These authors contributed equally to this work

*Correspondence: zon@enders.tch.harvard.edu

Attributions

T. E. North and W. Goessling performed the initial chemical screen, made the figures and wrote the paper. They were also involved in most of the experiments. M. Peeters and E. Dzierzak performed the mouse embryo experiments. P. Li confirmed the blood flow-related chemicals with the same embryo assays, performed comprehensive dose titration and chemical treatment time window optimization which directly led to the discovery of nitric oxide as the important signaling mediator, helped designing the experiments, participating in discussions, and editing the manuscript (Figure 1, 3 and 4). C. Ceol performed the blastula transplantation. A.M. Lord, G. J. Weber, J. Harris, C. C. Cutting, P. Huang provided technical support. L. I. Zon was involved in the conception of the project, writing the manuscript, and contributed to the paper intellectually at all levels.

Hematopoietic Stem Cell Development Is Dependent on Blood Flow

Trista E. North,[1,2,8] Wolfram Goessling,[1,3,4,5,8] Marian Peeters,[6] Pulin Li,[1] Craig Ceol,[1] Allegra M. Lord,[1] Gerhard J. Weber,[1] James Harris,[2] Claire C. Cutting,[3] Paul Huang,[7] Elaine Dzierzak,[6] and Leonard I. Zon[1,*]

[1]Stem Cell Program and Hematology/Oncology, Children's Hospital, Howard Hughes Medical Institute, Harvard Stem Cell Institute, Harvard Medical School, Boston, MA 02115, USA

[2]Department of Pathology, Beth Israel Deaconess Medical Center, Boston, MA 02115, USA

[3]Genetics Division

[4]Gastroenterology Division

Brigham and Women's Hospital, Boston, MA 02115, USA

[5]Medical Oncology, Dana-Farber Cancer Institute, Boston, MA 02115, USA

[6]Erasmus Stem Cell Institute, Erasmus Medical Center, 3000 DR Rotterdam, The Netherlands

[7]Cardiovascular Research Center, Massachusetts General Hospital, Boston, MA 02114, USA

[8]These authors contributed equally to this work

*Correspondence: zon@enders.tch.harvard.edu

DOI 10.1016/j.cell.2009.04.023

SUMMARY

During vertebrate embryogenesis, hematopoietic stem cells (HSCs) arise in the aorta-gonads-mesonephros (AGM) region. We report here that blood flow is a conserved regulator of HSC formation. In zebrafish, chemical blood flow modulators regulated HSC development, and *silent heart* (*sih*) embryos, lacking a heartbeat and blood circulation, exhibited severely reduced HSCs. Flow-modifying compounds primarily affected HSC induction after the onset of heartbeat; however, nitric oxide (NO) donors regulated HSC number even when treatment occurred before the initiation of circulation, and rescued HSCs in *sih* mutants. Morpholino knockdown of *nos1* (*nnos/enos*) blocked HSC development, and its requirement was shown to be cell autonomous. In the mouse, *Nos3* (*eNos*) was expressed in HSCs in the AGM. Intrauterine Nos inhibition or embryonic *Nos3* deficiency resulted in a reduction of hematopoietic clusters and transplantable murine HSCs. This work links blood flow to AGM hematopoiesis and identifies NO as a conserved downstream regulator of HSC development.

INTRODUCTION

Definitive hematopoietic stem cells (HSCs) that are capable of self-renewal and production of all mature blood lineages arise during embryogenesis. Both the timing of HSC induction and the gene programs regulating this process are well conserved across vertebrate species (Orkin and Zon, 2008). Additionally, factors that affect HSC specification during embryogenesis often similarly function in HSC maintenance and/or recovery after marrow injury. The identification of factors that regulate HSC induction during embryogenesis is of significant therapeutic interest.

Murine transplantation studies revealed that adult-type long-term repopulating (LTR) HSCs arise in the aorta-gonads-mesonephros (AGM) region between embryonic day 10.5 (e10.5) and e11.5 (Dzierzak and Medvinsky, 2008). Transplantable HSCs localize to the ventral wall of the dorsal aorta and express phenotypic markers of mesenchymal, endothelial, or hematopoietic cell types. *Runx1*, commonly affected in childhood and adult leukemia (Downing et al., 1993; Golub et al., 1995), is required for the formation of functional HSCs (North et al., 1999, 2002; Wang et al., 1996); its expression is highly conserved across vertebrate species (Orkin and Zon, 2008). Based on the functional conservation of AGM hematopoiesis from fish to man, an evolutionary advantage or necessity for the production of stem cells within the aorta must exist. To identify genes that regulate HSC formation, we conducted a chemical genetic screen for regulators of *runx1/cmyb*+ cells in the zebrafish AGM at 36 hr postfertilization (hpf). We have previously identified PGE2 as a potent regulator of both HSC induction and marrow repopulation across vertebrate species (North et al., 2007). The wnt pathway similarly regulates stem cell production during embryogenesis, and genetically interacts with PGE2 (Goessling et al., 2009). The identification of novel regulators of this process will aid in connecting the complex network of signaling pathways that control both HSC development during embryogenesis and marrow regulation in the adult.

Nitric oxide (NO) plays a key role in the regulation of vascular tone, angiogenesis, and endothelial migration (Davies, 1995; Lucitti et al., 2007). As HSCs are derived from hemogenic endothelial cells within the dorsal aorta, NO produced locally in endothelial cells could link blood flow and HSC formation. NO has been detected in blood cells and extends replating ability in hematopoietic culture, presumably by maintaining HSCs in a quiescent state in vitro (Krasnov et al., 2008). While NO function in the adult hematopoietic stroma is thought to have a positive effect on hematopoiesis, data from knockout mice imply that NO production is detrimental to hematopoietic repopulation and recovery after injury (Michurina et al., 2004); this effect, however,

may be due to NO-related superoxide complexes induced by irradiation (Epperly et al., 2007). The role of NO in HSC induction in the vertebrate embryo is currently uncharacterized.

Here, we show that a diverse group of compounds that regulate blood flow affect the production of *runx1/cmyb*+ HSCs. In general, compounds that increased blood flow enhanced HSC number, whereas chemicals that decreased blood flow diminished HSCs. *silent heart* (*sih*) embryos that lack a heartbeat and fail to establish blood circulation had impaired HSC formation. Compounds that increase NO production could modify HSC formation when exposure occurred prior to the initiation of circulation and rescue HSC production in *sih* mutants. Inhibition of NO production blocked the inductive effect of several blood flow modulators on HSCs, suggesting that NO serves as the connection between blood flow and HSC formation. In the mouse, *NO synthase 3* (*Nos3; eNos*) is expressed in AGM endothelium and hematopoietic clusters, and marks LTR-HSCs. Intrauterine Nos inhibition reduced transplantable HSCs; similar results were found for the *Nos3*$^{-/-}$ knockout mice. Our work provides a direct link between the initiation of circulation and the onset of hematopoiesis within the AGM and identifies NO signaling as a conserved regulator of HSC development.

RESULTS

Modulators of Blood Flow Regulate HSC Formation

A chemical genetic screen was conducted to identify regulators of AGM HSC formation (North et al., 2007). Of the chemicals found to regulate *runx1* and *cmyb* coexpression by in situ hybridization at 36 hpf, several were known modulators of heartbeat and blood flow. These compounds were categorized into distinct classes on the basis of their hemodynamic mechanism of action (Figure S1A available online). Well-established agonists and antagonists of each category were secondarily screened for effects on HSCs (Figures 1A–1L). The adrenergic signaling pathways affect both cardiac and vascular physiology. Exposure to the α1-adrenergic blocker doxasozin (10 μM) enhanced HSCs (58 increased [inc]/86 scored), while the α-agonist ergotamine (10 μM) decreased HSC number (Figures 1B and 1H, 42 decreased [dec]/82). Similarly, the β1-adrenergic blocker metoprolol increased (49 inc/77) and the β1-agonist epinephrine decreased *runx1/cmyb* staining (Figures 1C and 1I, 40 dec/70). Changes in electrolyte balance potently regulate cardiac and vascular reactivity. The Ca^{2+}-channel blocker nifedipine enhanced HSC formation (48 inc/85), while BayK8644 diminished HSC number (Figures 1D and 1J, 34 dec/79). The cardiac glycoside digoxin, a modulator of Na^{+}/K^{+} fluxes, also increased HSCs (Figure 1G, 56 inc/79). NO is a well-established direct regulator of vascular tone and reactivity, thereby influencing blood flow. The NO donor S-nitroso-N-acetyl-penicillamine (SNAP) (10 μM) caused a significant increase in HSC development (69 inc/93). In contrast, the Nos inhibitor N-nitro-L-arginine methyl ester (L-NAME) (10 μM) diminished *runx1/cmyb* expression (Figures 1E and 1K, 58 dec/90). Exposure to the angiotensin-converting enzyme (ACE) inhibitor enalapril decreased HSC number (Figure 1F, 42 dec/81). These findings were corroborated by qPCR for *runx1* (Figure 1M).

Conserved vascular responses of each chemical class were demonstrated by in vivo confocal microscopy of *fli:GFP; gata1:dsRed* transgenic zebrafish (n = 5/compound) at 36 hpf (Figures 1N and S2) (Eddy, 2005). These data correlated with prior zebrafish studies (Fritsche et al., 2000). Vasodilation of the artery and vein was accompanied by increased passage of total blood volume, as seen by digital motion analysis of gata1+ red blood cells (RBCs; data not shown); vasoconstriction caused RBCs to traverse only in single file. Together with the in situ hybridization studies, these experiments reveal that increases in vessel diameter typically were coincident with increased *runx1* expression, and vice versa.

We have previously utilized microarray analysis of sorted cell populations isolated during various stages of embryogenesis to document cell-type and developmental specificity of genes of interest (North et al., 2007; Weber et al., 2005). We found components of the NO (*nos1*), angiotensin (*ace2, agtrl1a, agt*), and adrenergic signaling (*adra2b, adra2 da, adra2c*) pathways expressed in the HSC compartment (Figure S1B). Most were more highly expressed during the definitive wave of hematopoiesis after the onset of the heartbeat and circulation, consistent with their role in regulating hemodynamic homeostasis. These data confirm that vascular tone and flow-modifying components are present and responsive to chemical manipulation in the AGM and imply that modulation of blood flow could have a significant impact on HSC formation during embryonic development.

Absence of a Heartbeat Causes Failures in Definitive HSC Development

In the zebrafish, the occurrence of vigorous blood circulation through the tail is coincident with HSC formation in this region (T.E.N. and L.I.Z., unpublished data). In order to establish the importance of blood flow for initiation of HSC formation, we examined *sih* mutant zebrafish embryos, which lack a heartbeat due to a mutation in *cardiac troponin T* (Sehnert et al., 2002). *runx1/cmyb* expression was dramatically reduced in *sih*$^{-/-}$ embryos (Figures 2A and 2E, 69 dec/77). In contrast, the vascular marker *flk1* was minimally affected (Figures 2B and 2F), consistent with previous observations (Isogai et al., 2003). *ephrinB2*, a marker of arterial identity, was reduced in *sih* embryos (Figures 2C and 2G, 55 dec/74), while expression of the venous marker *flt4* was increased (Figures 2D and 2H, 33 inc/61). These results were confirmed by qPCR (Figure 2I, $p < 0.05$, n = 3). In contrast, benzidine staining for RBCs as well as in situ hybridization for the erythroid marker *globin* and the myeloid marker *myeloperoxidase* (*mpo*) show distribution differences due to lack of blood circulation in *sih* mutants, but no gross quantitative changes (Figures 2J, 2K, and S3A–S3H). *Myosin heavy chain* (*mhc*), a marker of somitogenesis, and the endodermal progenitor marker *foxa3* were also not affected. These data demonstrate that the absence of a beating heart and subsequent failure to establish circulation specifically impairs arterial identity and HSC formation.

Nitric Oxide Signaling Can Affect HSC Formation prior to the Initiation of Flow

To further investigate the role of circulation in the initiation of HSC development, we exposed zebrafish embryos to blood

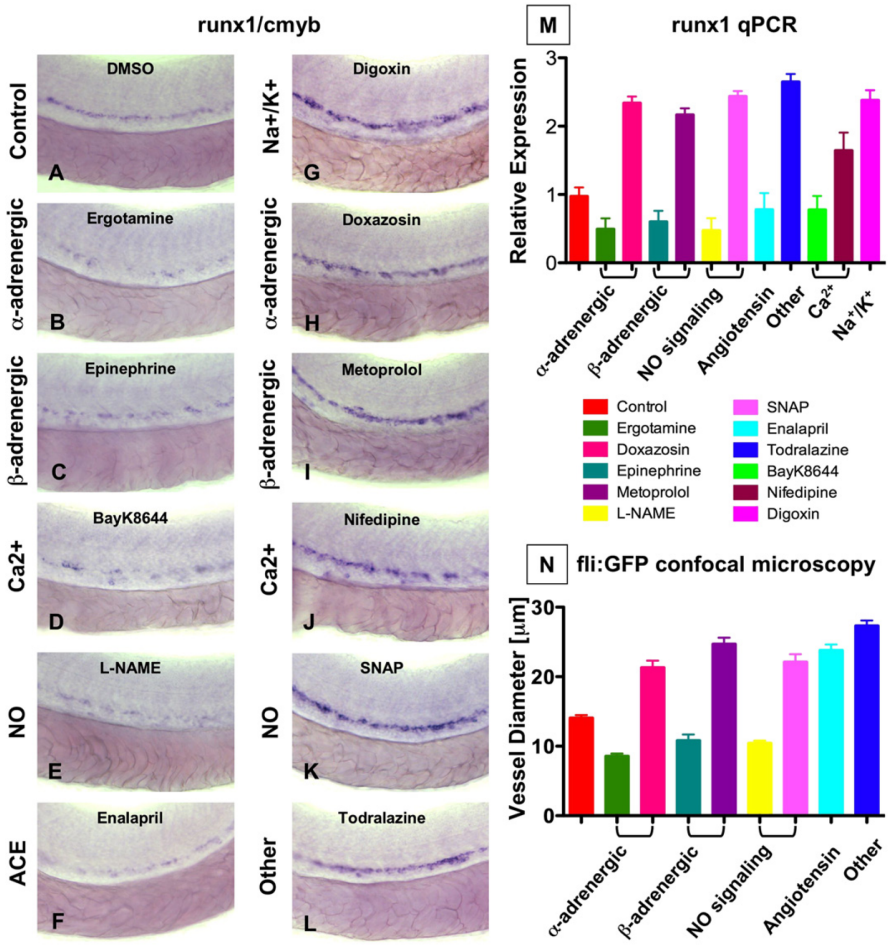

Figure 1. Modulation of Vascular Flow Affects HSC Formation in Zebrafish

(A–M) Effect of blood flow modifiers on *runx1/cmyb*+ HSC formation. Zebrafish were exposed to chemicals (10 μM) from 10 somites–36 hpf and subjected to *runx1/cmyb* in situ hybridization. Photomicrographs were taken with Nomarski optics at 40× magnification. Representative examples from after drug treatment are shown.

(L) Effect of todralazine (10 μM; 67 inc/84).

(M) Effect of drug treatment on *runx1* expression, quantified by qPCR (mean ± SD).

(N) Effect of drug treatment on the diameter of the dorsal aorta in vivo. Transgenic *fli:GFP* fish were treated with chemicals and imaged by confocal microscopy at 36 hpf; all treatments were statistically significant from the control (mean ± SD, ANOVA, $p < 0.001$).

flow-modulating agents either before (10 somites–23 hpf) or after (26–36 hpf) the onset of heartbeat and assessed HSC development at 36 hpf. All compounds examined increased HSC formation when used after the heartbeat began (Figures 3A, 3C, 3E, and 3G). In contrast, only SNAP was capable of enhancing HSC number at 36 hpf when treatment was completed before the heartbeat was established (Figures 3B, 3D, and 3F). Likewise, the NO inhibitor L-NAME could reduce HSC formation when treatment occurred prior to the initiation of the heartbeat (Figure 3A). The effects of L-NAME and SNAP were dose dependent over a range of 1–100 μM (Figures S4A–S4L) and specific to the HSC compartment, with mild effects on the vasculature, but not on *globin*, *mpo*, *mhc*, or *foxa3* expression (Figures S5A–S5R). Additionally, changes were only observed during the definitive hematopoietic wave and were maintained into larval stages (Figures S6A–S6O). In addition to SNAP (Figure 3K, 18 inc/25), NO donors sodium nitroprusside (SNP; Figure 3N, 20 inc/31) and L-arginine (L-arg; Figure 3I, 15 inc/25) (Pelster et al., 2005; Pyriochou et al., 2006) enhanced *runx1/cmyb* expression (Figures 3I, 3K, and 3N), while the nonspecific nos inhibitor, N-monomethyl-L-arg acetate (L-NMMA; Figure 3O, 17 dec/29) diminished HSCs like L-NAME (Figure 3L, 16 dec/26). Inactive

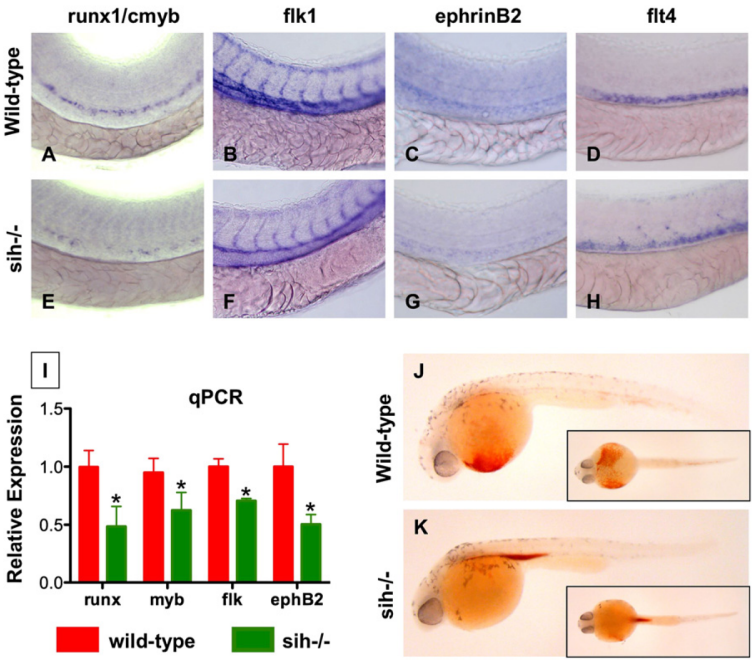

Figure 2. A Beating Heart Is Required for HSC Formation and Artery Development

(A–H) Effect of *sih* mutation on HSC and vascular formation at 36 hpf.

(A and E) *runx1/cmyb* expression is greatly reduced in *sih*$^{-/-}$ embryos compared to WT siblings.

(B and F) *flk1* expression reveals a grossly normal vascular pattern in *sih*$^{-/-}$ embryos; changes in the development of the intersomitic vessels and vascular plexus were noted in some animals.

(C and F) *ephB2* expression is diminished in *sih*$^{-/-}$ embryos.

(D and H) *flt4* expression is expanded in *sih*$^{-/-}$ embryos.

(I) The expression levels of HSC (*runx1, cmyb*), vascular (*flk*), and arterial (*ephB2*) markers are significantly decreased in *sih*$^{-/-}$ embryos compared to sibling controls (mean ± SD, t test, $p < 0.05$, $n = 3$), as measured by qPCR at 36 hpf.

(J and K) The *sih* mutation has no effect on primitive hematopoiesis as seen by benzidine staining at 36 hpf; in the absence of a heartbeat blood is pooled in the major vessels.

D-enantiomers had no effect (Figures 3J, 3M, and 3P). To assess whether modification of *runx1/cmyb* expression correlated with a quantifiable effect on HSC number, we utilized *cmyb:GFP; lmo2:dsRed* reporter fish (North et al., 2007). Confocal microscopy revealed increased HSC (yellow) numbers after SNAP exposure, and a reduction after L-NAME treatment (Figures 3Q–3S and S5S, $p < 0.001$, $n = 5$). TUNEL analysis indicated that L-NAME could affect HSC by induction of apoptosis (Figures S7A–S7D). These analyses indicate that HSC modulation by the majority of flow-modifying compounds requires the establishment of blood circulation and that NO signaling is the mediator of blood flow in this process.

HSC Formation Is Affected by Signals Downstream of NO

To clarify that the effect of flow on HSCs was mediated by NO signaling, we studied downstream components of the NO signaling cascade by chemical manipulation. The soluble guanyl cyclase inhibitor 1H-oxadiazolo-quinoxalin-1-one (ODQ) prevents cGMP formation in response to NO signaling; it regulates vascular remodeling and blood flow in zebrafish in a dose- and time-dependent manner (Pyriochou et al., 2006). ODQ (10 μM) caused a profound decrease in HSCs (Figures 3T and 3U, 27 dec/43) and also blocked the effects of SNAP (Figures 3W and 3X, 8 inc/38). Phosphodiesterase (PDE) V converts cGMP to GTP. The PDEV inhibitor 4-{[3′,4′-methylene-dioxybenzyl]amino}-6-methoxyquinazoline (MBMQ, 10 μM) increased HSCs (Figure 3V, 35 inc/43) and further enhanced the effects of SNAP (Figure 3Y, 40 inc/46). These data highlight the specificity of cGMP as a downstream effector of NO signaling in HSC formation.

NO Signaling Rescues HSCs in *sih*$^{-/-}$ Embryos

To confirm a direct role for NO in HSC induction, we exposed *sih* embryos to SNAP. SNAP rescued *runx1/cmyb* expression toward wild-type (WT) levels in the majority of *sih* embryos examined (Figures 4A–4D, 31 normal/51). These results were confirmed by qPCR (Figure 4E). SNAP also normalized *ephB2* defects in *sih* mutants (Figures 4F–4I, 18 inc/27; Figure S8A). L-arg and SNP (data not shown), as well as bradykinin, a potent vasodilator that stimulates NO production, increased HSCs, and rescued the *sih* hematopoietic defect (Figures S8B–S8E). To further characterize the relationship between blood flow, NO signaling, and HSC induction, we concomitantly exposed WT embryos to flow-modifying drugs and L-NAME (10 μM). As the majority of flow-regulating compounds that enhance HSCs also cause vasodilation and increase total blood flow through the aorta, they may directly trigger NO production by alterations in sheer stress, pulsatile flow, or soluble signaling components. L-NAME treatment prevented the increase in HSC formation caused by most compounds tested (Figures 4J–4U). These data further point to NO signaling as the direct link between blood flow and HSC development.

Nos1 Is Required for HSC Formation

Zebrafish lack genomic evidence for endothelial NO synthase (*enos, nos3*); however, we, and others (Pelster et al., 2005), observed eNos immunoreactivity in the tail region, where the HSCs develop (Figures S9J–S9L). Phylogenetic and genomic examination demonstrates that neuronal *nos* (*nnos, nos1*) (Poon et al., 2003) and *nos3* (*enos*) are highly related. Morpholino antisense oligonucleotide (MO) knockdown of *nos1* had a

Compound	Class	10 ss - 23 hpf	26 hpf - 36 hpf
A		HSC Formation	
Doxazosin	Adren	normal	↑ 62%
Metoprolol	Adren	normal	↑ 66%
Digoxin	Na+/K+	normal	↑ 74%
Nifedipine	Ca+	normal	↑ 58%
SNAP	NO	↑ 65%	↑ 71%
Todralazine	Unknown	↑ 52%	↑ 79%
L-NAME	NO	↓ 60%	↓ 64%

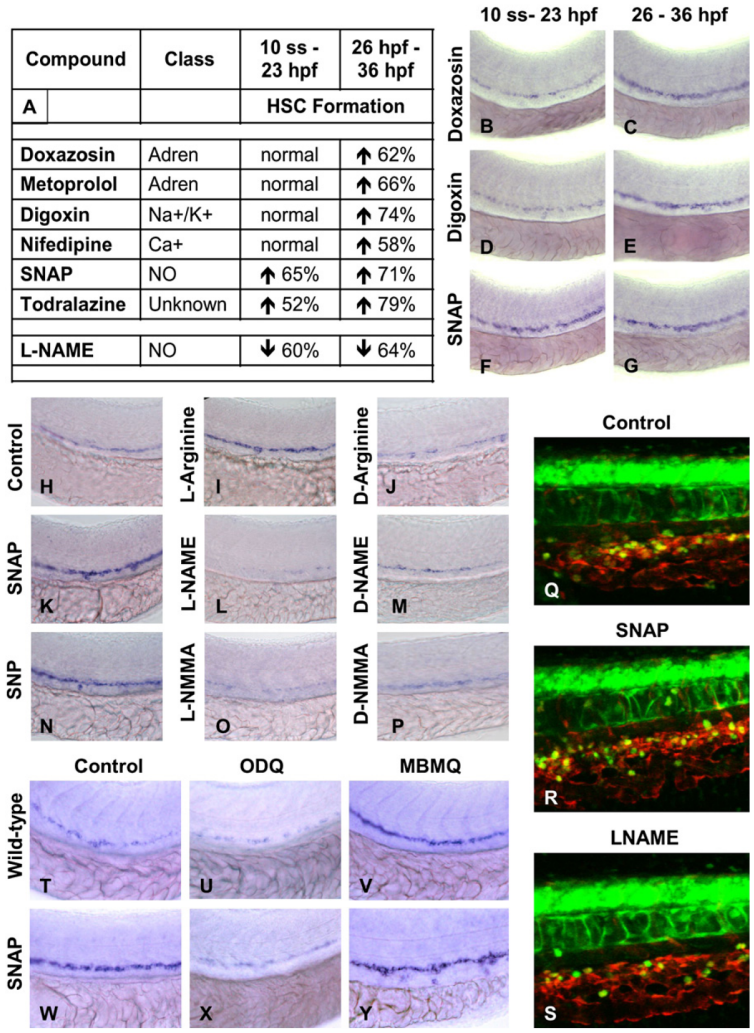

Figure 3. NO Signaling prior to the Onset of Cardiac Activity can Affect HSC Formation

(A–G) Effect of vasoactive drugs (10 μM) on HSC formation before and after the onset of heartbeat at 24 hpf, after exposure to chemicals from either 10 somites–23 hpf or from 26–36 hpf.

(A) Most vasoactive drugs do not affect HSC formation when applied prior to the onset of heartbeat, while NO modifiers influenced HSC development even prior to heart beat initiation. The percentage of embryos ($n > 20$) with altered *runx1/cmyb* expression is indicated.

(B–G) Representative examples of flow-modifying drugs on *runx1/cmyb* expression.

(H–P) Specificity of NO signaling in HSC formation. NO donors enhanced and inhibitors diminished HSCs; inactive D-enantiomers had no effect.

(Q–S) Effects of NO modulation on HSC number by in vivo confocal imaging in *cmyb:GFP; lmo2:dsRed* transgenic embryos.

(T–Y) Effects of downstream modifiers of NO signaling on *runx1/cmyb* expression.

(U and X) Inhibition of soluble guanyl cyclase by ODQ (10 μM) decreases *runx1/cmyb* expression in WT and SNAP treated embryos.

(V and Y) Inhibition of PDE V by MBMQ (10 μM) increases HSC formation in WT embryos and further enhances the effects of SNAP.

profound dose-dependent impact on HSC development (Figures 5A, 5C, and 5E; 63 dec/89 ATG MO, 48 dec/64 splice MO; Figures S9A–S9E), while knockdown of *nos2* (*inducible nos, inos*) did not affect *runx1/cmyb* expression (Figures 5D, and 5F; 9 dec/98 ATG MO, 10 dec/65; Figures S9F–S9I). The potent effect of *nos1* was confirmed by chemical inhibition of NO synthesis (Figures 5B, 5G, and 5H): selective inhibition of *nos1* by S-methyl-L-thiocitrulline (10 μM; 30 dec/44) severely diminished HSC number, whereas the *nos2* (*inos*)-specific inhibitor 1400W (10 μM; 4 dec/49) only minimally affected HSCs. These data suggest that *nos1* (*nnos/enos*) is required for HSC formation in zebrafish, which is supported by *nos1* expression in both endothelial cells and HSCs (Figure S1B). Interestingly, in $sih^{-/-}$ embryos, *nos1* was significantly decreased (Figure 5I, $p < 0.001$); in contrast, *nos2* was not significantly changed. Further, *nos1*, but not *nos2*, was significantly altered in response to chemical alteration of blood flow (Figures 5J and 5K, $p < 0.003$). These data support the hypothesis that *nos1* is the functionally relevant connection between blood flow and HSC development.

The Effect of NO Signaling on HSC Formation Is Cell Autonomous

In order to examine cell autonomy and delineate the role of NO signaling in the HSC and surrounding hematopoietic niche, we employed a blastula transplant strategy. Cells harvested from *cmyb:GFP* embryos injected with control or *nos1* MO were transplanted at the blastula stage into *lmo2:dsRed* recipients. In this transplant scheme, donor-derived HSCs appear green (Figure S10A) in the red fluorescent endothelial/HSC compartment (Figures 6A and S10B). Sixty-two and a half percent of embryos examined had GFP+ HSC formation derived from control-injected donor cells (Figures 6B and 6D), while none of the *nos1* MO injected donor cells gave rise to green HSCs (Figures 3C and 3D, $p = 0.0065$); successful transplants were indicated by the contribution of *cmyb*+ donor cells to the recipient eye. In a reciprocal experiment, we found that uninjected *lmo2:dsRed* donor cells contributed to endothelial and HSC development in *cmyb:GFP* recipients (Figure S10C), particularly after MO knockdown in the recipient. These experiments formally demonstrate that *nos1* acts in a cell-autonomous manner in the hemogenic endothelial cells.

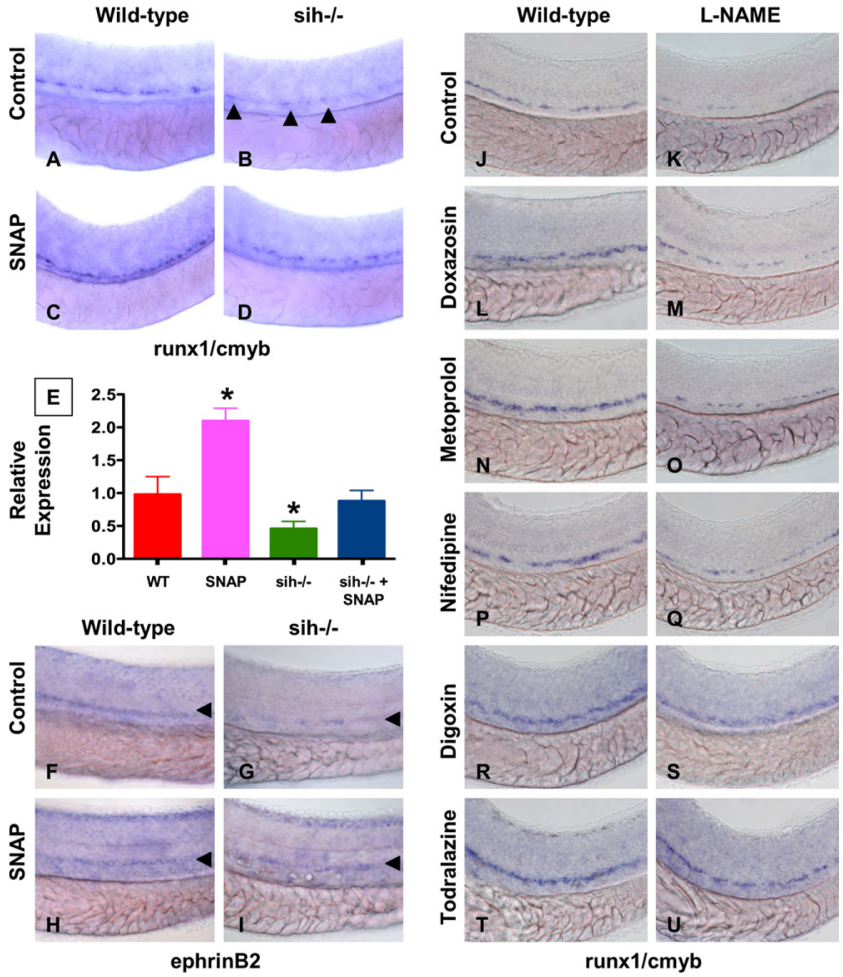

Figure 4. NO Signaling Affects Zebrafish HSC Formation Independent of Heartbeat

(A–I) WT and *sih*$^{-/-}$ mutants were exposed to DMSO and SNAP (10 μM) from 10 somites–36 hpf.

(A–D) In situ hybridization for *runx1/cmyb*. SNAP rescues HSC formation in *sih*$^{-/-}$ mutants.

(B) Remaining *runx1/cmyb*+ cells are highlighted by arrowheads.

(E) qPCR for *runx1*. * statistically significant versus the WT, mean ± SD, ANOVA, $p < 0.001$, $n = 5$.

(F–I) Effect of heartbeat and SNAP on *ephrinB2* expression, highlighted by arrowheads.

(J–U) Effect of L-NAME on HSC formation in embryos concurrently treated with blood flow-modifying agents. L-NAME inhibits the effects of doxazosin ([M], 7 inc/36 observed), metoprolol ([O], 3 inc/31) and nifedipine ([Q], 4 inc/28), but not of digoxin ([S], 16 inc/ 29) and todralazine ([U], 20 inc/33).

Developmental Signaling Pathways Interact with NO in HSC Formation

Developmental regulators such as the notch and wnt pathways have been linked to HSC formation and self-renewal (Burns et al., 2005; Goessling et al., 2009). Due to the effect of NO on HSC specification and expansion, potential interaction with notch and wnt signaling was examined. The notch pathway influences arterial/venous identity and functions upstream of *runx1* in HSC specification; *mindbomb* (*mib*) mutants lack HSCs because of a deficiency of notch signaling (Burns et al., 2005) (33 dec/47). SNAP rescued HSC formation in these mutants (Figures S11A–S11D; 27 normal/43). Transgenic zebrafish embryos expressing an activated form of the notch intracellular domain (NICD) exhibit enhanced HSC numbers (55 inc/62); L-NAME blocked the HSC increase (Figures S11E–S11H; 16 inc/63) and inhibited NICD-mediated elevation of *ephB2* expression in the aorta (Figures S12A–S12D). These studies imply that NO functions downstream of notch in regulation of arterial identity and/or in HSC induction.

Recent studies have shown that modulation of the wnt pathway affects HSCs (Goessling et al., 2009; Reya et al., 2003). We used heat-shock-inducible transgenic zebrafish embryos expressing negative (*dkk*) and positive (*wnt8*) regulators

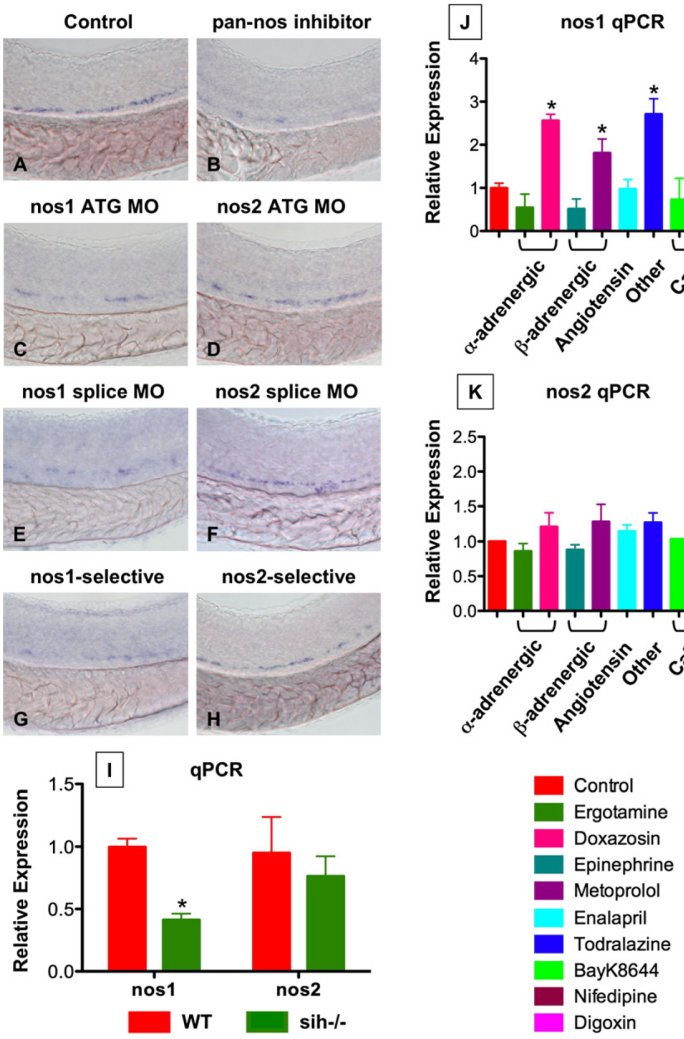

Figure 5. nos1 Is Required for HSC Formation in Zebrafish

(A–H) In situ hybridization for *runx1/cmyb* at 36 hpf. (C and E) *nos1* knockdown (40 μM) decreased HSC formation.

(D and F) MO (ATG and splice site) against *nos2* (40 μM) had no effect on HSC development.

(B, G, and H) Chemical nos inhibition confirmed the specific requirement for *nos1*: embryos exposed to nonspecific (L-NAME; 10 μM) and *nos1*-selective (S-methyl-L-thiocitrulline; 10 μM) inhibitors demonstrated decreased HSC formation; *nos2*-selective inhibition (1400W; 10 μM) had minimal impact.

(I) WT and *sih*$^{-/-}$ embryo extracts (n = 20) were subjected to qPCR (mean ± SD; * *nos1*, WT versus *sih*, t test, $p < 0.001$, n = 3; *nos2*, WT versus *sih*, $p = 0.385$, n = 3.).

(J and K) Effect of flow-modifying chemicals (10 μM, 10 somites–36 hpf) on *nos1* and *nos2* expression; *nos1* is significantly regulated by most compounds tested. Mean ± SD; * significant versus control, ANOVA, $p < 0.01$, n = 3.

of wnt signaling to evaluate the interaction between the wnt and NO signaling cascades (Goessling et al., 2008). Induction of *dkk* reduced HSC number (16 dec/8) and was rescued by SNAP (Figures S13A–S13D; 5 dec/33). In contrast, *wnt8* enhanced HSC formation (22 inc/30), which was blocked by L-NAME (Figures S13E–S13H; 9 inc/28). In support of these findings, previous studies have shown an interaction of both the notch and wnt pathways with NO, although the directionality of these interactions varies (Du et al., 2006; Ishimura et al., 2005; Prevotat et al., 2006).

The Relationship between NO and HSC Induction Is Conserved in the Mouse

To document a role for NO in murine HSC formation, we examined *Nos3:GFP* expression in the AGM. Histological sections of e11.5 embryos showed endothelial cells lining the dorsal aorta expressing high levels of Nos3 (Figures S14A–S14D). Hematopoietic clusters and adjacent endothelium on the ventral wall of the aorta expressed *Nos3* at a lower level; this expression pattern was reminiscent of the embryonic HSC markers such as *Runx1* and *c-Kit* (North et al., 2002). Fluorescence-activated cell sorting (FACS)-based coexpression analysis confirmed that the majority of e11.5 cKit^{hi}CD34^{med}CD45^{med}VE-cadherin^{med} AGM HSCs (E.D., unpublished data) were Nos3^{med} (Figure S14E). Transplantation of Nos3 AGM subfractions into irradiated adult recipients demonstrated that LTR-HSCs are enriched within the Nos3^{med} population (Figure S14F).

To demonstrate a conserved functional requirement for NO signaling in HSC/progenitor formation, we exposed pregnant mice to L-NAME (2.5 mg/kg intraperitoneally) or vehicle control and compared effects on the AGM HSC and progenitor populations at e11.5. NO inhibition produces implantation defects in early pregnancy (Duran-Reyes et al., 1999) and can alter yolk sac angiogenesis (Nath et al., 2004); interestingly, *Nos3* deficiency caused significant lethality from e8.5 to 13.5 during the time when definitive HSCs are formed (Pallares et al., 2008). L-NAME treatment at e8.5 produced severely delayed embryos that lacked the majority of both extra- and intra-embryonic blood vessels (data not shown). L-NAME treatment at e9.5 and e10.5 at prevented gross morphological abnormalities of the yolk sac, placenta, or embryo. Histological analysis of the AGM region revealed that L-NAME caused the disappearance of hemogenic endothelial clusters, which was confirmed by phenotypic FACS analysis (Figures 7A–7L and S15A–S15G). Similarly,

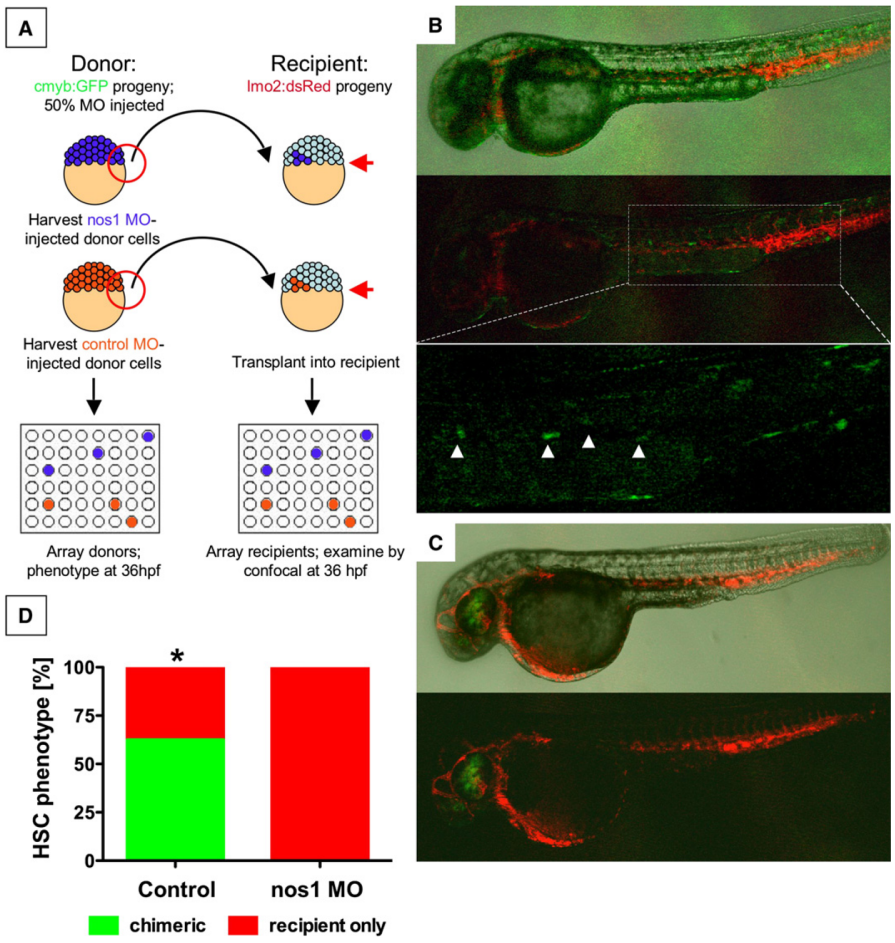

Figure 6. The Effect of NO Signaling on HSC Development Is Cell Autonomous

(A) Cells from *cmyb:GFP* transgenic donor embryos, injected with *nos1* ATG MO or control MO, were transplanted into *lmo2:dsRed* recipients at the blastula stage.

(B) Donor contribution to HSC formation assessed by confocal microscopy at 36 hpf. Shown are the merged picture on the top, red/green merge in the middle, and a high-magnification view of green fluorescence only on the bottom. *cmyb:GFP* donor-derived HSCs in recipients are highlighted by arrowheads.

(C) *nos1* MO donors never contributed to HSC formation; the presence of *cmyb:GFP*-derived donor cells in the eye is indicative of a successful transplant.

(D) HSC chimerism in transplanted embryos (control versus *nos1* MO, Fisher's exact test, $p = 0.0065$, $n \geq 8$).

analysis of e11.5 *Nos3*$^{-/-}$ embryos revealed a significant decrease in the AGM Sca1+/cKit+ and CD45+/VE-Cadherin+ populations, which was confirmed histologically; *Nos3*$^{-/-}$ embryos displayed a reduction in the number and size of the hematopoietic clusters (Figure 7K). HSC induction was grossly normal in *Nos1*$^{-/-}$ animals (Figure 7L).

To examine effects on HSC function, we performed transplantation studies using single-cell suspensions of subdissected AGM tissue from WT, L-NAME-exposed, and *Nos3*$^{-/-}$ embryos at e11.5. Progenitor activity as measured by spleen colony formation at days 8 and 12 after transplantation was diminished in L-NAME-exposed (Figure S15J, $p < 0.001$) and *Nos3*$^{-/-}$ (Figure 7M, $p < 0.001$) embryos. Multilineage repopulation after 6 weeks revealed significantly diminished peripheral blood (PB) chimerism (Figures 7N and S15K, $p > 0.05$) and engraftment rates (Figure S15L) for recipients of both L-NAME-exposed and *Nos3*$^{-/-}$ AGM cells. These results indicate a conserved role for NO signaling in the regulation of hematopoietic stem/progenitor formation and function during embryonic development. Although at reduced numbers, *Nos3*$^{-/-}$ embryos develop to adulthood and lack significant steady-state peripheral blood abnormalities; our data suggest that while impaired initially, some functional HSCs do arise in *Nos3*$^{-/-}$ embryos. Interestingly, although the *Nos3*$^{-/-}$ animals exhibit some residual HSC production, L-NAME-exposed embryos do not possess AGM HSCs, implying that functional redundancy with other Nos family members must occur.

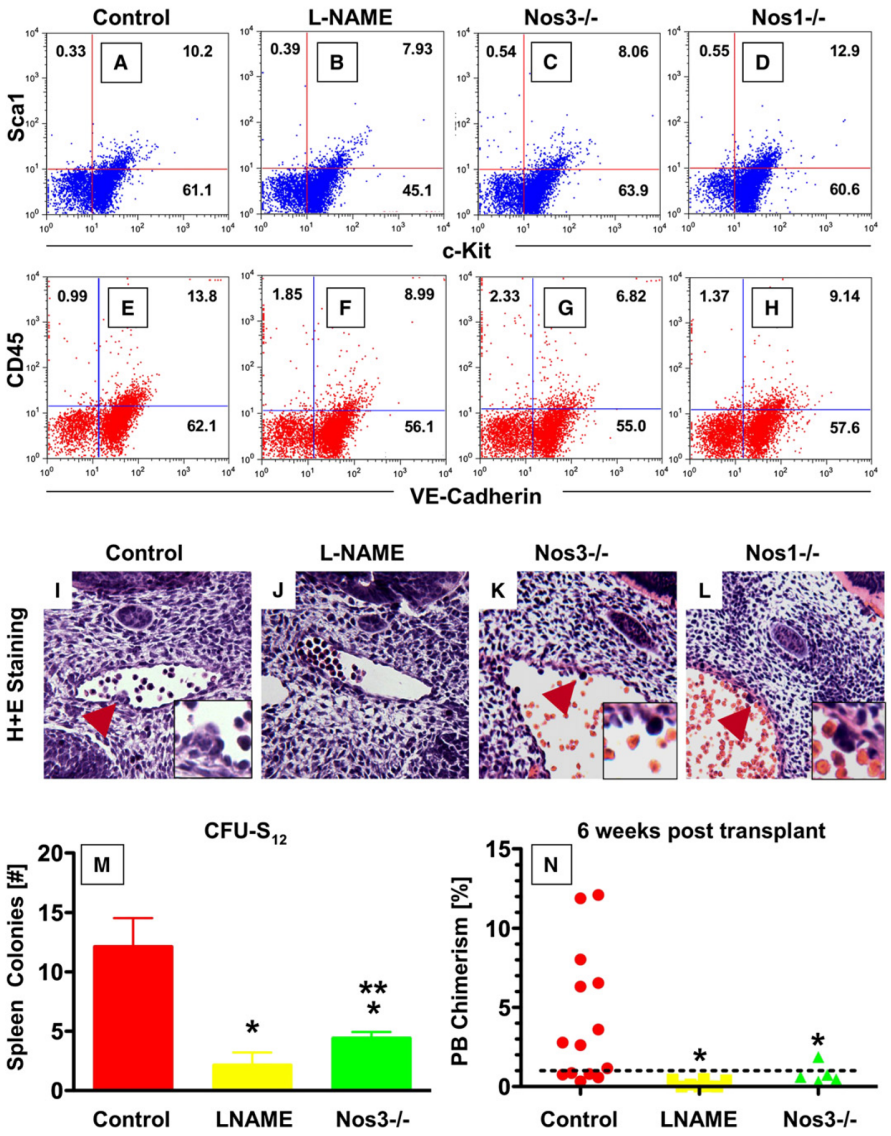

Figure 7. The Effect of NO Signaling on HSC Development in the AGM Is Conserved in Mice

(A–H) FACS analysis of dissociated AGM cells in WT and *Nos* KO mice at e11.5. *Nos3*$^{-/-}$ mice exhibited a decrease in the Sca1+/cKit+ and CD45+/VE-Cadherin+ populations, while deletion of *Nos1* had no significant effects.

(I–L) Histological sections through the AGM region of e11.5 embryos; the inset represents a high-magnification view around the hematopoietic clusters. L-NAME exposure causes absence of hematopoietic clusters; *Nos3*$^{-/-}$ mice exhibit smaller cluster size, while *Nos1*$^{-/-}$ does not impair cluster formation. Serial sections through the entire aorta of at least ten embryos per genotype/treatment were analyzed.

(M and N) Effect of NO signaling on AGM HSC function. AGM regions of somite stage-matched WT, L-NAME treated or *Nos3*$^{-/-}$ progeny were subdissected at e11.5 and transplanted into sublethally irradiated recipients. L-NAME exposure or *Nos3* deletion in embryos significantly reduced CFU-S12 spleen colony formation (mean ± SD; * sig versus control; $p < 0.001$; ** sig versus L-NAME; $p < 0.05$; ANOVA, $n \geq 5$) (M). Diminished NO signaling significantly decreased embryonic donor cell chimerism rates in individual recipient mice at 6 weeks after transplant (* sig versus control, $p < 0.05$, ANOVA, $n \geq 5$) (N).

DISCUSSION

The purpose of a beating heart and circulation at embryonic stages where diffusion is still sufficient for oxygenation of developing tissue has long been a source for speculation (Burggren, 2004; Pelster and Burggren, 1996). Through a chemical screen in zebrafish, small molecules that regulate vascular dynamics were found to influence HSC development; intriguingly, changes in HSC formation were coupled to blood flow and NO production. Our data imply that circulation itself, through NO induction, signals to trigger the onset of definitive hematopoiesis, thereby ensuring proper timing of blood cell development to support additional hematopoietic requirements during accelerated growth in fetal/larval stages. Significantly, we found that the enhancing role of NO in HSC induction is conserved from fish to mammals.

NO production can be induced by sheer stress and alterations in blood flow (Fukumura et al., 2001). The coincident timing of HSC induction with the achievement of vigorous pulsatile flow implies that the latter may serve as the physiologic inductive signal for NO in the AGM. Pulsatile flow achieved by a regular heartbeat has been shown to trigger NO production in the endothelium (White and Frangos, 2007). The data from the *silent heart* embryos—as well as observations in *Ncx1*$^{-/-}$ mice (Lux et al., 2008; Rhodes et al., 2008), which also fail to establish circulation due to heart-specific defects—indicate that in the absence of flow there are alterations in specification, budding, and shedding of HSCs from endothelial hematopoietic clusters. It will be intriguing to further decipher the correlation between flow rate and total AGM HSC number; MO knockdown of *tnnt2* (*sih*) (Bertrand et al., 2008; Murayama et al., 2006; Jin et al., 2009) and analysis of incompletely penetrant *sih* mutants with occasional heartbeats (data not shown) show less-severe reductions in HSC number, implying that small bursts of NO production may be sufficient to trigger HSC induction. As NO can regulate endothelial cell movement and processes resembling HSC budding, such as podokinesis, by altering cell-cell adhesions and actin conformation (Noiri et al., 1998), it could directly control the formation and stability of hematopoietic clusters once flow is established. Confirming this conjecture, we determined that there is a cell-autonomous role of NO signaling during hematopoietic development, where the hemogenic endothelial population must be capable of NO production to support subsequent HSC formation in the AGM.

We found that NO may additionally function to establish the AGM vascular niche prior to HSC formation; our data showing significant alterations in *ephrinB2* staining in the absence of flow support the concept that flow itself plays a role in maintaining vascular identity. NO is a well-characterized regulator of angiogenesis and is required for murine yolk sac vasculogenesis (Nath et al., 2004). Prior studies in the zebrafish embryo showed that chemical inhibition of NO production/signaling by L-NAME or ODQ during somitogenesis produces vascular abnormalities (Pyriochou et al., 2006). Since definitive HSCs are formed within the major embryonic arteries (de Bruijn et al., 2000), any alterations in NO signaling and subsequent vessel development would negatively impact HSC number. As ephrinB2 and arterial identity are established by notch signaling (Lawson et al., 2001), the interaction of the notch and NO pathways may be particularly relevant for HSC formation. NO may initiate arterial specification early during development and may maintain arterial identity once flow is established. This is in agreement with reports that demonstrate that arterialization is an ongoing and flow-dependent process, influenced by NO (Teichert et al., 2008). Similarly, vascular endothelial growth factor (VEGF), a potent vascular mitogen regulated by both notch and wnt, is a well-characterized inducer of NO production (Fukumura et al., 2001). In the dorsal aorta, VEGF may increase NO production and signaling to cause the vascular remodeling required for the production of the hematopoietic clusters.

Our data demonstrate both a requirement for and enhancing response to NO signaling for AGM HSC development. Several *nos* isoforms have been identified in zebrafish: *nos1*, which is expressed in developing neural tissues as well as the gut, kidney, and major vessels (Holmqvist et al., 2004; Poon et al., 2003), and two isoforms of *nos2*. While genomic evidence for the presence in zebrafish of *nos3* is lacking (Pelster et al., 2005), immunoreactivity to eNos antibodies suggests the conservation of the functional epitope (Fritsche et al., 2000). As NO-mediated vascular reactivity is clearly present in fish and *nos1* and *nos3* are highly related at both the sequence and structural levels, *nos1* likely assumes the role of vascular NO production in fish. *Nos1* is genetically complex with individual splice forms showing tissue-specific expression, and it is likely that one form of *nnos* acts *enos*-like in zebrafish. In support of this hypothesis, our microarray analysis demonstrated *nos1* expression in CD41+ HSCs and the vascular niche.

In the murine AGM, phenotypic and histological analysis showed that *Nos3* (*eNos*) is expressed in HSCs and required for stem cell function. Conversely, we found *Nos1* (*nNos*) not to be essential for HCS formation under normal developmental conditions. Interestingly, *Nos3* and *Nos1* are both expressed in the fetal liver shortly after AGM HSC formation and could play a role in the developmental regulation and expansion of HSC and progenitor populations (Krasnov et al., 2008). Their coexpression suggests a functional redundancy in mammalian HSCs that could explain the impaired, but present, HSC formation and adult viability of *Nos3*$^{-/-}$ embryos. Consequently, global NO inhibition by L-NAME had a much more severe effect on HSC formation. It remains to be determined whether differences in hematopoietic development occur in mice in which all *Nos* isoforms are disrupted.

NO donors positively affect multipotent hematopoietic progenitors in vitro (Michurina et al., 2004); additionally, the ability of stromal cell lines to support stem cell maintenance corresponds with NO production (Krasnov et al., 2008). In contrast, others have shown that NO inhibition enhances HSC engraftment after transplantation (Krasnov et al., 2008; Michurina et al., 2004). While these studies imply that NO may have a negative effect on adult HSCs, parallel work has shown that NO is induced by ionizing irradiation and that the absence of Nos diminishes superoxide and peroxide damage (Epperly et al., 2007). These data preclude a clear interpretation of transplantation/repopulation studies where the hematopoietic niche is cleared via irradiation. After 5-fluorouracil bone marrow injury, *Nos3*$^{-/-}$ mice show impaired regeneration, indicating an important role for *Nos3* in stem and

progenitor cell function in vivo after marrow injury (Aicher et al., 2003). Taken together with the results presented here, these studies indicate that the effects of NO are likely highly time and context dependent, and further work is needed to decipher the role of NO in regulating adult hematopoietic homeostasis and maintaining both the stromal and vascular niche.

Our study demonstrates that definitive hematopoietic stem cell formation in the developing embryo is dependent on the induction of the heartbeat and establishment of circulation. Two models have been proposed for the relationship of blood formation in murine extraembryonic tissues and the embryo proper: in one model, the stem cells arise independently in discrete locations in the embryo and extraembryonic tissues and subsequently colonize the fetal liver (Dzierzak and Speck, 2008; Rhodes et al., 2008), whereas the other proposes that cells from the extraembryonic tissues traverse circulation to colonize the intraembryonic hematopoietic sites (Palis and Yoder, 2001). A recent study using the *Ncx1*$^{-/-}$ mouse showed that yolk sac hematopoietic progenitors could form in the absence of blood flow, while the appearance of progenitors in the embryo proper was greatly impaired; these data were interpreted to show that it is yolk sac-derived embryonic progenitors that traverse the circulation and seed the fetal liver (Lux et al., 2008). Our data imply that the contemporaneous establishment of circulation and the appearance of HSCs within the embryo proper may not simply reflect the transit of HSCs formed in extraembryonic tissues to colonize the aorta and fetal liver, but rather that the circulation functions directly to provide inductive signals to specific regions of the embryonic vasculature, making it competent to produce HSCs de novo.

Here, we established a conserved role for NO in the developing hematopoietic system. NO can function in vessel formation and specification, blood flow regulation, and hematopoietic cluster formation, suggesting that it is required in the vascular niche for HSC production. Although the function of NO in the adult marrow is complex, our findings during embryogenesis indicate that modulation of blood flow or NO signaling might be therapeutically beneficial for patients undergoing stem cell transplantation.

EXPERIMENTAL PROCEDURES

Zebrafish Husbandry

Zebrafish were maintained according to Institutional Animal Care and Use Committee protocols. *fli:GFP, hs:gal4;uas:NICD, wnt8:GFP, dkk1:GFP* transgenic and *sih* and *mib* mutant fish were described previously (Burns et al., 2005; Goessling et al., 2009; Itoh et al., 2003; Lawson and Weinstein, 2002; Sehnert et al., 2002). Embryonic heat shock was conducted as described (Goessling et al., 2009).

Mice

Embryos were generated from *C57Bl/6*, *Runx1:lacZ* (North et al., 1999), *Nos3:GFP* transgenic (van Haperen et al., 2003), *Nos1*$^{-/-}$, and *Nos3*$^{-/-}$ mice. Vaginal plug identification was considered e0.5. Animals were handled according to institutional guidelines.

In Situ Hybridization

Paraformaldehyde-fixed embryos were processed for in situ hybridization according to standard zebrafish protocols (http://zfin.org/ZFIN/Methods/ThisseProtocol.html). The following RNA probes were used: *runx1*, *cmyb*, *flk1*, *ephrinB2*, *flt4*, *globin*, *mpo*, *mhc*, and *foxa3*. Changes in expression compared to WT controls are reported as the number altered/number scored per genotype/treatment (North et al., 2007); a minimum of three independent experiments was conducted per analysis.

Chemical Exposure

Zebrafish embryos were exposed to chemicals at the doses indicated; dimethyl sulfoxide (DMSO) carrier content was 0.1%. For evaluation of HSC development, exposure ranged from early somitogenesis (5+ somites) until 36 hpf, unless otherwise noted.

Morpholino Injection

Morpholino (MO; GeneTools) designed against the ATG and exon1 splice sites of *nos1* (5′-ACGCTGGGCTCTGATTCCTGCATTG; 5′-TTAATGACATCCCTC ACCTCTCCAC) and *nos2* (5′- AGTGGTTTGTGCTTGTCTTCCCATC; 5′-ATGC ATTAGTACCTTTGATTGCACA), and mismatched controls were injected into one-cell-stage embryos.

Confocal Microscopy

Fluorescent reporter embryos were exposed to blood flow modulators (10 μM, unless otherwise noted) as indicated, live embedded in 1% agarose, and imaged with a Zeiss LSM510 Meta confocal microscope at 36 hpf (North et al., 2007) or a Perkin Elmer UltaVIEW VoX spinning disk confocal microscope.

qPCR

qPCR was performed on cDNA obtained from whole embryos at 36 hpf (n = 20/variable; primers listed in Table S1) as previously described (North et al., 2007), with SYBR Green Supermix on the iQ5 Multicolor RTPCR Detection System (BioRad).

Blastula Transplantation

cmyb:GFP embryos were injected with nos1 or control MO at the one-cell stage. At the blastula stage, 100 cells were removed from the donor embryo and transplanted into stage-matched recipients. Embryos were analyzed by confocal microscopy at 36 hpf.

Murine AGM Histology

At e11.5 after timed mating, embryos dissected from the uterus and processed for histological evaluation. Paraffin serial sections were stained with hematoxylin and eosin; cryosections were assessed by fluorescence microscopy for GFP. X-Gal staining was performed as indicated.

Nos3:GFP AGM FACS Analysis

Embryos (e11.5) from *Nos3:GFP* transgenic animals were isolated, and AGM tissue was dissected and disaggregated. Flow cytometric analysis was performed for Nos3:GFP, VE-Cadherin, CD34, Sca-1, c-kit, and CD45 (BD Pharmingen).

Nos3:GFP AGM Transplantation

Transgenic AGM cells were sorted into Nos3:GFP fractions. AGM (one embryo equivalent) cell suspensions were injected into irradiated (9 Gy) *FVB* recipient mice with adult spleen carrier cells (2×10^5 per recipient). Recipient peripheral blood was analyzed at 4 months after transplantation for donor-derived cells by DNA PCR for *GFP* (donor marker) and *myogenin* (normalization control). Recipients with >10% donor-marked cells were considered positive.

AGM Transplantation and Progenitor and LTR HSC Analysis

AGM transplantations were performed with the CD45.1/45.2 allelic system. Pregnant *C57Bl/6* females were injected with DMSO or L-NAME (2.5 mg/kg) intraperitoneally on e9.5 and e10.5. WT, L-NAME, *Nos1*$^{-/-}$, and *Nos3*$^{-/-}$ AGM regions were dissected and disaggregated at e11.5 then injected into 8-week-old *C57Bl/6* sublethally irradiated recipients. For CFUS8 and 12 analyses, spleens were dissected, weighed, and fixed with Bouin's solution, and hematopoietic colonies were counted. For long-term transplants, PB obtained from recipient mice at 6 weeks was analyzed for donor chimerism and multilineage engraftment (>1%) by FACS.

SUPPLEMENTAL DATA

Supplemental Data include 15 figures and one table and can be found with this article online at http://www.cell.com/supplemental/S0092-8674(09)00448-6.

ACKNOWLEDGMENTS

We thank M. Lin and J. Loscalzo for helpful suggestions, D. Atochin for assistance with Nos knockout mice, and W. Davis for technical support with spinning-disk confocal microscopy. We thank K.R. Kopani, J. Ojeda, and A. Meyers for technical assistance with the zebrafish HSC screen. This work was supported by the National Institutes of Health (T.E.N., W.G., E.D., and L.I.Z) and a Netherlands Besluit Subsidies Investeringen Kennisinfrastructuur award (E.D.). L.I.Z. is a Howard Hughes Medical Institute investigator.

Received: September 17, 2008
Revised: December 23, 2008
Accepted: April 7, 2009
Published online: May 13, 2009

REFERENCES

Aicher, A., Heeschen, C., Mildner-Rihm, C., Urbich, C., Ihling, C., Technau-Ihling, K., Zeiher, A.M., and Dimmeler, S. (2003). Essential role of endothelial nitric oxide synthase for mobilization of stem and progenitor cells. Nat. Med. *9*, 1370–1376.

Bertrand, J.Y., Kim, A.D., Teng, S., and Traver, D. (2008). CD41+ cmyb+ precursors colonize the zebrafish pronephros by a novel migration route to initiate adult hematopoiesis. Development *135*, 1853–1862.

Burggren, W.W. (2004). What is the purpose of the embryonic heart beat? Or how facts can ultimately prevail over physiological dogma. Physiol. Biochem. Zool. *77*, 333–345.

Burns, C.E., Traver, D., Mayhall, E., Shepard, J.L., and Zon, L.I. (2005). Hematopoietic stem cell fate is established by the Notch-Runx pathway. Genes Dev. *19*, 2331–2342.

Davies, P.F. (1995). Flow-mediated endothelial mechanotransduction. Physiol. Rev. *75*, 519–560.

de Bruijn, M.F., Speck, N.A., Peeters, M.C., and Dzierzak, E. (2000). Definitive hematopoietic stem cells first develop within the major arterial regions of the mouse embryo. EMBO J. *19*, 2465–2474.

Downing, J.R., Head, D.R., Curcio-Brint, A.M., Hulshof, M.G., Motroni, T.A., Raimondi, S.C., Carroll, A.J., Drabkin, H.A., Willman, C., Theil, K.S., et al. (1993). An AML1/ETO fusion transcript is consistently detected by RNA-based polymerase chain reaction in acute myelogenous leukemia containing the (8;21)(q22;q22) translocation. Blood *81*, 2860–2865.

Du, Q., Park, K.S., Guo, Z., He, P., Nagashima, M., Shao, L., Sahai, R., Geller, D.A., and Hussain, S.P. (2006). Regulation of human nitric oxide synthase 2 expression by Wnt beta-catenin signaling. Cancer Res. *66*, 7024–7031.

Duran-Reyes, G., Gomez-Melendez, M.R., Morali-de la Brena, G., Mercado-Pichardo, E., Medina-Navarro, R., and Hicks-Gomez, J.J. (1999). Nitric oxide synthesis inhibition suppresses implantation and decreases cGMP concentration and protein peroxidation. Life Sci. *65*, 2259–2268.

Dzierzak, E., and Medvinsky, A. (2008). The discovery of a source of adult hematopoietic cells in the embryo. Development *135*, 2343–2346.

Dzierzak, E., and Speck, N.A. (2008). Of lineage and legacy: the development of mammalian hematopoietic stem cells. Nat. Immunol. *9*, 129–136.

Eddy, F.B. (2005). Role of nitric oxide in larval and juvenile fish. Comp. Biochem. Physiol. A Mol. Integr. Physiol. *142*, 221–230.

Epperly, M.W., Cao, S., Zhang, X., Franicola, D., Shen, H., Greenberger, E.E., Epperly, L.D., and Greenberger, J.S. (2007). Increased longevity of hematopoiesis in continuous bone marrow cultures derived from NOS1 (nNOS, mtNOS) homozygous recombinant negative mice correlates with radioresistance of hematopoietic and marrow stromal cells. Exp. Hematol. *35*, 137–145.

Fritsche, R., Schwerte, T., and Pelster, B. (2000). Nitric oxide and vascular reactivity in developing zebrafish, Danio rerio. Am. J. Physiol. Regul. Integr. Comp. Physiol. *279*, R2200–R2207.

Fukumura, D., Gohongi, T., Kadambi, A., Izumi, Y., Ang, J., Yun, C.O., Buerk, D.G., Huang, P.L., and Jain, R.K. (2001). Predominant role of endothelial nitric oxide synthase in vascular endothelial growth factor-induced angiogenesis and vascular permeability. Proc. Natl. Acad. Sci. USA *98*, 2604–2609.

Goessling, W., North, T.E., Lord, A.M., Ceol, C., Lee, S., Weidinger, G., Bourque, C., Strijbosch, R., Haramis, A.P., Puder, M., et al. (2008). APC mutant zebrafish uncover a changing temporal requirement for wnt signaling in liver development. Dev. Biol. *320*, 161–174.

Goessling, W., North, T.E., Loewer, S., Lord, A.M., Lee, S., Stoick-Cooper, C.L., Weidinger, G., Puder, M., Daley, G.Q., Moon, R.T., et al. (2009). Genetic interaction of PGE2 and Wnt signaling regulates developmental specification of stem cells and regeneration. Cell *136*, 1136–1147.

Golub, T.R., Barker, G.F., Bohlander, S.K., Hiebert, S.W., Ward, D.C., Bray-Ward, P., Morgan, E., Raimondi, S.C., Rowley, J.D., and Gilliland, D.G. (1995). Fusion of the TEL gene on 12p13 to the AML1 gene on 21q22 in acute lymphoblastic leukemia. Proc. Natl. Acad. Sci. USA *92*, 4917–4921.

Holmqvist, B., Ellingsen, B., Forsell, J., Zhdanova, I., and Alm, P. (2004). The early ontogeny of neuronal nitric oxide synthase systems in the zebrafish. J. Exp. Biol. *207*, 923–935.

Ishimura, N., Bronk, S.F., and Gores, G.J. (2005). Inducible nitric oxide synthase up-regulates Notch-1 in mouse cholangiocytes: implications for carcinogenesis. Gastroenterology *128*, 1354–1368.

Isogai, S., Lawson, N.D., Torrealday, S., Horiguchi, M., and Weinstein, B.M. (2003). Angiogenic network formation in the developing vertebrate trunk. Development *130*, 5281–5290.

Itoh, M., Kim, C.H., Palardy, G., Oda, T., Jiang, Y.J., Maust, D., Yeo, S.Y., Lorick, K., Wright, G.J., Ariza-McNaughton, L., et al. (2003). Mind bomb is a ubiquitin ligase that is essential for efficient activation of Notch signaling by Delta. Dev. Cell *4*, 67–82.

Jin, H., Sood, R., Xu, J., Zhen, F., English, M.A., Liu, P.P., and Wen, Z. (2009). Definitive hematopoietic stem/progenitor cells manifest distinct differentiation output in the zebrafish VDA and PBI. Development *136*, 647–654.

Krasnov, P., Michurina, T., Packer, M.A., Stasiv, Y., Nakaya, N., Moore, K.A., Drazan, K.E., and Enikolopov, G. (2008). Neuronal nitric oxide synthase contributes to the regulation of hematopoiesis. Mol. Med. *14*, 141–149.

Lawson, N.D., Scheer, N., Pham, V.N., Kim, C.H., Chitnis, A.B., Campos-Ortega, J.A., and Weinstein, B.M. (2001). Notch signaling is required for arterial-venous differentiation during embryonic vascular development. Development *128*, 3675–3683.

Lawson, N.D., and Weinstein, B.M. (2002). In vivo imaging of embryonic vascular development using transgenic zebrafish. Dev. Biol. *248*, 307–318.

Lucitti, J.L., Jones, E.A., Huang, C., Chen, J., Fraser, S.E., and Dickinson, M.E. (2007). Vascular remodeling of the mouse yolk sac requires hemodynamic force. Development *134*, 3317–3326.

Lux, C.T., Yoshimoto, M., McGrath, K., Conway, S.J., Palis, J., and Yoder, M.C. (2008). All primitive and definitive hematopoietic progenitor cells emerging before E10 in the mouse embryo are products of the yolk sac. Blood *111*, 3435–3438.

Michurina, T., Krasnov, P., Balazs, A., Nakaya, N., Vasilieva, T., Kuzin, B., Khrushchov, N., Mulligan, R.C., and Enikolopov, G. (2004). Nitric oxide is a regulator of hematopoietic stem cell activity. Mol. Ther. *10*, 241–248.

Murayama, E., Kissa, K., Zapata, A., Mordelet, E., Briolat, V., Lin, H.F., Handin, R.I., and Herbomel, P. (2006). Tracing hematopoietic precursor migration to successive hematopoietic organs during zebrafish development. Immunity *25*, 963–975.

Nath, A.K., Enciso, J., Kuniyasu, M., Hao, X.Y., Madri, J.A., and Pinter, E. (2004). Nitric oxide modulates murine yolk sac vasculogenesis and rescues glucose induced vasculopathy. Development *131*, 2485–2496.

Noiri, E., Lee, E., Testa, J., Quigley, J., Colflesh, D., Keese, C.R., Giaever, I., and Goligorsky, M.S. (1998). Podokinesis in endothelial cell migration: role of nitric oxide. Am. J. Physiol. *274*, C236–C244.

North, T., Gu, T.L., Stacy, T., Wang, Q., Howard, L., Binder, M., Marin-Padilla, M., and Speck, N.A. (1999). Cbfa2 is required for the formation of intra-aortic hematopoietic clusters. Development *126*, 2563–2575.

North, T.E., de Bruijn, M.F., Stacy, T., Talebian, L., Lind, E., Robin, C., Binder, M., Dzierzak, E., and Speck, N.A. (2002). Runx1 expression marks long-term repopulating hematopoietic stem cells in the midgestation mouse embryo. Immunity *16*, 661–672.

North, T.E., Goessling, W., Walkley, C.R., Lengerke, C., Kopani, K.R., Lord, A.M., Weber, G.J., Bowman, T.V., Jang, I.H., Grosser, T., et al. (2007). Prostaglandin E2 regulates vertebrate haematopoietic stem cell homeostasis. Nature *447*, 1007–1011.

Orkin, S.H., and Zon, L.I. (2008). Hematopoiesis: an evolving paradigm for stem cell biology. Cell *132*, 631–644.

Palis, J., and Yoder, M.C. (2001). Yolk-sac hematopoiesis: the first blood cells of mouse and man. Exp. Hematol. *29*, 927–936.

Pallares, P., Garcia-Fernandez, R.A., Criado, L.M., Letelier, C.A., Esteban, D., Fernandez-Toro, J.M., Flores, J.M., and Gonzalez-Bulnes, A. (2008). Disruption of the endothelial nitric oxide synthase gene affects ovulation, fertilization and early embryo survival in a knockout mouse model. Reproduction *136*, 573–579.

Pelster, B., and Burggren, W.W. (1996). Disruption of hemoglobin oxygen transport does not impact oxygen-dependent physiological processes in developing embryos of zebra fish (Danio rerio). Circ. Res. *79*, 358–362.

Pelster, B., Grillitsch, S., and Schwerte, T. (2005). NO as a mediator during the early development of the cardiovascular system in the zebrafish. Comp. Biochem. Physiol. A Mol. Integr. Physiol. *142*, 215–220.

Poon, K.L., Richardson, M., Lam, C.S., Khoo, H.E., and Korzh, V. (2003). Expression pattern of neuronal nitric oxide synthase in embryonic zebrafish. Gene Expr. Patterns *3*, 463–466.

Prevotat, L., Filomenko, R., Solary, E., Jeannin, J.F., and Bettaieb, A. (2006). Nitric oxide-induced down-regulation of beta-catenin in colon cancer cells by a proteasome-independent specific pathway. Gastroenterology *131*, 1142–1152.

Pyriochou, A., Beis, D., Koika, V., Potytarchou, C., Papadimitriou, E., Zhou, Z., and Papapetropoulos, A. (2006). Soluble guanylyl cyclase activation promotes angiogenesis. J. Pharmacol. Exp. Ther. *319*, 663–671.

Reya, T., Duncan, A.W., Ailles, L., Domen, J., Scherer, D.C., Willert, K., Hintz, L., Nusse, R., and Weissman, I.L. (2003). A role for Wnt signalling in self-renewal of haematopoietic stem cells. Nature *423*, 409–414.

Rhodes, K.E., Gekas, C., Wang, Y., Lux, C.T., Francis, C.S., Chan, D.N., Conway, S., Orkin, S.H., Yoder, M.C., and Mikkola, H.K. (2008). The emergence of hematopoietic stem cells is initiated in the placental vasculature in the absence of circulation. Cell Stem Cell *2*, 252–263.

Sehnert, A.J., Huq, A., Weinstein, B.M., Walker, C., Fishman, M., and Stainier, D.Y. (2002). Cardiac troponin T is essential in sarcomere assembly and cardiac contractility. Nat. Genet. *31*, 106–110.

Teichert, A.M., Scott, J.A., Robb, G.B., Zhou, Y.Q., Zhu, S.N., Lem, M., Keightley, A., Steer, B.M., Schuh, A.C., Adamson, S.L., et al. (2008). Endothelial nitric oxide synthase gene expression during murine embryogenesis: commencement of expression in the embryo occurs with the establishment of a unidirectional circulatory system. Circ. Res. *103*, 24–33.

van Haperen, R., Cheng, C., Mees, B.M., van Deel, E., de Waard, M., van Damme, L.C., van Gent, T., van Aken, T., Krams, R., Duncker, D.J., et al. (2003). Functional expression of endothelial nitric oxide synthase fused to green fluorescent protein in transgenic mice. Am. J. Pathol. *163*, 1677–1686.

Wang, Q., Stacy, T., Binder, M., Marin-Padilla, M., Sharpe, A.H., and Speck, N.A. (1996). Disruption of the Cbfa2 gene causes necrosis and hemorrhaging in the central nervous system and blocks definitive hematopoiesis. Proc. Natl. Acad. Sci. USA *93*, 3444–3449.

Weber, G.J., Choe, S.E., Dooley, K.A., Paffett-Lugassy, N.N., Zhou, Y., and Zon, L.I. (2005). Mutant-specific gene programs in the zebrafish. Blood *106*, 521–530.

White, C.R., and Frangos, J.A. (2007). The shear stress of it all: the cell membrane and mechanochemical transduction. Philos. Trans. R. Soc. Lond. B Biol. Sci. *362*, 1459–1467.

Appendix 4

Resolving the Controversy about N-Cadherin and Hematopoietic Stem Cells

Pulin Li[1], Leonard I. Zon[1,*]

[1] Howard Hughes Medical Institute, Stem Cell Program, Hematology/Oncology, Children's Hospital, Harvard Medical School, Boston, MA 02115, USA

*Correspondence: zon@zon.tchlab.org

Resolving the controversy about N-Cadherin and Hematopoietic Stem Cells

Discrepancies in published results about the role of N-cadherin in hematopoietic stem cells have led to confusion in the field. Attempting to settle the disagreements and reach a consensus, we undertook a collective discussion approach. This process clarified a number of issues but left some questions still unresolved.

Background

One of the fundamental principles in biology is that cells in multicellular organisms interact and communicate with surrounding cells to acquire or maintain certain properties. This principle is relevant for stem cell biologists as they examine the ‘‘niche’’ hypothesis. The ‘‘stem cell niche’’ concept was first applied to the mammalian hematopoietic stem cell (HSC) field in 1978 (for a review of this area, see Voog and Jones, 2010); however, because of the rarity and low accessibility of HSCs, as well as the lack of specific HSC markers, it has been difficult to examine the specific contact of HSCs with niche cells.

Drosophila researchers adopted the niche concept and demonstrated that DE-cadherin and β-catenin interact at the interface between germline stem cells (GSCs) and niche cells. Loss of DE-cadherin leads to the loss of GSCs. These observations in Drosophila gonads encouraged the mammalian HSC field to examine the role of cadherin in the marrow niche.

Bone marrow contains a variety of cells that make up stem cell niche. There is evidence suggesting that some cells in the bone marrow express N-cadherin. Three papers published in 2003 and 2004 proposed that bone marrow osteoblasts are HSC niche cells, and two of them additionally showed that osteoblasts and HSCs are positive for immunohistochemical staining with a polyclonal anti-N-cadherin antibody (YS, Japan) (Calvi et al., 2003; Zhang et al., 2003; Arai et al., 2004). However, none of the studies identified a functional role for N-cadherin in the HSC niche. Wilson et al. (2004) found that KLS (c-kit+lineage-Sca-1+) cells are a mixture of N-cadherin-positive and -negative cells based on staining with the YS antibody, but whether those YS antibody-positive cells were long-term repopulating HSCs was unclear. In their model, HSCs lacking *c-myc* maintain a high level of N-cadherin and other adhesion molecules to enhance stem cell-niche interaction and therefore promote HSC expansion, whereas HSCs with high *c-myc* repress the adhesion molecules, causing the loss of stem cell-niche interaction and progressive exhaustion of stem cell pool. Later, Hosakawa et al. demonstrated that reactive oxygen species downregulated expression of N-cadherin in LSK-SP (c-kit+lineage-Sca-1+-side population) cells by quantitative RT-PCR and proposed a role of N-cadherin in the HSC-niche interaction (Hosokawa et al., 2007). Another follow-up study detected N-cadherin expression in Flk2-LSK HSCs by flow cytometry with a monoclonal N- cadherin antibody (MNCD2) that was verified by RT-PCR. This study indicated that the YS polyclonal antibody does not reliably indicate N-cadherin and instead concluded that flow cytometry with MNCD2 can be used to identify distinct subpopulations of HSCs (Haug et al., 2008). The authors concluded that Flk2LSK

cells that express intermediate levels of N-cadherin (N-cadherin^{int}) are quiescent HSCs that lack significant reconstituting potential upon transplantation into irradiated mice, whereas cells expressing low levels of N-cadherin (N-cadherin^{lo}) are primed/active HSCs with the capacity to reconstitute irradiated mice (Haug et al., 2008). However, two other papers reported no evidence of N-cadherin expression in Flk2-LSK cells or a further enriched population, SLAM-LSK HSCs, by a variety of techniques, including antibody staining and RT-PCR (Kiel et al., 2009; Kiel et al., 2007). In addition, these authors found that N-cadherin conditional knockout mice had no observable phenotype in HSC frequency, hematopoiesis, long-term competitive repopulation, or serial transplantation (Kiel et al., 2009). The observations from the different groups were therefore at odds with one another.

A Collaborative Discussion Process

The discrepancies described above were generating confusion in the published literature and thus in the field. With the aim of resolving the controversy and providing clarification of the issues involved, we embarked on an interactive discussion approach. At our (L.I.Z.) request, the principal investigators from the two groups that have generated the majority of the conflicting published data, Linheng Li and Sean Morrison, participated in a telephone conference in which each investigator presented and discussed pertinent data slides. This meeting also included another investigator, Toshio Suda, who has published work suggesting a positive role for N-cadherin in the bone marrow, and the editor of Cell Stem Cell, Deborah Sweet. This joint discussion was followed by a series of one-on-one phone

meetings and two other telephone conferences with L.I.Z. During the discussion, it became clear that the disagreement centered on three major questions: (1) Do HSCs express N-cadherin? (2) Is the MNCD2 monoclonal antibody specific for N-cadherin? (3) Does N-cadherin play a role in HSC maintenance and regulation? Involving the groups who had previously come to differing conclusions in a joint discussion provided an efficient mechanism for critical analysis of key experimental data and honest expression of opinion about the relevant issues.

With the available information, some conclusions about the first two issues became clear, and these will be outlined below. However, we were not able to reach an agreement on the third question on the basis of the available data. Upon the senior scientist's suggestion, the Li and Morrison labs agreed to independently perform a limiting dilution competitive transplantation with the exact same experimental conditions and N-cadherin conditional knockout mice, with a view to comparing data and coming to a consensus conclusion. Several emails between the groups outlined in detail the methods, doses of cells, and mechanism of conditional inactivation of N-cadherin. Six months later, we set up a phone call to examine the data from the two laboratories.

Agreements and Outstanding Issues During our initial discussions, we were able to come to agreement on a number of points relating to detection of N-cadherin expression in bone marrow cells. In previous studies, the expression of N-cadherin in HSCs has been examined at the mRNA level. The Li and Suda groups found that N-cadherin mRNA can be detected in highly enriched populations of stem cells by quantitative RT-PCR (Haug et al., 2008; Hosokawa et al., 2007; Hosokawa et al.,

2010), but Morrison and colleagues did not detect any expression by qRT-PCR or by microarray analysis (Kiel et al., 2007). Indeed, even in the Li and Suda groups' qRT-PCR assays, the expression level in HSCs was found to be very low compared with some non-HSC control populations. Moreover, no microarray analysis by any group has ever reported the enrichment of N-cadherin in HSCs. With very low levels of expression, divergent findings could potentially be explained by differences in experimental methods and assay sensitivities. The overall conclusion from these data is that N-cadherin RNA is either present at very low levels or absent in HSCs.

The majority of the protein expression data presented by Haug et al. were obtained using a monoclonal antibody against N-cadherin, MNCD2 (Haug et al., 2008). Therefore, challenges to the conclusion that HSCs might express varying low levels of N-cadherin on their surface have centered on concerns about the specificity of the MNCD2 reagent. MNCD2 was originally developed by Matsunami and Takeichi in 1995 (Matsunami and Takeichi, 1995), and its specificity for N-cadherin in western blots was demonstrated by Radice et al., who compared wild-type and N-cadherin null mice (Radice et al., 1997). The Morrison and Li groups also independently con- firmed that MNCD2 was specific for N-cadherin by western blotting and immunostaining using neonatal forebrain cells and cell lines in which N-cadherin is abundantly expressed (Kiel et al., 2009; Haug et al., 2008). To examine whether N-cadherin is expressed in enriched HSCs, Kiel et al. sorted 105 LSK cells and carried out western blot analysis with MNCD2. They failed to detect any N-cadherin protein despite readily detecting N-cadherin in a few thousand fore- brain cells (Kiel et al., 2009). Thus, the available data suggest that MNCD2 does give a

specific signal by Western blot in tissues in which N-cadherin is highly expressed, but Western blotting with MNCD2 has not been able to confirm N-cadherin expression in the LSK cells. These observations provide further support for the idea that N-cadherin is expressed in a very limited hematopoetic cell population and/or at extremely low levels, or may in fact be absent. Using improved Western blotting techniques and a large number of highly purified cells might reveal the answer.

The above conclusions about the expression level of N-cadherin in HSCs raise the possibility that signals obtained for MNCD2 with other assays could be the result of nonspecific binding. Use of the MNCD2 antibody for flow cytometry with enriched HSCs has proved problematic. Haug et al. did see a shift in MNCD2 staining with Flk2-LSK cells compared with the control omitting MNCD2, but in their published study they did not compare this staining with isotype controls to assess staining above background or non-specific antibody binding (Haug et al., 2008). Kiel et al. (2007, 2009) were unable to detect any staining of SLAM-LSK or Flk2-LSK HSCs using MNCD2 or other commercially available anti-N-cadherin antibodies. Moreover, both Kiel et al. and Foudi et al. found that MNCD2 strongly stained surface B220+ B cells in the bone marrow, but when these cells were sorted and analyzed by Western blot, no N-cadherin band was evident (Foudi et al., 2009; Kiel et al., 2009). The Morrison and Hock groups also examined HSCs enriched by multiple combinations of markers, such as SLAM-LSK and Flk2-LSK, and neither group observed any effect of N-cadherin deficiency on the MNCD2 staining of HSCs or other bone marrow cells (Foudi et al., 2009; Kiel et al., 2009). To some extent the differences in results could be due to variation in flow cytometry technique between

the labs, different sub-clones of hybridoma used to produce the antibody, or the conditional knockout efficiency. However, the Morrison laboratory tested multiple aliquots of MNCD2 antibody obtained from the Li laboratory as well as directly from the Developmental Studies Hybridoma Bank and confirmed in all of their experiments that N-cadherin deletion was complete or nearly complete by PCR (S.M. unpublished data). Concerns about these technical differences are heightened by the very low level of proposed N-cadherin expression and the non-specific binding of MNCD2 to HSCs/progenitors. There is no indication from any group that HSCs express high levels of N-cadherin, and instead the accumulated data are consistent with a low level of expression, if any at all, that might be limited to a very small subset of HSCs. Although very low levels of proteins can have a function in cell biology, these data currently cannot be used to support an important HSC function of N-cadherin. These conclusions formed the backdrop against which we discussed our viewpoints on functional studies.

To address the question of whether N-cadherin is required for HSC maintenance, Kiel et al. (2009) studied N-cadherin conditional knockout mice, as the germline knockout is embryonic lethal. They did not observe any change of HSCs or hematopoiesis in homeostatic situations up to 5 months after N-cadherin deletion (using *Mx-1-Cre*). To further challenge the HSCs, they transplanted 10^6 bone marrow cells from the N-cadherin conditional knockout mice with comparable numbers of competitive bone marrow cells, and did not observe a significant difference in chimerism relative to wild-type donor cells, even in secondary transplantation. From these experiments, they concluded that HSCs ‘‘do not depend on N-cadherin to

regulate their maintenance.'' N-cadherin could potentially still be required during regeneration or the response to certain types of stresses, and testing the N-cadherin knockout animals for their response during various stresses or irradiation could be interesting. However, the Morrison group failed to see any effect of N-cadherin deletion on the recovery of mice in response to 5-fluorouracil treatment (Kiel et al., 2009), indicating that N-cadherin does not play an important role in at least this stress condition.

During the discussion, the transplantation data by Kiel et al. (2009) were questioned. One potential issue related to the knockout efficiency in the donor mice, and it was suggested that using reporter mice that can indicate the *Cre*-mediated recombination activity could be helpful. However, with such an approach it is still possible that the recombination efficiency at the reporter locus could be different from the N-cadherin locus, or could vary between cell populations. As an alternative approach, Morrison's group purified the LT-HSC for clonal culture and per- formed PCR on each individual colony, showing the knockout efficiency was almost 100%. In addition, the donor-derived cells in the recipients' peripheral blood are also N-cad$^{-/-}$, further confirming the knockout efficiency (Kiel et al., 2009). Based on these results, it seems unlikely that the failure to observe a phenotype is due to incomplete knockout.

Even though transplantation is considered the gold standard for testing stem cell functionality, the field has not been able to agree on standardized procedures, and there are substantial inter-lab variances in aspects of hematopoietic transplantation protocols such as donor cell numbers and the cut-off for long- term

multi-lineage reconstitution. In an attempt to address the controversy in a rigorous way, L.I.Z. suggested that both groups perform a limiting dilution competitive transplantation indepentdently and compare results, and they agreed to do so. The agreed experiment was that 20,000, 60,000 and 200,000 wild-type or N-cad conditional knockout whole bone marrow cells would be trans- planted together with 200,000 competitor cells, and the results examined 16 weeks after transplantation. Six months later, however, only the Morrison lab presented data from the agreed experiment (M. Acar, M. Kiel, and S. Morrison, unpublished data). We examined the resulting data with a biostatistician using standard software for calculating the frequency of hematopoietic stem cell engraftment and ANOVA analysis, and found that there was no difference between the wild-type and N-cadherin deficient groups, consistent with the conclusions published previously by Kiel et al. (2009). For additional verification, we also showed the entire analysis to an independent investigator in the hematopoietic stem cell field, who also ran the data through statistical software and came to the same conclusion. Complete N-cadherin deletion was confirmed in these experiments by PCR of genomic DNA from donor cells sorted from the reconstituted mice. However, instead of the agreed set of experiments the Li lab independently chose to undertake a different approach involving using a *Cre-loxP* reporter system to indirectly indicate the recombination/knockout efficiency and trans- planting purified reporter positive and reporter negative cells separately. They observed a difference between these two subsets of cells, which they interpreted as indicating a role for N-cadherin in HSCs (L. Li, unpublished data). However, in our view these experiments are not

straightforward to interpret and are therefore not informative for resolving the question at hand. Thus, at this point our conclusion is that no substantial HSC phenotype associated with N-cadherin conditional deletion has been observed, suggesting that N-cadherin does not play an essential functional role in HSCs.

Future Questions

Although the data available at this point do not indicate an essential role of N-cadherin in HSCs, redundancy in cadherin function in HSCs remains a possibility. Early experiments showed that HSCs do not express E-cadherin (Zhang et al., 2003). However, in this issue of Cell Stem Cell Toshio Suda's group show that the N-cadherin mRNA level in LSK cells differs between mouse strains by qRT-PCR (Hosokawa et al., 2010). They found that the C57BL/6 strain has significantly higher N-cadherin level than the 129/Sv strain, from which the N-cadherin$^{fl/-}$ mice were originally derived (Kostetskii et al., 2005). In contrast, the 129/Sv strain has higher expression of other cadherins than the C57BL/6 strain. This could indicate that different cadherins are used by different strains. Interestingly, the Suda group found that overexpressing a dominant-negative (DN) N-cadherin inhibits the lodgment and long-term repopulating activities of HSCs, while overexpressing wild-type N-cadherin has the opposite effect (Hosokawa et al., 2010). Because of the non-specific blocking of cadherin family members by the DN-N-cadherin (Fujimori and Takeichi, 1993), this result leaves open the possibility that cell adhesion mediated by the redundant cadherin family members might be involved in HSC activities.

However, it is worth noting that Kiel et al. were not able to detect N-cadherin mRNA in C57BL HSCs and studied knockout mice that were backcrossed with C57BL/6 for at least six generations, arguing against the idea that strain background is a basis for the discrepancy in results (Kiel et al., 2009). Thus, although potential strain differences are intriguing, currently it does not appear likely they can provide an explanation for the different conclusions drawn.

In summary, therefore, although there are still differences of opinion among the investigators involved in this process regarding the potential for N-cadherin function in HSCs, it is our view that to move the research in the field forward we need to acknowledge the current observations and set a common foundation for the stem cell community. The current observations on the N-cadherin conditional knockout model indicate that the maintenance of adult HSCs does not appear to depend on N-cadherin homophilic interactions. This conclusion does not support or argue against the potential role of osteoblasts or perivascular cells in the HSC niche, and it does not entirely rule out the idea of cadherin-mediated niche-HSC interaction model as cadherin redundancy is still a possibility. However, convincing evidence to support this idea would require demonstration of a clear HSC defect in knockout mice, either alone or in combination with the N-cadherin knockout, using limiting dilution competitive repopulation studies in the mouse. Our conclusion is that until clearcut data along these lines are forthcoming, the field should not base further experiments on the concept that there is a functionally significant cell-autonomous role for N- cadherin in HSCs.

Bullet Point Summary

- N-cadherin expression in HSCs is either low or undetectable; if N-cadherin is expressed in HSCs it is present at a very low level and/or in a small subset of cells.
- The N-cadherin monoclonal antibody, MNCD2, is not specific for N-cadherin expression in the hematopoietic compartment. This antibody should not be used for experiments that require flow-cytometric sorting of HSCs, although it still can be used to detect N-cadherin expression by Western blot or immunostaining in tissues that express high levels of N-cadherin, such as liver.
- Currently available data lead to the conclusion that the maintenance of adult HSCs does not depend on a cell-autonomous role of N-cadherin. To argue against this conclusion, future experiments would need to demonstrate that genetic deficiency of another component, such as a different cadherin, causes a substantial HSC phenotype in N-cadherin conditional knockout mice.

References

Arai, F., Hirao, A., Ohmura, M., Sato, H., Matsuoka, S., Takubo, K., Ito, K., Koh, G.Y., Suda, T. (2004). Tie2/Angiopoietin-1 signaling regulates hematopoietic stem cell quiescence in the bone marrow niche. Cell 118, 149-161.

Calvi, L.M., Adams, G.B., Weibrecht, K.W., Weber, J.M., Olson, D.P., Knight, M.C., Martin, R.P., Schipani, E., Divieti, P., Bringhurst, F.R., et al. (2003). Osteoblastic cells regulate the haematopoietic stem cell niche. Nature 425, 841-846.

Cobas, M., Wilson, A., Ernst, B., Mancini, S.J., MacDonald, H.R., Kemler, R., and Radtke, F. (2004). Beta-catenin is dispensable for hematopoiesis and lymphopoiesis. J Exp Med 199, 221-229.

Foudi, A., Hochedlinger, K., Van Buren, D., Schindler, J.W., Jaenisch, R., Carey, V., and Hock, H. (2009). Analysis of histone 2B-GFP retention reveals slowly cycling hematopoietic stem cells. Nat Biotechnol 27, 84-90.

Haug, J.S., He, X.C., Grindley, J.C., Wunderlich, J.P., Gaudenz, K., Ross, J.T., Paulson, A., Wagner, K.P., Xie, Y., Zhu, R., et al. (2008). N-cadherin expression level distinguishes reserved versus primed states of hematopoietic stem cells. Cell Stem Cell 2, 367-379.

Hosokawa, K., Arai, F., Yoshihara, H., Nakamura, Y., Gomei, Y., Iwasaki, H., Miyamoto, K., Shima, H., Ito, K., Suda, T. (2007). Function of oxidative stress in the regulation of hematopoietic stem cell-niche interaction. Biochem Biophys Res Commun 363, 578-583.

Kiel, M.J., Acar, M., Radice, G.L., and Morrison, S.J. (2009). Hematopoietic stem cells do not depend on N-cadherin to regulate their maintenance. Cell Stem Cell 4, 170-179.

Kiel, M.J., Radice, G.L., and Morrison, S.J. (2007). Lack of evidence that hematopoietic stem cells depend on N-cadherin-mediated adhesion to osteoblasts for their maintenance. Cell Stem Cell 1, 204-217.

Koch, U., Wilson, A., Cobas, M., Kemler, R., Macdonald, H.R., and Radtke, F. (2008). Simultaneous loss of beta- and gamma-catenin does not perturb hematopoiesis or lymphopoiesis. Blood 111, 160-164.

Kostetskii, I., Li, J., Xiong, Y., Zhou, R., Ferrari, V.A., Patel, V.V., Molkentin, J.D., and Radice, G.L. (2005). Induced deletion of the N-cadherin gene in the heart leads to dissolution of the intercalated disc structure. Circ Res 96, 346-354.

Maillard, I., Koch, U., Dumortier, A., Shestova, O., Xu, L., Sai, H., Pross, S.E., Aster, J.C., Bhandoola, A., Radtke, F., et al. (2008). Canonical notch signaling is dispensable for the maintenance of adult hematopoietic stem cells. Cell Stem Cell 2, 356-366.

Matsunami, H., and Takeichi, M. (1995). Fetal brain subdivisions defined by R- and E-cadherin expressions: evidence for the role of cadherin activity in region-specific, cell-cell adhesion. Dev Biol 172, 466-478.

Radice, G.L., Rayburn, H., Matsunami, H., Knudsen, K.A., Takeichi, M., and Hynes, R.O. (1997). Developmental defects in mouse embryos lacking N-cadherin. Dev Biol 181, 64-78.

Schofield, R. (1978). The relationship between the spleen colony-forming cell and the haemopoietic stem cell. Blood Cells 4, 7-25.

Song, X., Zhu, C.H., Doan, C., and Xie, T. (2002). Germline stem cells anchored by adherens junctions in the Drosophila ovary niches. Science 296, 1855-1857.

Zhang, J., Niu, C., Ye, L., Huang, H., He, X., Tong, W.G., Ross, J., Haug, J., Johnson, T., Feng, J.Q., et al. (2003). Identification of the haematopoietic stem cell niche and control of the niche size. Nature 425, 836-841.